THE EFFECT OF THERMAL-MECHANICAL PROCESSING ON THE PHYSICAL AND MECHANICAL PROPERTIES OF Al-Fe-Co ELECTRICAL CONDUCTOR ALLOY

A THESIS

Presented to

The Faculty of the Division

of Graduate Studies

by

Enrique Henry Chia

In Partial Fulfillment

of the Requirements for the Degree

Doctor of Philosophy

In the School of Chemical Engineering

Georgia Institute of Technology

June, 1975

Dedicated to Dr. Niels N. Engel
who introduced the author to
the subject of Metallurgy

ACKNOWLEDGEMENTS

The author wishes to thank his thesis advisor, Dr. Pieter Muije, for his guidance, encouragement and fruitful discussions during this research. The genuine interest and guidance extended by Drs.N. N. Engel and Edgar A. Starke, Jr. are gratefully acknowledged. The very generous amount of time they spent appraising this work was invaluable and is sincerely appreciated.

I am very grateful to Dr. Bruce G. LeFevre and to my reading committee Drs. H. Grenga and S. Spooner for their time and constructive criticism.

I am indebted to my boss, Mr. D. B. Cofer, Senior Vice President of Southwire Company for his encouragement and patience throughout the entire course of this research. Thanks are also extended to Mr. Roy Richards, President and Mr. Roger Schoerner, Vice-President of Southwire Company.

The invaluable contribution of Mr. Phil Jackson in the compilation and assembling of this work is very much appreciated. Also, vital help was provided by Mr. Oscar Roberts and George Keller during the experimental stage of this work. Thanks are extended to Messrs. James W. Wallis and Sloan Barrow for their invaluable assistance and to Messrs. Stanley Jones and Kenneth McColley for their help in Mechanical Testing.

I am very grateful to Mr. Phineas Clower for his excellent drafting work. I am also indebted to Messrs. Kenneth Chadwick, Frank Powers, Ron Adams and Doug Cole for their helpful suggestions.

Finally, I am extremely grateful to my wife, Diana, for her encouragement and endurance which made the present work a reality. Also, I express my love to my daughters Laura and Lisa, who were a definite driving force for the completion of this work.

TABLE OF CONTENTS

TABLE OF CONTENTS (Continued)

LIST OF TABLES

LIST OF FIGURES

LIST OF FIGURES (Continued)

LIST OF FIGURES (Continued)

LIST OF FIGURES (Continued)

LIST OF FIGURES (Continued)

LIST OF FIGURES (Continued)

LIST OF FIGURES (Continued)

LIST OF FIGURES (Continued)

LIST OF FIGURES (Continued)

LIST OF FIGURES (Continued)

LIST OF FIGURES (Continued)

LIST OF FIGURES (Continued)

SUMMARY

The effect of the speed of solidification and the thermal-mechanical processing of a newly developed aluminum alloy containing 0.5 weight percent cobalt and 0.5 weight percent iron was investigated using transmission electron microscopy and mechanical testing. The present research has shown that in order to produce a final wire product with small, uniformly distributed precipitate particles, rapid solidification producing a small interdendritic spacing is necessary.

Optimum hot rolling conditions consist of a high strain rate with the maximum cooling attainable during deformation to produce an effective dispersion of particles and a small cell structure.

Annealing the hot rolled rod before cold drawing was proven to have a detrimental effect on the mechanical properties of the finish wire. This is due to the excessive growth of the subgrains before cold work and to the precipitation of the compounds before the final anneal.

It was also found that the obtained dispersion of particles in the cold drawn wire act as barriers to the movement of the subgrain boundaries during annealing. It was shown that the high degree of thermal stability achieved in this alloy was due to the pinning effect produced by the precipitate particles on the growing subgrain boundaries after primary recrystallization. The combination of subgrain strengthening and precipitate dispersion hardening produces the

strengthening mechanisms in this alloy. These effects are responsible for producing a finish wire which possesses a stable subgrain structure and consequently excellent mechanical and electrical properties.

CHAPTER I

INTRODUCTION

In recent years the use of aluminum as an electrical conductor has increased significantly. An electrical grade conductor with a minimum of 99.45% aluminum was first used for overhead transmission lines in the early 1890's and has been used extensively since then with great success. There are other electrical applications where aluminum could be used only if certain physical and mechanical properties are achieved. These include building wire, telephone cable, battery cable, automotive harness wiring, aircraft cable, transformer wire, magnet wire and appliance cord. Inspection of these uses indicates that a material which possesses high strength and a high degree of connectability, coupled with a minimum loss in electrical conductivity, would be required for successful performance.

Electrical Conductor grade aluminum,[1] in the fully annealed condition, possesses acceptable ductility and electrical conductivity. However, it is seriously handicapped by its poor mechanical properties and thermal stability. This precludes its use in applications where a strong, reliable connection is required. The connection or termination of the system is one of the most critical parts of any electrical system. The termination or connection is also the part that is handled by the public, and consequently is very often subjected to careless or poor workmanship. An ideal system would consist of conductor

and termination designed in such a way that it would produce a "fool proof" system.

One of the integral components of the system, the conductor itself, which was the object of this research, could be made stronger and with higher thermal stability simply by alloying the aluminum with magnesium, silicon, copper, etc., as has been done in the past for many structural applications.[2-5] However, the decrease in electrical conductivity associated with the high solubility of these alloying additions prohibits their use in electrical conductor aluminum. Another way that the mechanical properties of the aluminum can be increased is to subject it to a certain amount of cold work in order to produce extensive work hardening in the matrix. This method, however, will render the aluminum unusable as it yields an unstable cold worked structure with both low ductility and extremely low thermal stability.

The method used in this research consisted of producing, by thermo-mechanical processing, a conductor which possessed improved mechanical properties and an electrical conductivity above 61 percent of the International Annealed Copper Standard (IACS). This was achieved by obtaining a fine, stable cell structure in the aluminum matrix containing a fine dispersion of stable, insoluble intermetallic phase particles. The alloy used was an aluminum alloy containing 0.5 weight percent iron and 0.5 weight percent cobalt.

In non-heat-treatable, commercial alloys, it is difficult to obtain a completely uniform distribution of the insoluble precipitate particles in the matrix. Usually, the particles are found in groups in

an essentially precipitate-free matrix. The spacing of the particles determines the minimum cell size obtainable by mechanical-thermal processing.[6] The presence of large precipitate particles in the matrix decreases the recrystallization temperature of the alloy; whereas, small precipitate particles can increase its recrystallization temperature.[7] In other words, small precipitate particles distributed uniformly throughout the matrix would be desirable to obtain optimum stability of mechanical properties. The casting operating controls the dendritic grain size and arm spacing, and the size and distribution of the precipitate particles. Thus, the interprecipitate distance is controlled by the solidification conditions. Solution heat treatments cannot affect the alloy in this respect once it has solidified, since the precipitates are insoluble, and the only alternative available to influence the precipitate-matrix morphology is by deformation and thermo-mechanical treatments. Deformation of the material can cause the precipitates to be broken and strung out causing the number of particles present to increase, and the inter-precipitate spacing to decrease. However, the precipitates break up only if they are brittle and if sufficient deformation is applied prior to annealing. The ductile matrix will tend to form a cell structure in the presence of a second phase if the stacking fault energy is sufficient to allow cross slip.

An aluminum alloy containing 0.5 weight percent iron and 0.5 weight percent cobalt was successfully developed based on the stability of the compound formed, effect of alloying additions on electrical conductivity, and manufacturing feasibility. The developed aluminum-iron-

cobalt alloy met the above mentioned requirements of improved mechanical properties without sacrificing the electrical conductivity.

Since unalloyed aluminum (Electrical Conductor grade aluminum) has been used for several of the previously mentioned applications, and since the Al-Fe-Co alloy thermo-mechanically processed represents a definite improvement over the EC aluminum a side-by-side comparison was performed on the effect of the studied parameters. This included the effect of speed of solidification, the cell formation during hot working, the effect of rod annealing before cold working, and the study of annealing parameters.

CHAPTER II

LITERATURE SURVEY

The mechanical properties of the finished aluminum alloy wire and their stability at higher temperatures are enhanced significantly by the characteristics of the substructure produced during the hot working operation.[8]

Aluminum and its alloys develop a well-defined cell structure[9] when subjected to various degrees of deformation.[10] This is attributed to the high stacking fault energy of aluminum which by the prevention of dislocations splitting into partials, aids in the cross-slip process necessary for subgrain formation.[11,12] During deformation, the dislocation density increases and well-defined cells are formed until an equilibrium cell size and dislocation density is reached. The equilibrium state is a function of temperature and deformation obeying the following relationship as pointed out by Amelinckx[12]

$$\rho = K\ (1/d)^n$$

where ρ is the dislocation density, d the cell size, and K and n are constants, n usually between two and three.

Aluminum, when deformed at temperatures from 50 to 70 percent of its melting temperature, softens by dynamic recovery.[13] This term implies recovery taking place during deformation. McQueen[14] investigated the effect of the hot working temperature on the dynamic

recovery of metals of high stacking fault energy such as aluminum. He found that with increasing deformation temperature, a greater amount of recovery was responsible for reducing the strain hardening in such metals. The arrangement of dislocations into sub-boundaries during the hardening stage was found[15] to be caused by simultaneous dynamic recovery. The subgrain network formed during deformation will influence the properties of the finished product even if the aluminum is partly or completely recrystallized. The presence of small precipitates in the aluminum matrix has a pronounced effect on the stabilization of the formed subgrain boundaries.[16]

Softening Processes

A cold worked metal will soften during annealing by the following processes: recovery, recrystallization and grain growth. In aluminum and its alloys, the recovery stage is composed of (a) dislocation clearing (annihilation), (b) polygonization and (c) partial coalescence.

During dislocation clearing and polygonization, the dislocations existing in the cell interiors are attracted to the cell walls where annihilation of the redundant dislocations takes place. This results in sharply defined subgrains separated by delineated, thin boundaries.[7] This was confirmed by Gay, et al.[17] and Perryman[18] who concluded from their X-ray microbeam studies that the substructural changes taking place during the recovery of aluminum was due to the rearrangement and subsequent movement of dislocations from the interior of the cells to the cell walls. The movement and rearrangement of dislocations in aluminum during the recovery stage produces significant changes in the

mechanical properties of the metal. This has been reviewed in detail by Vandermeer and Gordon[19] who extensively investigated the property changes taking place during the recovery and recrystallization of aluminum. Polygonization of aluminum cells was first reported by Cahn[20] in 1949. He found that transmission Laue patterns of the aluminum specimen before and after annealing showed a difference in the continuity of the asterisms. When the aluminum was annealed, the asterisms became discontinuous due to the formation of walls of dislocations perpendicular to the glide planes that were active during the bending. This mechanism lowers the total elastic strain energy of the crystal since the edge dislocations are arranged one above the other instead of the random way they are before annealing. The decrease of energy provides the driving force for the process. A polygonized substructure is characterized by sharp, delineated subgrains which can coalesce and grow. Leighly, et al.[2] pointed out that if high-purity aluminum is allowed to polygonize extensively prior to recrystallization, the decrease in internal energy taking place during polygonization would delay, and in some cases prevent the formation of recrystallization nuclei during further annealing. This is due to the fact that both processes have the elimination or lowering of the stored energy of cold work as their driving force.

The coalescence of subgrains during recovery and recrystallization has been clearly explained by Li[22] who devised a model for coalescence of subgrains in aluminum. Figure 1 shows the schematic of the coalescence process as explained by Li. The process involves the movement of the atoms around the subgrains to produce a rotation of one subgrain with

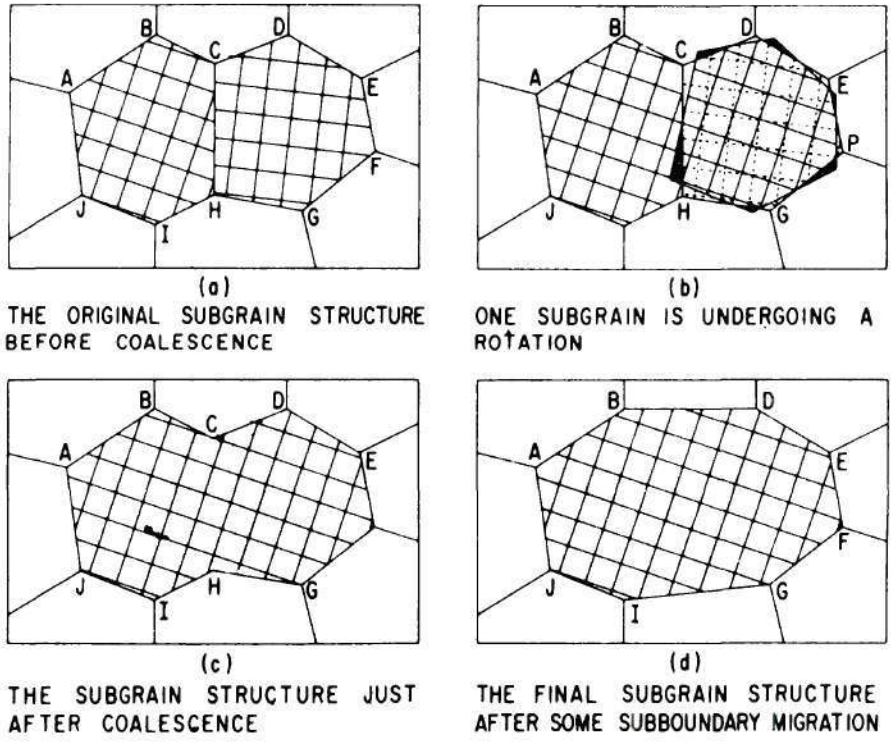

Figure 1. Schematic of the Coalescence Process by Subgrain Rotation as Explained by Li.[22]

respect to the other and dislocation climb along the disappearing subgrain boundary.

In 1962 Bailey and Hirsch[23] stated that recrystallization took place in copper by boundary migration. They found that grains which subtended misorientations as high as ten degrees with their neighbors become recrystallization nuclei and proceeded to grow by boundary migration. Beck and Sperry[24] also found a type of recrystallization which did not involve nucleation but only grain boundary migration which they called strain induced boundary migration. This mechanism consists of the movement of the boundary away from its center of curvature, leaving behind a strain-free material of the same orientation as the parent grain. They also found this type of recrystallization predominated in high-purity aluminum which was cold rolled in increasing amounts up to 40 percent reduction. Cottrell[25] stated that a recrystallization nucleus would occur in regions of heavy lattice curvature which subtend high misorientation angles with their neighbors and consequently would be favorable for grain boundary migration. Doherty[28] suggested that the high boundary mobility associated with misorientations greater than 10-18 degrees is the origin of preexisting grain boundaries and transition bands acting as sites for nucleation. He also suggested that coalescence may play an important role in the initial growth of subgrain nuclei. However, Hu[26] investigated the recrystallization of silicon-iron single crystals under the electron microscope and suggested that the recrystallization nuclei form by a coalescence mechanism, as suggested by Li and not by grain boundary migration.

It definitely appears that aluminum recrystallizes by subgrain coalescence, that is, subgrains favorably oriented start to coalesce to the point where the misorientation angle is large enough to become a recrystallization nucleus which will then grow at the expense of other subgrains as suggested by Dunn and Koh[27] and shown in Figure 1. This will continue simultaneously in several areas until they impinge on each other. Weissman[112] confirmed that recrystallized grains are formed by subgrain growth. He followed the emergence of strain-free subgrains from a cluster of subgrains by the process of subgrain coalescence. He also found that subgrains with high degrees of misorientations grew faster and derived from regions associated with the grain edges of the deformed matrix.

Fujita[29] studied the recrystallization of aluminum after cold work and found that if there is an absence of recrystallized grains when the specimen is observed under the optical microscope after chemical etching, the structure is considered to be recovered, but not recrystallized. However, the specimen showed a high degree of subgrain coalescence when examined by electron microscopy. He observed subgrains which were as large as 10 microns in diameter. Fujita stated that recrystallization was started when a boundary was formed across many subgrain boundaries due to the coagulation of lattice defects and that their positions are originally decided during cold working. According to Fujita, annealing causes subgrain growth which is effected by these two mechanisms (a) sub-boundary migration and (b) subgrain group formation. He pointed out that these groups are composed of subgrains having small misfit angles. Fujita's results were (1) remarkable growth of subgrains was observed before recrystallization, (2) large subgrains were observed within the

recrystallized grain, (3) in the unrecrystallized grains, small subgrains were observed, (4) prior to recrystallization, subgrain boundaries were not well defined and broad. The precise details of mechanisms of how the sub-boundaries disappeared was not explained by Fujita.

The kinetics of recrystallization have been described by an equation of the type

$$N = 1 - e^{(-Bt^n)}$$

where N is the fraction of recrystallized volume, B the temperature - dependent factor, t the time at temperature, and n the constant. This formula implies that if a specimen is held within its recrystallization temperature range, isothermal recrystallization will occur if the specimen is held in that range long enough. However, Schweizer and Form[30] found by using the photoemission electron microscope that within the "range of partial recrystallization", complete recrystallization will not take place regardless of the length of time the specimen is held at that temperature. Their results show that at each temperature within this range, the amount recrystallized reaches a limiting value, which was termed by the authors as a "saturation value." The temperature where saturation reaches 100% is defined as the "upper recrystallization temperature." They attribute the divergence from the Avrami equation to the blocking of the moving boundaries either by impurities or special dislocation configurations.

Considering the work performed on the recovery and recrystallization of aluminum and the diversity of interpretations reached, one can conclude that the process is not completely understood at the present

time. However, several key conclusions can be drawn from the previous work. It can be stated that a majority of investigators now agree that recrystallization in aluminum takes place by subgrain coalescence whereby a subgrain is formed with a misorientation angle which differs from that of the adjacent subgrains. Once a subgrain is formed with high angle boundaries, these migrate during the rest of the process. The recrystallization process follows the recovery stage in which polygonization and subgrain coalescence takes place.

Subgrain Structure

The effect of grain size on the yield strength of metal was first studied by Hall in 1951[31] and Petch[32] in 1953 in iron. Their experimental results could be described by a relationship of the type

$$\sigma = \sigma_o + k\, d^{-1/2}$$

where σ is the yield strength, σ_o the frictional stress, and d the grain size. Several investigations[32,33,34,35,39] have been carried on the effect of subgrain size on the yield strength of different materials and also found it to obey a Hall-Petch type relation.

Korbel and Swiatkowski[38] studied the effect of the cell (subgrain) size on the mechanical properties of pure aluminum. They found that a Hall-Petch type relationship existed in cold deformed material between strength and cell size. They also concluded that the constant K in the Hall-Petch equation was independent of the angle of misorientation across the cells. The results of Abson and Jonas,[39] however, do not agree with those of Korbel and Swiatkowski. They

attributed this difference to the fact that the increase in the angle of misorientation was obtained by varying the cell wall thickness (dislocation tangles forming the subgrain boundary) while the dislocation density was kept constant. Determination of the angles of misorientation by the width of the cell boundaries is subject to a large error due to the imperfection of the cell boundaries.

A previous investigation by Ball[40] resulted in a strong correlation between flow stress and subgrain size in polycrystalline aluminum deformed in tension. He found a Hall-Petch type relation with the exponent of d equal to -1/2. However, this plot yielded a negative σ_o which would cast a doubt on the validity of this correlation since a negative σ_o is a physical absurdity.

Other investigators[36,37,38] have found that in pure cubic metals the dislocation density increases with increasing deformation forming thick tangles which adhere to subgrain boundaries separating areas of low dislocation density. An increase in the flow stress and the misorientation between the cells accompanies this increase in dislocation density.

Langford and Cohen[45] investigated the strain hardening of iron during cold drawing. They concluded that the strengthening achieved by cold drawing is a linear function of $\bar{d}^{-1}$ where $\bar{d}$ is the mean linear intercept between cell walls on a transverse section. This linear relationship has also been found by Jonas and McQueen[44] in aluminum which was hot extruded and cold worked. Langford and Cohen[45] also found that 99 percent of the dislocation generated during strain hardening are lost by annihilation at cell walls, 0.8 percent are lost

by coalescence and 0.2 percent is incorporated into the remaining cell walls as stored energy.

Another investigation[46] yielded that aluminum and copper did not follow the Hall-Petch relation

$$\sigma_{\epsilon} = \sigma_{o\epsilon} + k\, d^{-1/2}$$

in the areas of high strain. σ_{ϵ} is the flow stress at a particular value of strain, σ and $\sigma_{o\,\epsilon}$ and k_{ϵ} are the experimental constants appropriate to a particular strain value and d is the subgrain diameter. The authors pointed out that a good correlation would be found if an approach is taken which centers on the concept of different regions of slip within grains, one in the grain boundaries and the other in the interior of the grain, a concept which has been discussed by several investigators.[47, 48, 49]

Subgrains Formed During Hot Working

Kosik, et al[50] obtained data on the effect of subgrains on the room temperature strength of hot extruded aluminum which was applied to a Hall-Petch type equation. They measured the strength of the aluminum samples in the form of hardness and found that substructures produced by hot extrusion at high strain rates produced an increase in strength which was comparable to that produced by grain refinement in the submicron range. They attributed this increase in strength to the effect produced by the increase in dislocation density as the subgrain size decreases and by the subboundary misorientation.

Subgrains formed during hot working have been observed by Lequet et al[51] who found that the average size of the cells formed depend on the rolling temperature; the higher the working temperature, the larger the resulting subgrain size. Thornton, et al.[15] and Auld, et al[52] also found that a higher hot working temperature produced larger subgrains and a lower dislocation density. They studied this mechanism in relation to the decreasing tendency to recrystallize at a fixed annealing temperature. The morphology and density of precipitate particles in a matrix can also influence the recrystallization temperature of the material.[57]

Effect of Impurity Content and Precipitates on Recrystallization

An increase of the impurity content in metals results in an increase in stored energy with deformation and it also increases the recrystallization temperature of the alloy. The probability of dynamic recovery by cross slip decreases with increasing impurity content since impurities inhibit dislocation motion.[53]

The retardation of the recrystallization process has been related to the second phase inter-particle spacing by several authors.[54,55,56,57] They suggested that an inter-particle spacing less than one micron is the critical size for retardation of recrystallization.

Embury[58] has recognized that when large, (greater than 300Å in diameter) incoherent, rigid particles are present, localized dislocation tangles are formed in the area surrounding the particles. Glide dislocations interact with prismatic dislocation loops punched out from the particle producing a high degree of dislocation tangling.

A cell size is developed which is of comparable size with the interparticle spacing. This takes place by the increasing accumulation of the glide dislocations and linking of the dislocation tangles formed between particles. Embury also stated that the presence of particles was useful, not only to delineate the cell size, but also for stabilizing the cell structure during a subsequent thermally induced effect such as recovery.

The effect of second phase particles on the formation of recrystallization nuclei was investigated by Cahn[59] in 1956. He stated that recrystallization nuclei form preferentially at second phase matrix interfaces, on pre-existing grain boundary surfaces and the trihedral angles formed by adjacent grains. Mould and Cotterill[6] also studied the effect of second phase particles on the recrystallization kinetics of aluminum-iron alloys. They found that the interparticle spacing and the particle distribution and size were the determining factor on the recrystallization kinetics of the alloy. Mould and Cotterill found that $FeAl_3$ particles which had an interparticle spacing larger than four microns accelerated the isochronal and isothermal recrystallization of aluminum-iron alloys. They concluded that nucleation at particle-matrix interfaces becomes difficult when the interparticle spacing becomes of the order of twice the diameter of the subgrain structure of the cold worked matrix.

The retardation of primary recrystallization as a function of interparticle spacing was investigated by Preston and Grant[60] who found that a spacing smaller than one micron retards the recrystallization process. Other investigations[56,61] on this subject yielded similar

results. Brimhall, et al.[114] stated that interparticle spacings of the order of one micron decreases the misorientation between neighbor subgrains and precludes the formation and growth of recrystallization nuclei. Coarse precipitate particles, even if present in large numbers, can increase the rate of isothermal recrystallization and consequently lower the recrystallization temperature of the material.[7,80] Coarse particle-matrix interfaces serve as nucleation points for recrystallization and also as sinks for line and point defects during annealing.

Hornbogen[57] studied the precipitation of second phase particles during the recrystallization annealing of iron, nickel, copper and aluminum alloys. He found that in an aluminum alloy containing 0.042 weight percent iron which was deformed 95 percent and then annealed at 440 degrees centigrade for two minutes, the precipitation of small particles of $FeAl_3$ immobilized the grain boundaries by hindering the rearrangement of dislocations and therefore inhibited the movement of the recrystallization front. Hornbogen also stated that large, hard, incoherent particles serve as nucleation sites for recrystallization since nucleus formation is favored by a high localized degree of deformation in conjunction with an incoherent boundary surface.

The pinning of subgrain boundaries by precipitates was investigated by Humphreys and Martin,[62] who found that high angle boundaries lose their mobility due to the pinning effect provided by the precipitates. This was also postulated by Preston and Grant[60] and Gatti and Fullman.[63] The effect of impurities on grain boundary migration was investigated by Lucke and Detert.[64] They found that

at high concentrations, migrating grain boundaries are pinned by foreign atoms. However, they observed that at high temperatures and low particle concentrations, the boundary breaks away from the pinning particle and continues its motion. The effect of second phase particles can be also extended to the grain growth stage. Higgins[81] studied the effect of impurity inhibition during grain growth and found that a recrystallized grain size can be stabilized by a dispersion of second phase particles. He stated that secondary recrystallization would take place if either the second phase dispersion does not reduce the local driving force to zero or if resolution of the particles or coalescence takes place. He also found that any grains which are both larger than the average size and have a different orientation from the primary texture may develop preferentially during secondary recrystallization. According to Higgins, the presence of second phase particles inhibits grain growth in all but colonies of recrystallized grains that differ in size and orientation characteristics. These favored colonies will preferentially increase in size producing secondary recrystallization or abnormal grain growth.

Al-Fe-Co Compound

Several authors[65,66] have reported that aluminum, cobalt and iron do not form a ternary compound in equilibrium with the alpha phase in the aluminum rich end of the diagram. Mondolfo[67] confirmed that the compounds formed are of the type Co_2Al_9 and $FeAl_3$ (or $FeAl_6$ depending on the solidification rate).[68,69] According to Mondolfo, the iron can be soluble in the Co_2Al_9 compound up to 10.8 weight percent

while the $FeAl_3$ can take up to 12.4 weight percent cobalt in solution. This would indicate that under non-equilibrium conditions, the compounds formed would be $(Co,Fe)_2\ Al_9$ which has a Co_2Al_9 lattice with a small variation in lattice parameter plus $FeAl_3$ ($FeAl_6$) compounds. However, in the alloy used in this investigation, the $FeAl_3$ compound did not contain any cobalt in solution.(67)

Strengthening Mechanism Due to Precipitates Not Sheared by Dislocations

Orowan's original equation to determine the stress needed by a dislocation to break away from an obstacle is given by(77)

$$\tau = \frac{2\ To}{bL} \qquad (1)$$

where To = line tension of the dislocation, b = Burger's Vector and L = planar interparticle spacing. The basic bowing model used by Orowan is shown in Figure 2. In this model if $\varphi > 0$, the particle can be cut by the gliding dislocation and if $\varphi = 0$ the gliding dislocation cannot shear the particle and consequently Orowan strengthening takes place.

The planar interparticle spacing (L) was converted to the effective interparticle spacing by Foreman and Makin(78) with a value of 1.23 for a random array of particles. Also, the effective interparticle spacing (L) was corrected for the diameter of the particle replacing it with (L-2R) where R is the radius of the particle. A final equation for the Orowan mechanism is given by

$$\tau = \frac{0.8\ G\ b}{2\pi(1-\nu)} 1/2 \qquad \frac{\ln\ (2R/r_o)}{(L-2R)}$$

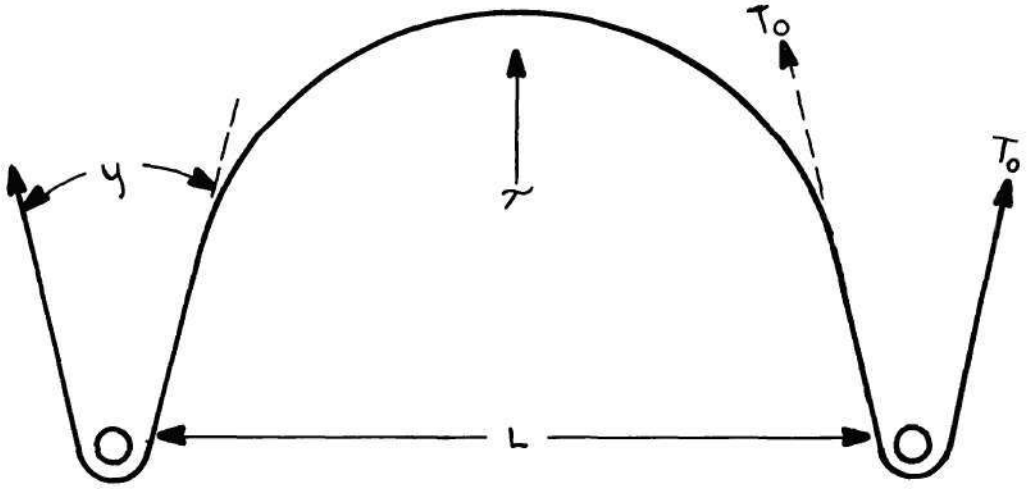

Figure 2. Orowan's Basic Bowing Model to Treat Particle Strengthening.

where G = shear modulus, b = Burger's Vector, ν = Poisson's Ratio and r_o = dislocation core radius.

The line tension (To) can be calculated using Ashby's relation[79]

$$To = \frac{G\,b^2}{4\,\pi\,(1-\nu)^{\frac{1}{2}}} \qquad \ln \frac{1.6\,R}{r_o}$$

CHAPTER III

EXPERIMENTAL PROCEDURES

Production Procedures

Aluminum ingots with the chemical composition shown in Table 1 were melted in a reverberatory furnace. The metal was heated to 1350°F prior to adding UCAR alloy #1[70] briquettes containing 41% cobalt-35% iron and 24% aluminum to make a 0.5 weight percent cobalt 0.5 weight percent iron alloy. The alloy briquette addition was made in the launder between the melter and holding furnaces during the transfer of the metal. The necessary amount of briquettes was placed in the trough, with a dam at the lower end to prevent the briquettes from being washed into the holding furnace without first being taken into solution with the aluminum. The metal was stirred after alloying in order to facilitate the homogenization of the alloy. After a 30 minute period, the alloy was sampled through two doors located on opposite sides of the furnace. The molten metal was then transferred to the pouring crucible and continuously cast. The metal temperature in the holding furnace was 1350°F $\pm$ 10°F which resulted in a crucible temperature of 1290°F $\pm$ 10°F. The temperatures at intermediate stages of processing are given in Figure 3.

A bar entry temperature of 1025 $\pm$ 25°F was used in all hot rolling operations.

Table 1. Chemical Composition of Aluminum Ingots

CHEMICAL COMPOSITION OF ALUMINUM INGOTS

(Weight Percent)

Fe	Si	Cu	Mn	Mg	Cr	Ni	Zn
0.15	0.04	0.001	0.003	0.008	0.001	0.001	0.02

Ti	V	Ga	B	Na	Al
0.001	0.005	0.006	0.001	0.001	Balance

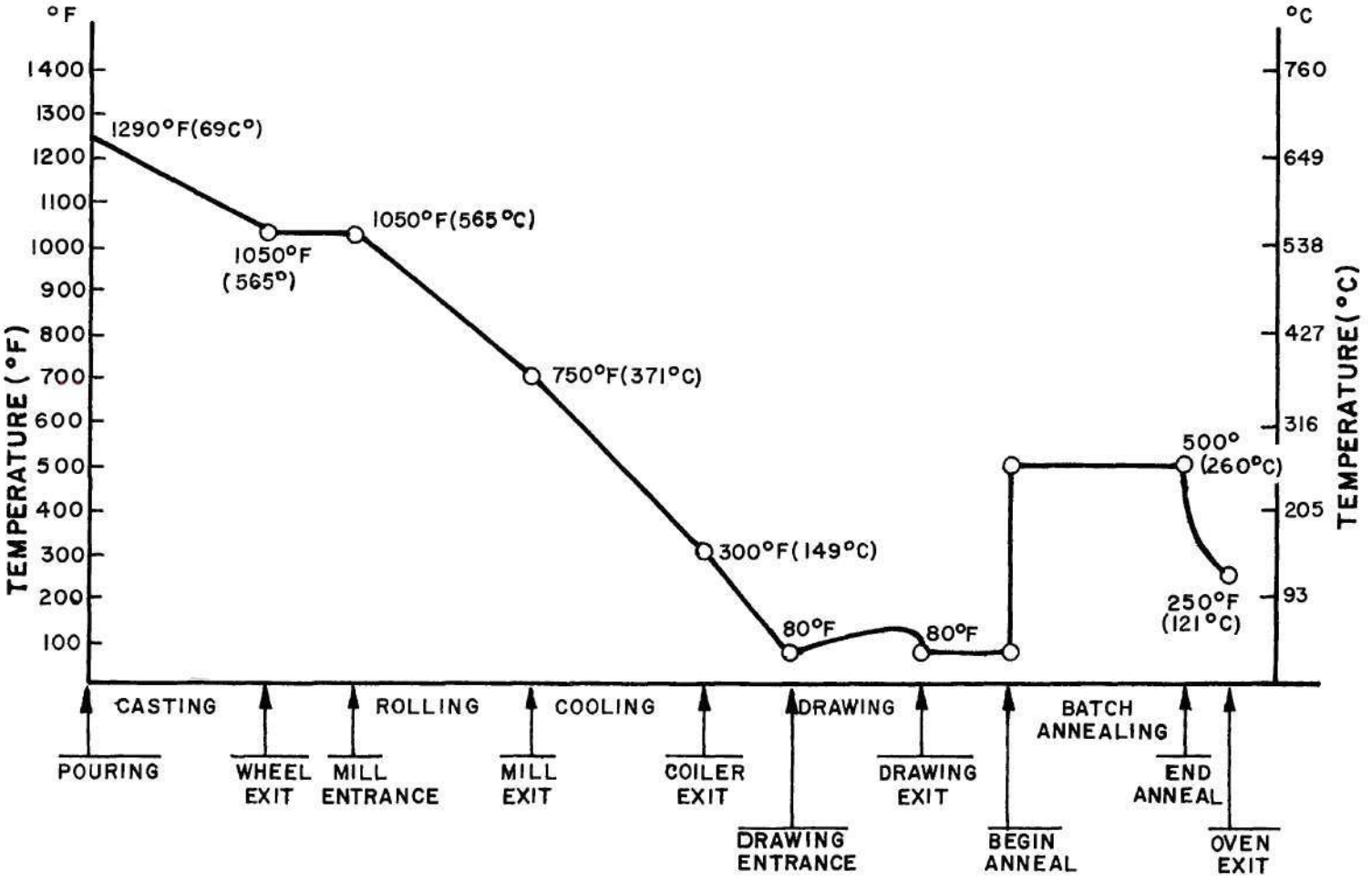

TEMPERATURE-PROCESS RELATIONS IN AL-FE-CO ALLOY

Figure 3. Temperature - Process Relations During Production.

Table 2 lists the speed of deformation of each reduction pass during hot rolling. This was based on a casting speed of 28 feet per minute.

To lubricate the material during hot rolling, Shell Oil Company's Type Dromus B soluble oil was used at a flow of 300 gallons per minute and a pressure of two atmospheres. The solution temperature was 130 $\pm$ 10^{o}F and its concentration was 10 to 20 percent by volume. The temperature of the rod exiting the rolling mill was 700 $\pm$ 50^{o}F. A cooling lubricant (Shell Dromus B and water) was used in the coiling pipe to cool the rod to a temperature of 300 $\pm$ 25^{o}F. This was done to prevent static recovery and recrystallization of the coiled rod. Figure 4 shows the schematic diagram of the production process for the Al-Fe-Co alloy rod.

The cross section of the cast bar was 8.24 square inch and it was reduced to a 0.375 inch diameter rod. (0.113 square inch) The reduction schedule is shown in Table 2. Macrographs of the etched cross sections of the hot rolled material are shown in Figure 5.

A Syncro C-13 drawing machine was used for cold drawing all production material. The 0.375 inch diameter rod entered the machine and was reduced to 0.105 inch diameter wire using the standard Brown & Sharpe reduction schedule. See Table 3.

The material was reduced a total of 92.2 percent using silicon carbide dies with an approach angle of 16 degrees. Dies and wire were lubricated during cold drawing with E.F. Houghton No. 4683 lubricant at room temperature. Cold drawing was performed at an exit speed of 4000 feet per minute.

Table 2. Rolling Speed Per Pass During Hot Deformation

Hot Rolling (pass no.)	Area (sq.inches)	Total Reduction of area (percent)	Speed of Each Roll (Feet/ Minute)
As-Cast	8.240	0	28
1	5.150	37.3	45
2	3.342	59.2	69
3	2.523	69.2	91
4	1.794	78.1	129
5	1.410	82.8	164
6	0.953	88.4	242
7	0.712	91.3	324
8	0.493	94.0	468
9	0.372	95.5	620
10	0.263	96.8	877
11	0.192	97.7	1202
12	0.148	98.2	1559
13	0.116	98.6	1989

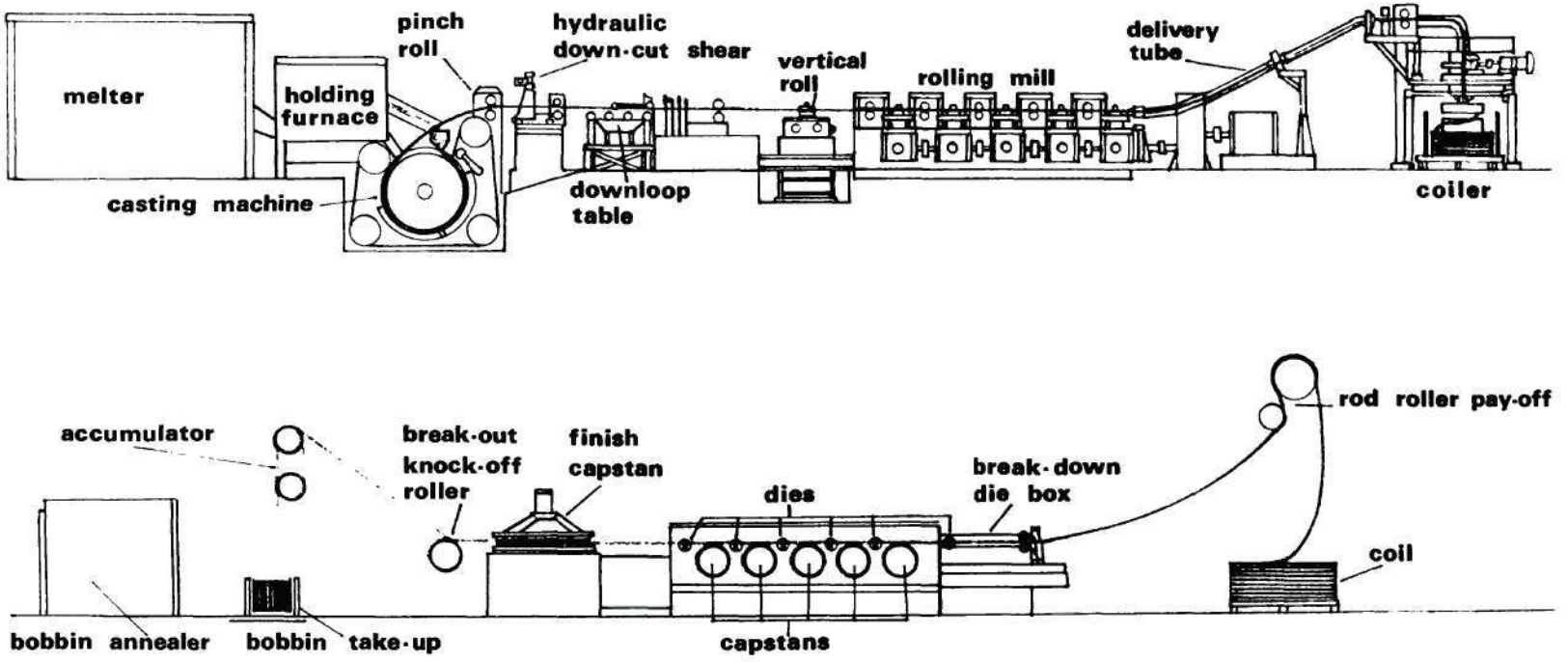

Figure 4. Schematic Diagram of Production Process of Al-Fe-Co Alloy.

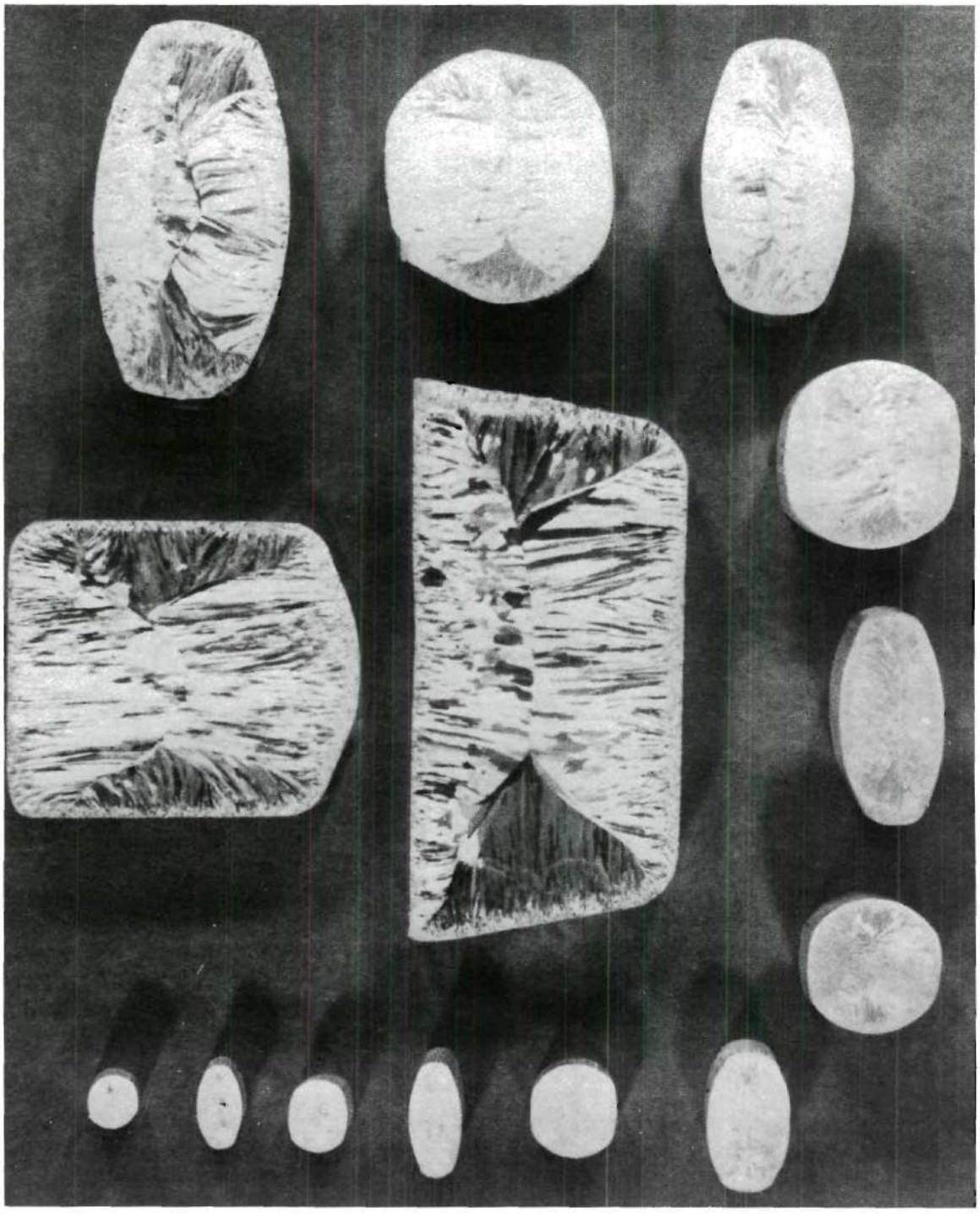

Figure 5. Macrograph of Hot Rolled Sections.

Table 3. Reduction in Cross Sectional Area During Cold Drawing

DIAMETER (Inches)	DIAMETER (mm)	REDUCTION OF AREA (percent per pass)
.365	9.27	20.67
.325	8.25	20.73
.289	7.35	20.44
.258	6.55	20.95
.229	5.83	20.70
.204	5.19	20.69
.182	4.62	20.70
.162	4.12	20.68
.144	3.67	20.69
.129	3.26	20.73
.114	2.91	20.69
.105	2.59	

Total Percentage of Reduction: 92.20

Annealing cycles were performed to determine the optimum annealing temperature and time for Al-Fe-Co and EC alloys. The criteria for this selection were based on the finished wire properties as required by the application. The cycles were performed in a Blue-M air circulating oven, Model POM-8000PRFX. An automatic temperature cycle cam with a temperature control of $\pm$ 1°F was used with the oven.

Preparation of Laboratory Specimens

Experimental laboratory cast bars were produced using a base metal with the chemical analyses as shown in Table 1. The base metal was melted in a 15 KW high frequency induction furnace, Lepel Model #T-15-3-KC-RP-SW equipped with a 5.3 inch diameter water cooled copper coil.

The base metal was placed in an aluminum oxide crucible, melted and heated to a temperature of 1350°F. The surface of the melt was skimmed in order to eliminate detrimental inclusions. Alloying was performed by adding the necessary amount of high-purity briquette hardener (41% cobalt, 35% iron, and 24% aluminum) to make an aluminum 0.5 weight percent cobalt, 0.5 weight percent iron alloy. The alloying briquettes were added to the molten aluminum at 1350°F and stirred to facilitate the dissolving of the iron and cobalt. After stirring, skimming and homogenizing at 1350°F for 30 minutes, a sample for spectrographic analyses was taken. The temperature of the melt was continuously recorded using a chromel alumel thermocouple.

The molten metal was then cast at 350°F into a low carbon steel mold which was initially at 72°F. The mold was 18 inches high and

contained a cavity 1.5 inch in diameter. The cast bar was kept in the mold until completely solidified. The bar was kept in the mold until completely solidified. The bar was extracted from the mold, its temperature recorded, and then immediately introduced into the rolling mill for hot rolling.

Experimental Method for the Effect of Solidification

The effect of the solidification rate on the properties of the Al-Fe-Co alloy was studied by casting the alloy using two different mold materials which would produce widely divergent cooling rates. A fast solidification rate was obtained by casting into a steel mold at room temperature, as explained above. The slow solidification rate was obtained by casting the alloy into a sand mold and containing the casting until the temperature was below 400°F. It was decided that for the purpose of this investigation these extreme rates would provide enough information to determine the effect of the solidification rate on the properties of the finished wire.

The cooling rate after casting was determined by measuring the temperature as a function of time using thermocouples at the middle and 0.75 inches from the surface of the bar, placed 9 inches from the bottom of the mold.

Typical cooling curves are given in Figure 6. The average cooling rates from 1222°F to 600°F were 311°F and 28°F per minute for the fast solidification and slow solidification samples, respectively. The cooling periods from 1222°F to 600°F were two minutes for the fast solidification and 22.3 minutes for the slow solidification.

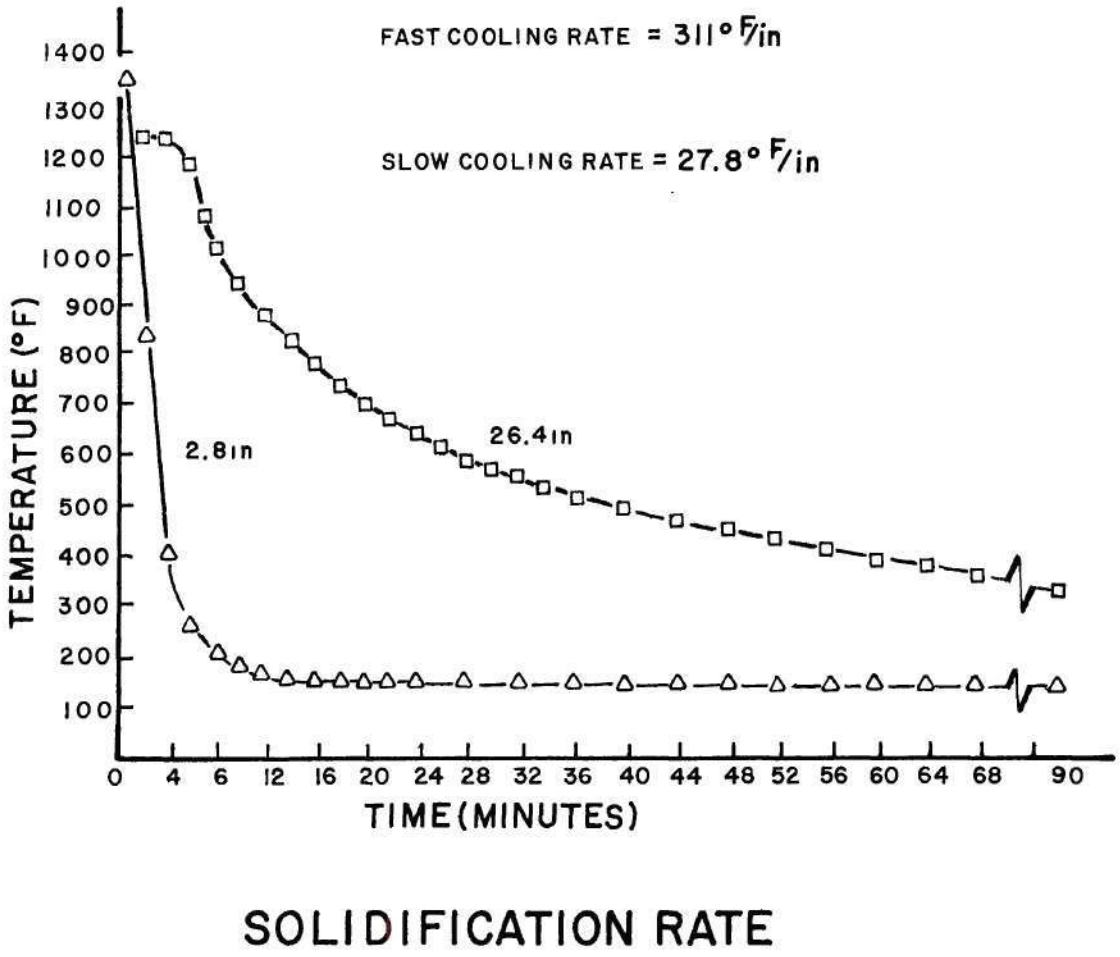

Figure 6. Plot of Temperature vs. Time (Solidification).

Hot Rolling of Lab-Cast Bars

The cast bars were introduced into the rolling mill at 1050°F and hot rolled to a 0.375 inch diameter rod. The number and amount of reductions used were the same for all the experiments throughout the entire investigation. The speed of the exiting rod produced from the laboratory cast bars was 610 feet per minute, and the lubricating soluble oil, Shell Oil Type Dromus B, was kept at 140°F and at a flow rate of 300 gallons per minute. The rod was cooled to room temperature immediately after exiting the rolling mill to avoid static recrystallization.

Cold Drawing and Annealing

The rod as-rolled was cold drawn in a laboratory model, single die drawing machine. The rod was successively reduced from 0.375 inch diameter to 0.105 inch diameter using standard Brown and Sharpe reductions as shown in Table 3. The dies and wire were lubricated during cold drawing using E. F. Houghton No. 4683 lubricant at room temperature. Drawing was performed at a speed of 72 feet per minute. The cold draw wires were annealed in a Blue-M air circulating oven, Model POM-800 PRFX. This oven is equipped with an automatic temperature cycle cam with a temperature control of $\pm$ 1°F.

Metallographic Examination

Optical Microscopy: The specimens to be examined microscopically were mounted in Bakelite and mechanically ground using 600 grit silicon carbide grinding paper. The samples were cleaned in an ultrasonic water bath to remove all the coarse particles. They were then

polished employing 6 micron size diamond paste. Final mechanical polishing was accomplished with a 1 micron size cerium oxide suspension (Miromet compound by Buehler) on a silk polishing cloth. To eliminate fine surface scratches, a 0.5 second electropolishing treatment was finally performed using a potential of 40 volts.

The specimens were etched either in 0.5 percent by volume hydrofluoric acid in water or electroetched 1 minute in a 4 percent by volume solution of fluoroboric acid in water using a potential of 20 volts. The specimens were rinsed in distilled water, ethyl alcohol, and dried. Optical microscopy was performed utilizing a Research II Bausch and Lomb Metallograph equipped with polarized light and a tiltable sensitive tint device.

Electron Microscopy: The specimens for transmission electron microscopic examination were cut in a Buehler Isomet low speed saw, model 11-1180 to a 0.025 inch thickness and punched to a 0.120 inch diameter. The wafers were mechanically polished to approximately 0.015 inches using 600 grit silicon carbide paper. The dimpling process was performed using a jet polishing apparatus as described elsewhere.[71] The specimen was placed at 0.5-1.5 cm from the orifice, depending on the temper of the sample, and a solution of 75 percent methanol, 25 percent nitric acid (by volume) was jetted to the center of the water which was made the anode. A voltage of 180 volts and a current of 50-100 MA were used for 30-90 seconds on each side of the specimen. This reduced the center of the specimen to a thickness of approximately 0.002 inches.

Once the sample was dimpled to the desired center thickness, final polishing was accomplished by submerging the specimen in a 75 percent methanol - 25 percent by volume nitric acid solution at -28 $\pm$ 2°C. Polishing was performed at 18 volts until a small hole appeared.[71] A stereo microscope adjacent to the polishing was used to allow visual inspection of the polishing surface and to aid in stopping the process at the appearance of a hole. The polished specimen was rinsed in methanol and dried for examination. Transmission electron microscopy was performed in a Siemens Elmiskop IA electron microscope equipped with a metallurgical stage, using an accelerating voltage of 125 KV.

Subgrain Size Determination

The average subgrain size of the studied specimens was determined using a radial line intersect method.[72] The number of boundaries crossed by each radial line is counted every 10 degrees and added for the total length of the radii. By dividing the total number of subgrains crossed by the total radial length and correcting for the magnification, the average subgrain size was obtained.

Interparticle Spacing Determination

The interparticle spacing was obtained using the grid intercept method. A rectangular grid with horizontal and vertical intercept lines is placed over the transmission electron micrographs. The number of intercepts of precipitates with the lines in the horizontal and vertical positions is counted. Calculation of the interparticle spacing is obtained by using the total number of intercepts and the magnification of the micrograph.

The acceptance criteria used was that

$$N = N_H + N_v \geq 20$$

where N_H = number of particles in the horizontal grid and N_v = number of particles in the vertical grid.

Method and Equipment Used in the Determination Of Desired Properties

Determination of the actual service performance of an electrical conductor is not feasible in most cases. It is for this reason that performance criteria have to be formed based on the results of several mechanical tests performed on the conductor. Ultimate tensile strength, yield tensile strength, percentage of elongation, and electrical conductivity are among the most significant tests performed on electrical conductors.

The ultimate tensile strength and yield strength were determined according to American Society for Testing and Materials specification E-8[73] using an Instron Universal Testing Instrument Model T.T.C. The specimens were deformed at a rate of 0.02 $minute^{-1}$ using a sample gauge length of 10 inches and an extensometer gauge lengths of 2.0 inches. The yield strength of conductors used for residential wiring is of importance since a minimum value is required in order to prevent pull down of the cable during installation. The yield strength was determined by the 0.2 percent offset using a Young's modulus of 10.0×10^6 PSI.[74]

The percentage of elongation indicates the degree of ductility of the conductor which is required in order to withstand the bending and

flexing during installation. This property has been determined by Underwriters' Laboratories to be of extreme importance for a successful termination in aluminum wire. UL has traced several failures of the terminations to low elongation materials which do not adjust during the screw tightening operation. The percentage of elongation during tension was measured in a gauge length of 10 inches using ASTM specification E-8.[73]

The importance of electrical conductivity cannot be overemphasized, a maximum being desired for economic reasons. Minimum electrical conductivity will be 61 percent of IACS based on the ASTM specification of electrical conductivity for aluminum conductors B-262-69.[75] The measurement of the electrical conductivity was performed in accordance with ASTM specification B-193-65[76] using a Precision Kelvin Bridge (Leeds and Northrup Model 4300 adjustable standard low resistance and a 4320 Kelvin Bridge Ratio Box).

CHAPTER IV

RESULTS AND DISCUSSION OF RESULTS

Theoretical Analysis of Strengthening Mechanism

To evaluate the effect of the subgrains and precipitates on the strength properties of the Al-Fe-Co alloy, isothermally annealed samples were used to determine the subgrain size and yield strength.[80,81] Table 4 contains the data obtained for use in this analysis. Figure 7 and 8 are the Hall-Petch plots of the obtained data for Al-Fe-Co alloy wire. The data were analyzed according to the following expressions;

$$\sigma = \sigma_o + k\, d^{-1/2} \quad \text{(Hall-Petch Relation)} \quad (1)$$

and

$$\sigma = \sigma_o + k\, d^{-1} \quad \text{(Langford-Cohen Model)} \quad (2)$$

The resulting least squares fit gave the following parameters:

(1) Hall-Petch

$$\sigma_o = 8.05 \frac{kg}{mm^2} = 11.4 \text{ KSI}^* \quad k = 4.19 \frac{kg}{mm^2}\, \mu^{1/2} = 0.13 \frac{kg}{mm^{3/2}},$$

The root mean squared deviation in is 0.372.

(2) Langford and Cohen

$$\sigma_o = 10.4 \frac{kg}{mm^2} = 14.8 \text{ KSI} \quad k = 1.88 \frac{kg}{mm^2}\, \mu = 1.88 \times 10^{-3} \frac{kg}{mm}$$

The root mean squared deviation in μ is 0.362 where the root mean

*Since this chapter contains data from the literature, the metric and English systems are used.

Table 4. Variation of Yield Strength and Subgrain Size During Isothermal Annealing of the 0.5 Percent Cobalt 0.5 Percent Iron Aluminum Alloy.

TIME (Minutes)	Yield Strength (kg/mm^2)	KSI	Average Subgrain Diameter $\bar{d}$ (Microns)
0	19.5	27.7	0.46
10	13.6	19.3	0.63
20	13.8	19.6	0.62
40	13.2	18.7	0.75
50	13.2	18.7	0.73
60	13.0	18.5	0.63
120	12.7	18.0	1.04
180	12.4	17.6	0.76
240	12.4	17.6	0.72
300	12.3	17.5	0.94
360	12.1	17.2	0.98
420	12.2	17.3	0.93

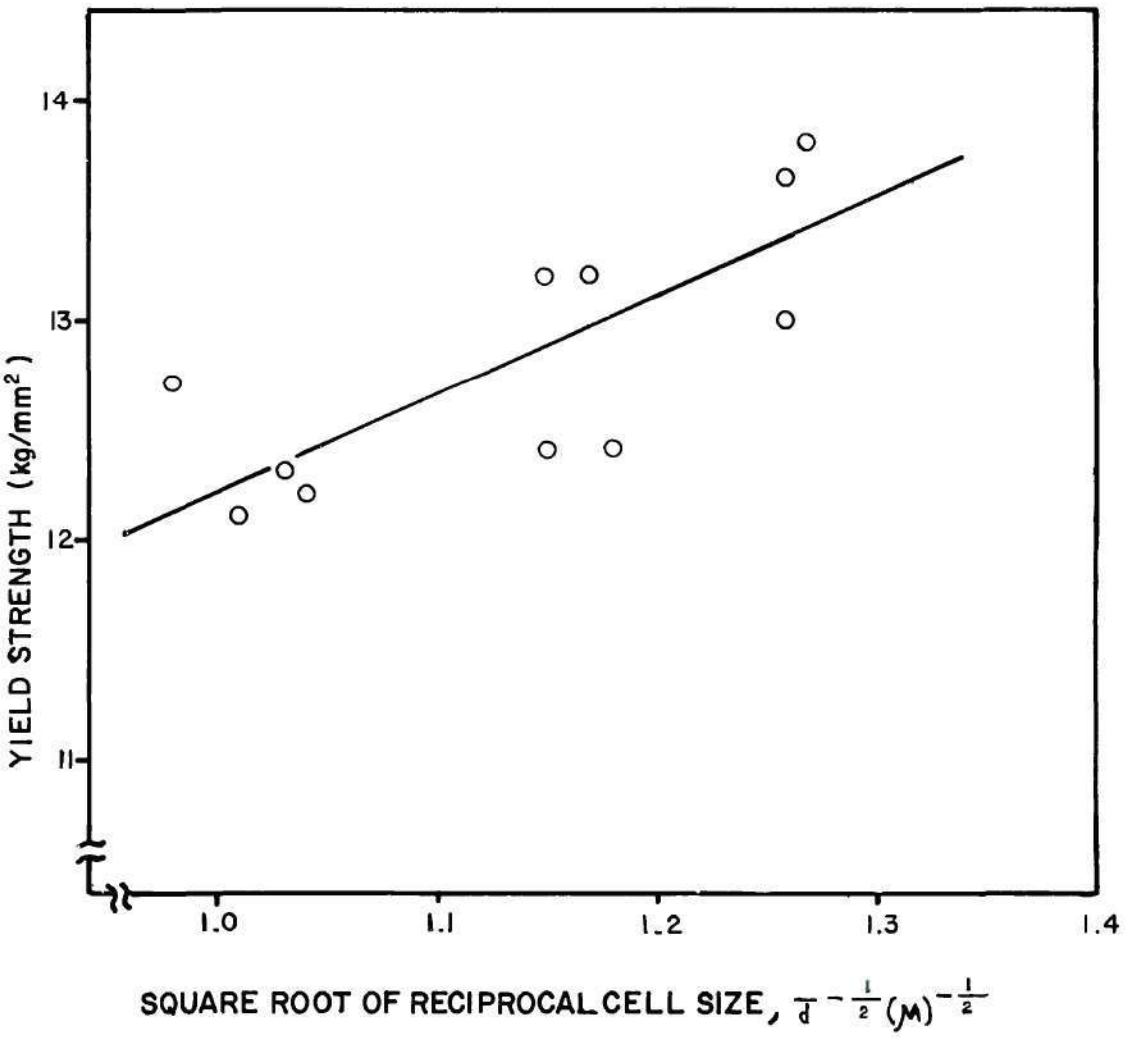

Figure 7. Hall-Petch Plot of the Data Obtained for Al-Fe-Co Alloy Wire.

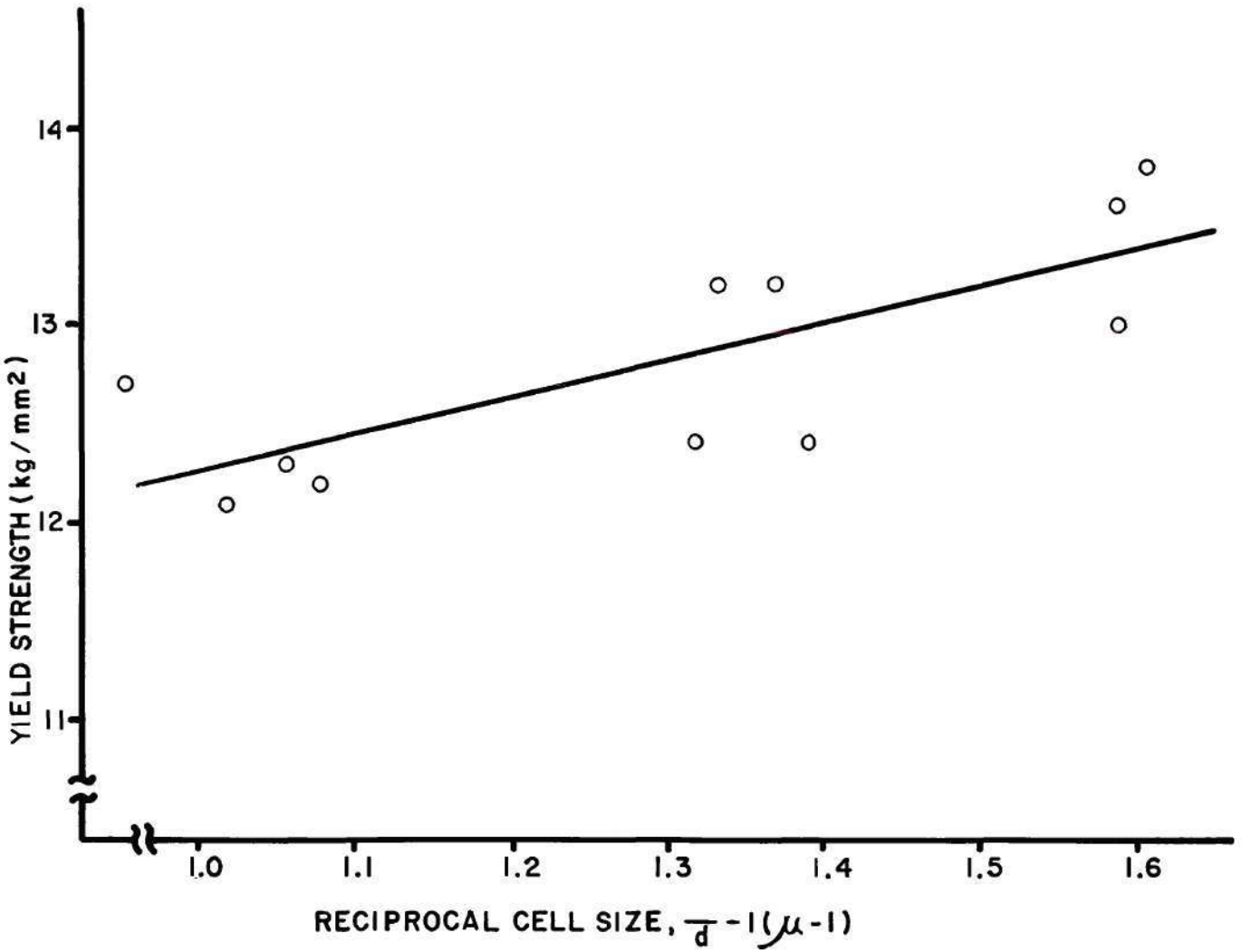

Figure 8. Langford-Cohen Plot of the Data Obtained for Al-Fe-Co Alloy Wire.

deviation is defined as: $$\sqrt{\frac{\sum_{i=1}^{N} (\sigma^i \text{ calc} - \sigma^i \text{ data})^2}{N}}$$

and σ^i calc. is the ith measured value of σ and N is the number of data points in the fit. Thus the smaller the value of root mean squared deviation better described by a Langford-Cohen expression than a Hall-Petch expression. However, this difference does not seem to be significant and one could quote the Hall-Petch results since this is the relation that has traditionally been used to describe aluminum data. The obtained results can be compared to the results of McElroy and Szkopiak[82] compiled from experiments on a wide range of aluminum alloys. These results are presented in Table 5.

From data we see that subgrain hardening for Al-Fe-Co alloy with our treatment shows only approximately one-half the subgrain hardening (k) of the other alloys in the table. For the Al-Fe-Co alloy, $k = 0.13$ and for the others $0.21 < k < 0.35$. This may be due to a more uniform distribution of subgrain sizes in Al-Fe-Co alloy whereas for others with less impurity content the strength is determined by the larger cell sizes rather than the average cell size.

The value of σ_o (8.05 kg/mm^2 11.4 KSI) obtained in this study is larger than that usually observed for pure aluminum. Consequently the strengthening is possibly due to a combination of subgrain and precipitate dispersion effects.

The parameters for Al-Fe-Co alloy obviously are well outside the range given in McElroy and Szkopiak for pure aluminum and actually compare best with the corresponding parameters for dispersion strengthened

Table 5. Frictional Stress and Subgrain Hardening Coefficient for Various Materials

MATERIAL & METHOD	σ_o (kg/mm^2)	k(kg/mm$^{3/2}$)
0.5 wt. percent Co-0.5 wt. percent Fe followed by annealing (1) (Present Study)	8.05	0.13
99.995% Al - hot and cold working followed by annealing (*)	-0.2	0.25
99.998% Al - hot and cold working followed by annealing (*)	-3.0	0.29
99.86% Al - hot working followed by rapid cooling to suppress recrystallization (*)	1.6	0.35
99.7% Al - hot working followed by rapid cooling to suppress recrystallization (*)	-1.3	0.29
99.5% Al - hot and cold working followed by annealing (*)	0.7	0.23
99.5% Al + 1.0% Al_2O_3 hot and cold working followed by annealing (*)	1.9	0.25
99.9% Al + 4.7% Al_2O_3 (*)	9.0	0.21

(*) Values obtained by McElroy and Szkopiak.

is possibly due to a combination of subgrain and precipitate dispersion effects.

The parameters for Al-Fe-Co alloy obviously are well outside the range given in McElroy and Szkopiak for pure aluminum and actually compare best with the corresponding parameters for dispersion strengthened aluminum (99.9% Al with 4.7% Al_2O_3 dispersion) which are:

$$\sigma_o = 9.0 \text{ kg/mm}^2$$

$$k = 0.21 \text{ kg/mm}$$

The strengthening effect appears to be due primarily to precipitated particles interacting with dislocations as in the case of dispersion strengthened aluminum.

Since the precipitates are hard intermetallic particles, incoherent with the matrix, one can assume that the Orowan Mechanism operates. The Orowan Mechanism can be described by[77]

$$\tau = 0.8 \frac{2 T_o}{b D} \qquad (3)$$

where τ = increase in flow stress due to interaction of gliding dislocations with dispersed particles for a single crystal, T_o = line tension of the dislocation in its position for the Orowan Mechanism, b = Burger's Vector = 2.86 $\mathring{A}$, D = measured interparticle spacing = $1.92 \pm 0.61\mu$. The interparticle spacing (D) was obtained using the line grid-intersection method on transmission electron micrographs from specimens annealed one hour at 425, 450, 275, 500, 575, 600, 650, 700, 750 and 800°F. Figure 9 is a plot of the obtained values for the interparticle spacings as a function of the annealing temperature.

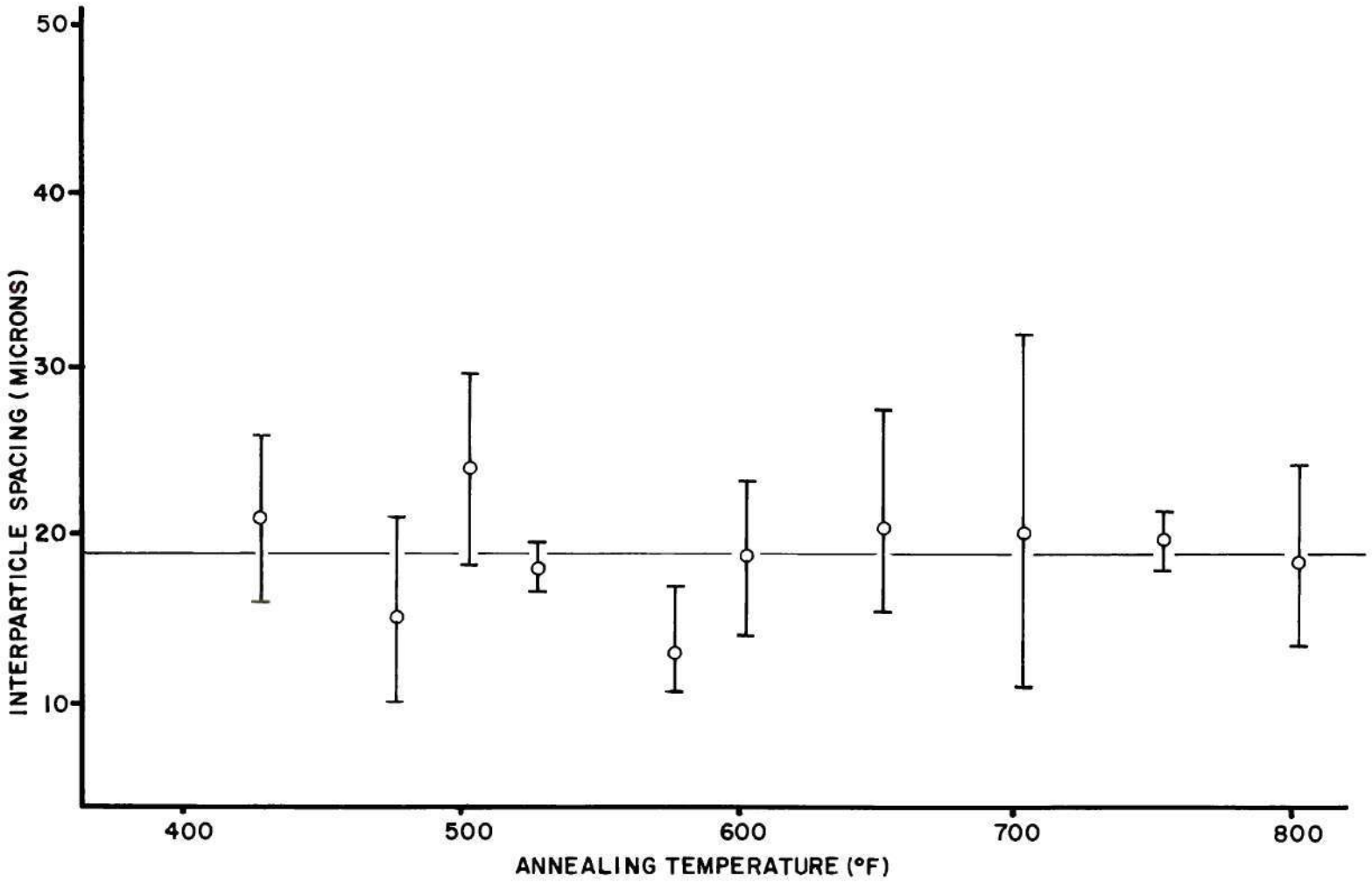

Figure 9. Variation in Measured Values of the Average Interparticle Spacing with Temperature.

The line tension (T_o) is determined by the following expression:

$$T_o = \frac{E\, b^2}{4\pi\ (1-\nu)^{1/2}} \quad \ln \frac{1.6}{r_o}$$

where E = Young's Modulus = 10^7 psi, ν = Poisson's Ratio = 0.33[8], R = average particle radius = 500 $\mathring{A}$, r_o = inner cut-off radius of the dislocation~b. Using these values the following are calculated:

$$T_o = 7.0 \times 10^{-10} \text{ pounds}$$

and

$$\Delta\sigma = 1.3 \times 10^3 \text{ psi} = 0.92 \text{ kg/mm}^2$$

This $\Delta\sigma$ is the value of a single crystal; for a polycrystalline material, this should be multiplied by the Taylor factor 2.89[86,87] which yields

$$\Delta\sigma = 3.76 \times 10^3 \text{ psi} = 2.65 \text{ kg/mm}^2$$

In order to compare the theoretical results with experimental values, wire specimens 0.105 inch in diameter, processed identically were annealed at 900°F for one hour and slowly cooled to room temperature after cold drawing using the same dies in order to obtain a structure basically free of subgrains. Figure 10 and 11 are the resulting photomicrographs of the Al-Fe-Co alloy and EC aluminum respectively after the thermal treatment showing absence of subgrains.

The experimentally obtained values of the proof stress of the Al-Fe-Co alloy and EC aluminum annealed at 900°F are 7.8×10^3 psi (5.5 Kg/mm^2) and 3.6×10^3 psi (2.5 kg/mm^2) respectively. The increase

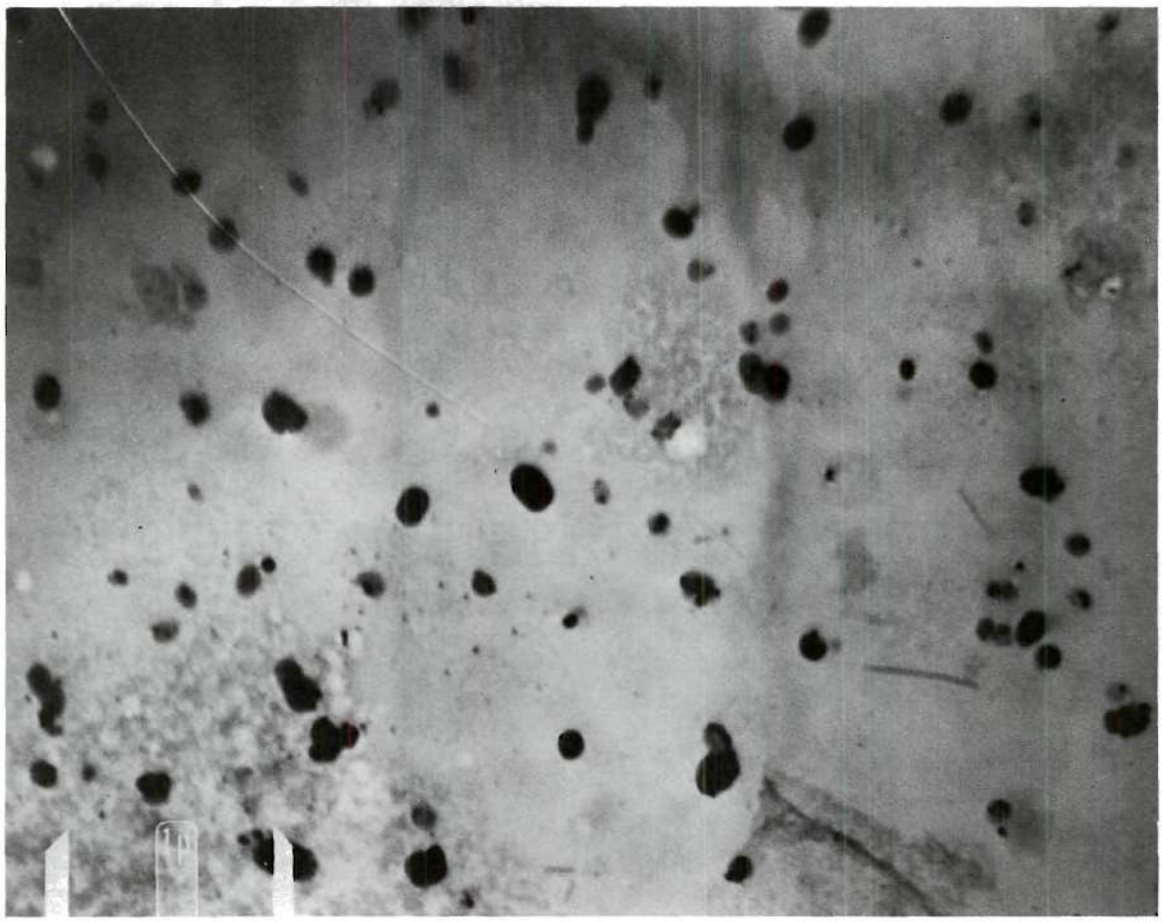

Figure 10. TEM of the Al-Fe-Co Alloy Wire Annealed at 900°F for One Hour and Slowly Cooled to Room Temperature After Cold Drawing. The Structure Shows Complete Absence of Subgrains.

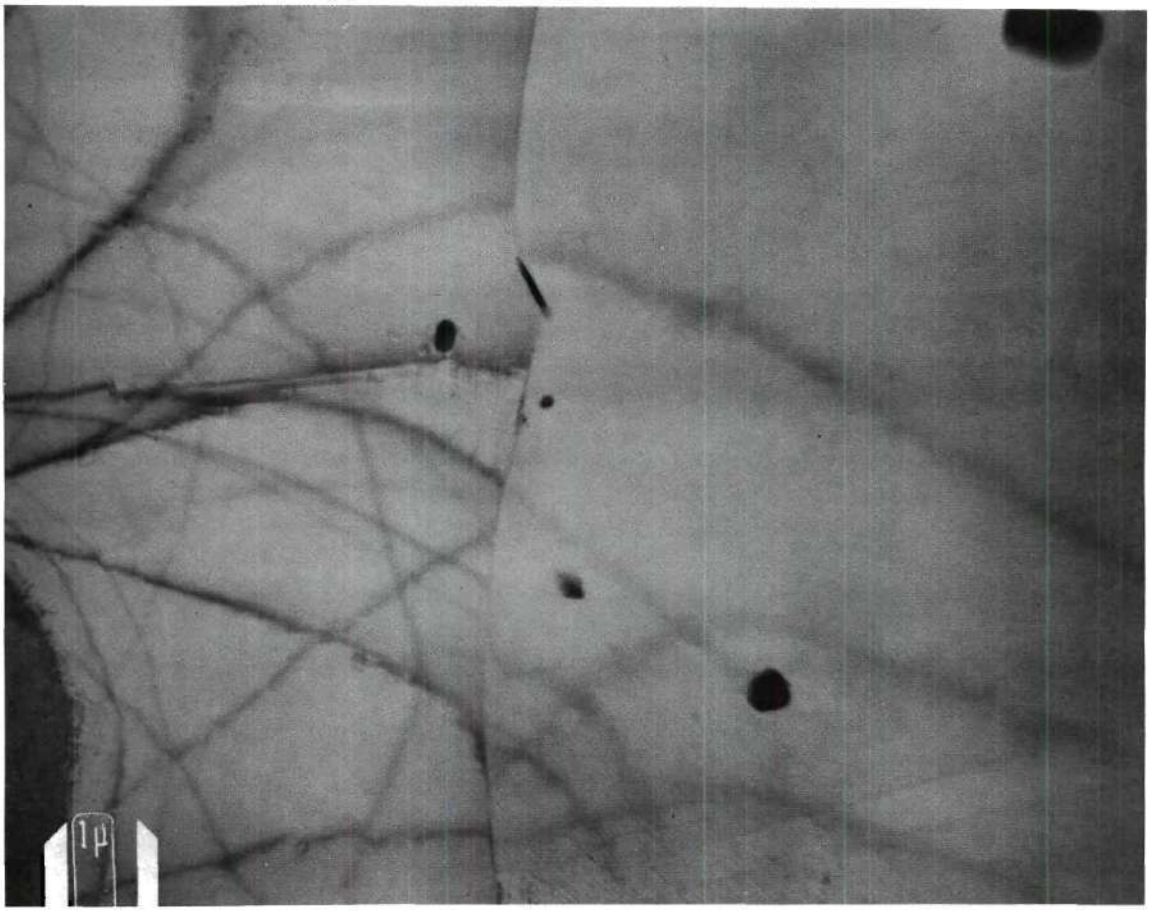

Figure 11. TEM of the EC Aluminum Wire Annealed at 900°F for One Hour after Cold Drawing Showing Absence of Subgrains.

in proof stress due to the presence of precipitates $\Delta\sigma$, is 4.2×10^3 psi. (3.0 kg/mm^2) This compares very favorably with the theoretical value obtained from equation (3), 3.76×10^3 psi (2.65 kg/mm^2).

It could be then ascertained that the Al-Fe-Co alloy obeys the Orowan mechanism in a matrix absent of subgrains; that is the particles are by-passed and not sheared. In a matrix containing subgrains such as those annealed below 800°F, the strength is determined by a combination of subgrain and precipitate effects. The complications of these duplex strengthening mechanisms probably prevents any direct comparison with either the Hall-Petch or the Langford-Cohen expressions.

In order to determine if the size dependence of the line tension determining the Orowan mechanism correlates with published results, a plot of the normalized increase in proof stress $0.8\left[\frac{2T_o}{G\,b^2}\right]$ versus the average particle radius (R) is shown in Figure 12 incorporating results of previous investigators as reported by Starke, et al.[88] As can be seen, the normalized $\Delta\sigma$ obtained by 0.87 for an average radius R = 500 Å which falls close to the line and normal within the values obtained by Ebeling and Ashby for Cu-Al_2O_3 dispersion.[89]

$$\frac{\Delta\sigma\, R}{Gb}\sqrt{\frac{2}{f}} = 0.8\left[\frac{2\ T_o}{G\ b^2}\right]$$

$$\frac{\Delta\sigma\ R}{G\ b}\sqrt{\frac{2}{f}} = 0.87$$

It could be stated that the strengthening of the Al-Fe-Co alloy is produced by a combination of subgrain strengthening and precipitate dispersion hardening. With small subgrains present, both mechanisms operate. However, in the absence of subgrains, such as after high

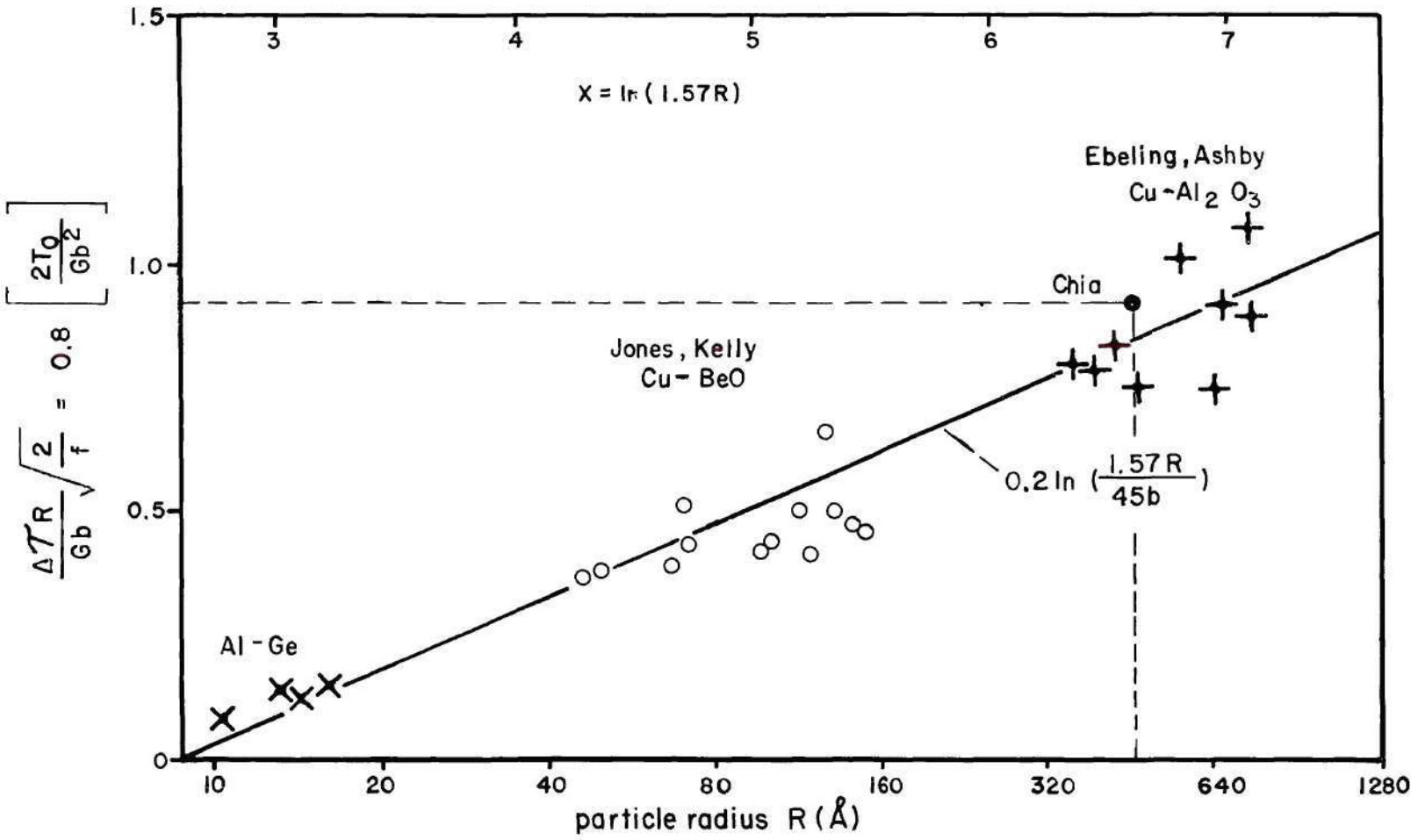

Figure 12. Normalized Increase in Critical Shear Stress, $\Delta\tau$ as a Function of Particle as Reported by Several Authors. The Noralized 0.8 $[2T_o/Gb^2]$ value obtained in this Investigation is Superimposed in this Graph.

temperature anneals, the operating strengthening mechanism becomes Orowan hardening.

Effect of the Speed of Solidification on the Substructure and Resulting Properties

Microstructures

The rapidly solidified cast bar shows well developed pure aluminum dendrites with a network of interdendritic eutectic (Figure 13(a). The eutectic consist of an aluminum matrix and Al-Fe-Co compounds. The compounds were identified by X-ray diffraction as $(Fe,Co)_2Al_9$ and $FeAl_6$. In the rapidly solidified specimen, the eutectic compounds are broken up and distributed throughout the aluminum matrix during hot deformation and cold drawing, which also results in a reduction of the interparticle spacing. The final spacing is proportional to the initial cast interdendritic spacing. (See Table 6) The precipitates act as barriers to the dislocation motion inhibiting subgrain growth and limiting the cell size of the finished wire.

The fine eutectic network of the rapid solidified bar (Figure 13(a) can be compared to the as-cast structure of the slowly solidified bar (Figure 13(b). The latter structure shows patches or colonies of eutectic compound distributed in a matrix of primary aluminum. The absence of a uniform eutectic network in the as-cast structure can be observed also in the finished wire structure as shown in Figure 15B and 16B. The fine eutectic networks formed during rapidly solidification Figure 13(a)can be traced through the hot-rolled rod (Figure 14A(a) and 14B(b) to the finished wire product (Figures 15(a) and 16(a)).

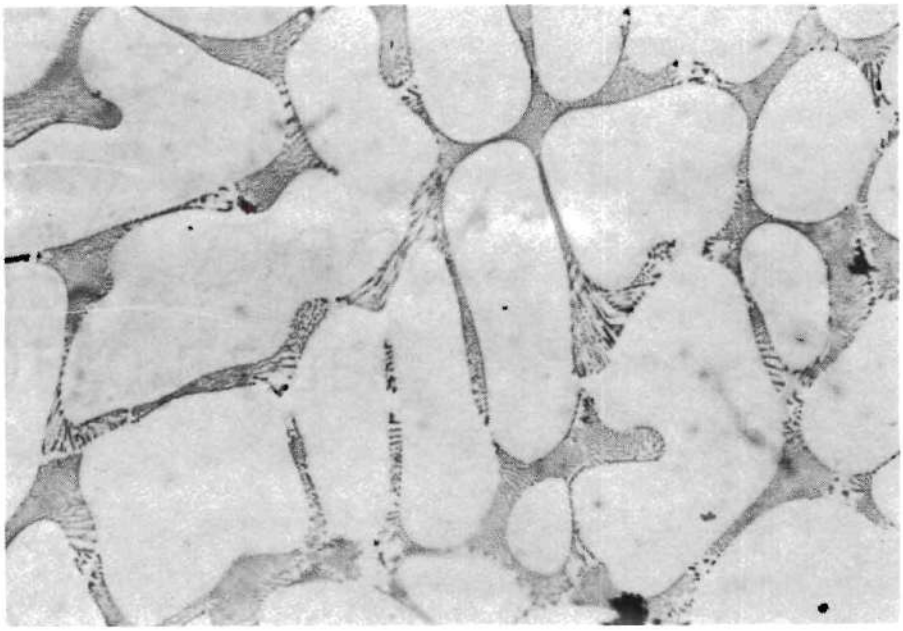

(a)

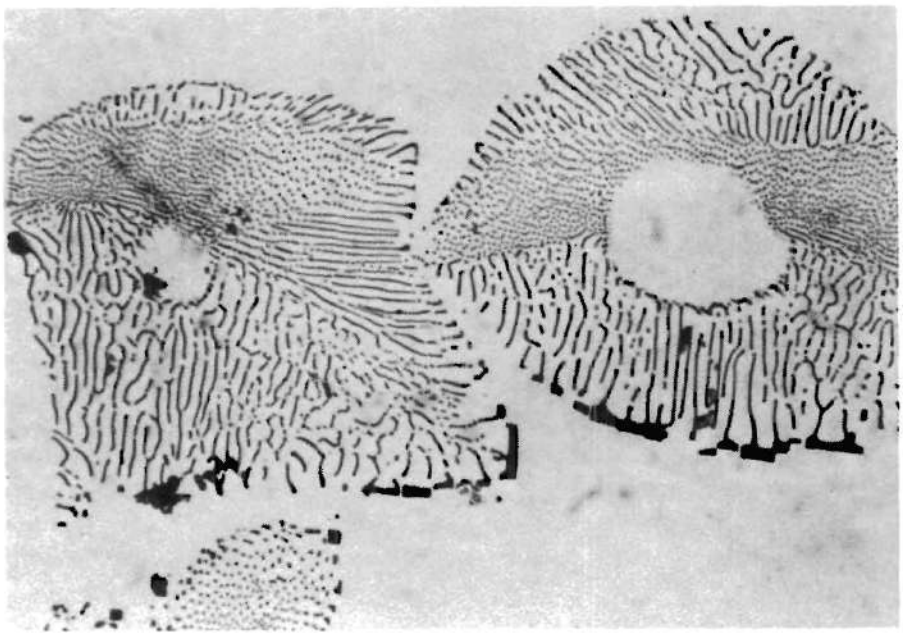

(b)

Figure 13. Grain Structure of Al-Fe-Co Cast Bars
(a) Rapidly Solidified and
(b) Slowly Solidified Showing the Dendrite Arm Spacing. 800X

Table 6. Solidification Parameters of Casting

Specimen	Ingot Dendrite Arm Spacing (Microns)	Inter-Precipitate Spacings Microns	Spacing Reduction Factor due to Deformation
As-Cast Rapidly Solidified	20	--	--
As-Cast Slowly Solidified	210	--	--
Rolled Rod from Rapidly Solidified Bar	--	2.5	8
Rolled Rod from Slowly Solidified Bar	--	40	5
Finished Wire from Rapidly Solidified Bar	--	0.8	25
Finished Wire from Slowly Solidified Bar	--	10.	21

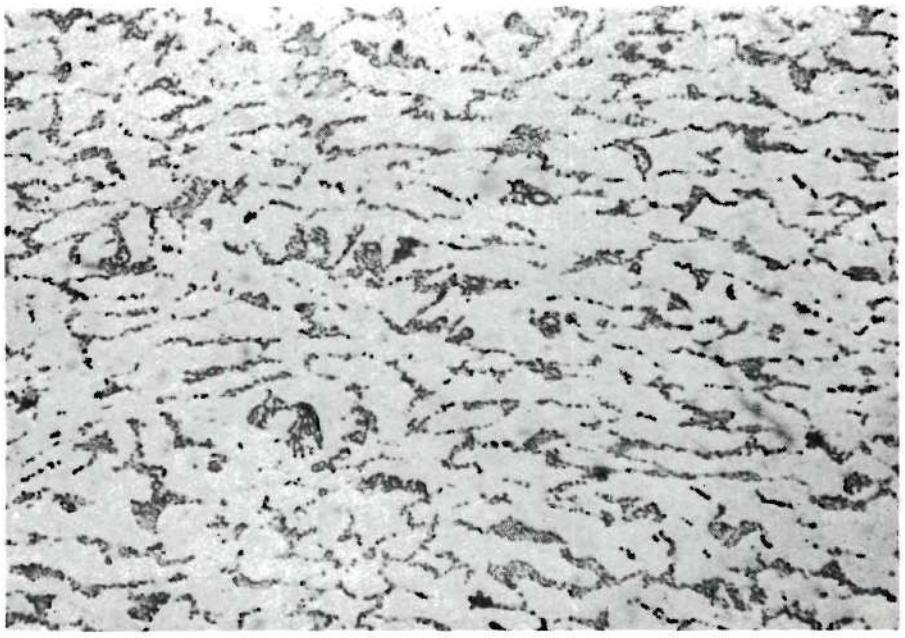

(a)

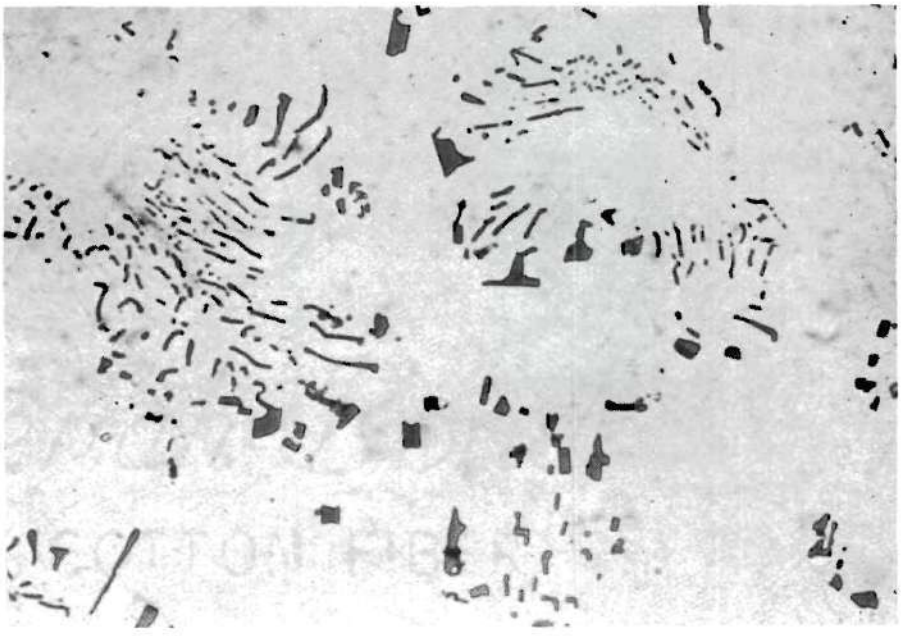

(b)

Figure 14A. Optical Photomicrograph of (a) Rapidly Solidified Sample and (b) the Slow Solidified Sample Taken in the Transverse Direction of the 0.375 Inch Hot-Rolled Rods of Al-Fe-Co Alloy. 800X

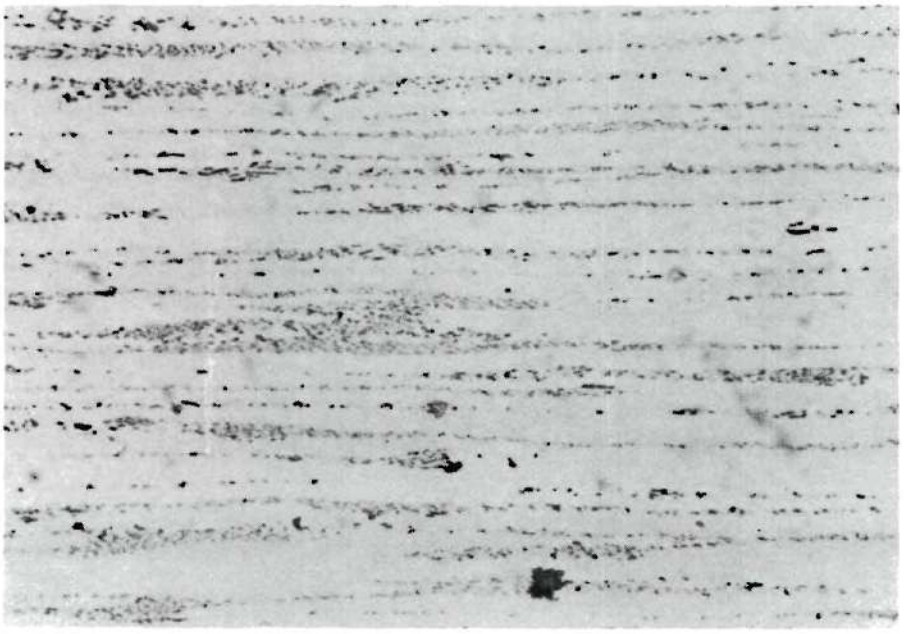

(a)

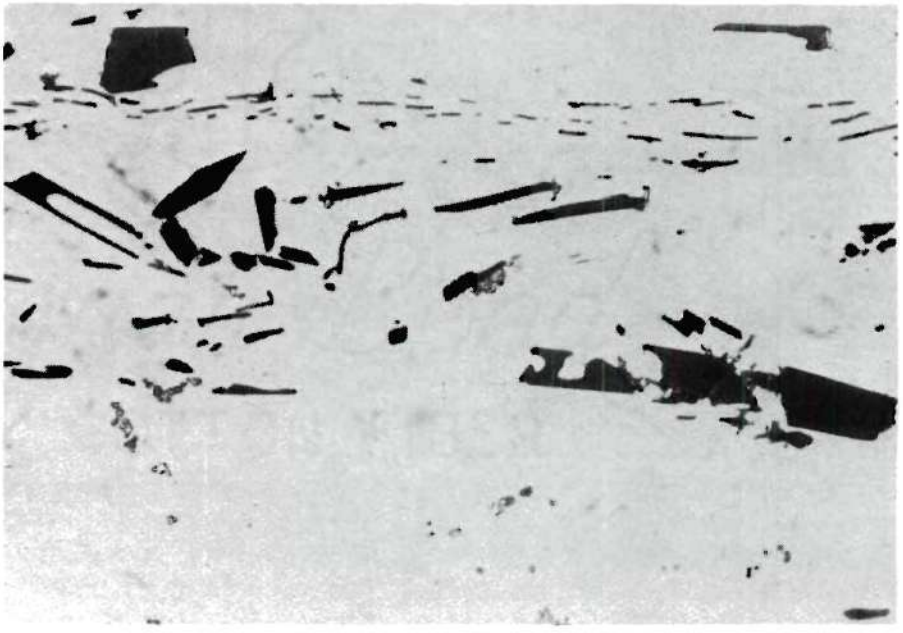

(b)

Figure 14B. Optical Photomicrographs of (a) Rapidly Solidified Sample and (b) a Slowly Solidified Sample Taken in the Longitudinal Direction of the 0.375 Inch Hot Rolled Rods of Al-Fe-Co Alloy. 800X.

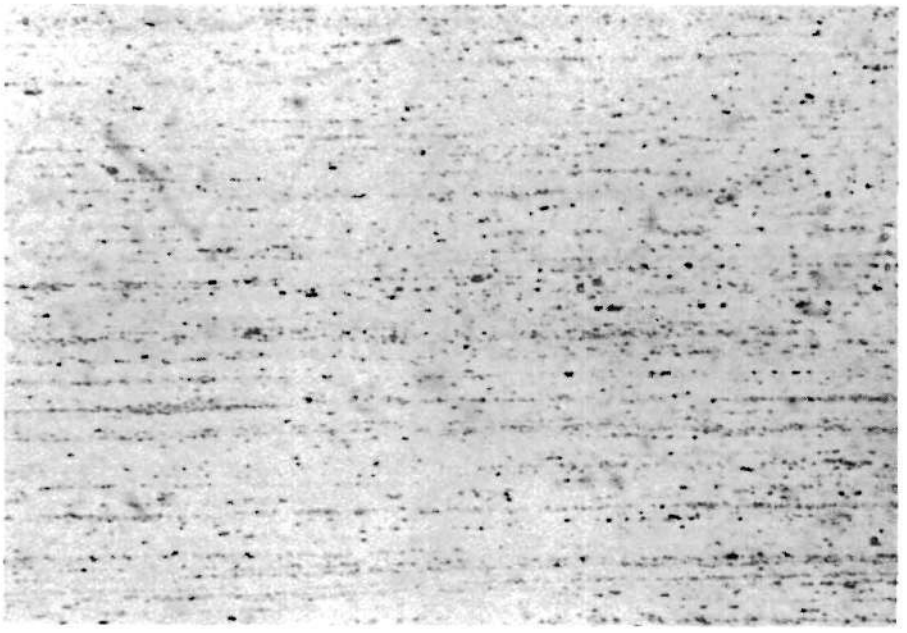

(a)

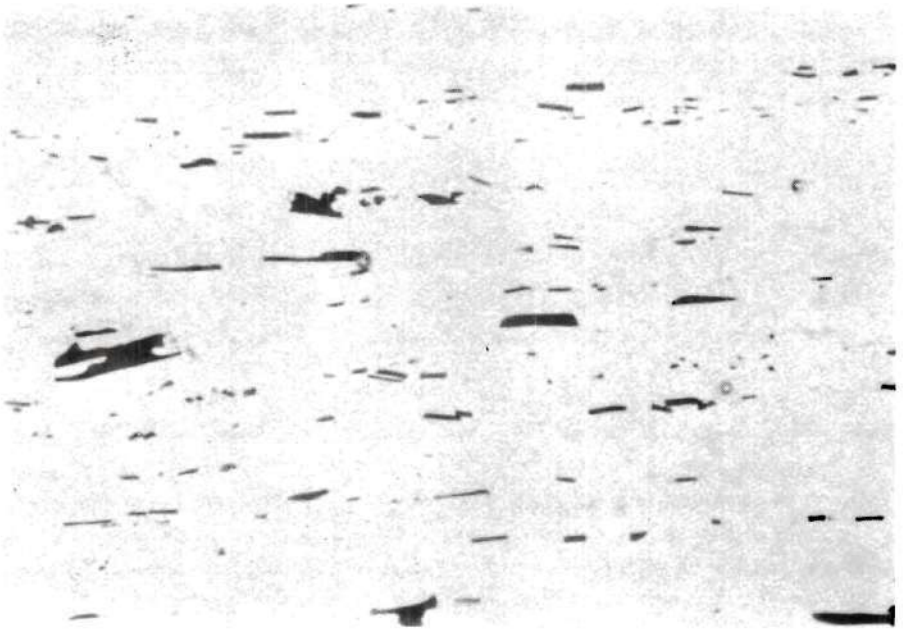

(b)

Figure 15. Optical Photomicrographs of Al-Fe-Co Alloy and EC Aluminum Annealed Wire Produced from (a) Rapidly Solidified Bar and (b) Slowly Solidified Bar in the Cross Sectional Direction. (800X) Showing Particle Distribution.

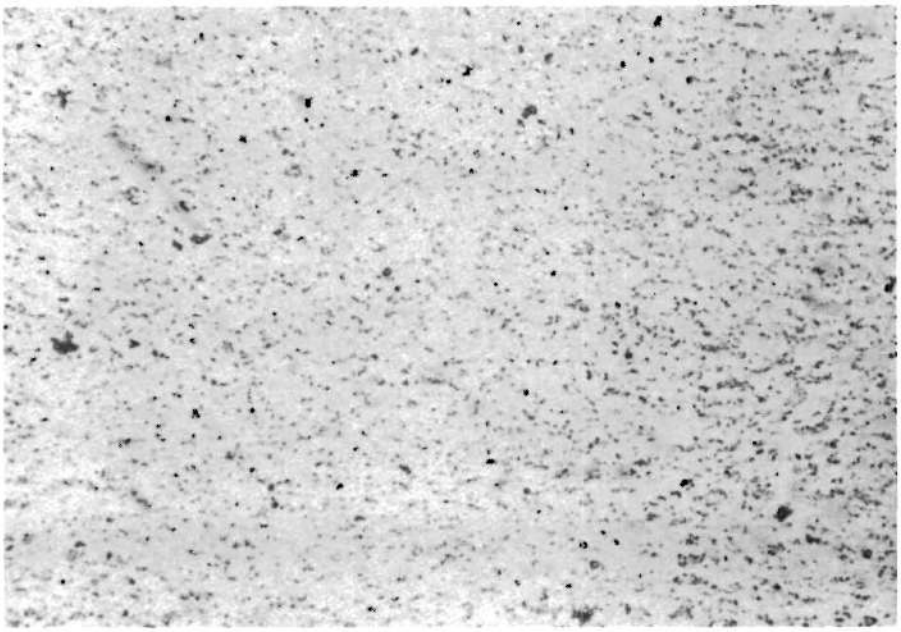

(a)

(b)

Figure 16. Optical Photomicrographs of Al-Fe-Co Alloy and EC Aluminum Annealed Wire Produced from (a) rapidly Solidified and (b) Slowly Solidified Cast Bar in the Longitudinal Direction Showing Particle Distribution. 800X

The Al-Fe-Co alloy microstructure of the rolled rod from the rapidly and slowly solidified bars are shown in Figures 14A and 14B (a) and (b). These micrographs show the uniformity of the eutectic network in the rapidly solidified specimen and the high degree of non-uniformity present in the rod obtained from a slowly solidified cast bar. Figures 17A and B are transmission electron micrographs of the Al-Fe-Co alloy rod from the rapidly and slowly solidified bars respectively. Figure 17A shows small cells formed between rows of eutectic particles while Figure 17B shows large cells formed in the rolled rod in the areas devoid of particles.

The EC aluminum cast bar which was rapidly solidified also show a uniform network of eutectic $FeAl_6$ in between the α aluminum dendrites with small dispersed eutectic regions as shown in Figure 18A. The microstructure of the rolled rod from the cast bars of EC is shown in Figure 19A and 19B showing the distribution of the eutectic in the aluminum matrix.

Al-Fe-Co Annealed Wire

Figure 15 is an optical photomicrograph of a transverse section of the Al-Fe-Co annealed wire processed from (a) rapidly solidified bar and (b) slowly solidified bar. It is obvious that the interparticle spacings have been proportionately reduced from the cast bar and rolled rod specimens. The annealed wire specimen from the rapidly solidified bar (Figure 15(b) and 16(b)) contains large precipitates and large precipitate-free regions, which are preserved from the cast bar and hot rolled rod. In order to observe the morphological features of the substructure, transmission electron microscopy was performed on the

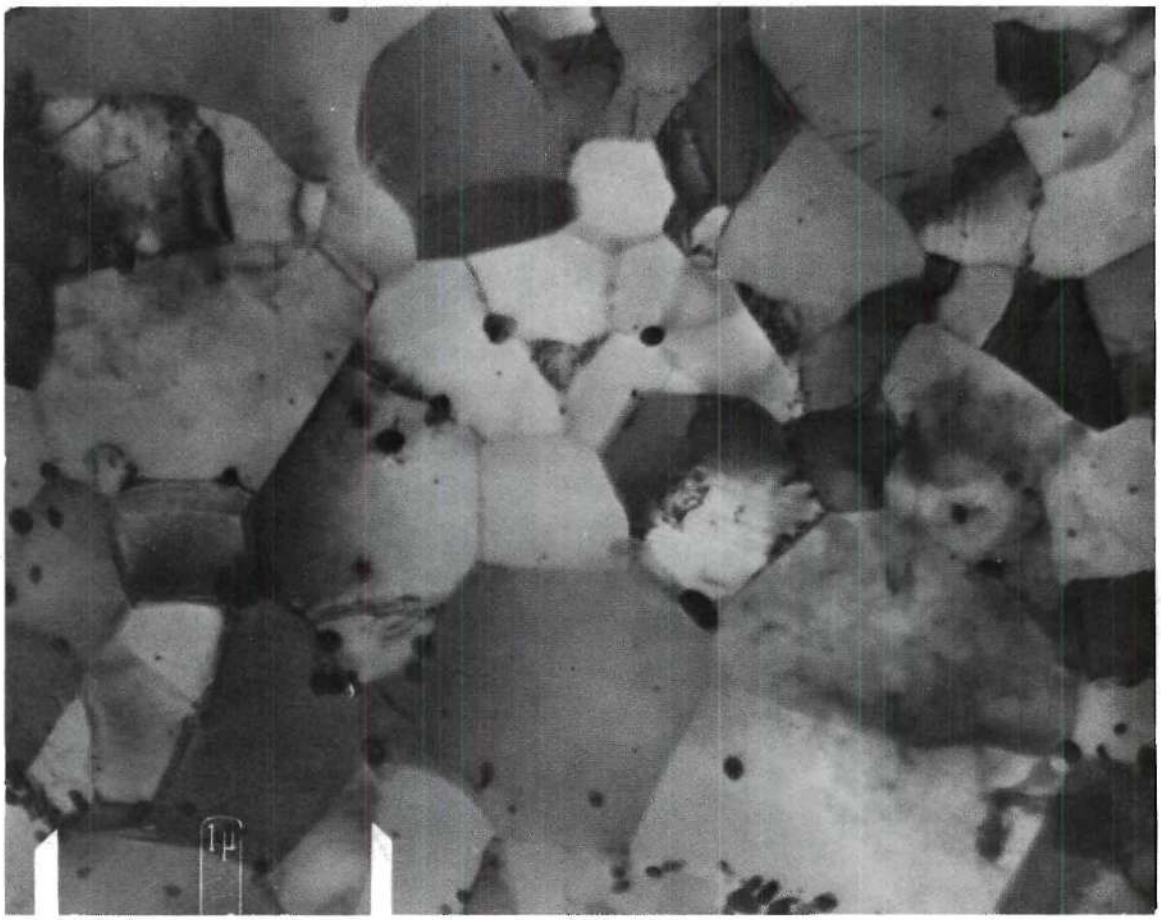

Figure 17A. TEM of the Al-Fe-Co Rolled Rod From the Rapidly Solidified Cast Bar Showing Subgrains Formed in Between Rows of Eutectic Particles.

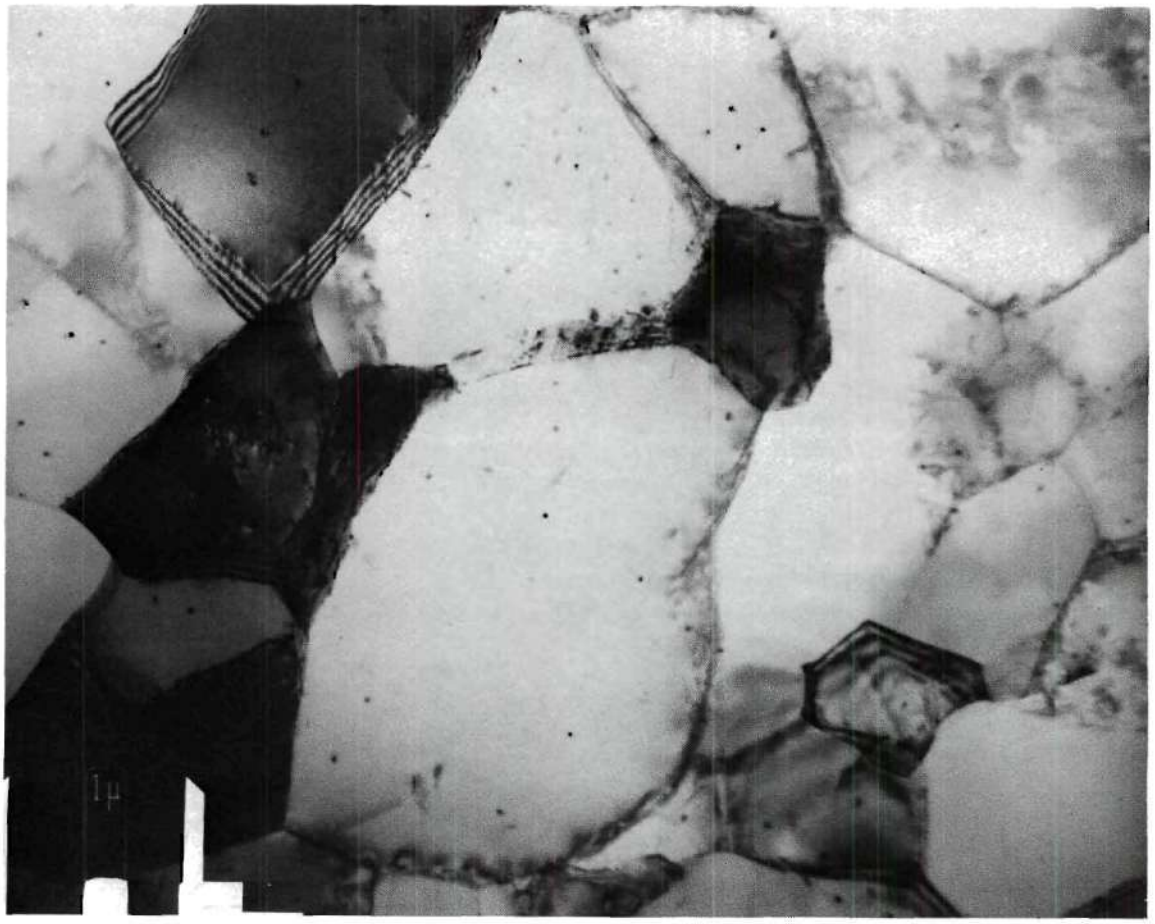

Figure 17B. TEM of Al-Fe-Co Rolled Rod from the Slowly Solidified Cast Bar Showing Large Cells in the Areas Devoid of Particles.

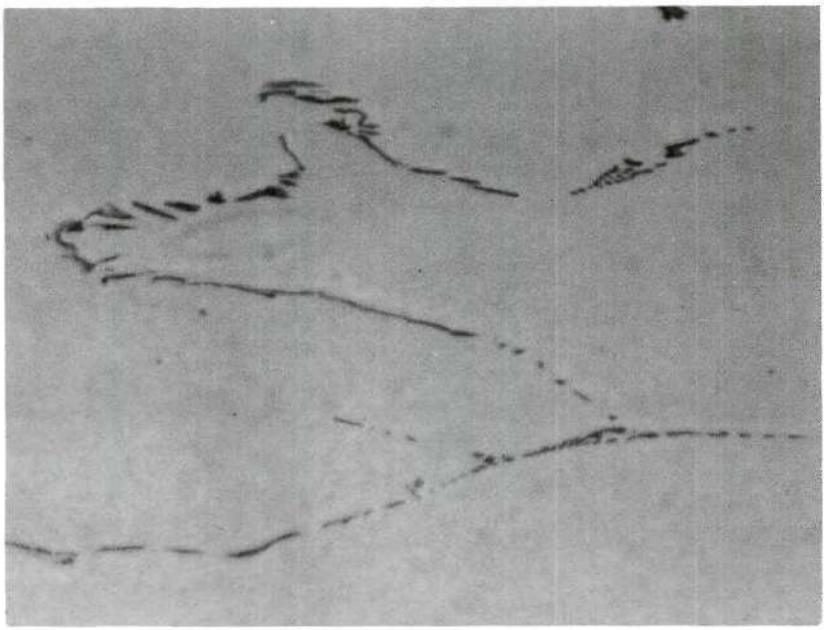

Figure 18A. Optical Micrographs of EC Aluminum Cast Which Was: (a) Rapidly Solidified Showing a Uniform Eutectic Network in Between The Aluminum Dendrites. 800X

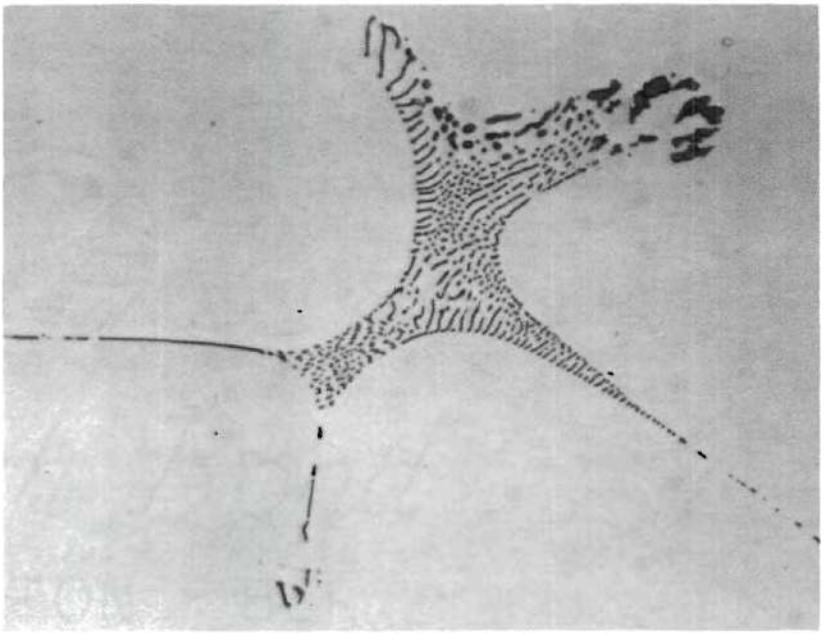

Figure 18B. Slowly Solidified Eutectic Grouped as Colonies. 800X

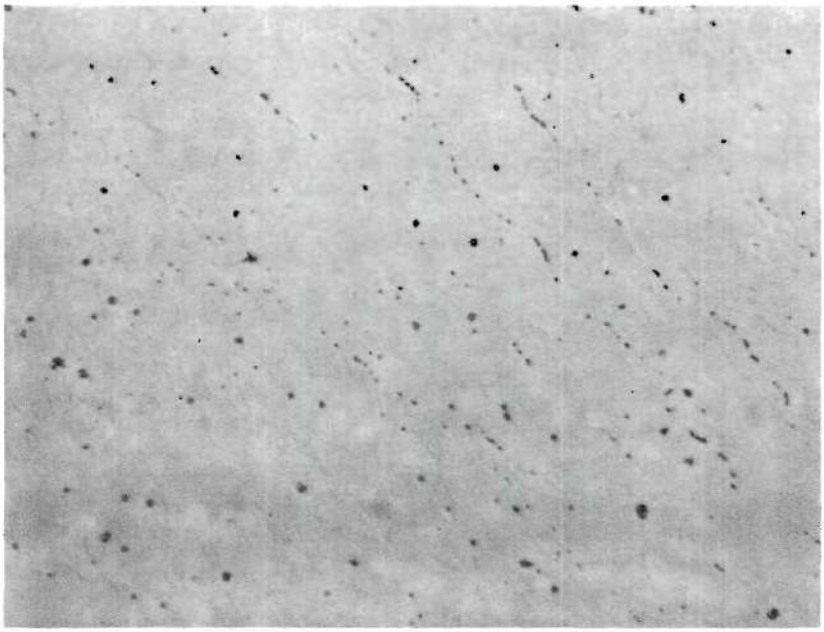

Figure 19A. Optical Micrographs of EC Aluminum Rod Hot-Rolled from: (a) Rapidly Solidified Bar. 800X

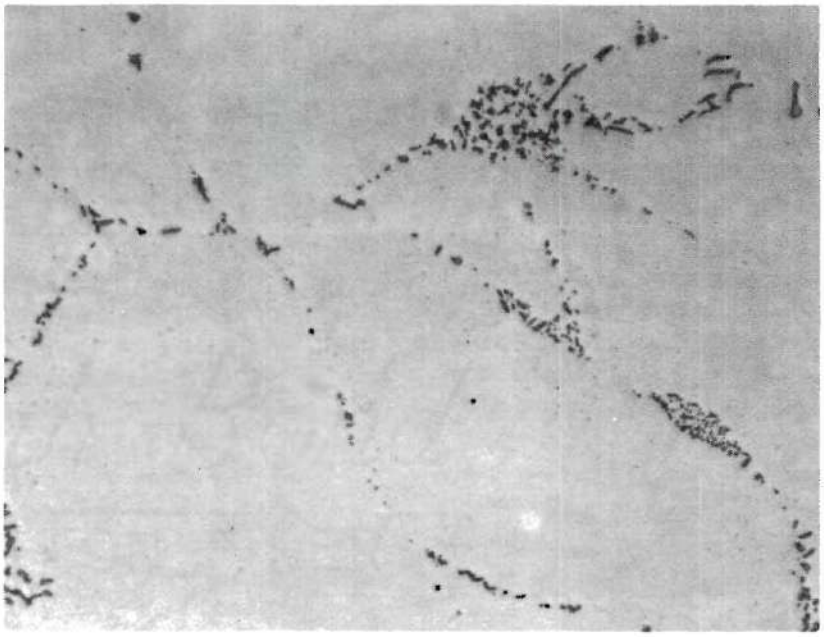

Figure 19B. Slowly Solidified Bar Showing the Distribution of Eutectic in the Aluminum Matrix. 800X

Al-Fe-Co annealed wire specimens produced from both rapidly and slowly solidified bars. Figure 20 is a TEM of the Al-Fe-Co alloy annealed wire produced from the rapidly solidified cast bar. This structure is composed of a uniform subgrain network with precipitates distributed throughout the entire structure. The subgrains of the annealed wire have sharp boundaries in contrast to the as-drawn condition. During the annealing process, dislocations present inside of the cold-drawn cells move to the cell walls producing thinner, more uniform, and higher angle subgrain boundaries. Subsequent references to boundary thickness in this thesis are based on observations of the dislocations at these boundaries. In addition, some coarsening occurs by the coalescence of subgrains, in which adjacent subgrains merge by the elimination of their common boundary. The average inter-precipitate distance corresponds to the average subgrain size. Thus the fine precipitate distribution seems to be directly responsible for retaining a small subgrain size. By suppressing cell coalescence, the precipitates stabilize the structure during recovery. The average subgrain size of this material is 0.8 microns, with a size range from 0.4 microns to 1.2 microns.

In the majority of the cases, the precipitate particles are located in the subgrain boundaries. Sometimes, a precipitate appears to be located in the center of a subgrain; however, usually, by tilting the specimen during observation in the electron microscope, a subgrain boundary, which goes through the precipitate, becomes visible.[90] This is due to a variation in the orientation of the specimen with respect to the electron beam, which results in variations in diffraction contrast.

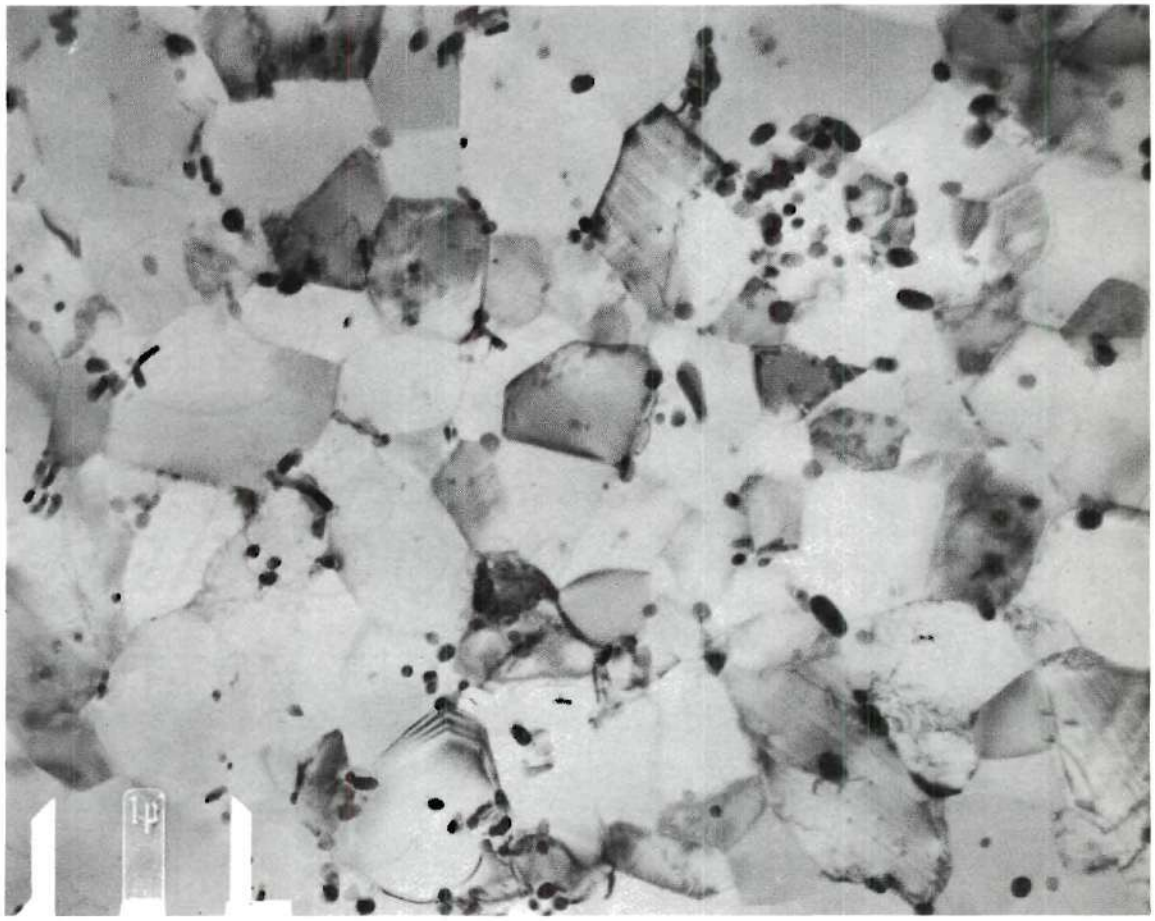

Figure 20. TEM of the Al-Fe-Co Alloy Annealed Wire Produced from the Rapidly Solidified Cast Bar Showing a Uniform Subgrain Structure with Precipitates Distributed Throughout the Entire Structure.

The Al-Fe-Co annealed wire drawn from the slowly solidified bar produced a finished wire product with the structure shown in Figure 21A. This structure is characterized by an absence of precipitates in 70 percent of the area examined. The precipitates were restricted to groups in widely spaced areas of the specimen, resulting in a complete lack of uniformity Figure 21B. The groups of precipitates correspond to the eutectic colonies which precipitated during solidification, as shown in Figure 13. The cast structure did not contain a fine, uniform distribution of the interdendritic eutectic compound. No precipitation takes place during subsequent processing after slow solidification, since iron and cobalt are not retained in solution. Consequently, the structure of the wire after annealing shows precipitate depleted matrix areas corresponding to those observed in the case and hot-rolled rod structures and large subgrains. The large subgrains are a result of the absence of sufficient uniformly dispersed fine particles which are necessary to restrict subgrains coalescence during annealing. The average cell size of this material was measured as 10 microns, with a range from 2 microns in the areas between precipitates to 20 microns in the precipitate depleted regions. The EC material showed the same effect of Al-Fe-Co alloy as shown in Figures 22 and 23, which are transmission electron micrographs of EC wire annealed at 550°F for three hours after cold drawing. These micrographs show the lack of stability of the subgrains due to the absence of pinning particles.

Physical Properties

The physical properties of the rolled rod, drawn wire and annealed

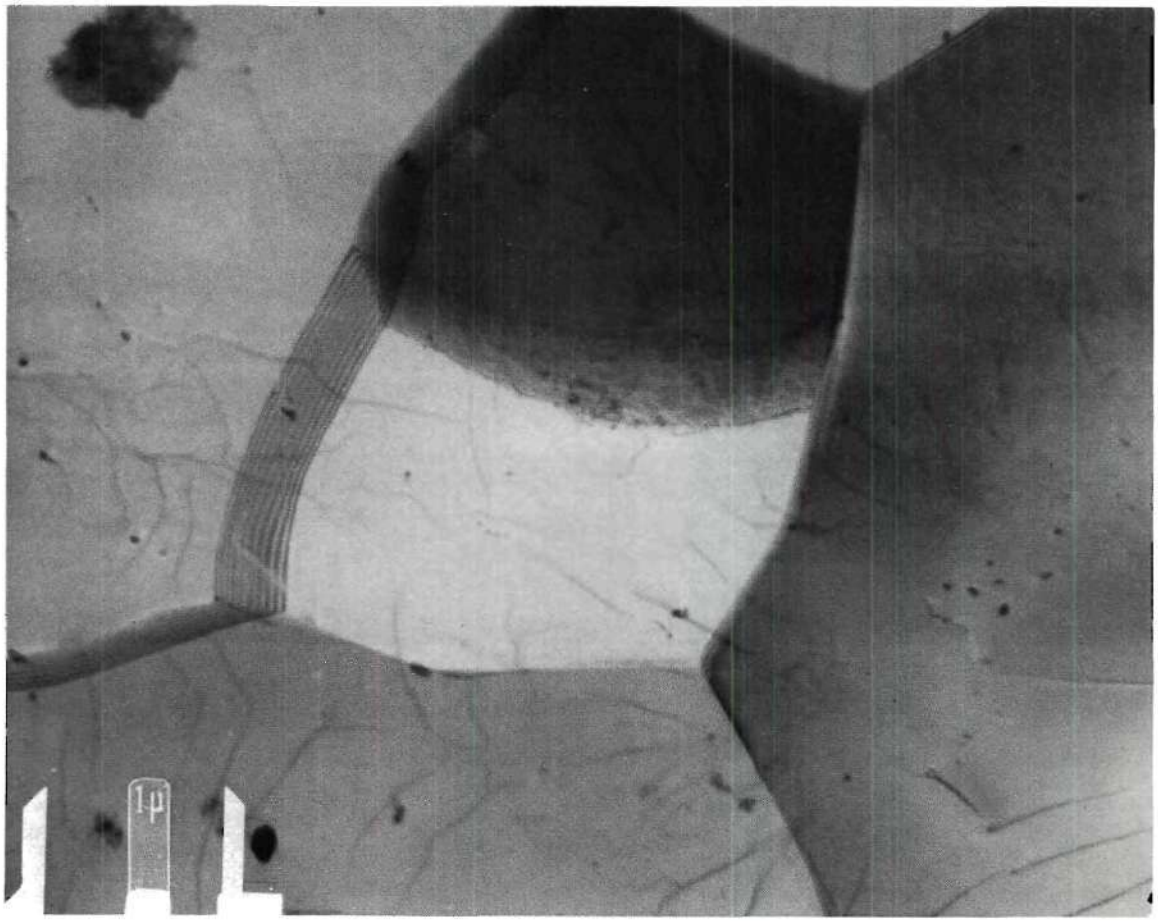

Figure 21A. TEM of the Al-Fe-Co Alloy Annealed Wire Produced from the Slowly Solidified Cast Bar Showing an Absence of Precipitates and Consequently Large Subgrains.

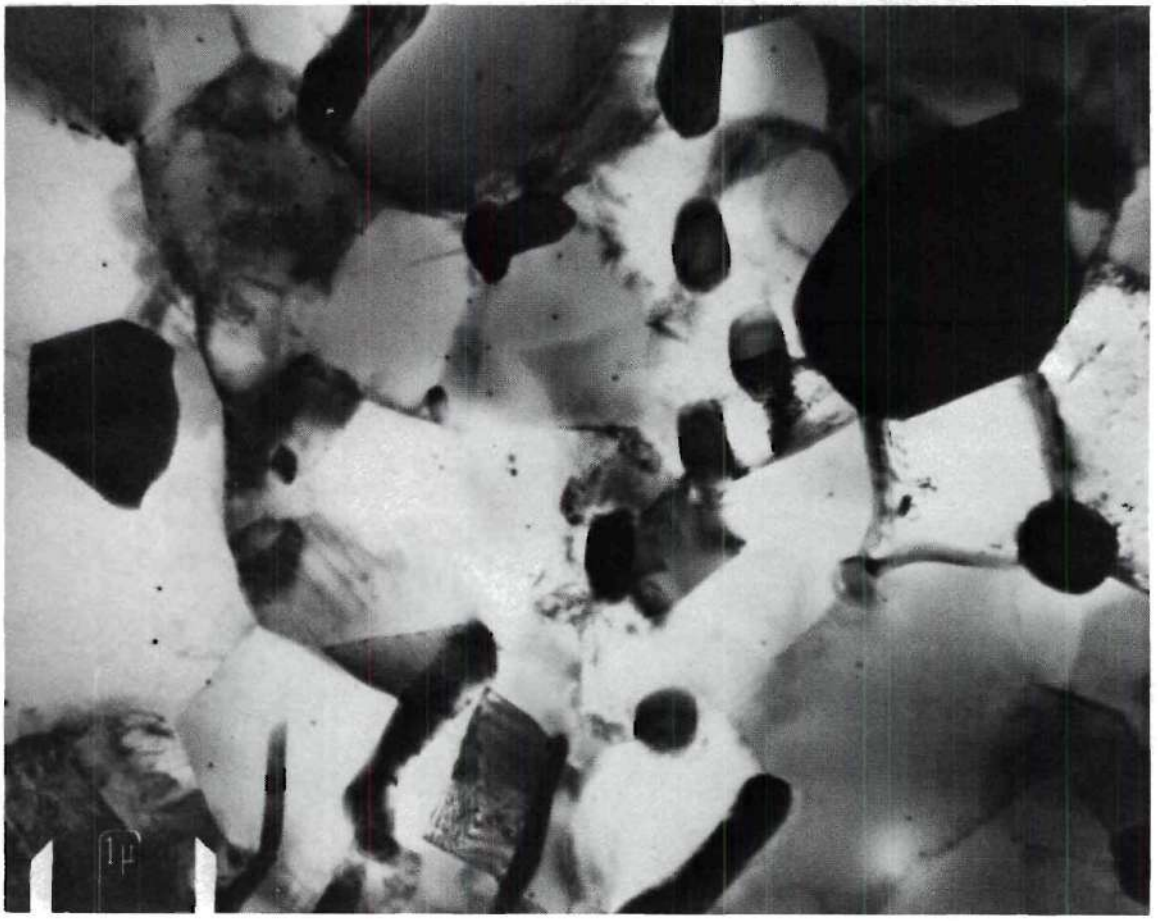

Figure 21B. TEM of the Al-Fe-Co Alloy Annealed Wire Produced from the Slowly Solidified Cast Bar Taken in the Eutectic Region Showing Large Particles and Non-Uniform Subgrain Structure.

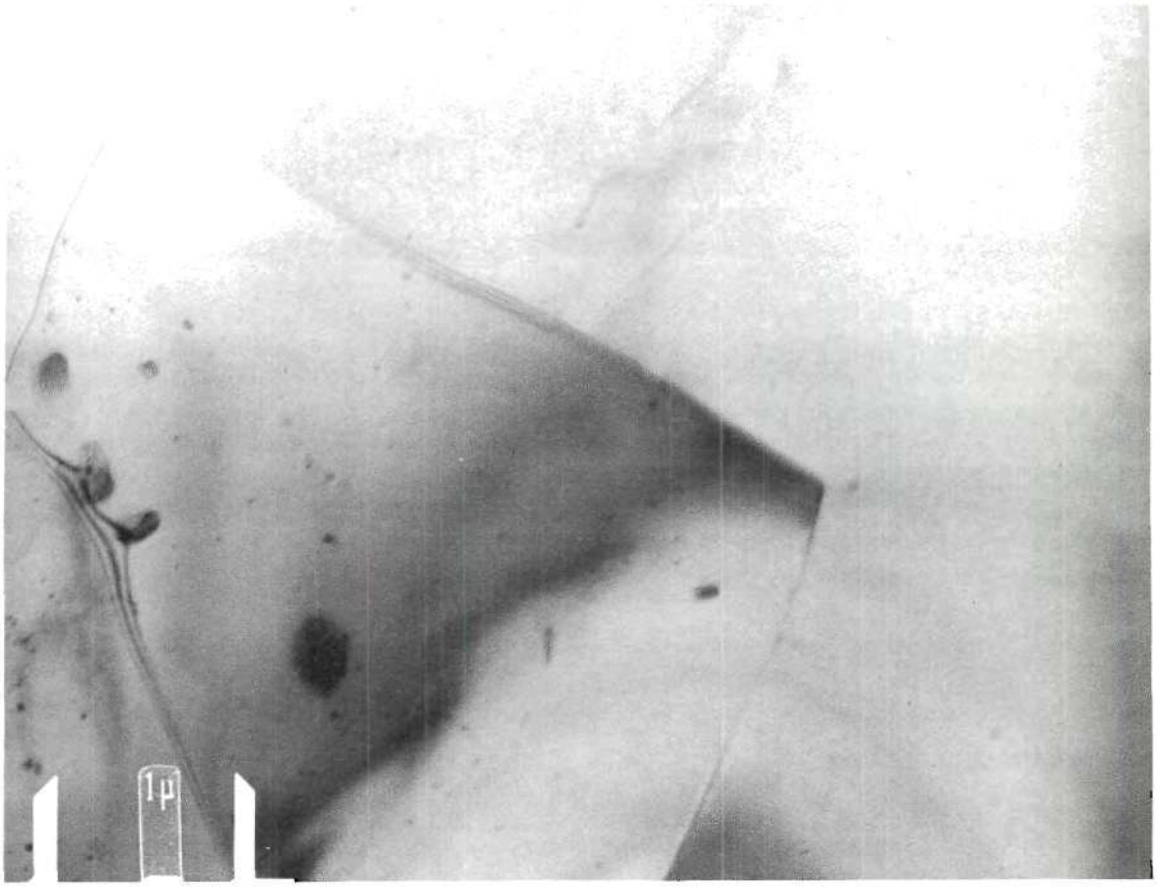

Figure 22. TEM of EC Wire from the Slowly Solidified Cast Bar Which was Annealed at 550°F for Three Hours After Cold Drawing Showing Large Subgrains.

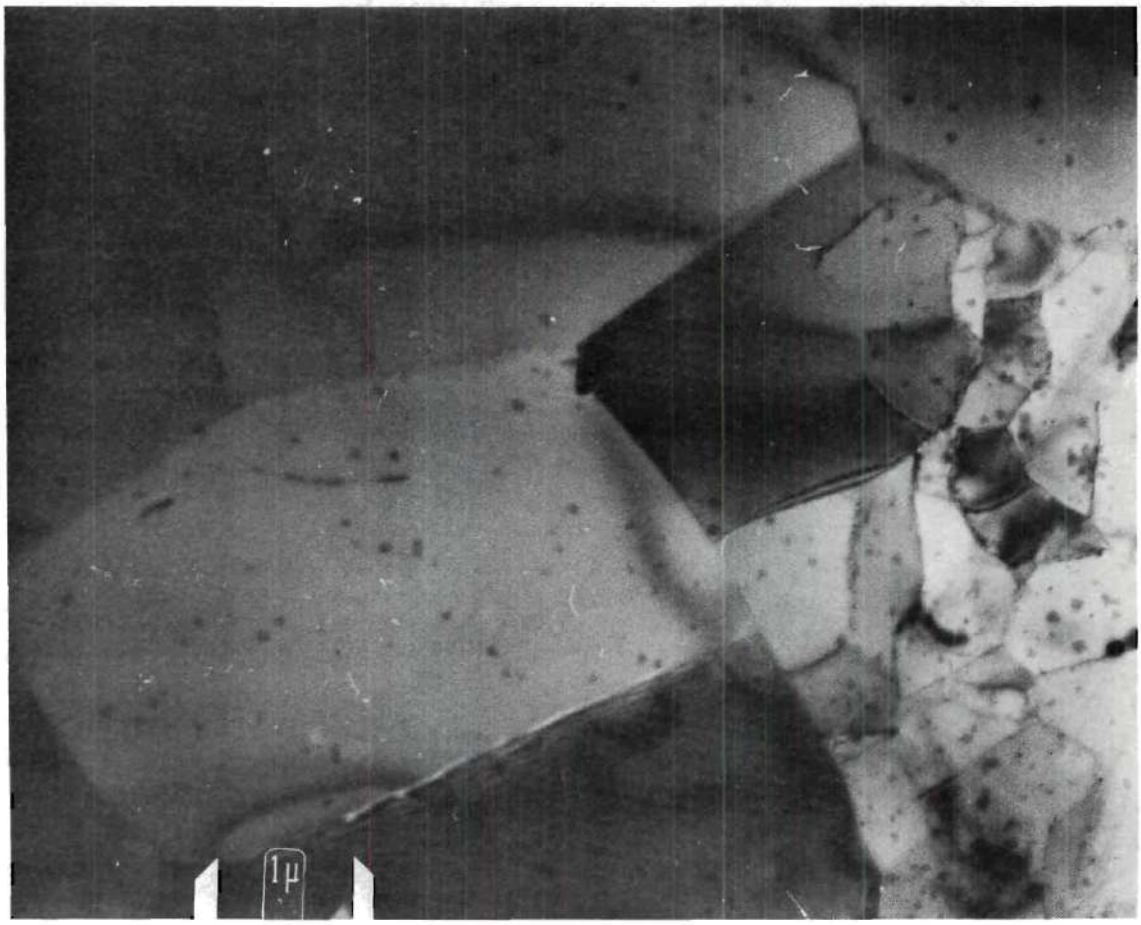

Figure 23. TEM of EC Wire from the Rapidly Solidified Bar Cold Drawn and Annealed at 550°F for Three Hours Showing a Non-Uniform Subgrain Structure Due to the Absence of Pinning Particles.

wire were determined for the rapidly solidified and slowly solidified Al-Fe-Co and EC samples and are contained in Figure 24. The annealed wire product from the rapidly solidified Al-Fe-Co alloy casting had an ultimate tensile strength of 18,200 psi, a yield strength of 15,300 psi, and an elongation of 23.0 percent. The significant difference in ultimate tensile strength and yield strength obtained between the rapidly and slowly solidified products can be attributed mainly to the effect of a stable, fine and uniform subgrain structure produced by the fine distribution of the precipitates throughout the aluminum matrix on the work-hardening characteristics. The solidification rate and alloy composition in aluminum-manganese alloys has been studied extensively[91,92,93] and found to have a significant effect on the size and precipitate distribution. This was found to have as great effect on the resulting mechanical properties of the alloy.

The elongation of the slowly cooled products reaches a value of 31.2 percent, which is equivalent to that of unalloyed electrical conductor grade aluminum. This demonstrates that the slow solidification of the Al-Fe-Co alloy produced a finished wire product which offers only a small improvement in mechanical properties over those of the unalloyed EC. The areas containing the large precipitates which were formed during the slow solidification do not produce enough strengthening effect to the entire matrix, and, furthermore, these large particles act as nucleation sites for microcracks and decrease the ductility of the material.

The effect of the solidification rate can be detected also in the EC finished wire product. The annealed wire from the rapidly

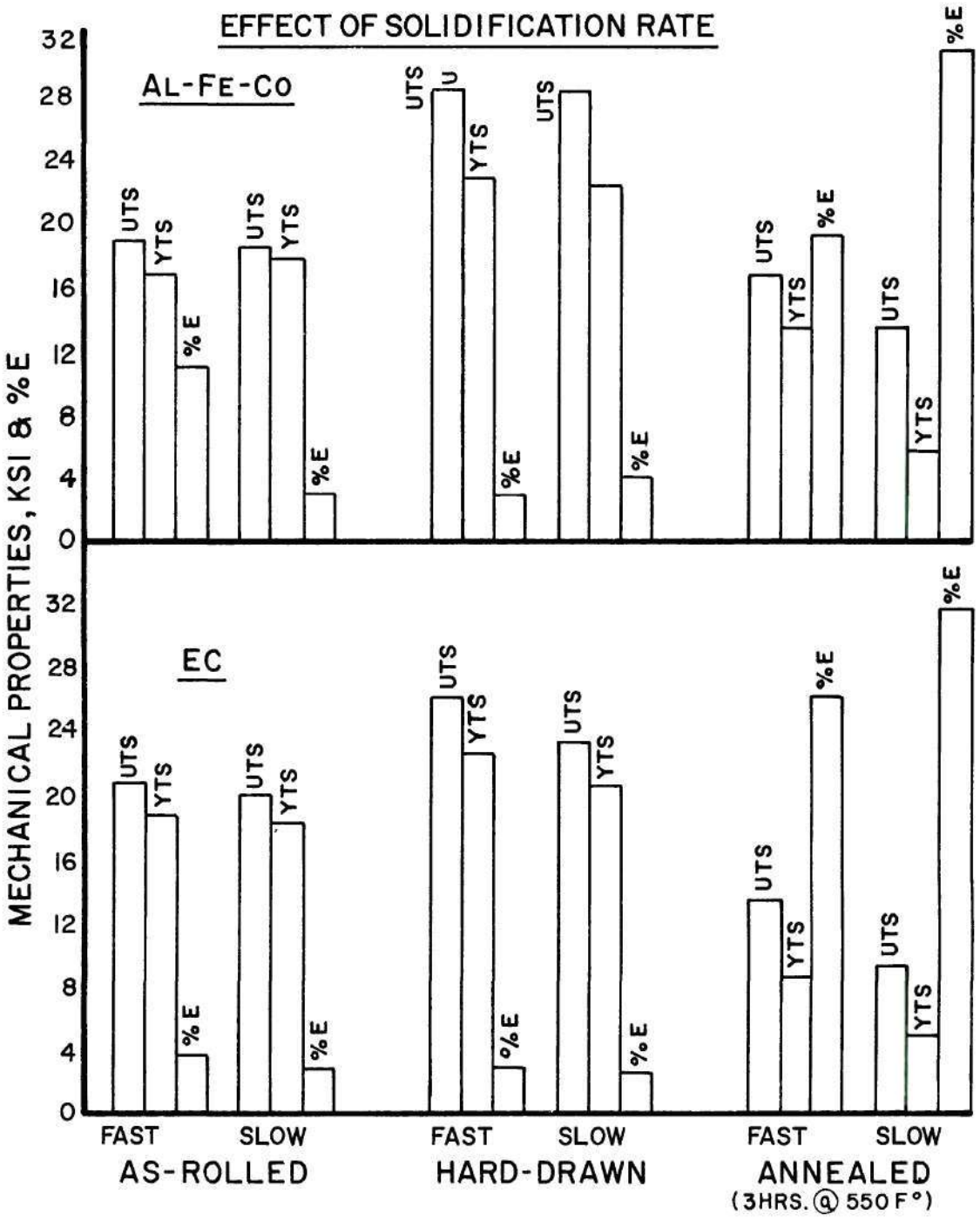

Figure 24. Mechanical Properties of Al-Fe-Co Alloy and EC Aluminum Specimens at Different Stages of Processing.

solidified bar had a tensile strength of 12,800 psi, a yield strength of 7,800 psi, and an elongation of 30 percent. This can be compared to the properties obtained from the EC annealed wire produced from the slowly solidified bar, e.g. 11,800 psi ultimate tensile strength, a yield strength of 6,700 psi and an elongation of 26 percent. The mechanisms for EC are essentially the same as those described for the Al-Fe-Co alloy. The precipitates in the case of EC are $FeAl_3$ formed from iron impurities. However, there is not sufficient iron in EC to produce the large effects observed for the Al-Fe-Co alloy.

Subgrain Size vs. Yield Strength

A correlation of subgrain size with yield strength for the different products is presented in Figure 25. This correlation shows that in all cases, a large cell size in the product corresponds to a low yield strength, independent of the processing history of the material. The high yield strength obtained in the Al-Fe-Co specimens which exhibit a fine subgrain size is due to the effective pinning of the dislocations by the precipitates which results in a fine, uniform cell structure. The precipitates are well distributed throughout the aluminum matrix and are located mainly in the subgrain boundaries, making them stable and resulting in a finished wire product with improved properties.

The slowly solidified Al-Fe-Co alloy yields a product which contains large regions of precipitate-free material. During recovery, the cells which are located in these areas are unstable and coalesce, resulting in large polygonized subgrains with thin walls, which are ineffective in producing the necessary resistance to the passage of

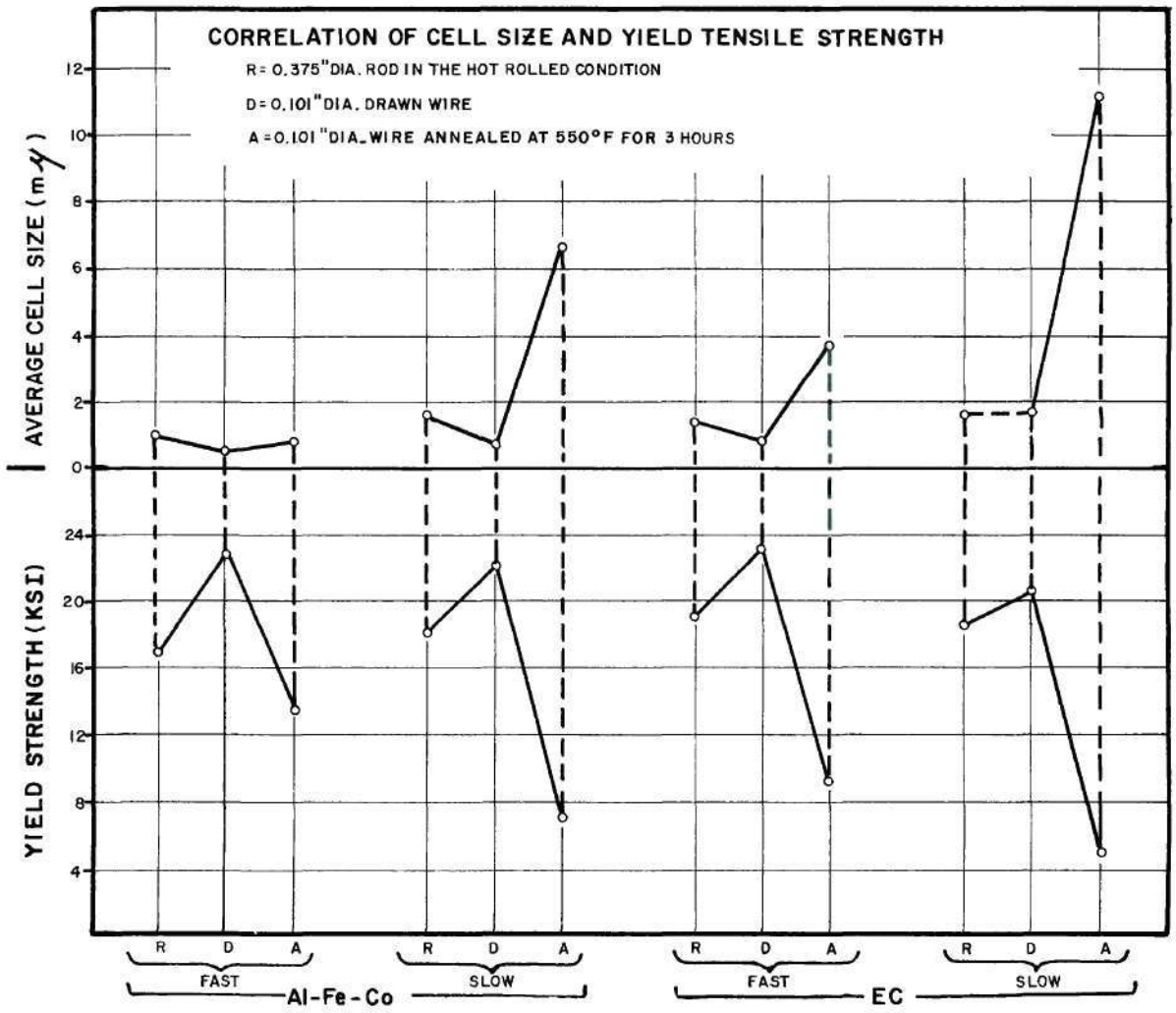

Figure 25. Correlation of Cell Size and Yield Tensile Strength of Al-Fe-Co Alloy and EC Aluminum Which were Solidified Rapidly and Slowly.

dislocations and consequently are not able to provide the necessary strengthening effect, as evidenced by the low yield strength.

Effect of Sequential Reductions During Hot Working on Subgrain Formation

The effect of successive stages of hot rolling was investigated for the Al-Fe-Co continuously (rapidly solidified) cast alloy. The rolling passes and corresponding reductions in area are presented in Table 7, together with the measured mechanical properties. Figure 26 is a plot showing the variation in ultimate tensile strength and yield tensile strength with the reduction in area.

The ultimate tensile and yield strengths steadily increase with increased reductions to 26 KSI and 24 KSI respectively. The elongation (Figure 27) of the cast-bar material was measured as 22.5 percent and increased to 37.0 percent after 37.3 percent reduction. This increase in ductility can be due to the uniformity of the structure produced by the hot deformation which also seals microporosity. In addition, the as-cast structure contains large grains which are unfavorably oriented for plastic flow with respect to the stress axis.

These results are similar to those of Decroix, et al.[94] who studied the hot workability of nickel-chromium steels and found that the ductility of the as-cast material at room temperature and at elevated temperatures was lower than after hot deformation. He attributed this increase in elongation to the decrease in interdendritic segregation and non-uniformity which existed in the cast structure. A similar conclusion was reached by Sellars and Tegart[95] and by Leech

Table 7. Mechanical Properties of Bars During Hot-Rolling for Al-Fe-Co Alloy

HOT ROLLING PASS NO.	AREA (Sq.In.)	TOTAL REDUCTION IN AREA(%)	ULTIMATE TENSILE STRENGTH (lbs./sq.in)	YIELD TENSILE STRENGTH (lbs./ sq. in.)	ELONGATION (4 Inches) (percent)
Cast	8.240	0	12,400	4,500	22.5
1	5.150	37.3	13,900	6.900	37.0
2	3.342	59.2	14.600	8,200	30.0
3	2.523	69.2	15,000	9,700	30.0
4	1.794	78.1	16,100	10.800	33.8
5	1.410	82.8	16,700	12,800	17.5
6	0.953	88.4	17,100	13,100	11.8
7	0.712	91.3	19,800	18,300	1.0
8	0.493	94.0	-	-	-
9	0.372	95.5	21,900	19,400	1.5
10	0.263	96.8	21,800	21,400	0.8
11	0.192	97.7	23,600	20,900	1.3
12	0.148	98.2	26,000	21,200	1.3
13	0.116	98.6	24,900	24,000	4.0

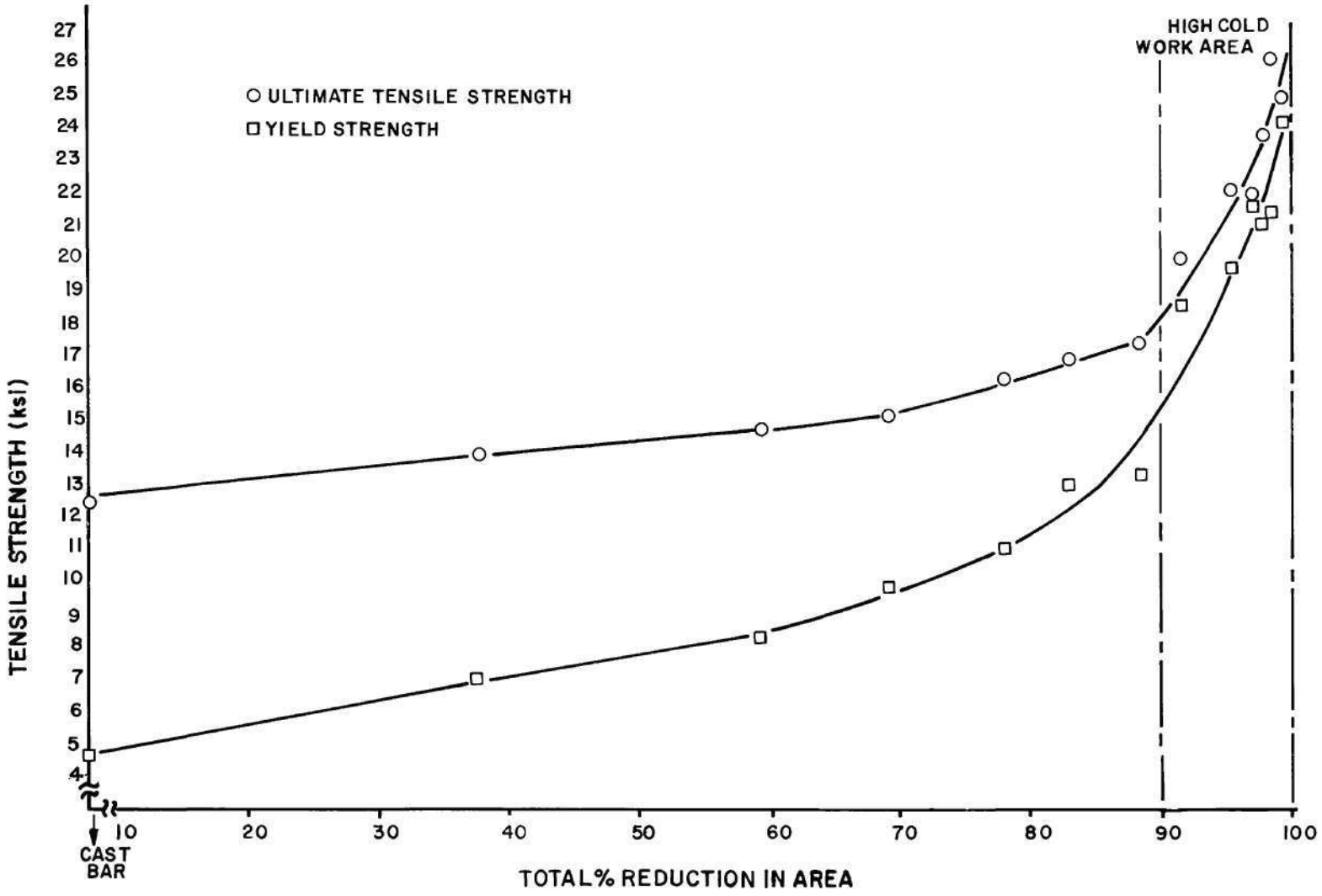

Figure 26. Variation of Ultimate Tensile Strength and Yield Strength With Percentage of Hot Deformation.

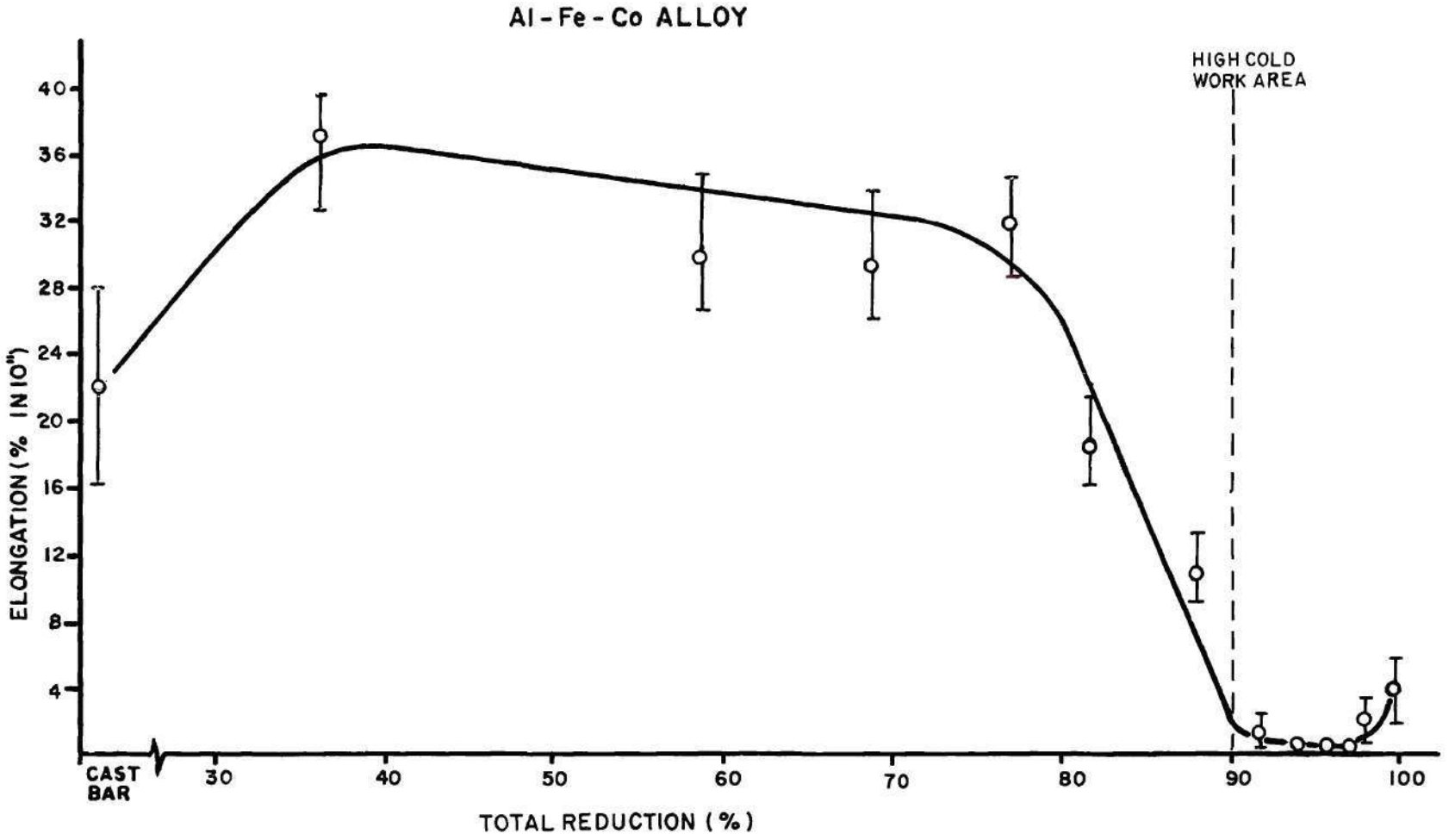

Figure 27. Variation of Percentage of Elongation with Percentage of Hot Deformation.

et al.[96] who attributed the increase in ductility during hot working mainly to the decrease in chemical heterogeneity which in turn decreases the amounts of non-equilibrium second phase present and to the grain refinement effect produced by the recrystallization taking place during deformation. After the first reduction, the elongation remains essentially constant due to the lack of work hardening resulting from dynamic recovery. After the fourth reduction (78.1%) the elongation rapidly decreases to less than 2% after 91.3% reduction.

The elongation of the rolled Al-Fe-Co bar remained constant with increasing deformation after 91.3% reduction. This reduction corresponds to the beginning of extensive cold work and the development of a constant cell size.

This can be attributed to the increase in dislocation density in the presence of precipitate particles and the lack of total recrystallization during the hot-rolling process.[102] The elongation decreases to 17.5 percent after an 82.8 percent reduction in area and drops below 4 percent after a 90 percent reduction in area. Starke and Spooner[97] also found that essentially no cold working takes place until a reduction in area of 85 to 90 percent is performed. They measured the hardness after each rolling stage and plotted this versus the percent reduction as shown in Figure 28. The work hardening, and thus the hardness, significantly increased after 90 percent reduction. During the last stages, the rate of dislocation generation significantly dominates over the process of dislocation annihilation producing significant work hardening. In this region, the yield values become very close to the ultimate tensile strength values, which also

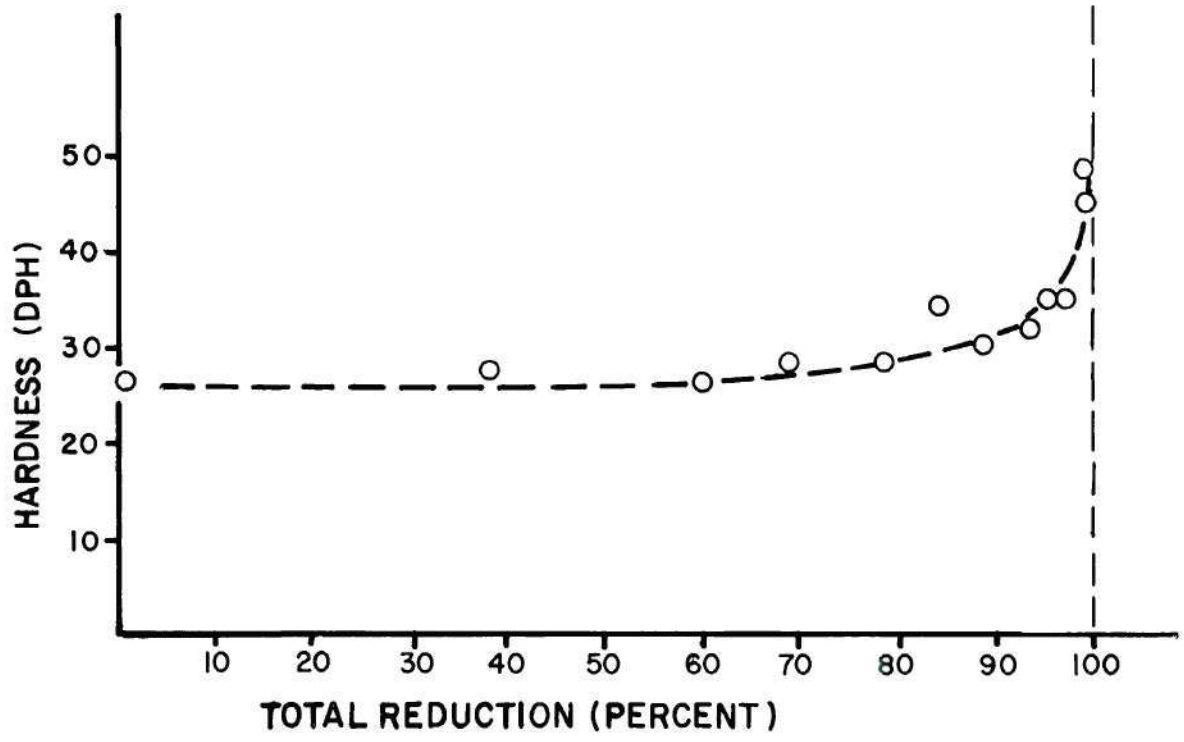

Figure 28. Hardness as a Function of the Percentage of Total Reduction of EC Aluminum During Hot Working.

indicates a high degree of work hardening. It should be recognized here that dynamic recovery is suppressed to a great extent during the last seven reductions. This is probably due to the fact that the last reductions take place at extremely high speeds (2000 feet per minute) and at relatively low temperatures (650 to 800°F) and the combination of the two makes dynamic recovery negligible. Lee, et al.[98] showed that dynamic recovery during tensile deformation becomes less significant as the strain rate is increased and the deformation temperature is decreased.[99,100] Additional evidence for this statement is provided by Figure 30 which shows the cell structure formed during the last sequential reduction of hot rolling. Microscopic examination and tilting of the specimen revealed that the cell structure present in this sample contained a high dislocation density without thin, well defined cell walls, features which are characteristic of cold worked or partially cold worked structures that have not dynamically or statically recovered.

Figure 29 shows that the yield to ultimate strength ratio becomes significantly larger after 91.3 percent reduction during hot working. This is another indication that the rate of dynamic recovery has decreased in the last reductions.

The microstructures of the cast bar and of the rolled bar at intermediate stages were studied using transmission electron microscopy. The cast bar shows a complete absence of subgrains in the matrix, Figure 31. This micrograph shows the presence of the eutectic compound which precipitated during casting and a negligible dislocation density.

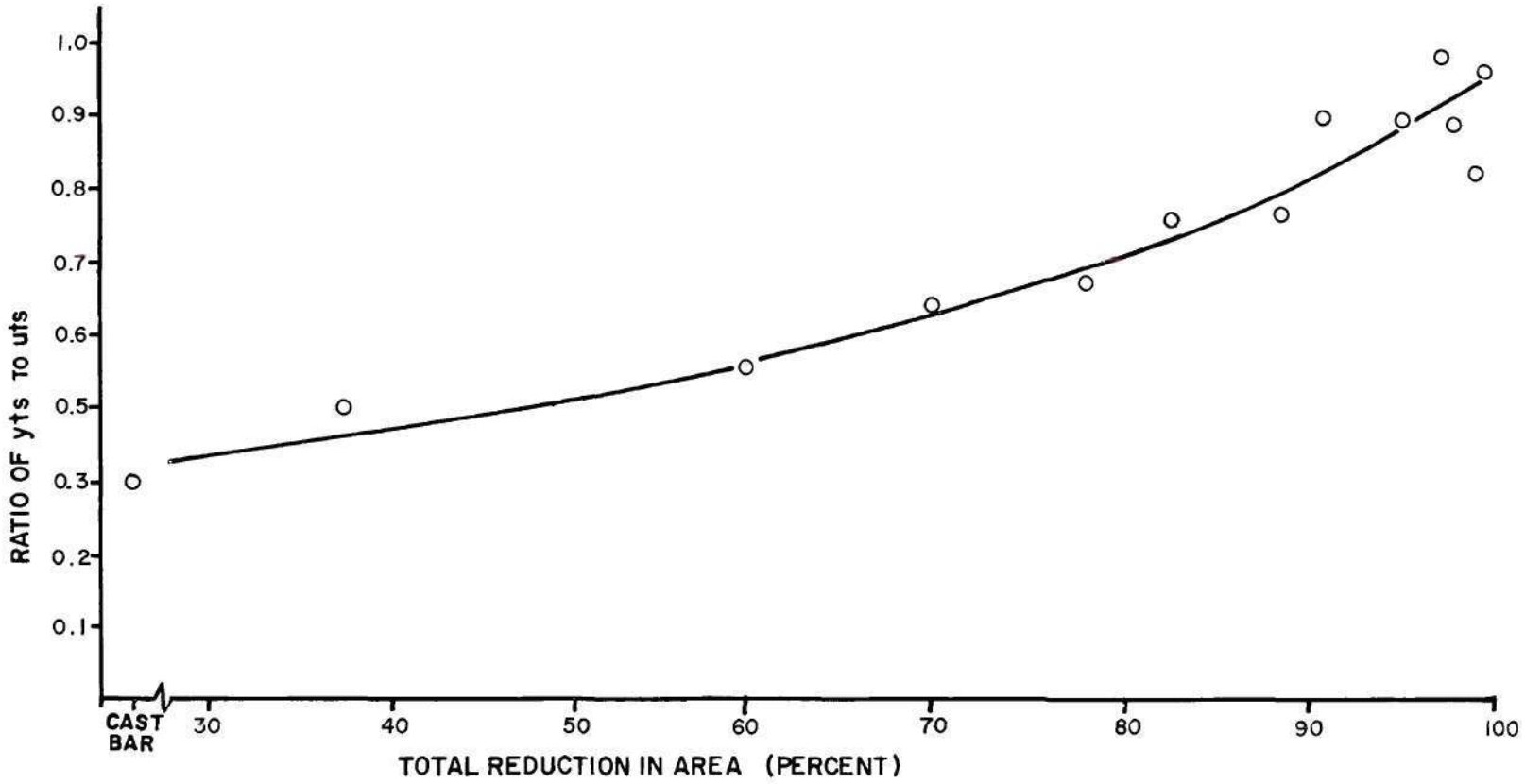

Figure 29. Variation of the Ratio of Yield to Ultimate Tensile Strength During Hot Rolling.

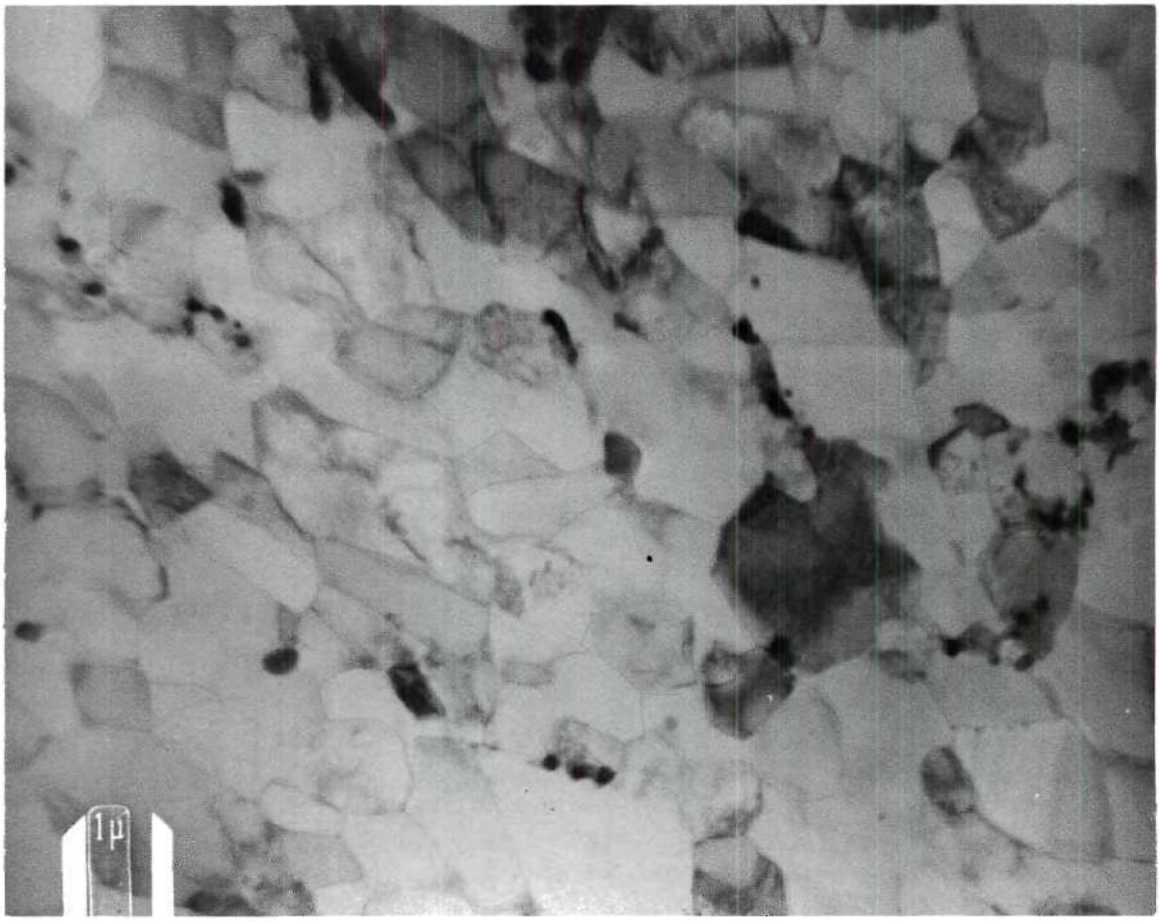

Figure 30. T.E.M. of the Al-Fe-Co Rod Microstructure After the Thirteenth Pass (98.6 Percent Reduction).

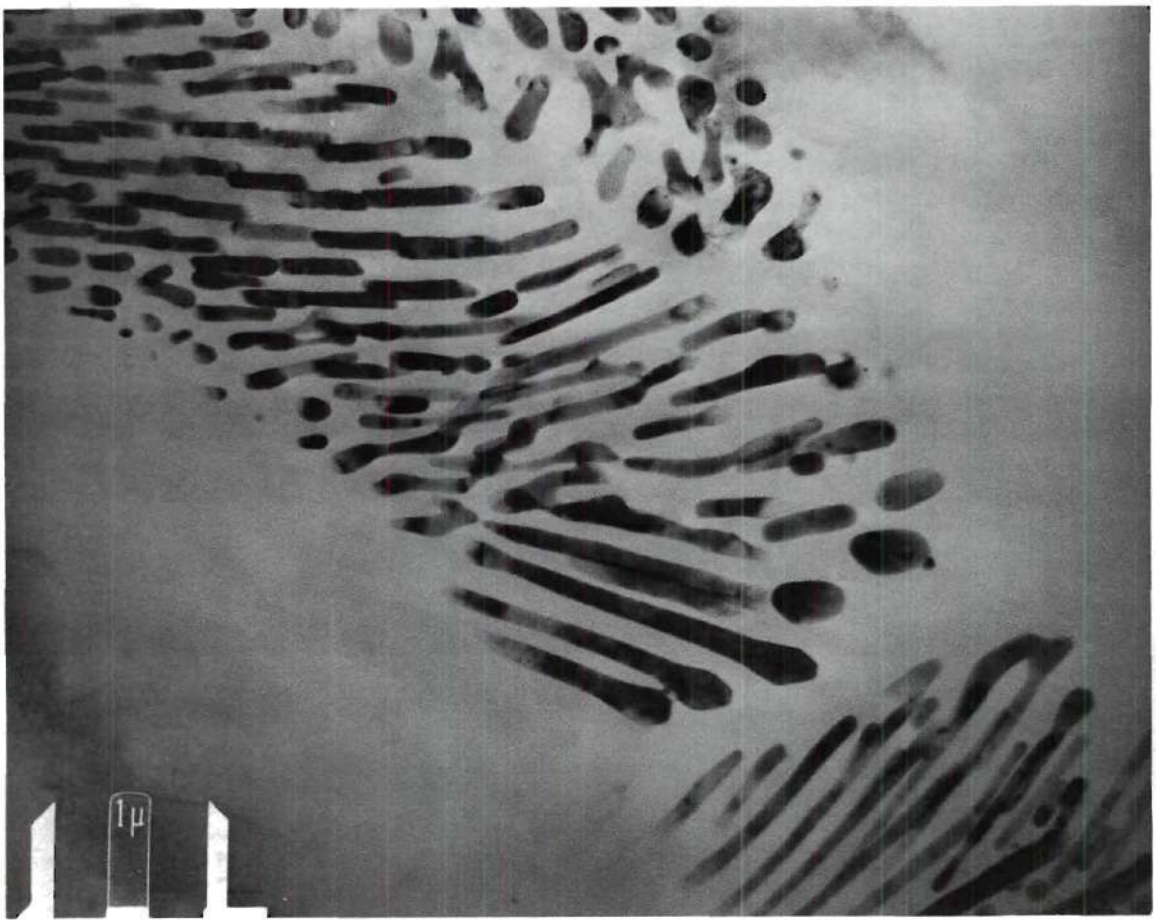

Figure 31. TEM of a Al-Fe-Co Cast Bar Sample, Showing Colony of (Fe Co) Al_9 and Fe Al_6 Eutectic in the Aluminum Matrix.

The cell structure in the bar begins to form between rows of precipitates after an initial reduction in cross section of 37.3 percent as shown in Figures 32 and 33. The rows of precipitates act as dislocation sources during deformation and as initial barriers to the motion of dislocations, causing pile-ups and subsequent subgrain formation. At this stage, the areas of the matrix devoid of precipitates do not show significant subgrain formation. There are, however, dislocations randomly dispersed in the matrix and associated with the beginning of subgrain formation, Figure 34. After a reduction of 59.2 percent by rolling, the Al-Fe-Co alloy exhibits a slightly high degree of subgrain formation, Figure 35 and a higher concentration of dispersed dislocations which in some areas appear to be aligned in a position to form subgrain boundaries. Subgrains are more numerous between precipitate colonies but still relatively absent in the precipitate-free areas of the aluminum matrix.

The average subgrain size after 59.2 percent total reduction by hot working is 5.0 microns. After a total reduction of 69.2 percent during hot rolling, the substructure becomes significantly smaller, having an average cell size of 2.9 microns and becomes uniform throughout the matrix, even in areas devoid of precipitates, Figure 36. The Al-Fe-Co alloy material possesses an average cell size of 2.5 microns after 78.1 percent total reduction (Figure 37) showing a good cell uniformity throughout. The remaining reductions are shown in Figures 39 to 45 which show that as the total hot rolling reduction in area increases, the cell size and size distribution of the rod decreases continuously up to

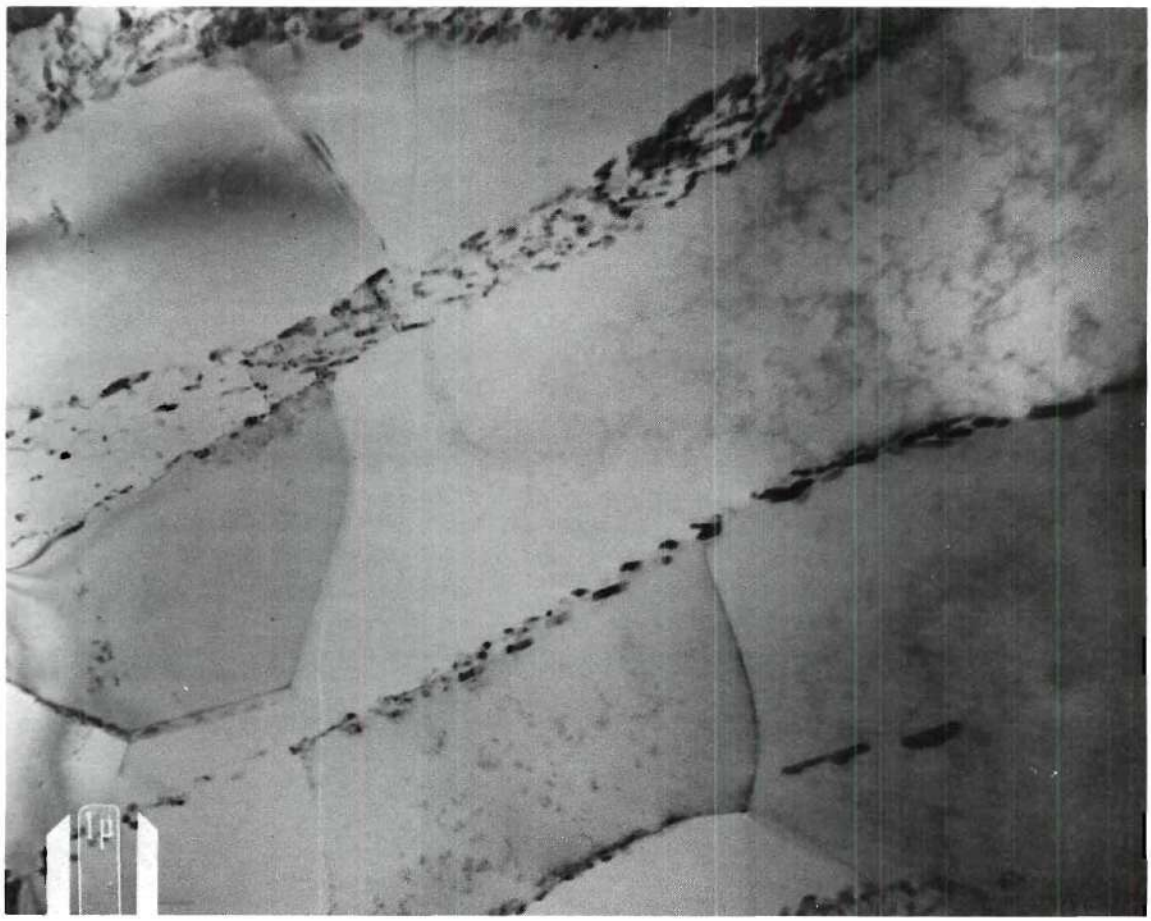

Figure 32. TEM of the Al-Fe-Co Microstructure After the First Pass (37.3 percent Reduction in Area), Showing the Onset of Subgrain Formation During Hot Rolling. The Subgrains form Initially Between Rows of Eutectic.

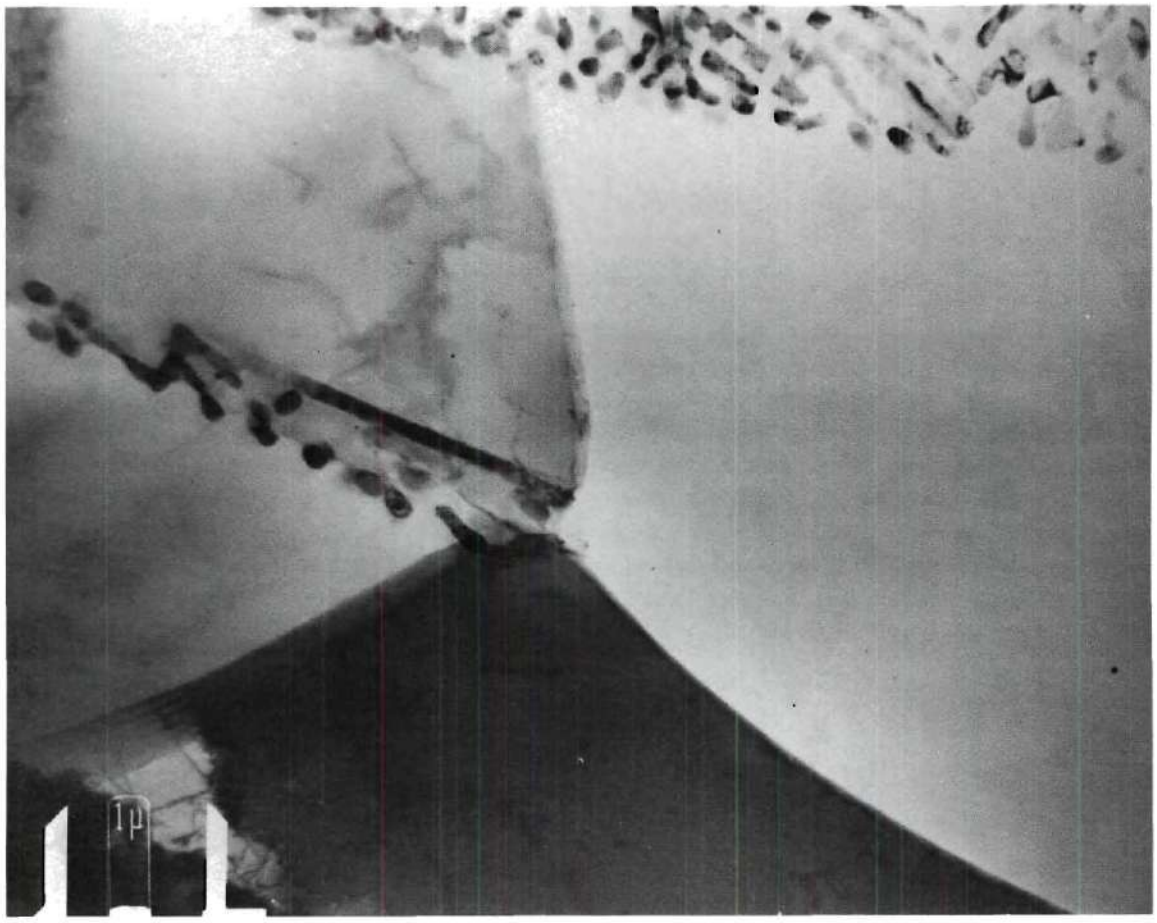

Figure 33. TEM of the Al-Fe-Co Microstructure After the First Pass (37.3 Percent Reduction in Area), Showing the Effect of the Precipitates on the Formation of the Cells.

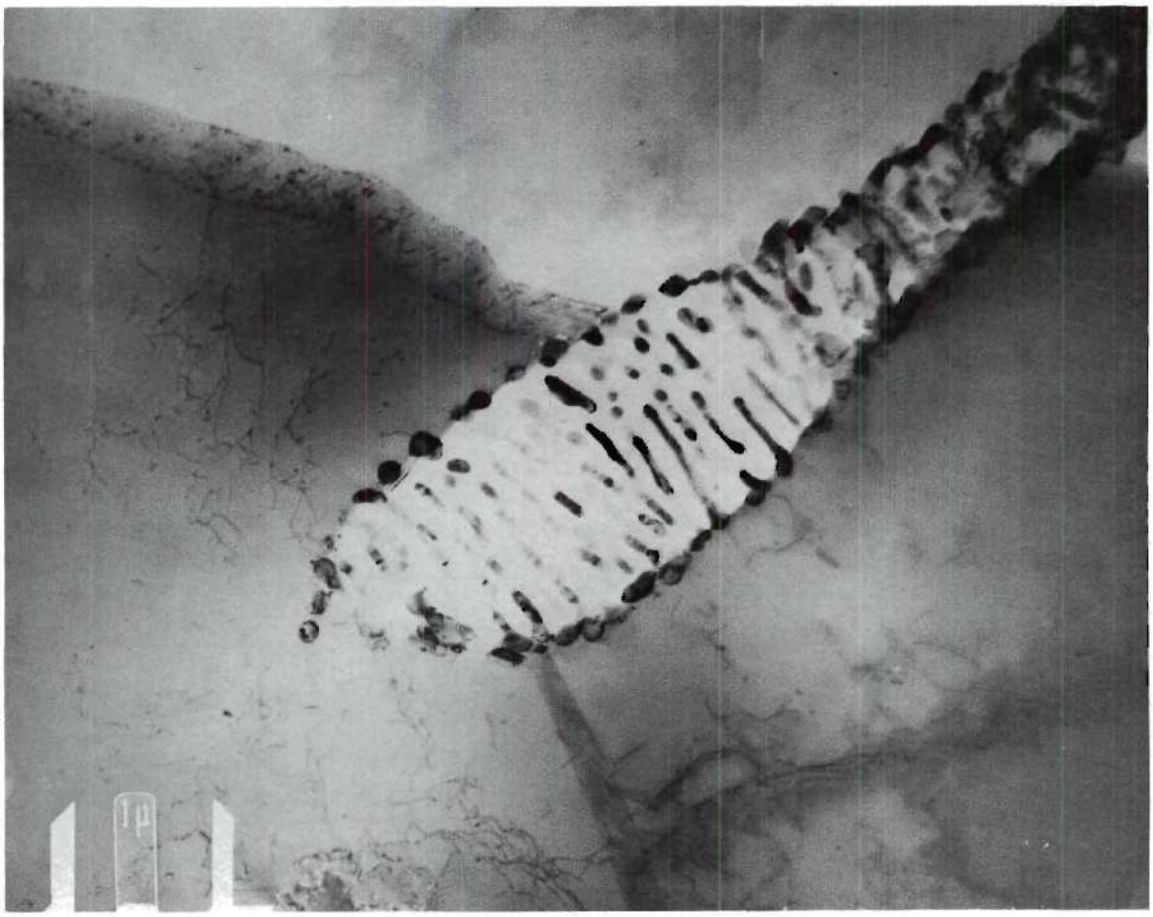

Figure 34. TEM of the Al-Fe-Co Microstructure after the First Pass, Showing Dislocations Forming Cells in the Vicinity of Precipitates.

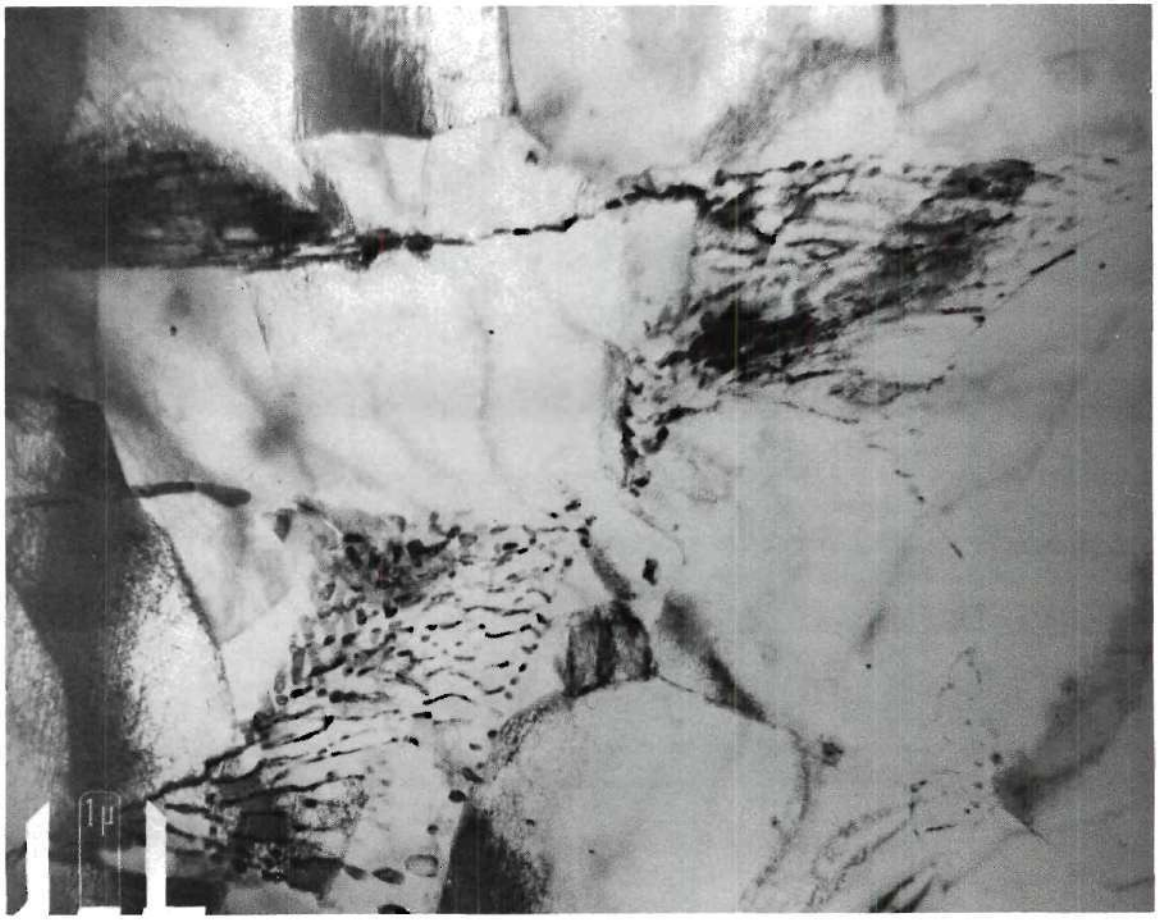

Figure 35. TEM of the Al-Fe-Co Microstructure After the Second Pass (59.2 Percent Reduction).

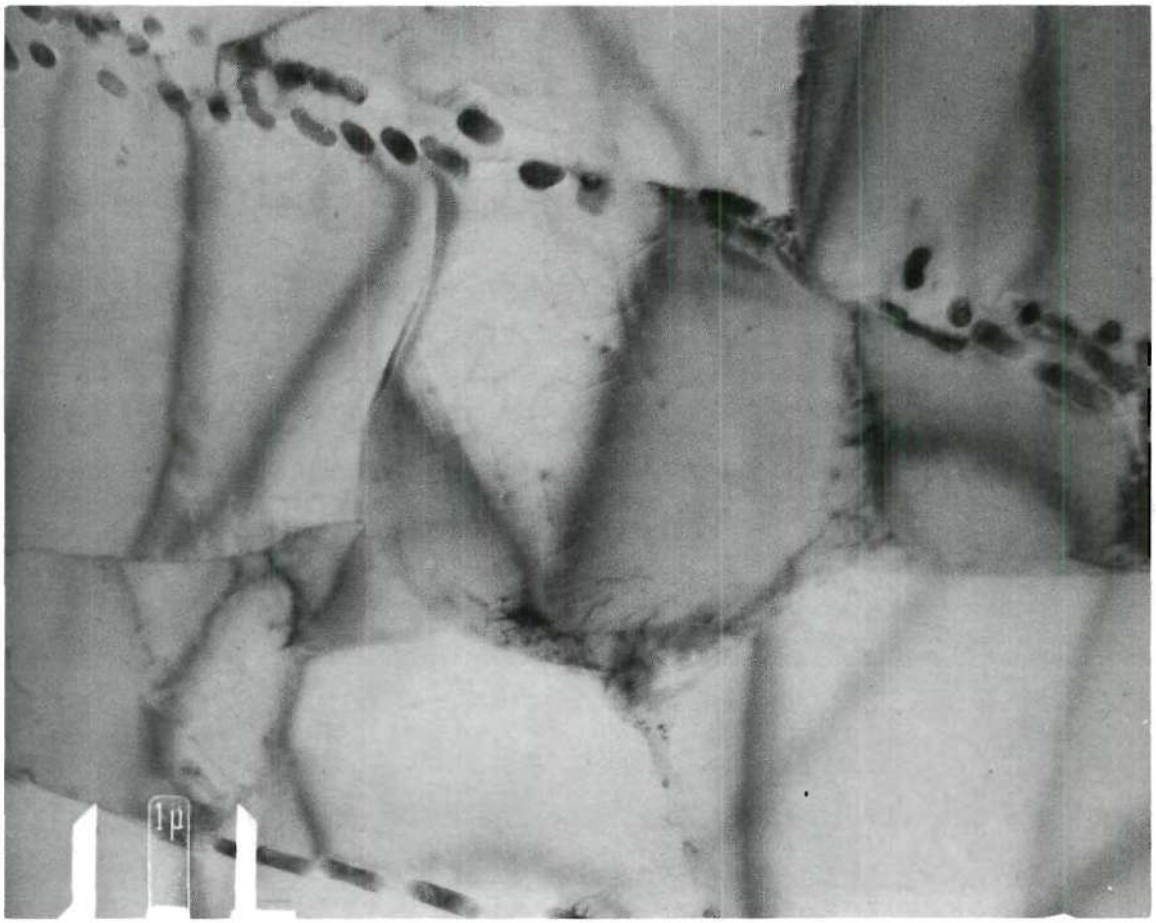

Figure 36. TEM of the Al-Fe-Co Microstructure After the Third Pass (69.2 Percent Reduction), Showing Further Cell Formation During Hot Rolling. Notice Refinement of the Cells Even in Areas Devoid of Precipitates.

Figure 37. TEM of the Al-Fe-Co Microstructure After the Fourth Pass (78.1 Percent Reduction), Showing Eutectic Colonies Surrounded by Cells.

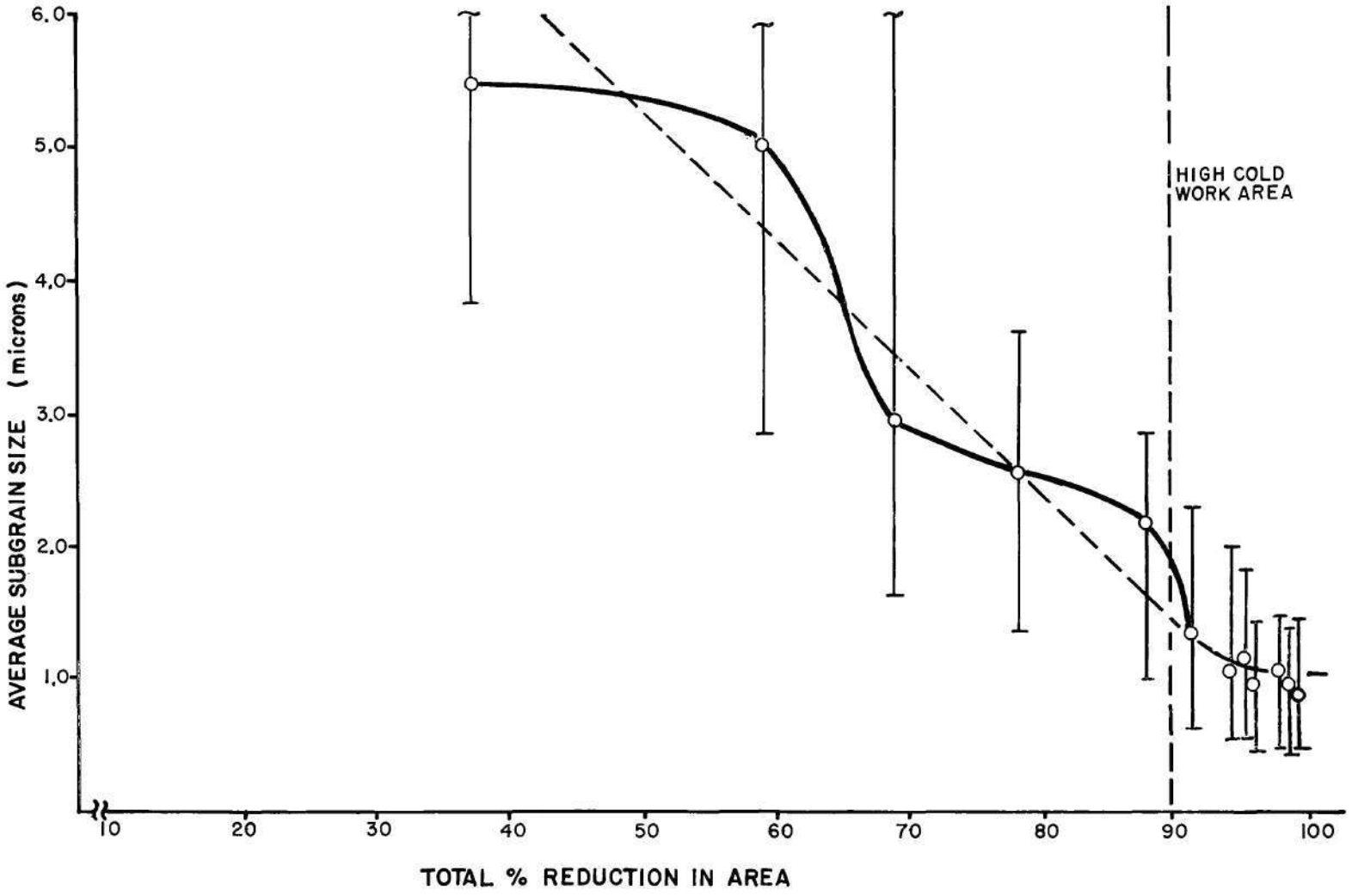

Figure 38. Decrease in Subgrain Size During Hot Rolling Al-Fe-Co Alloy.

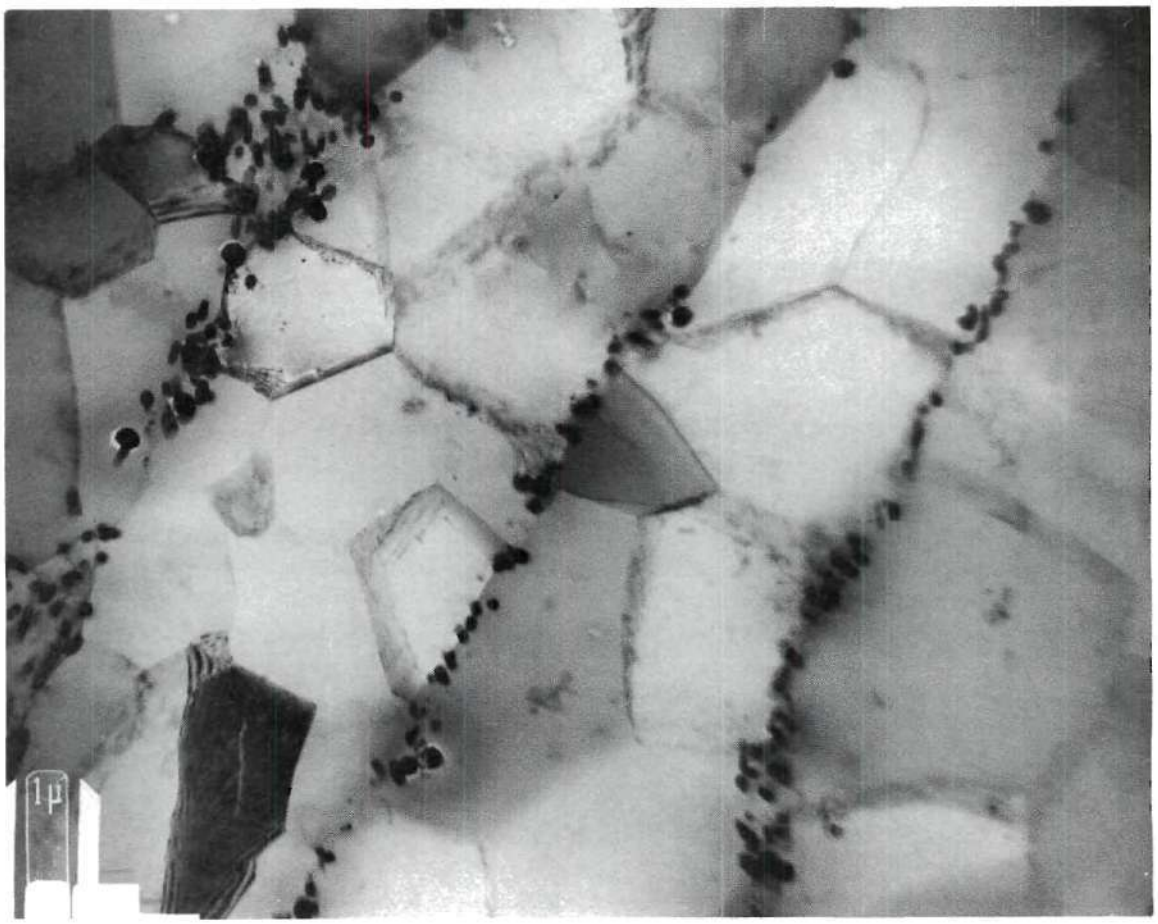

Figure 39. TEM of the Al-Fe-Co Microstructure After the Sixth Pass (88.4 Percent Reduction). A Higher Degree of Cell Uniformity is Present in this Specimen.

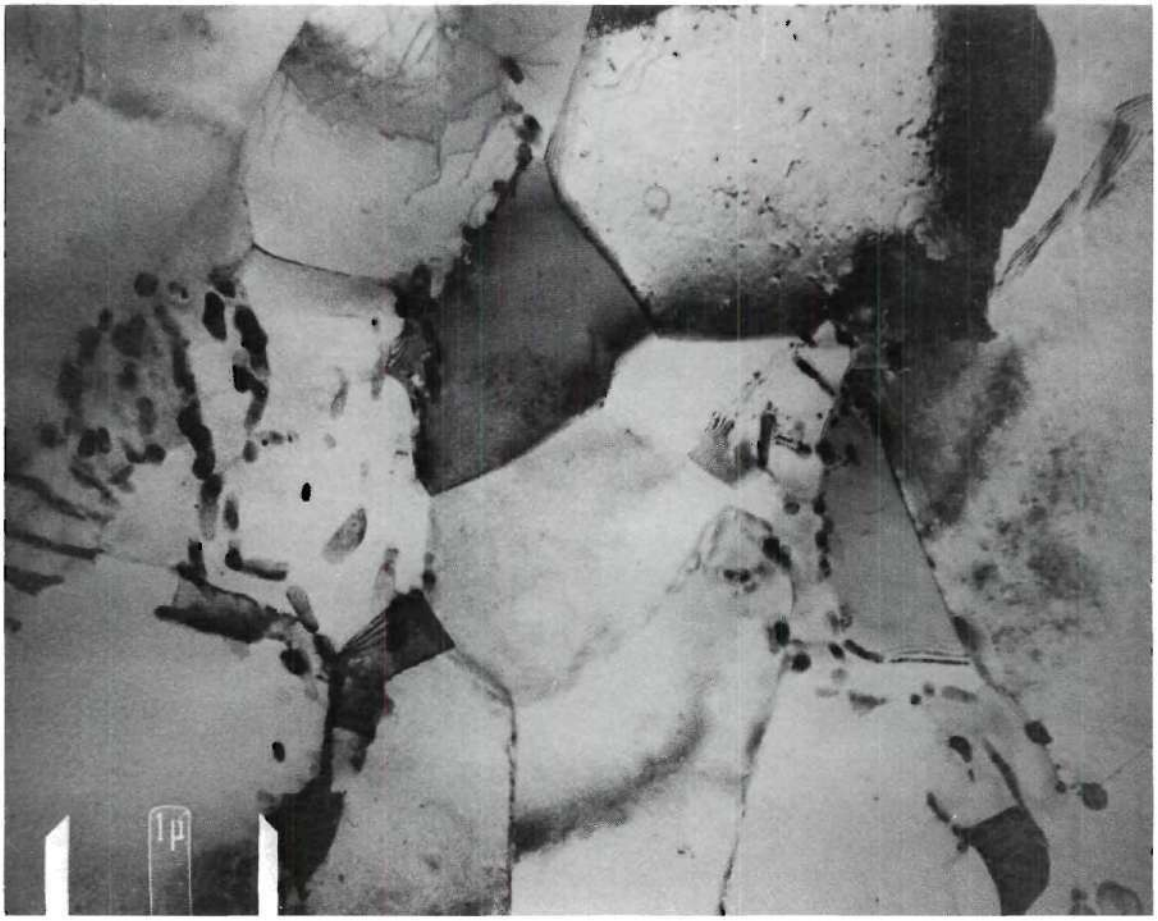

Figure 40. TEM of the Al-Fe-Co Microstructure After the Seventh Pass (91.3 Percent Reduction), Showing Increasing Dislocation Density Within the Cells Due to a Decrease in Dynamic Recovery at this Stage.

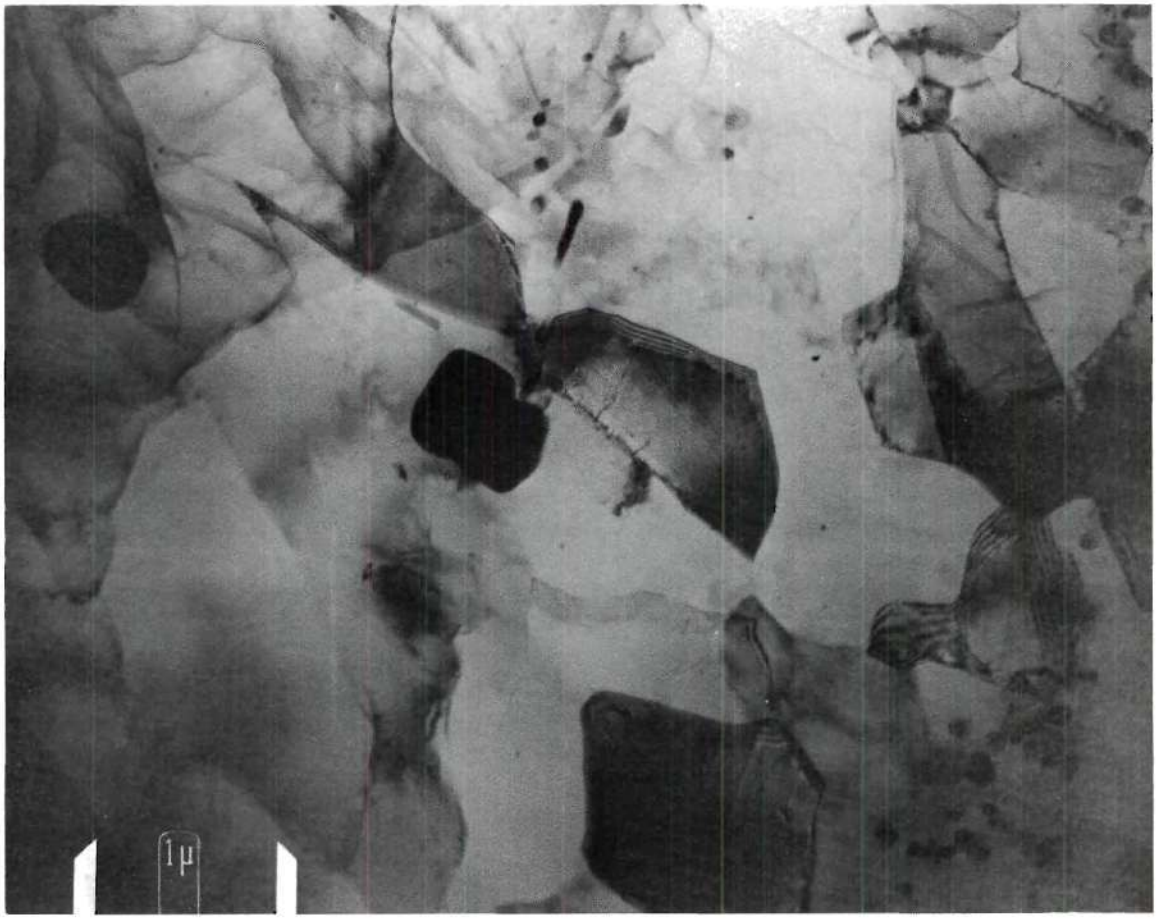

Figure 41. TEM of the Al-Fe-Co Microstructure After the Eighth Pass (94.0 Percent Reduction).

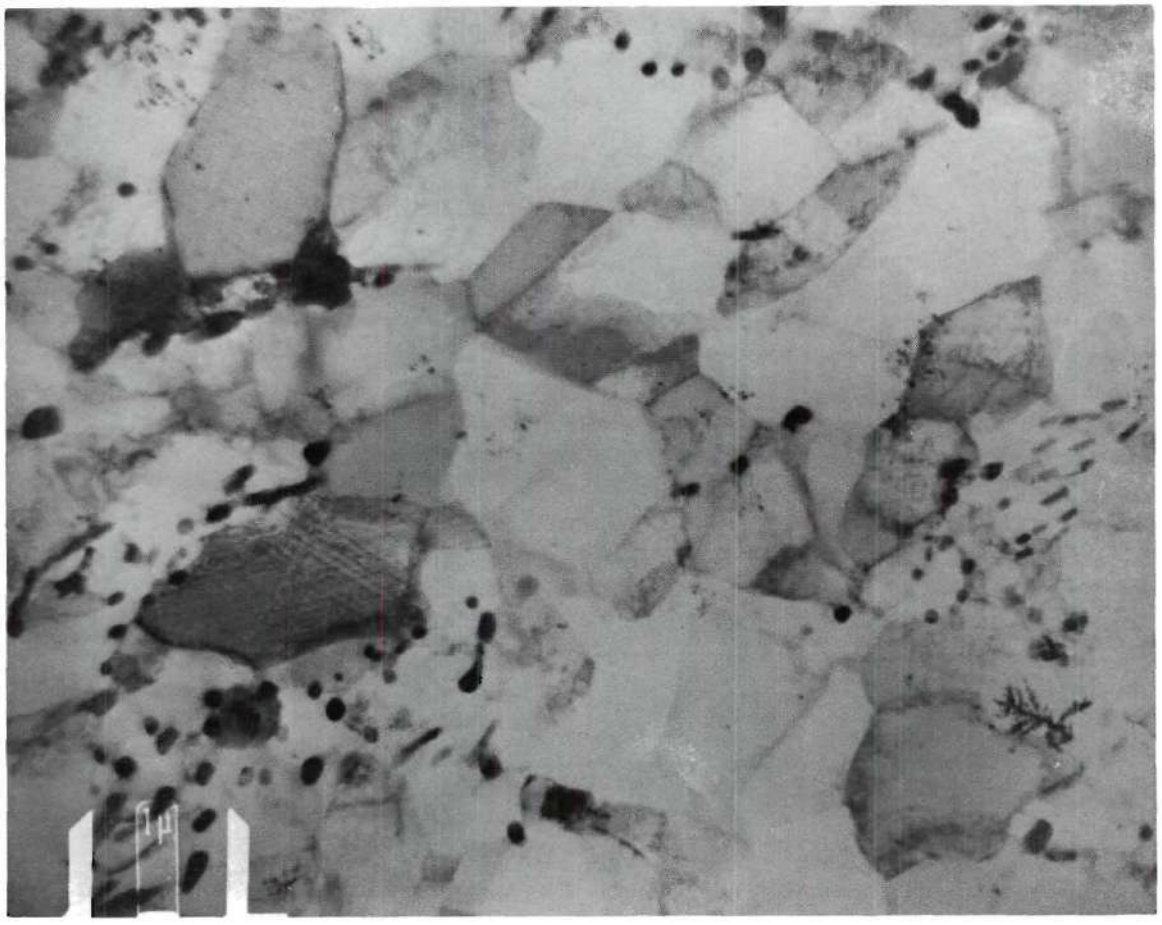

Figure 42. TEM of the Al-Fe-Co Microstructure after the Ninth Pass (95.5 Percent Reduction), Showing an Increasing Dislocation Density and a Significant Decrease in Cell Size.

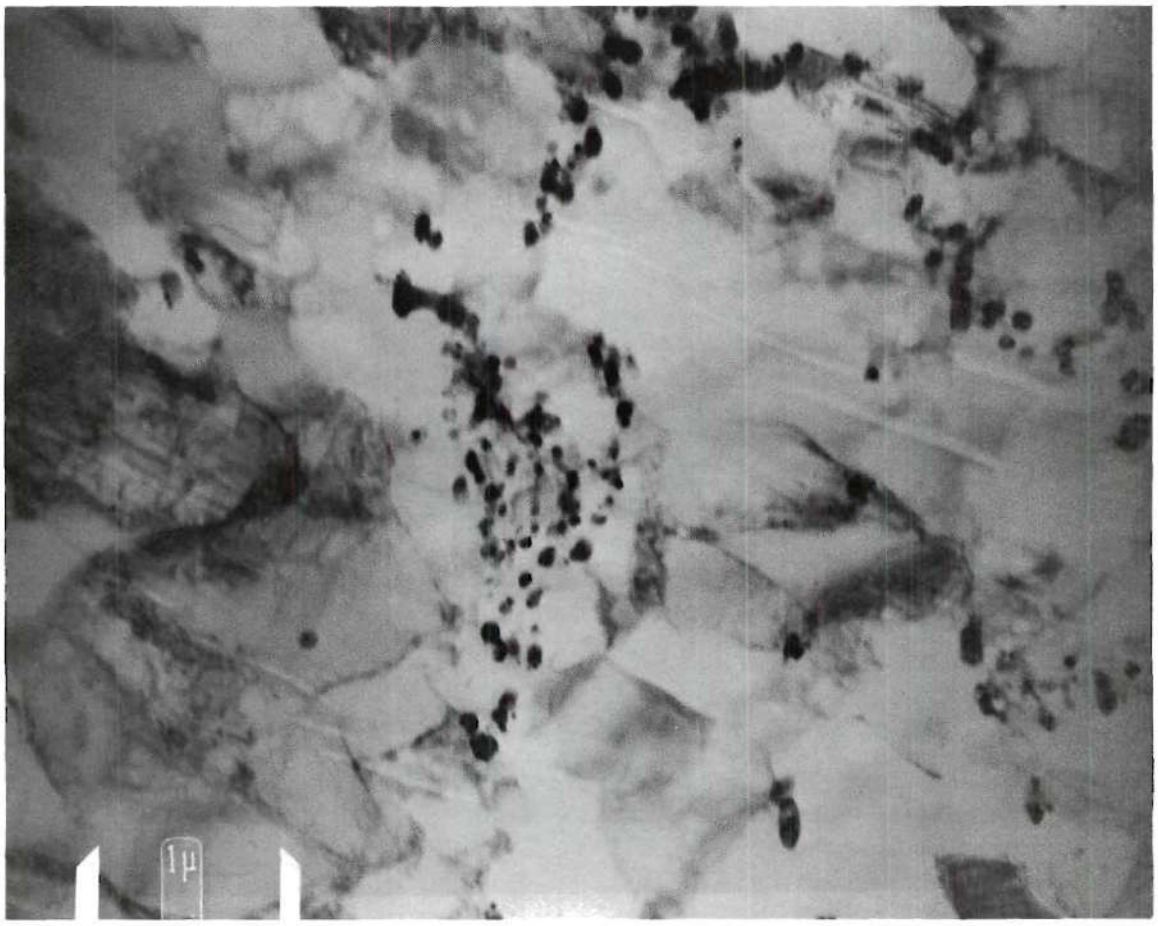

Figure 43. TEM of the Al-Fe-Co Microstructure after the Tenth Pass (96.8 Percent Reduction), and Showing Continuing Refinement of the Cell Size and Increasing Number of Dislocation Tangles.

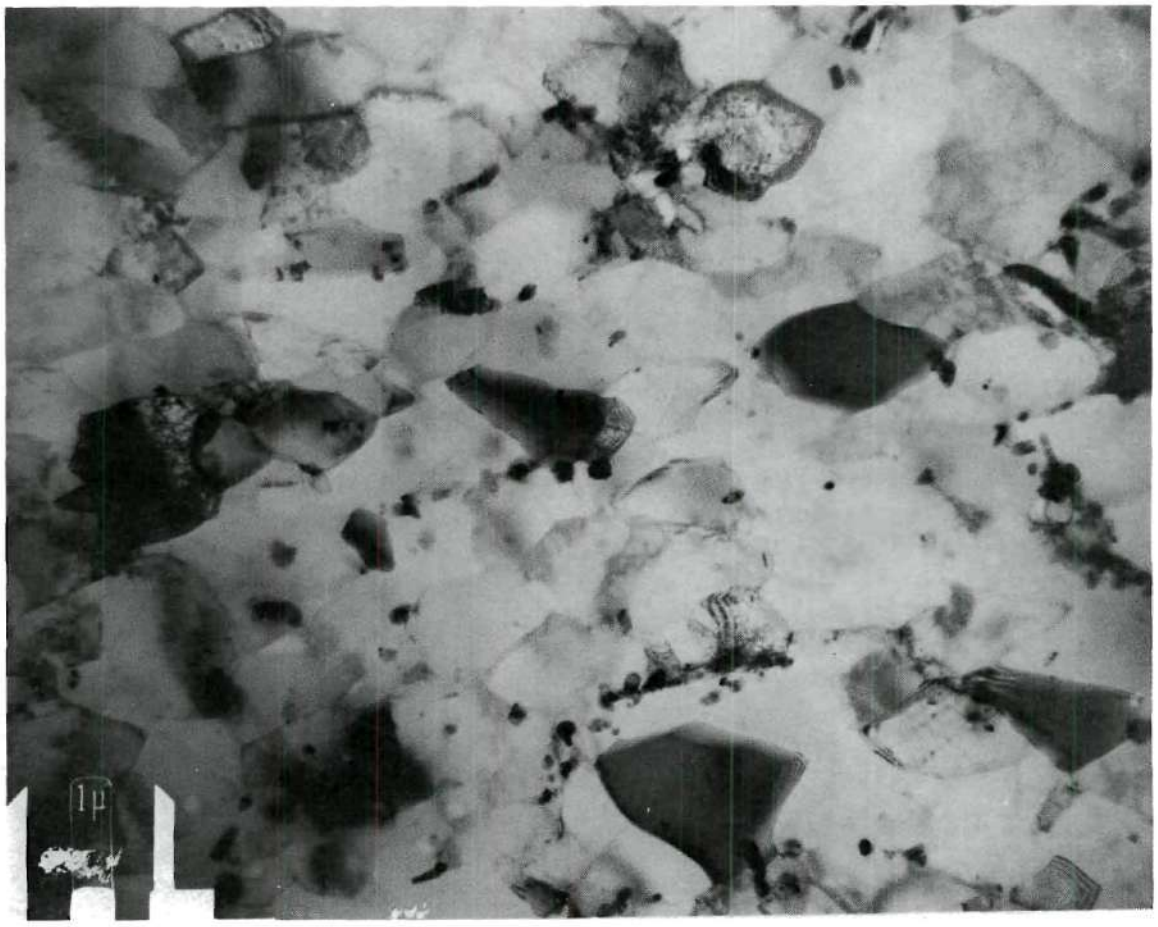

Figure 44. TEM of the Al-Fe-Co Microstructure after the Eleventh Pass (97.7 Percent Reduction), Showing a High Dislocation Density.

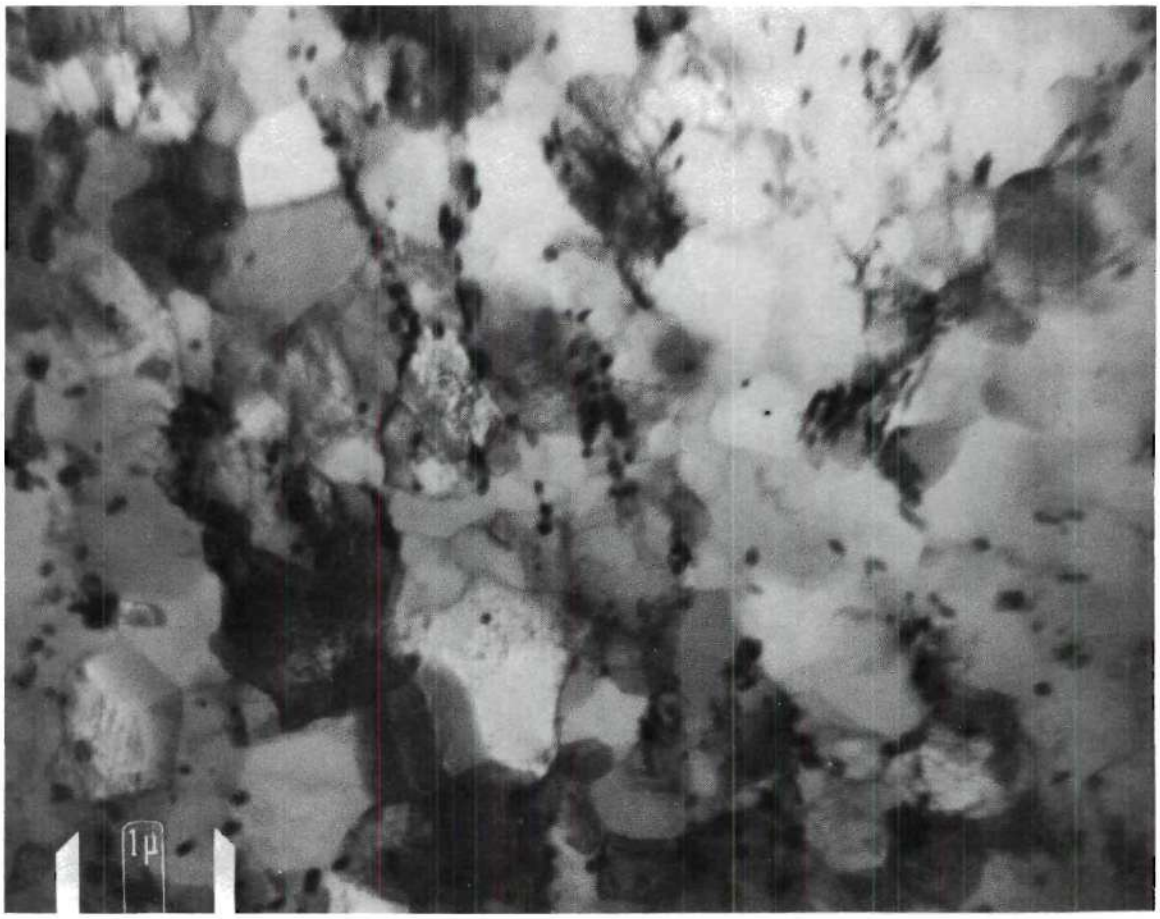

Figure 45. TEM of the Al-Fe-Co Microstructure after the Twelfth Pass (98.2 Percent Reduction).

a total reduction of 98.6 percent, Figure 30. Table 8 contains the cell size and size distribution after each stage of hot rolling. Figure 38 is a plot of cell size versus rolling pass number.

From Figure 38, which is a plot of the cell size versus the hot rolling reduction sequence, it can be observed that the cell size decreases progressively until the 9th pass (95.5 percent area reduction), and that there after there is no further decrease in cell size. Figure 26 shows that the ultimate tensile strength and yield strength continue to increase throughout the entire rolling process which indicates that the strengthening is due to other factors besides subgrain strengthening. It can be observed in Figures 39 through 45 that although the cell size remains constant, the dislocation density apparently increases as evidenced by the increase in cell wall thickness, "raggedness", and dislocation debris in the cell interior. This is produced by the cold work of the last seven reduction passes. Jonas, et al.[101] found that during hot extrusion and after the cell size becomes fixed, the dislocation density remains constant. When rolling the Al-Fe-Co alloy, the stress is not independent of the strain as it is in hot extrusion; therefore, the dislocation density increases significantly, producing further strain hardening.

EC Aluminum

In order to have a basis for comparison, the behavior of EC aluminum was investigated during hot rolling. The mechanical properties of the EC bars during hot rolling are enumerated in Table 9. Figure 46 depicts the variation of the tensile properties of EC aluminum during hot deformation. This can be compared with Figure 26 which shows the

Table 8. Variation in Subgrain Size with Rolling Passes (Al-Fe-Co Alloy).

ROLLING PASS NO.	% AREA REDUCTION	AVERAGE SUBGRAIN SIZE (MICRONS)	MINIMUM SIZE(MICRONS)	MAXIMUM SIZE (MICRONS)
1	37.3	5.4	3.8	-
2	59.2	5.0	2.8	-
3	69.2	2.9	1.6	-
4	78.1	2.5	1.3	3.7
5	82.8	-	-	-
6	88.4	2.1	1.0	3.3
7	91.3	1.3	0.5	2.3
8	94.0	1.0	0.4	2.0
9	95.5	1.1	0.4	1.8
10	96.8	0.9	0.3	1.6
11	97.7	1.0	0.4	1.7
12	98.2	0.9	0.3	1.5
13	98.6	1.0	0.3	1.6

Table 9. Mechanical Properties of Bars During Hot-Rolling for EC Aluminum

HOT ROLLING PASS NO.	PERCENT TOTAL REDUCTION IN AREA	ULTIMATE TENSILE STRENGTH(KSI)	YIELD TENSILE STRENGTH(KSI)	ELONGATION (10 INCHES PERCENT)
CAST	0	8.1	4.4	25
1	37.3	8.3	4.7	35
2	59.2	8.8	5.0	20.4
3	69.2	9.7	5.6	17.0
4	78.1	10.7	7.7	21.0
5	82.8	12.4	10.1	20
6	88.4	13.3	12.0	11.4
7	91.3	14.5	14.0	3.0
8	94.0	16.6	15.2	8.6
9	95.5	17.9	16.4	9.4
10	96.8	17.4	16.6	1.6
11	97.7	17.9	17.2	2.0
12	98.2	20.3	17.3	5.6
13	98.6	20.3	18.0	7.6

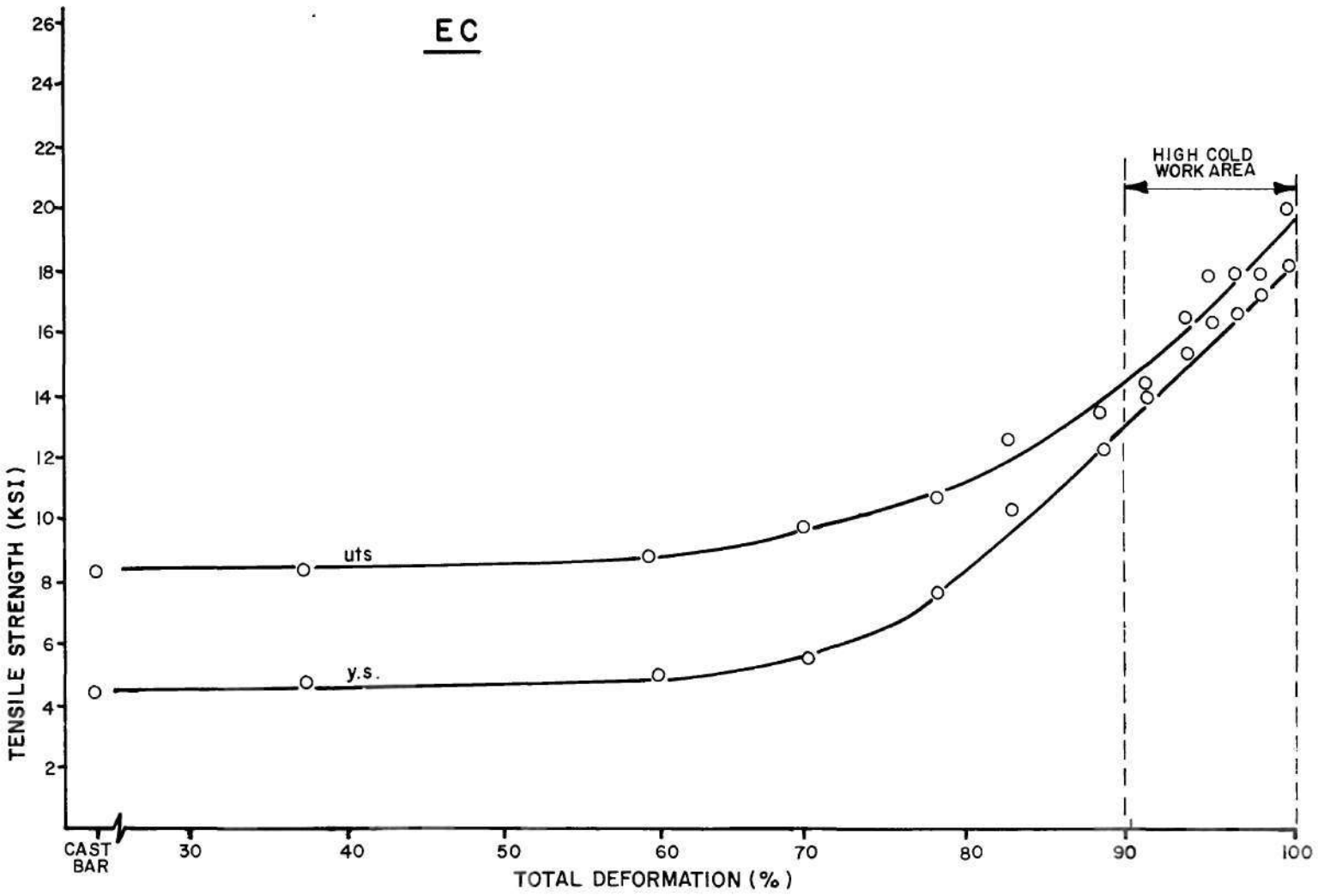

Figure 46. Variation of Ultimate Tensile Strength and Yield Strength with Percentage of Hot Deformation.

variation of tensile properties of Al-Fe-Co alloy during hot rolling. The main difference is observed in the high cold work area (above 90 percent reduction in area). The slope of the EC aluminum in this region is not as steep as that of Al-Fe-Co alloy as shown in Figure 28. This can be attributed to the presence of $(Co, Fe)_2 Al_9$ precipitates which produce a higher degree of work hardening in the region where dynamic recovery is negligible. This effect can be also observed in the behavior of the elongation during hot working as shown in Figure 47. The percentage of elongation sharply decreases above 90 percent reduction and remains basically the same for the remainder of the process.

Effect of Rod Annealing on the Substructure And Resulting Properties

The effect of rod annealing after hot rolling and before cold drawing was studied by comparing the physical and mechanical properties with the microstructure in the finished annealed wire. The Al-Fe-Co alloy hot rolled rod was annealed at 650°F for three hours, cold drawn to 0.105 inches diameter using standard B & S reductions and statically recovered at 550°F for three hours. The properties of this wire were compared to those of a wire produced without an intermediate anneal.

Figure 48 is a plot of the ultimate tensile strength, yield strength, percentage of elongation, and electrical conductivity for each of these products. The tensile strength of the rod decreased from 24.1 KSI to 16.4 KSI after annealing with a corresponding decrease in yield strength from 20.7 KSI to 10.9 KSI and a resulting increase in elongation from 7.0 percent to 28 percent. The significant changes in

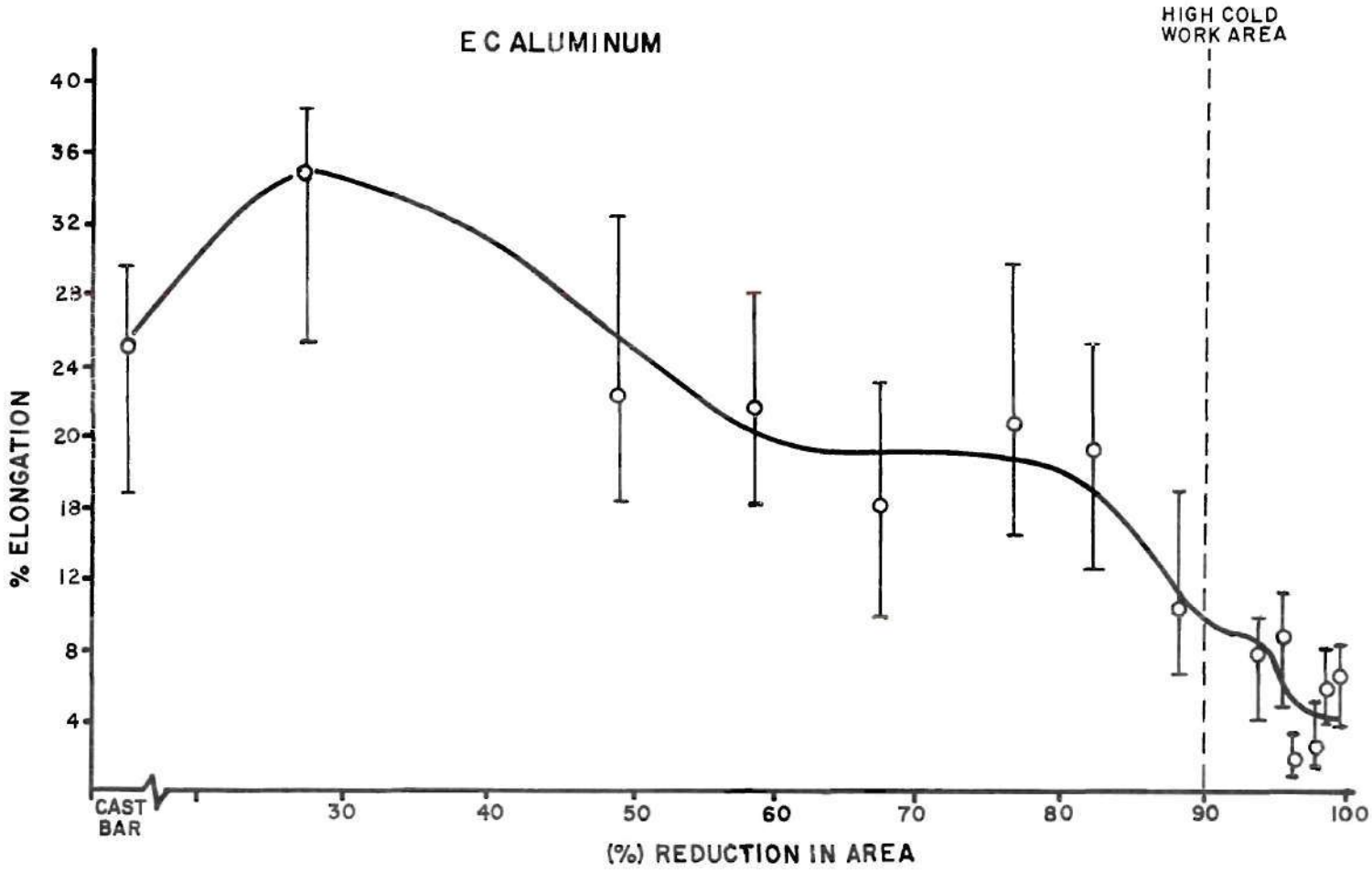

Figure 47. Variation of the Percentage of Elongation During Hot Deformation.

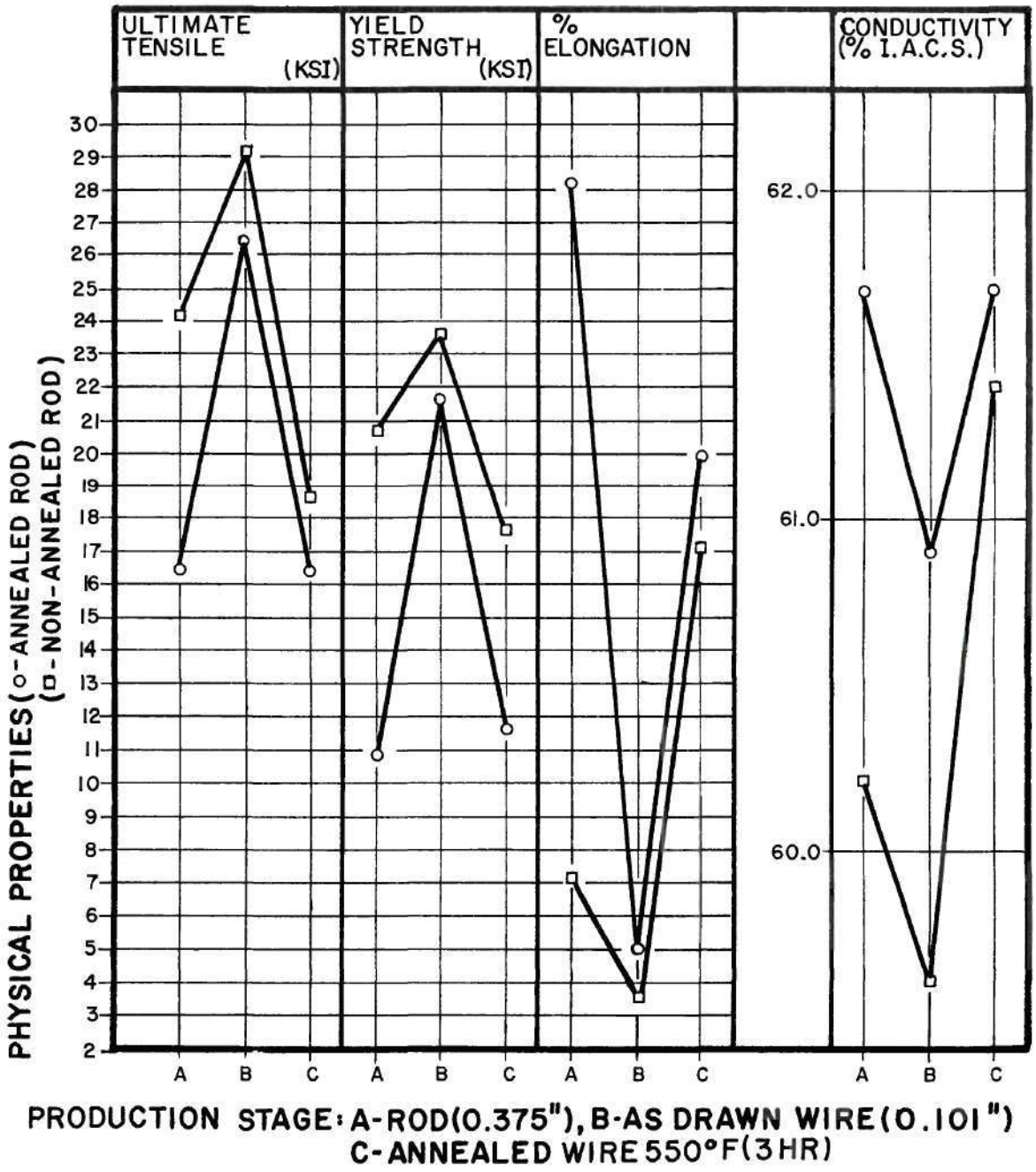

Figure 48. Comparison of the Physical and Mechanical Properties of Al-Fe-Co Products from Annealed Rod (650°F, Three Hours) to the Properties of the Corresponding Al-Fe-Co Products from Non-Annealed Rod.

physical and mechanical properties can be readily explained in terms of the microstructural changes taking place during annealing. Figure 49 is a TEM of the Al-Fe-Co alloy hot rolled rod showing a fine cell structure and several regions of precipitates. The average cell size of the material was measured as 0.9 microns. This structure shows a high density of dislocations between cell walls and around the precipitates. The fact that a certain degree of dynamic recovery has taken place during hot rolling is evidenced by the presence of well-defined, delineated polygonized subgrains in several areas of the specimens studied. In contrast, the substructure of the Al-Fe-Co alloy rod which was annealed showed sharply defined, large subgrains throughout the material (Figure 50). A structure containing delineated, polygonized subgrains is indicative of a fully recovered material.

The dramatic effect on properties and structure produced by annealing the hot-rolled rod remained after cold drawing. The ultimate tensile strength and yield strength of the annealed cold drawn wire produced from the non-annealed rod are 18.6 KSI and 17.6 KSI respectively. This can be compared to the 16.3 KSI and 11.7 KSI for the ultimate tensile strength and yield strength of the annealed wire produced from annealed rod. The greatest difference was obtained in the yield strength, while basically no difference was seen in the percent elongation and the electrical conductivity of the two finished wire products. This, of course, would be expected since the yield strength is the mechanical property which is most affected by microstructural changes produced by recovery treatments. This microstructure is observed in Figure 51 which is a TEM of the Al-Fe-Co alloy finished wire produced from non-

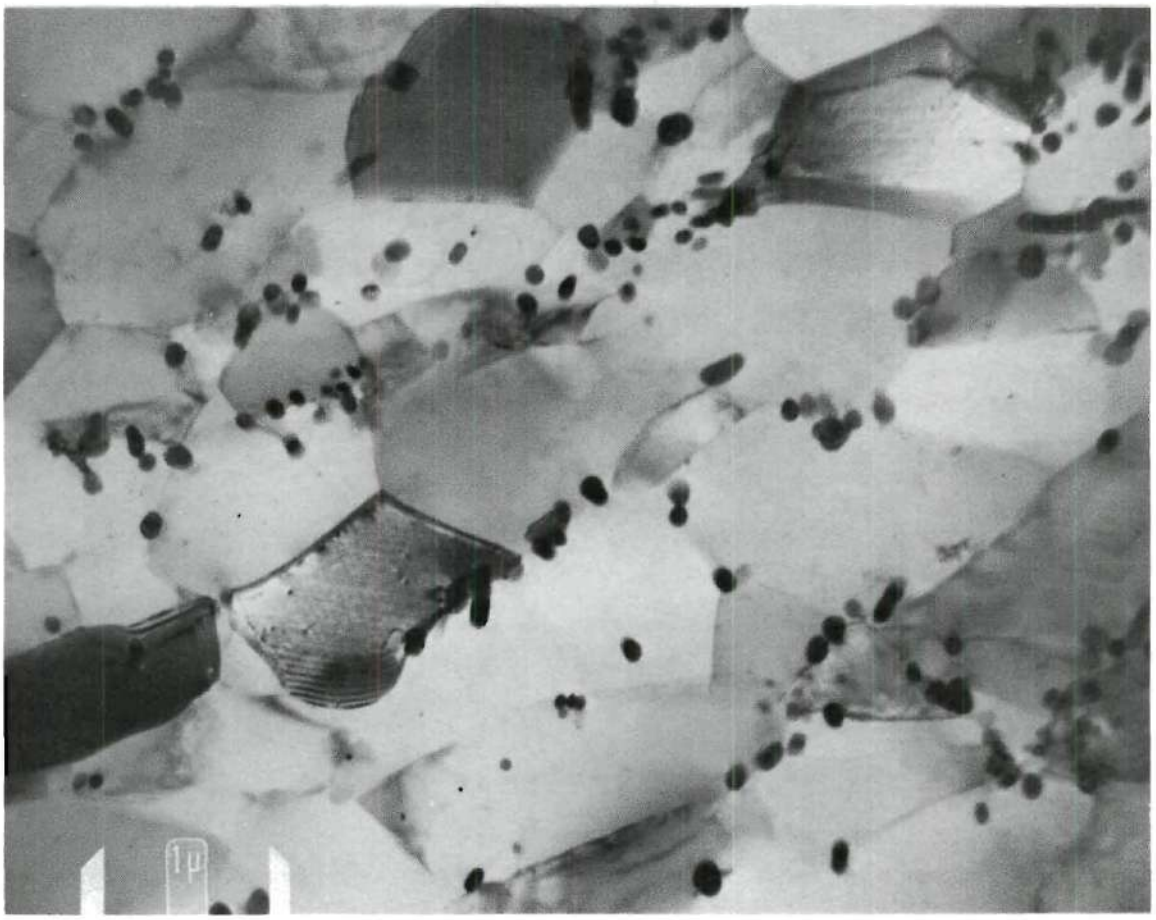

Figure 49. TEM of the Al-Fe-Co Alloy Hot-Rolled Rod Showing a Fine Cell Structure and the Precipitate Distribution.

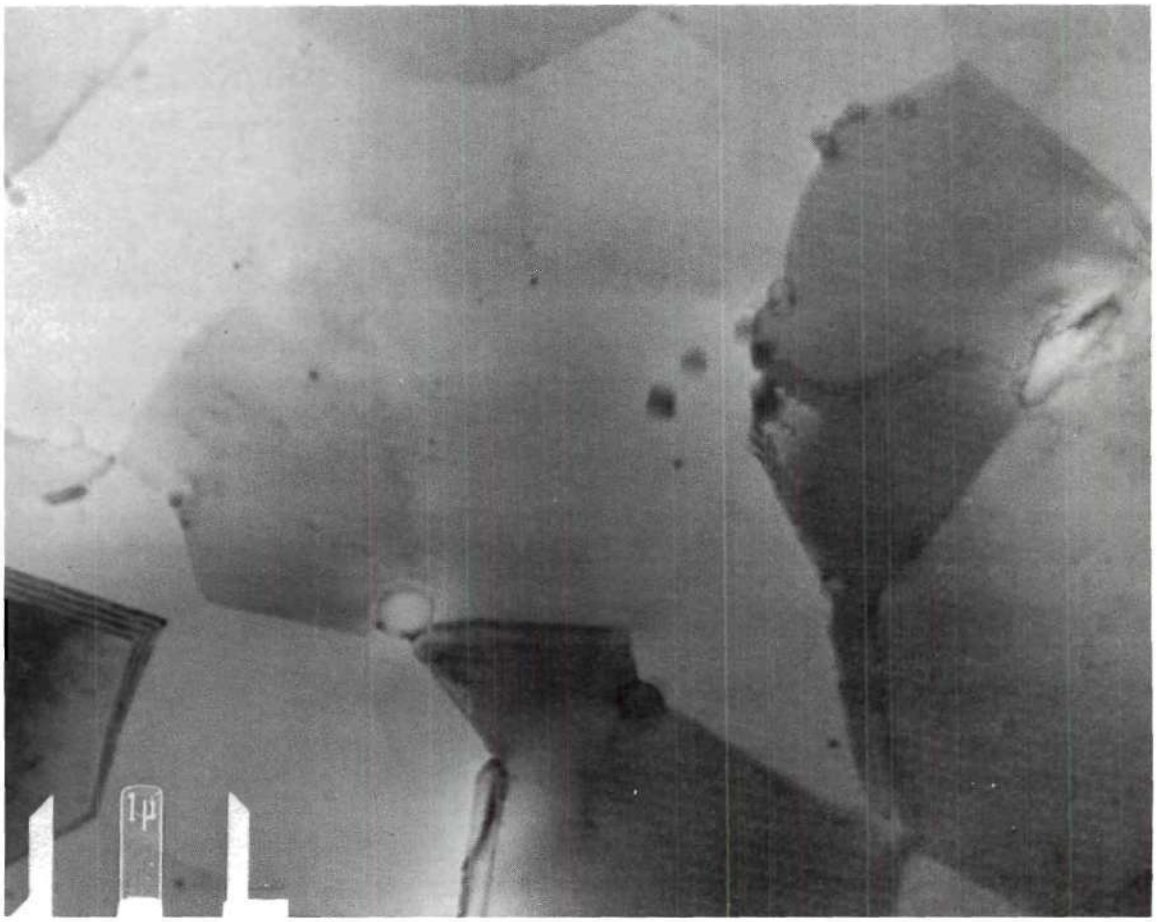

Figure 50. TEM of the Al-Fe-Co Alloy Rod Annealed at 650°F For Three Hours Resulting in a Conglomeration of Precipitates and in a Sharply Defined, Polygonized Subgrain Wall.

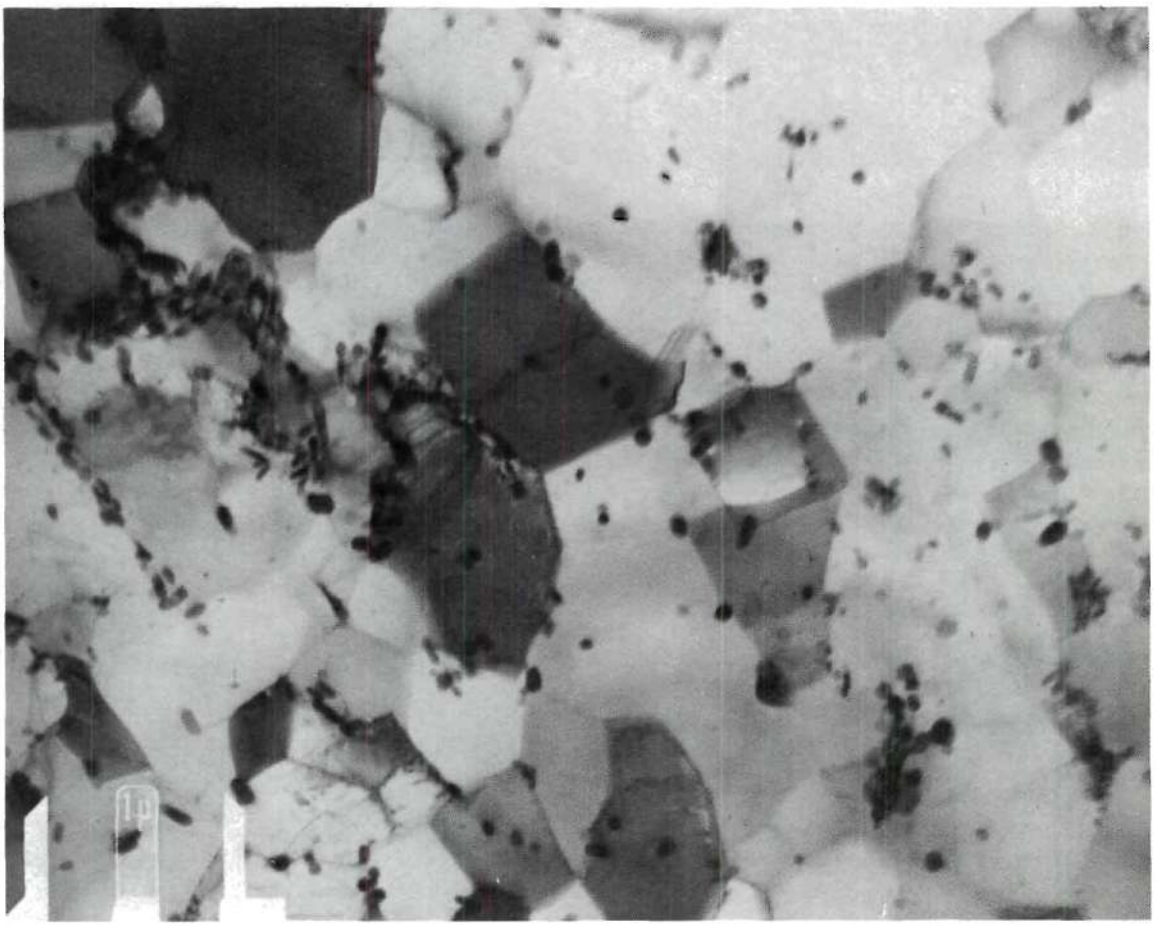

Figure 51. TEM of the Al-Fe-Co Alloy Annealed Wire Produced from Rod Annealed at 650°F for Three Hours.

annealed rod. The substructure consists of a fine dispersion of precipitates which range in size from 200 angstrom to 1100 angstrom. The subgrain size in this material ranged from 0.2 microns to 0.9 microns with an average subgrain diameter of 0.5 microns. It is important to point out that the subgrain diameter is approximately of the same magnitude as the interprecipitate spacing in the matrix, which indicates the importance of the precipitates and their distribution for pinning the subgrain boundaries during the recovery process. This is further illustrated in Figure 52 which is a TEM of the Al-Fe-Co alloy rod annealed at 650^{o}F for three hours showing dramatically the pinning effect of the precipitates on the subgrain boundary.

The subgrains present in the wire produced from annealed rod (Figure 51) have well defined, thin walls and are basically devoid of internal dislocations.

TEM observations of the finished wire product (Figure 53) show that the substructure contains larger subgrains with an average subgrain size of 1 micron. The subgrain walls are not as delineated as those from Figure 50, and the precipitates are larger and not so uniformly distributed. The precipitates of the wire from annealed rod ranged in size from 600 angstroms to 2500 angstroms. In this case (Figure 51) inter-precipitate spacings were twice as large as those in the wire produced from non-annealed rod. It can be concluded that since both rod products (annealed after rolling and non-annealed after rolling) were cold drawn to the same size after cold drawing, the annealing treatment of the rod produced large precipitates, not as well distributed as those in the non-annealed product. It is possible that the increased

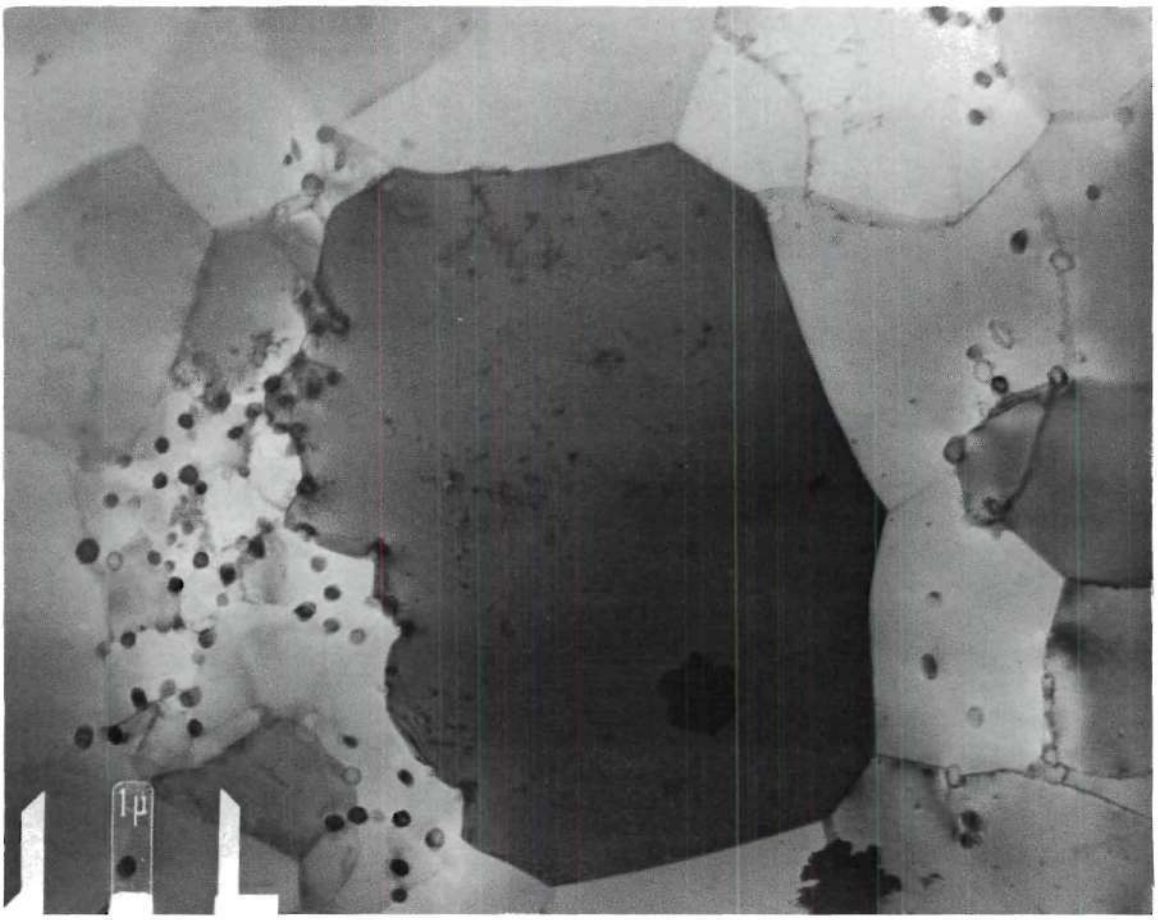

Figure 52. TEM of the Al-Fe-Co Alloy in the Rod Form Which was Annealed at 650°F for Three Hours Showing the $FeAl_3$ and $(Fe,Co)_2Al_9$ Precipitates Pinning the Cell Boundary from Further Coalescence During Annealing. Note the Fine Subgrains Present in the High Precipitate Density Area as Opposed to the Large Subgrains in the Precipitate-Free Regions.

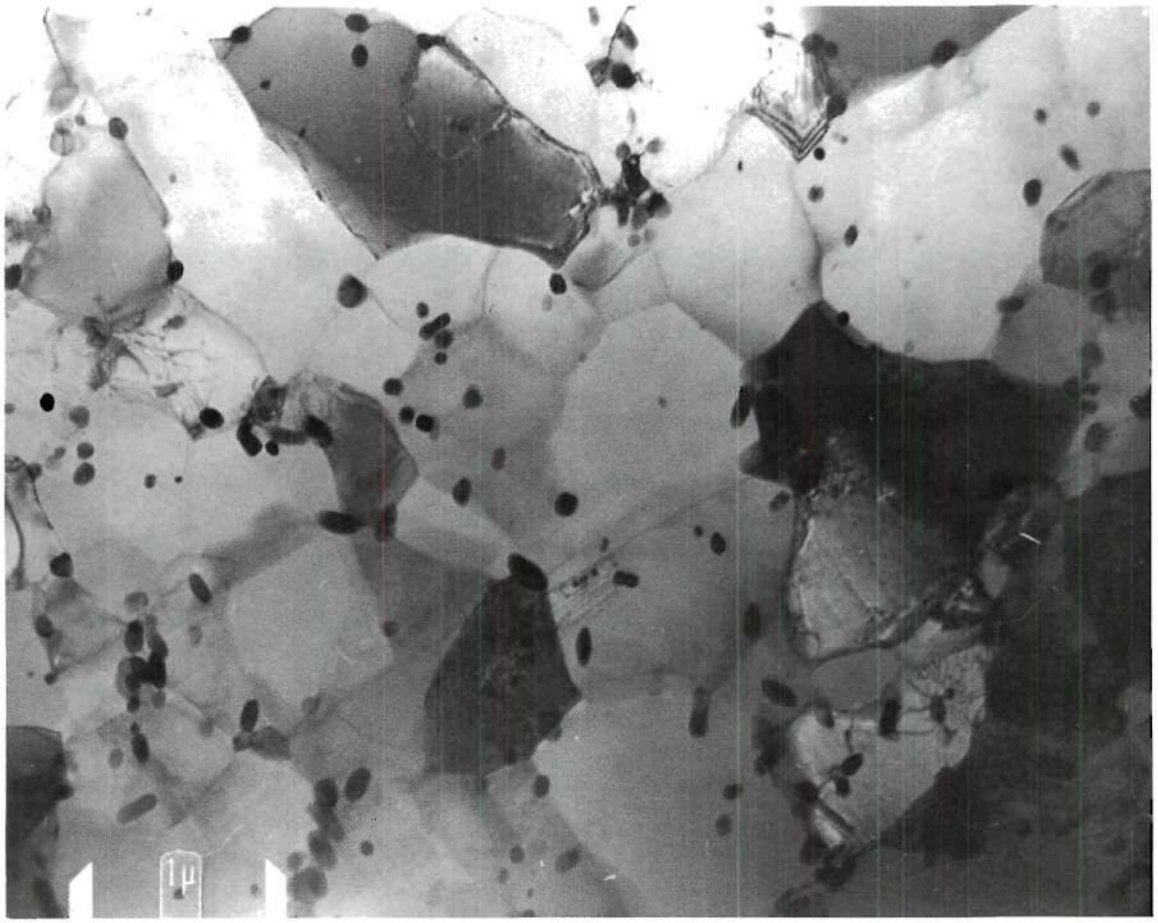

Figure 53. TEM of the Al-Fe-Co Alloy Annealed Wire Product from Annealed Rod Showing Large Subgrains with an Average Size of 1.1μm.

size of the particles takes place by the resolutioning of the particles below the critical size for that temperature. Diffusion of the iron and cobalt in solution to existing precipitates results in larger precipitate particles.[102] The solid solubilities of iron in aluminum and cobalt in aluminum at 300°C (572°F) are 0.002 weight percent and 0.01 weight percent respectively. Since the solid solubility of iron and cobalt at room temperature are negligible, the difference in solubility at 572°F is sufficient to produce reversion and reprecipitation.[67] In addition, the effect produced by secondary precipitation during annealing is absent since any iron and cobalt present in solution in the rod product would be precipitated out during rod annealing leaving a solute depleted matrix.

Effect on EC Material

A reduction of cell size similar to that produced in the Al-Fe-Co alloy product was found to take place in EC material. Figure 54 is a plot of the mechanical and physical properties of the EC after the different processes. A significant difference in yield strength of 4.6 KSI was obtained between finished wires produced from non-annealed and annealed rods. This difference can also be explained in terms of the resulting substructure. Figure 55 is a TEM of the hot-rolled EC rod showing a certain amount of dynamic recovery as evidenced by the presence of fine, delineated subgrain walls. The corresponding TEM of the finished wire from non-annealed rod is shown in Figure 56. This substructure contains an average cell size of 1.6 microns and exhibits a fully recrystallized structure as evidenced by the large, well-defined polygonized subgrains.

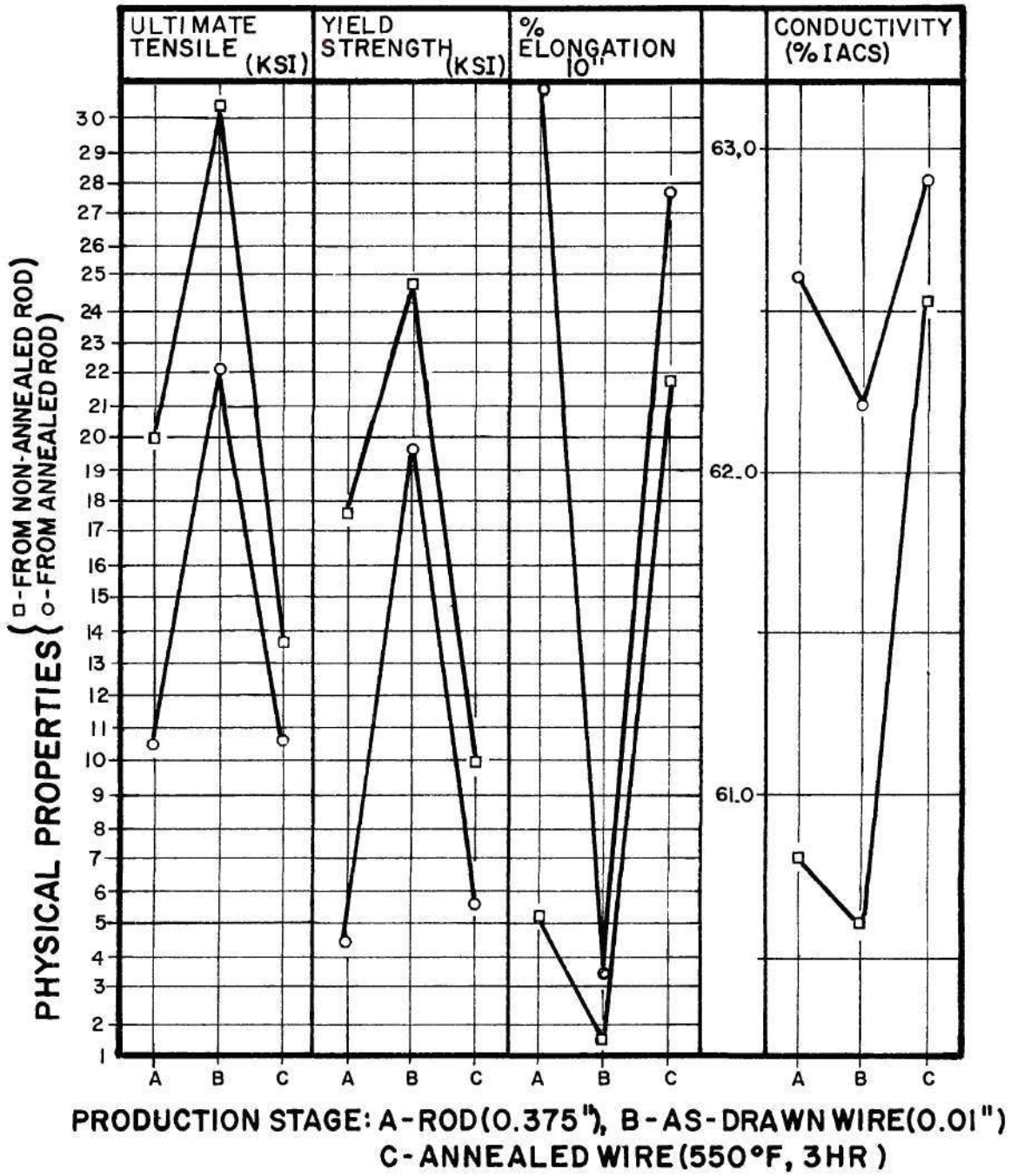

Figure 54. Comparison of the Physical Properties of EC Products Produced from Annealed Rod (650°F, Three Hours) to the Corresponding EC Products Produced from Non-Annealed Rod.

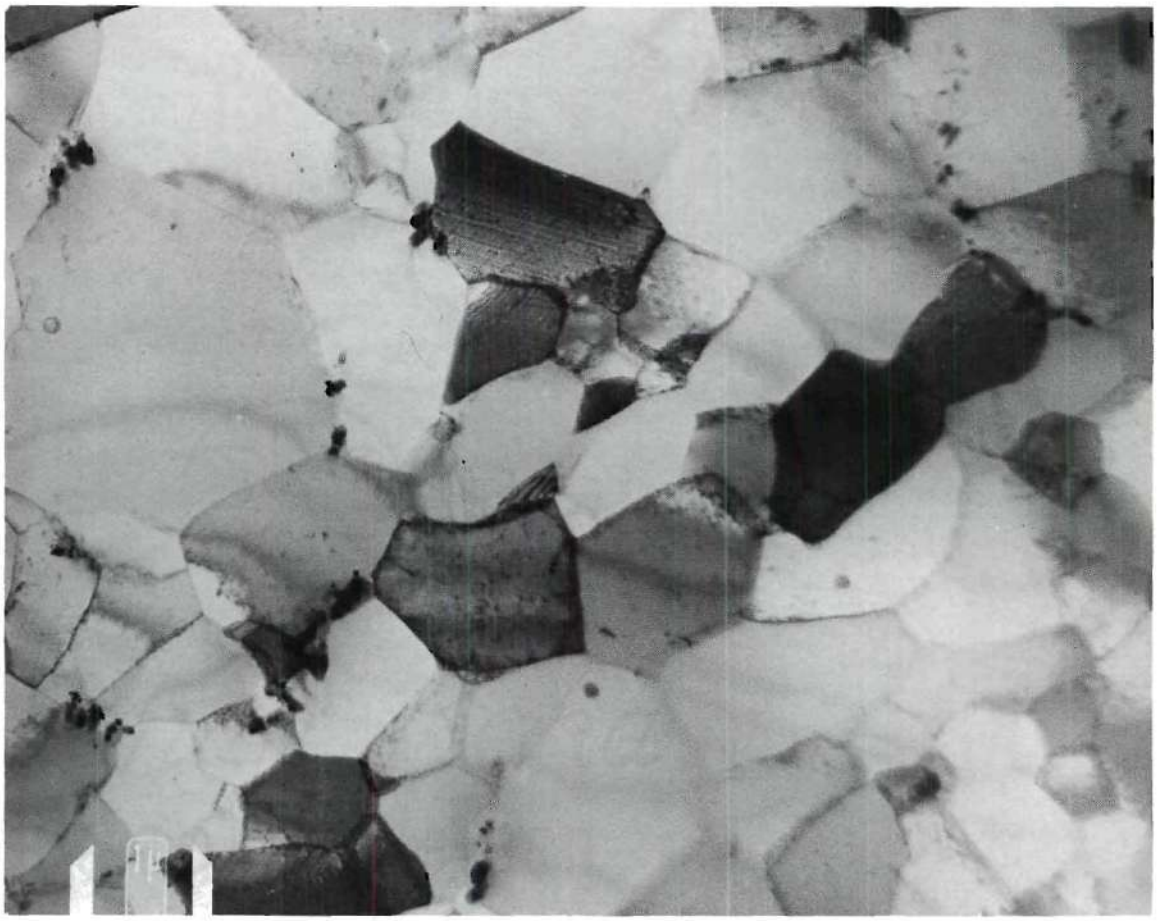

Figure 55. TEM of the Hot Rolled EC Rod Showing a Certain Amount of Dynamic Recovery as Evidenced by the Presence of Fine, Delineated Subgrain Walls.

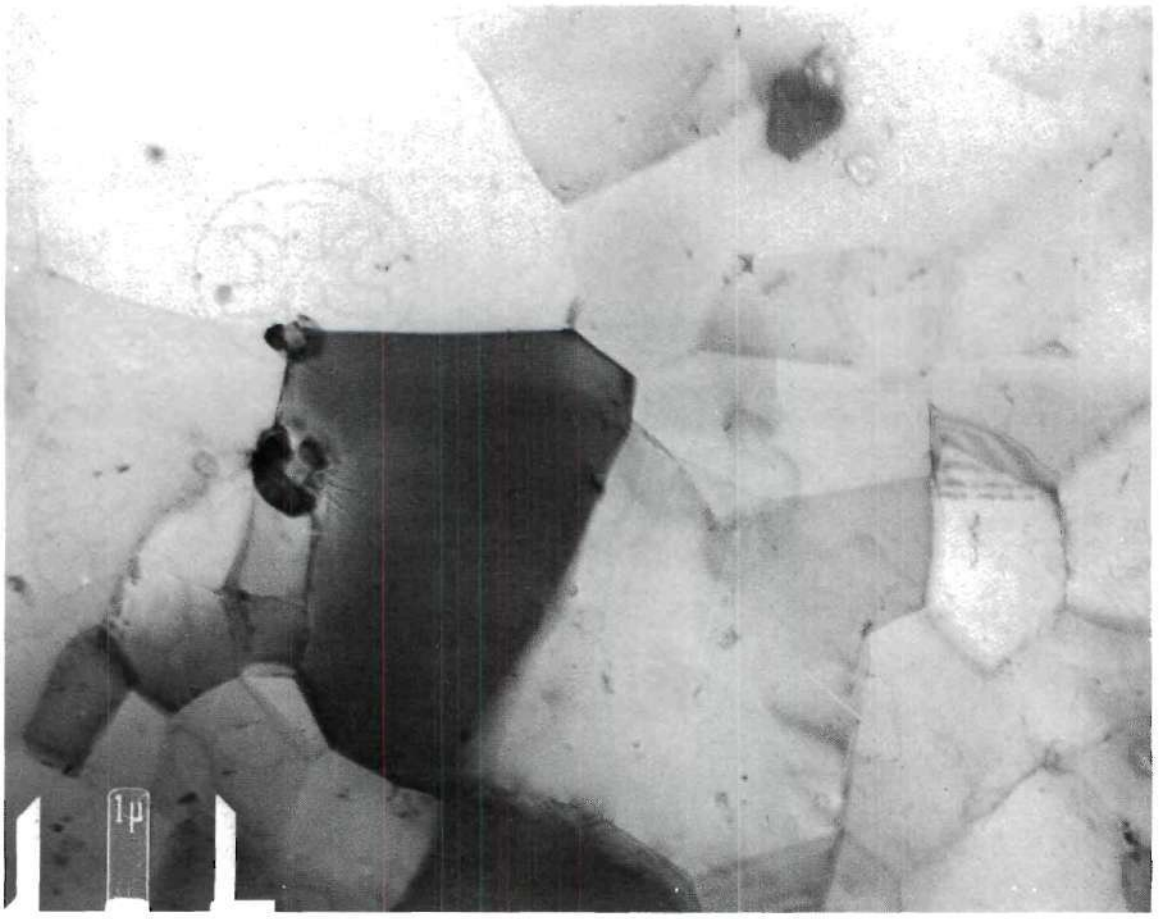

Figure 56. TEM of the Annealed Wire Produced from Non-Annealed Rod Exhibiting a Non-Uniform Structure Containing Large and Small Subgrains.

An even greater effect was obtained after annealing the EC wire from annealed rod as shown by a comparison of Figure 57 which is the TEM of the annealed rod and Figure 58 which exhibits the substructure of the annealed wire from annealed rod. The annealed rod exhibits some thicker non-linear walls and does not show signs of complete recrystallization as does the annealed wire (Figure 58). This can be explained by the fact that a certain amount of dynamic recovery took place during hot rolling and the resulting structure was not as unstable thermodynamically as the structure obtained after cold drawing.[103] The average cell size of the annealed EC wire from annealed rod is 4.1 microns with a range from 1.9 microns to 9.0 microns. Besides the large size of the annealed subgrains, an important feature present in the EC product is the high degree of non-uniformity present which can be evidenced by the subgrain size range.

Annealing Characteristics

The mechanical and electrical properties of the 0.105 inch diameter wire produced from the 0.5 percent Co, 0.5 percent Fe alloy which was continuously (rapidly solidified) cast and rolled rod were determined at room temperature after one-hour anneals. The results are shown in Figures 59, 62, 63. The ultimate tensile strength and yield strength increased between 500 and 3000 psi after annealing between 200°F and 350°F, as shown in Figure 59. The maximum increase of 3000 psi occurred at 300°F. Figure 62 shows that there was also a decrease in elongation during heating at these temperatures. Some solid state precipitation probably of the phases $FeAl_3$ and $(CoFe)_2Al_9$[67] took place as shown in Figure 60 and 61. These precipitates which were not present in the

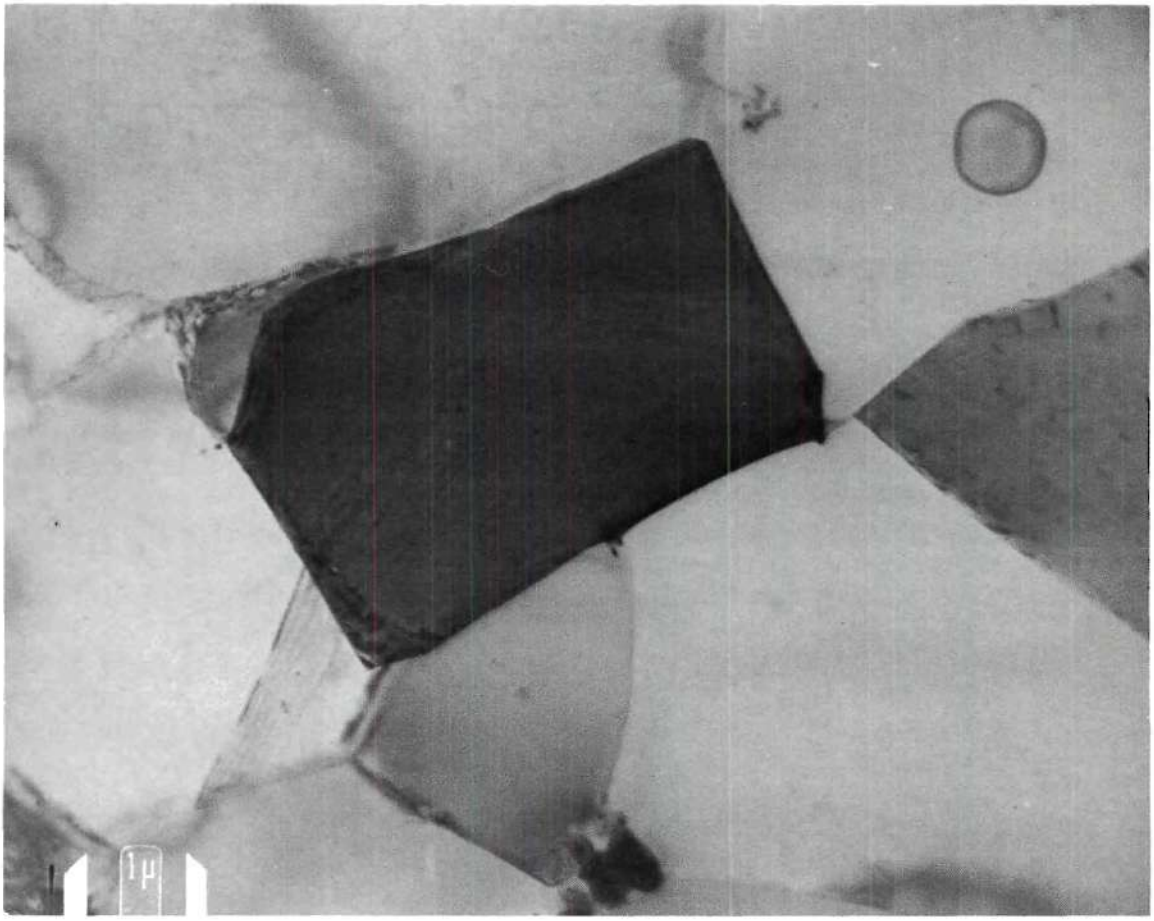

Figure 57. TEM of EC Rod Which was Annealed at 650°F for Three Hours Showing Large Polygonized Subgrains.

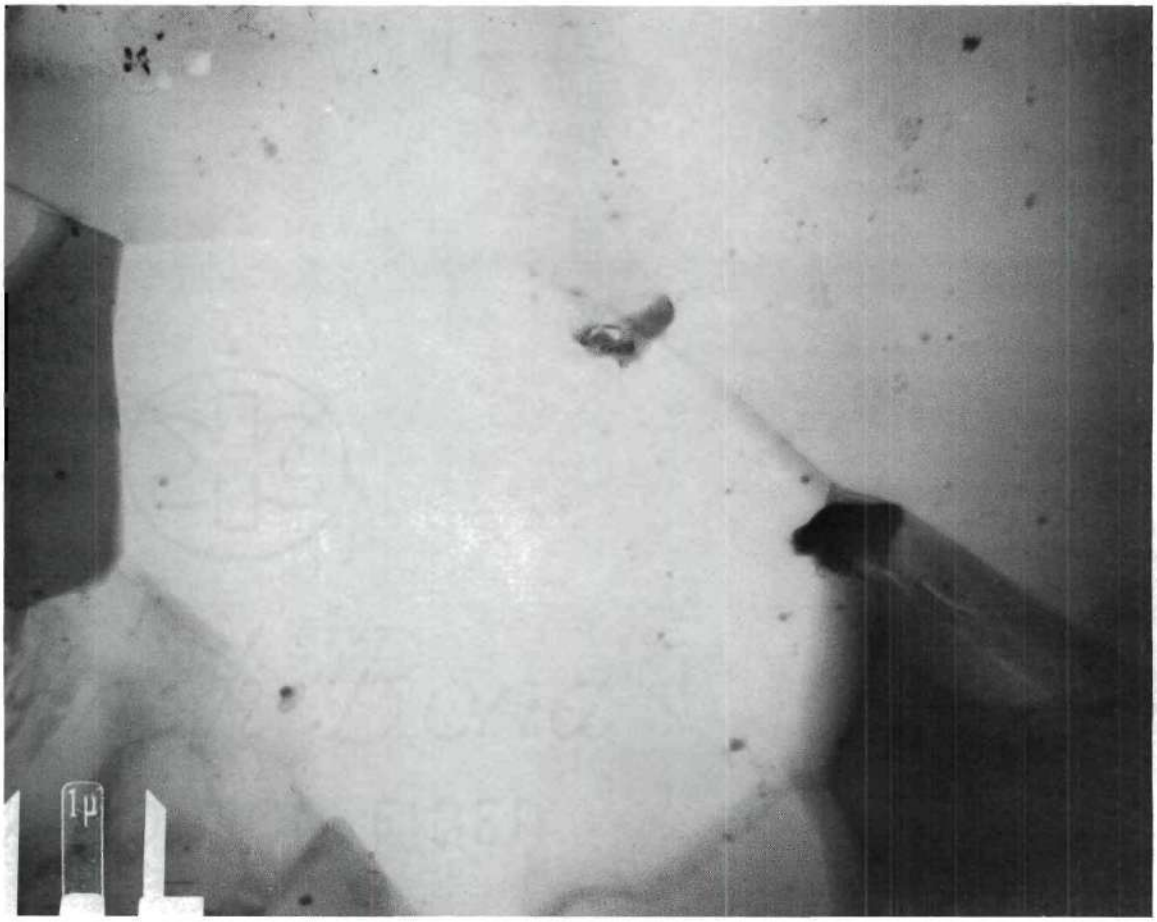

Figure 58. TEM of the EC Finished Wire Produced from Rod Which was Annealed at 650°F for Three Hours Showing Very Large, Recrystallized Subgrains.

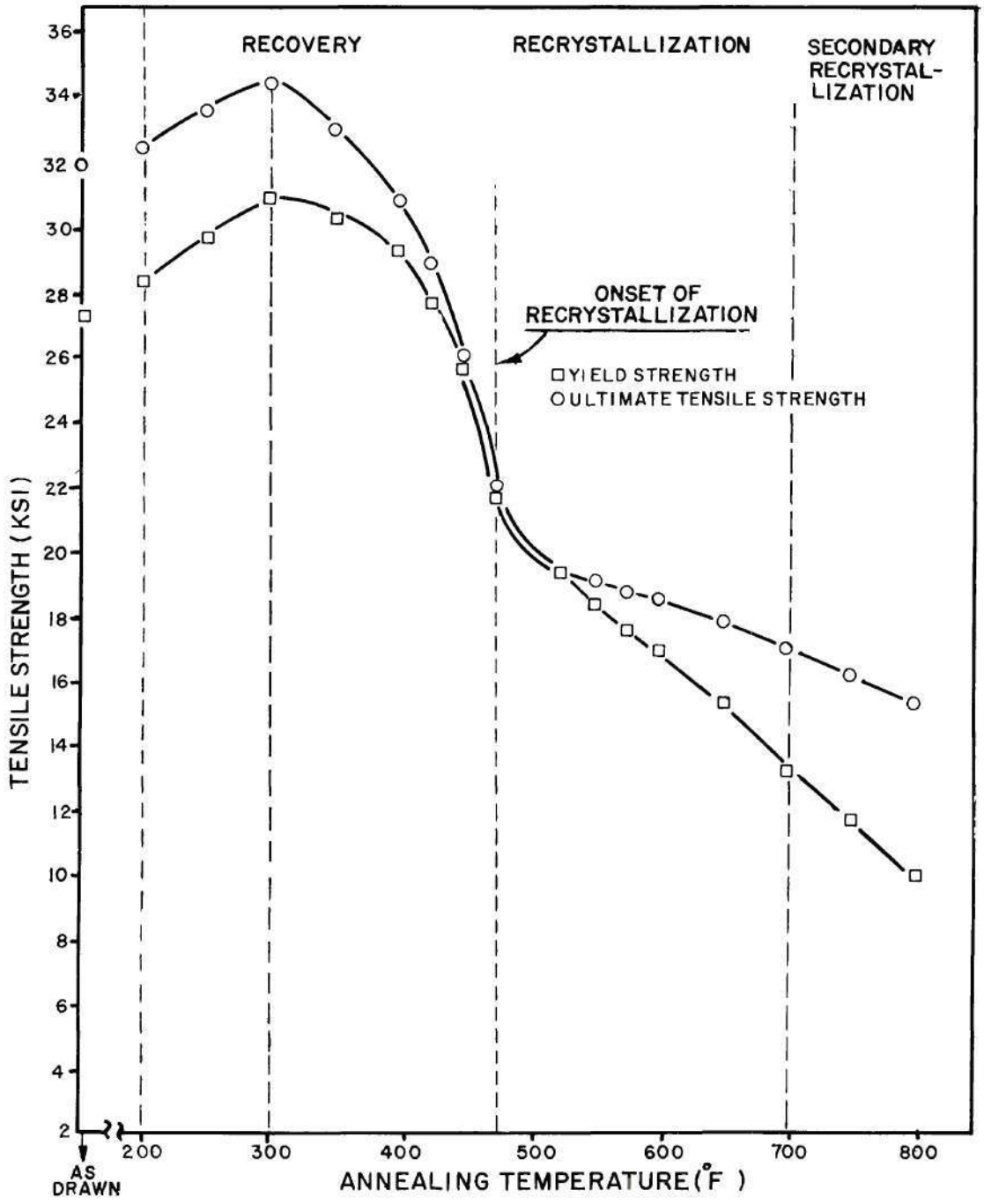

Figure 59. Effect of Isochronal One-Hour Annealing on Ultimate Tensile Strength of 0.105 Inch Diameter Al-Fe-Co Alloy Wire.

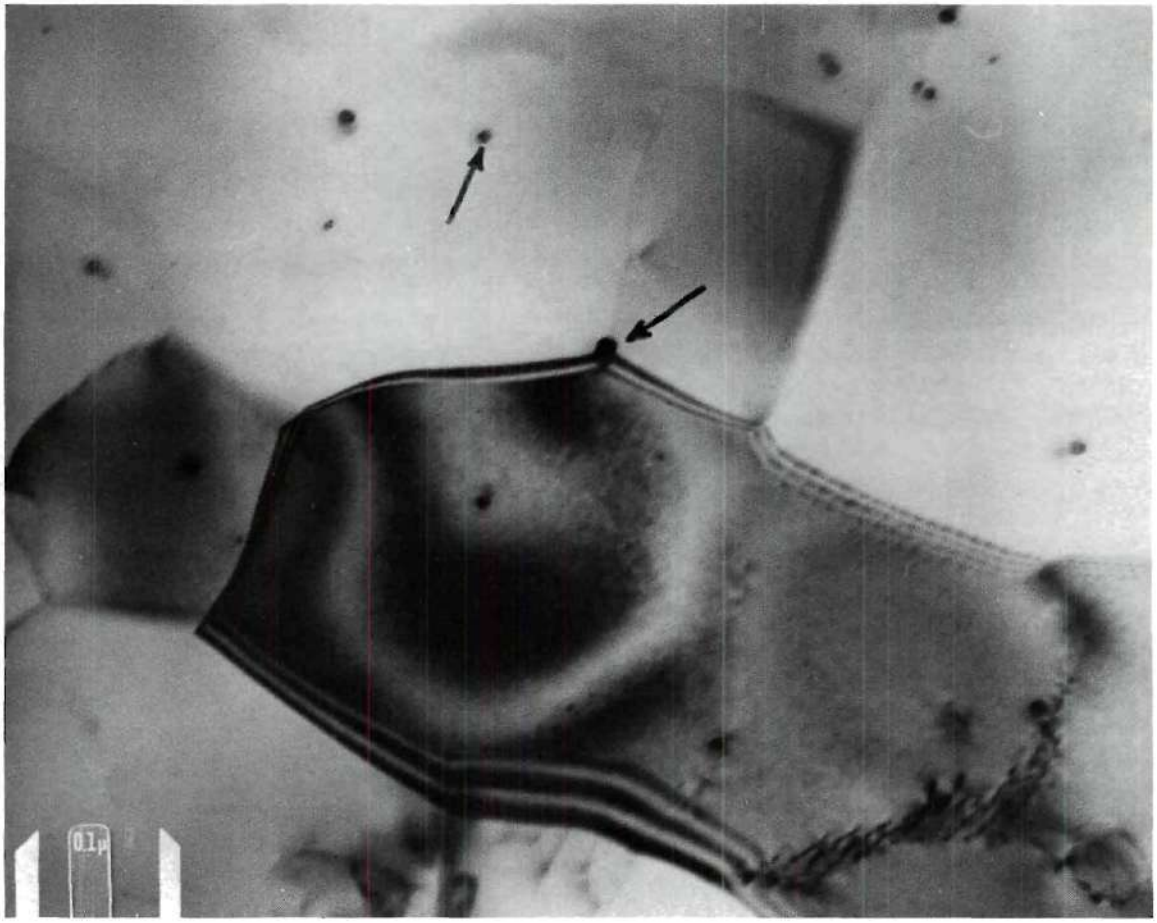

Figure 60. TEM of the Al-Fe-Co Alloy Wire Annealed 200°F for one Hour Showing the Small Precipitated $(Co,Fe)_2Al_9$ Particles Pinning a Subgrain Boundary.

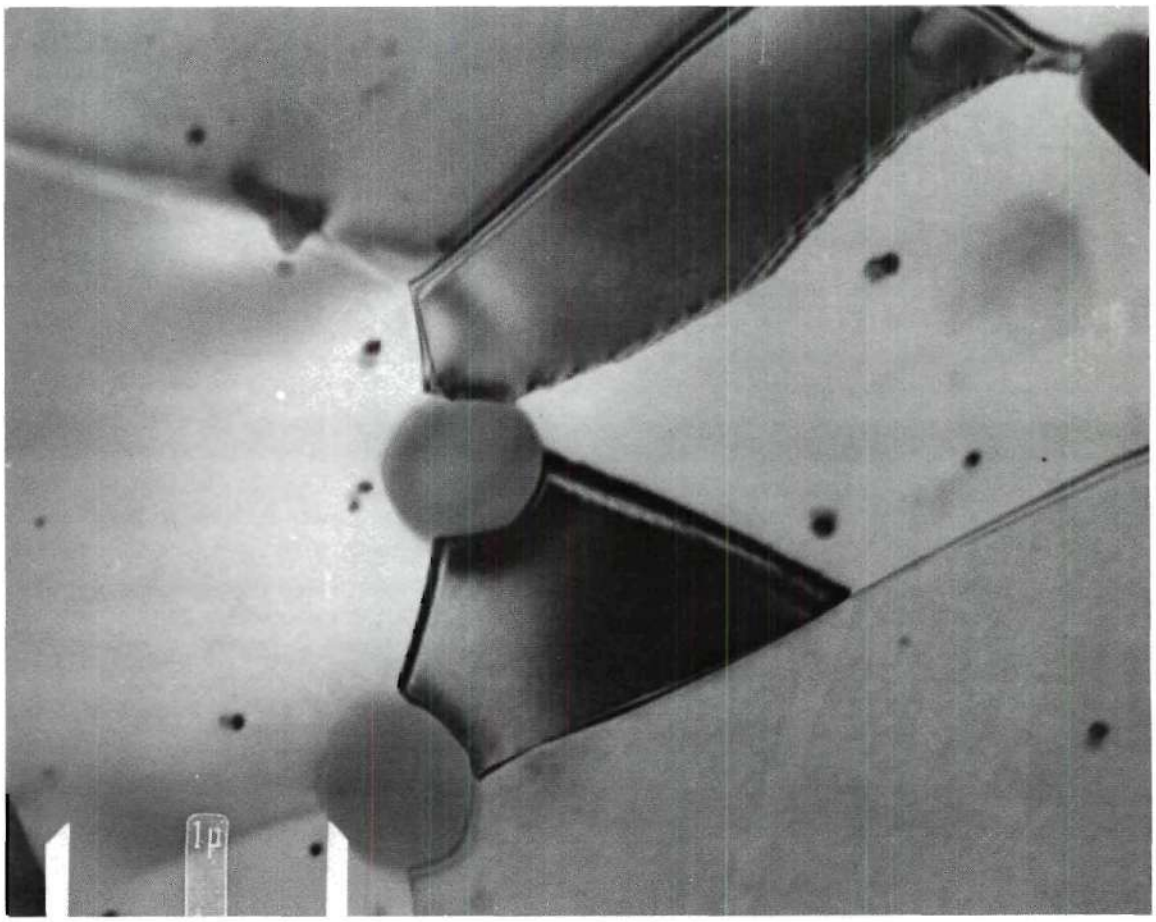

Figure 61. TEM of the Al-Fe-Co Alloy Wire Annealed One Hour at 475°F Showing the Presence of $(Co,Fe)_2 Al_9$ Precipitates Formed During Casting (large) and Precipitated During Isochronal Annealing. Note Pinning Effect of the Large Particles on the Subgrain Boundaries.

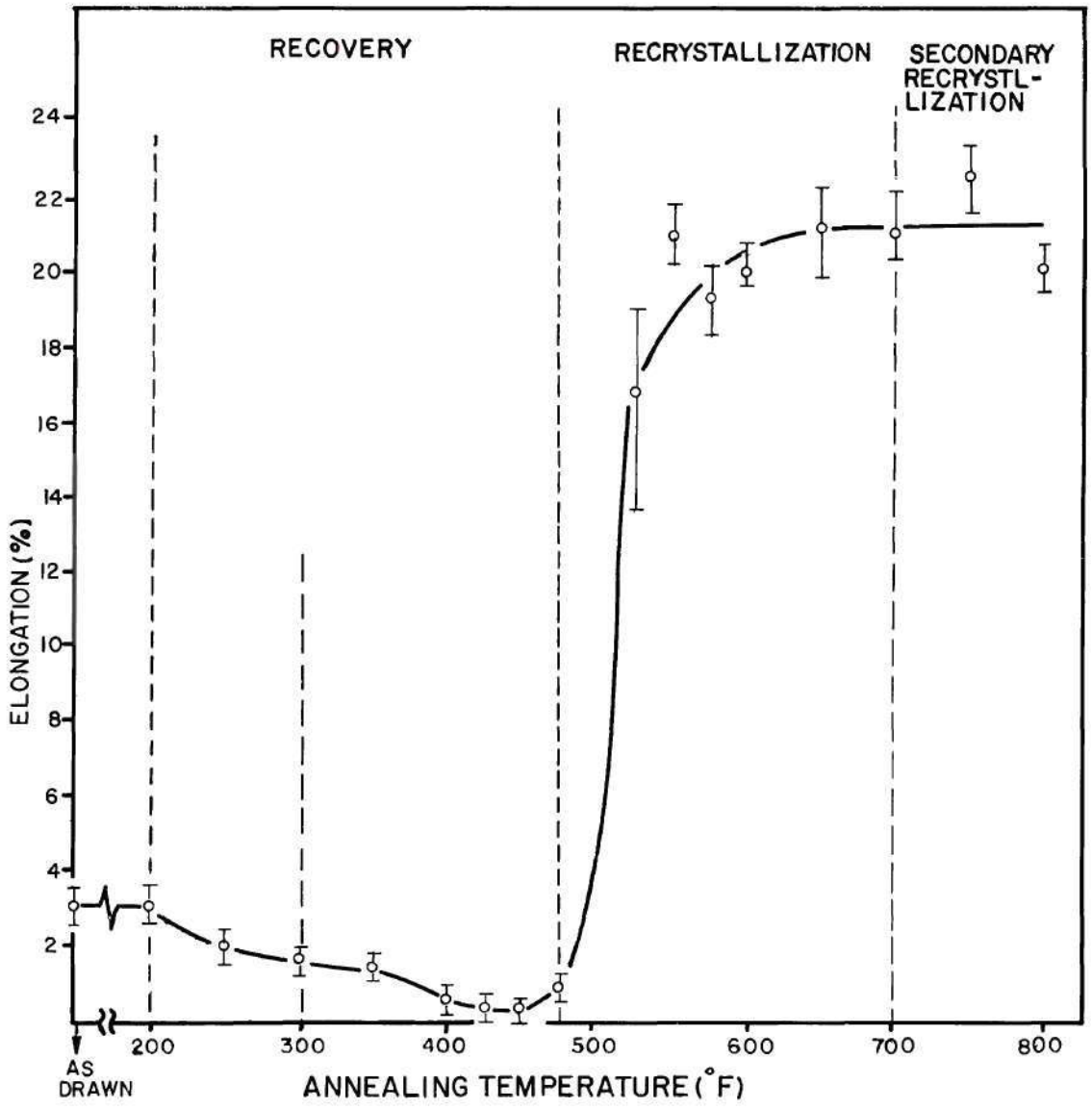

Figure 62. Effect of Isochronal One-Hour Annealing on Percent Elongation in Ten Inches of 0.105 Inch Diameter Al-Fe-Co Alloy Wire.

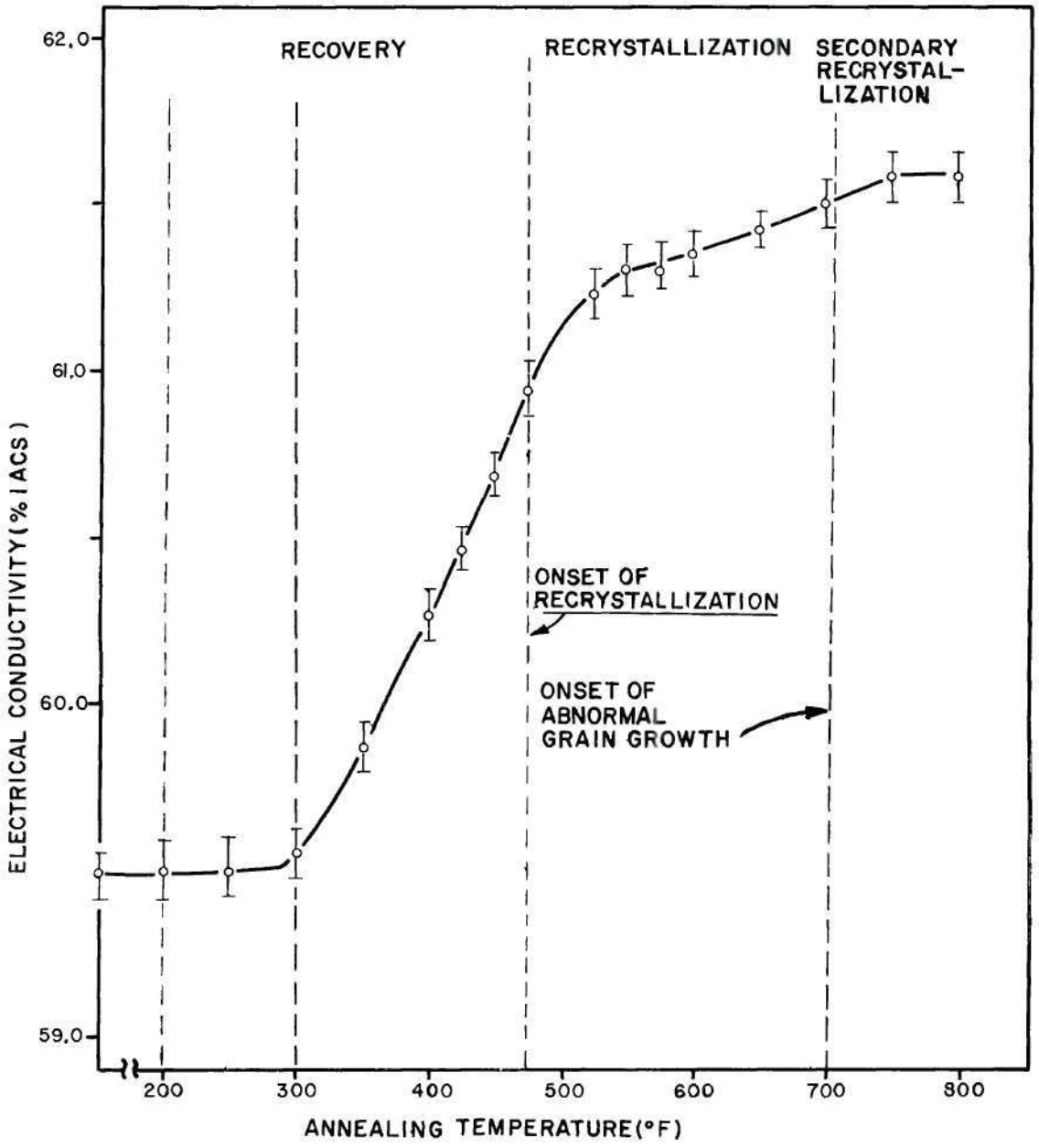

Figure 63. Effect of Isochronal One-Hour Annealing on Electrical Conductivity of 0.105 Inch Diameter Al-Fe-Co Alloy Wire.

as-drawn wire specimens were apparently responsible for the increase in strength and decrease in ductility taking place during annealing. In addition there was a higher rate of increase in electrical conductivity between 200°F and 350°F in the Al-Fe-Co alloy, Figure 63, than in EC, Figure 72. This supports the metallographic observations that precipitation occurred between 200°F and 350°F. However, the large amount of cold work still present did not allow a large increase in electrical conductivity in either material.

Static recovery was observed in wire samples annealed between 200°F and 475°F. The effects of recovery on structure may be seen by comparing the structure of the as-drawn wire shown in Figure 65 with the structures of the annealed wire shown in Figures 66, 67 and 68. Examination of the specimen after annealing, revealed a decrease in dislocation density inside the subgrains and a decrease in boundary thickness. However, the decrease in dislocation density was not significant at 200°F, so that this temperature was considered the start of recovery. The measured subgrain sizes of the wire, after annealing, are plotted in Figure 64. The error bars represent the range in size in the individual measurements. The subgrain size increased above 350°F indicating that subgrain coalescence during recovery begins at this temperature.

From the above it is clear that during recovery there was a progressive decrease in dislocation density with a definite increase in subgrain size by the process of coalescence. During this stage a certain amount of precipitation took place. However, the softening effect of recovery was less than the hardening effect of the precipita-

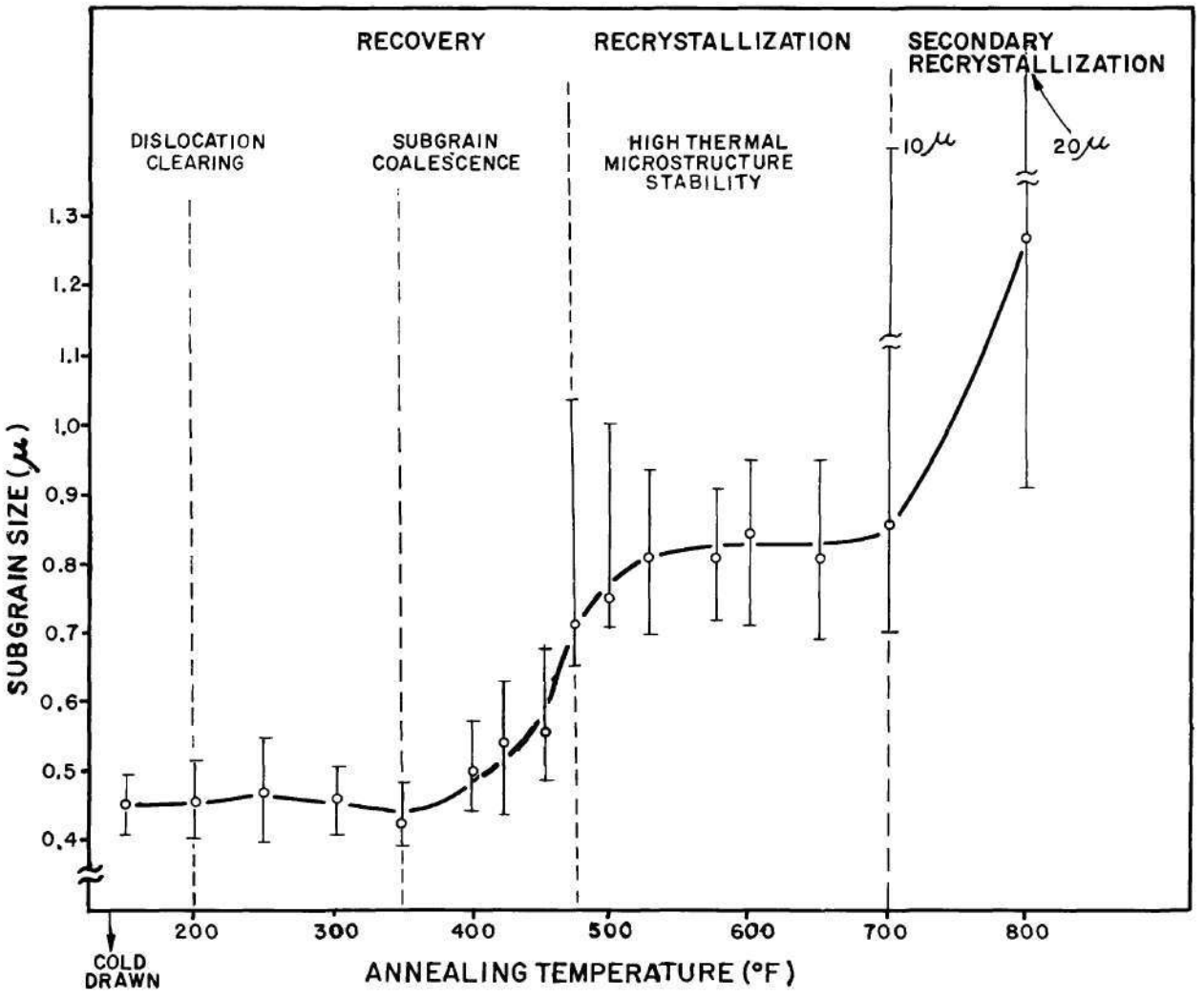

Figure 64. The Effect of Isochronal (one hour) Annealing on the Subgrain Size in 0.105 Inch Al-Fe-Co Wire. The Error Bars Represent the Range in Size due to the Statistical Standard Deviation in the Individual Measurements.

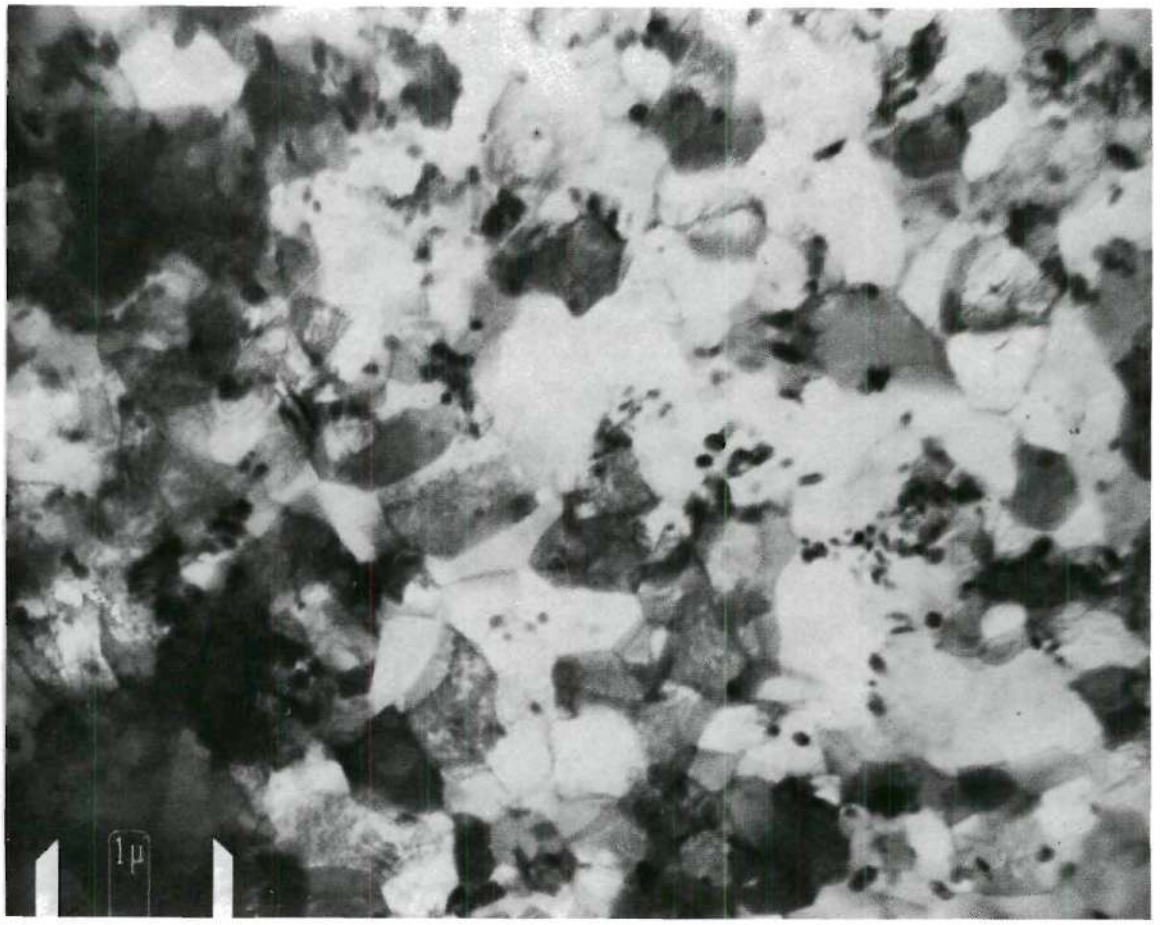

Figure 65. TEM of the Al-Fe-Co Alloy Wire in the As-Drawn Condition Showing Cell Structure Containing Heavy Dislocation Tangles and $(Co,Fe)_2Al_9$ and $FeAl_6$ Precipitates.

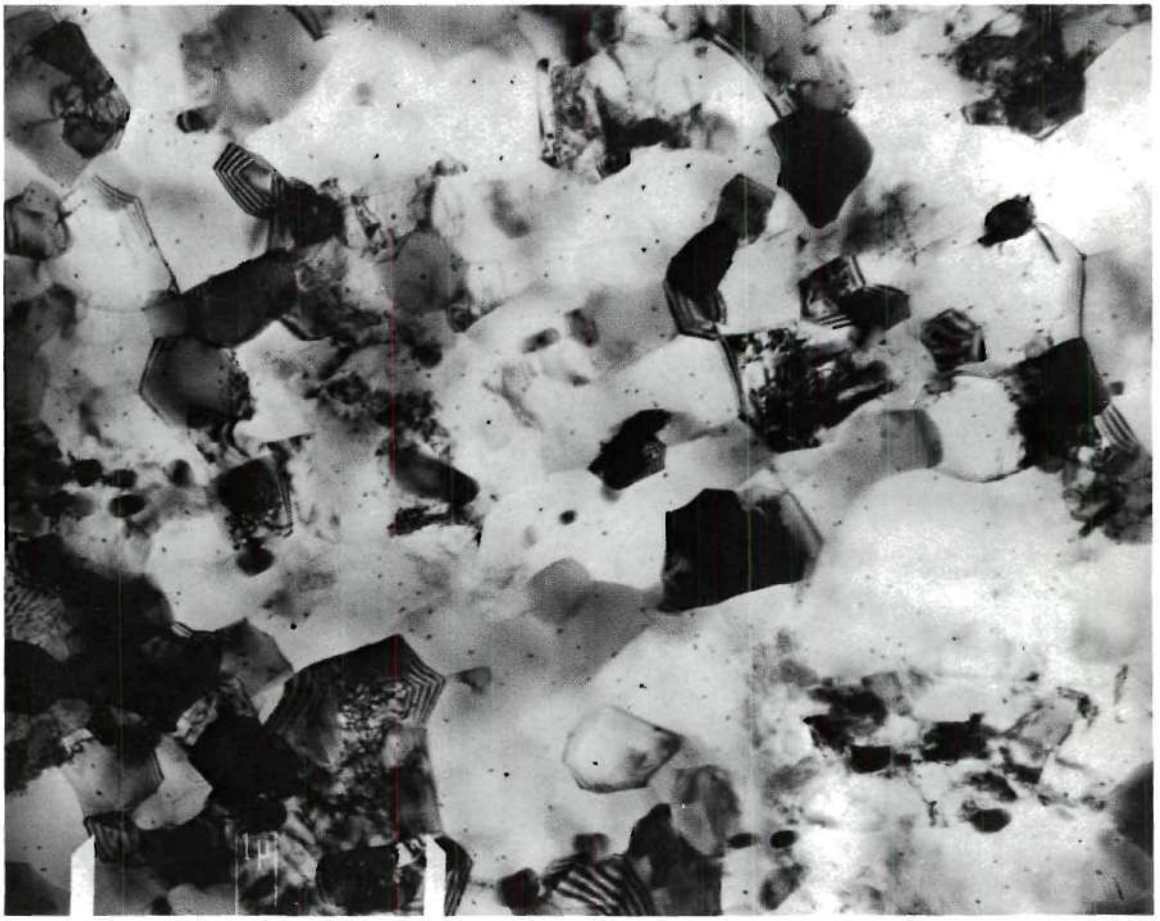

Figure 66. TEM of Al-Fe-Co Alloy Wire Annealed at 200°F for One Hour Showing Subgrain Structure with Small $(Co,Fe)_2Al_9$ Precipitates Distributed Throughout the Matrix. The Dislocation Density has not Decreased Significantly from that of the As-Drawn Wire.

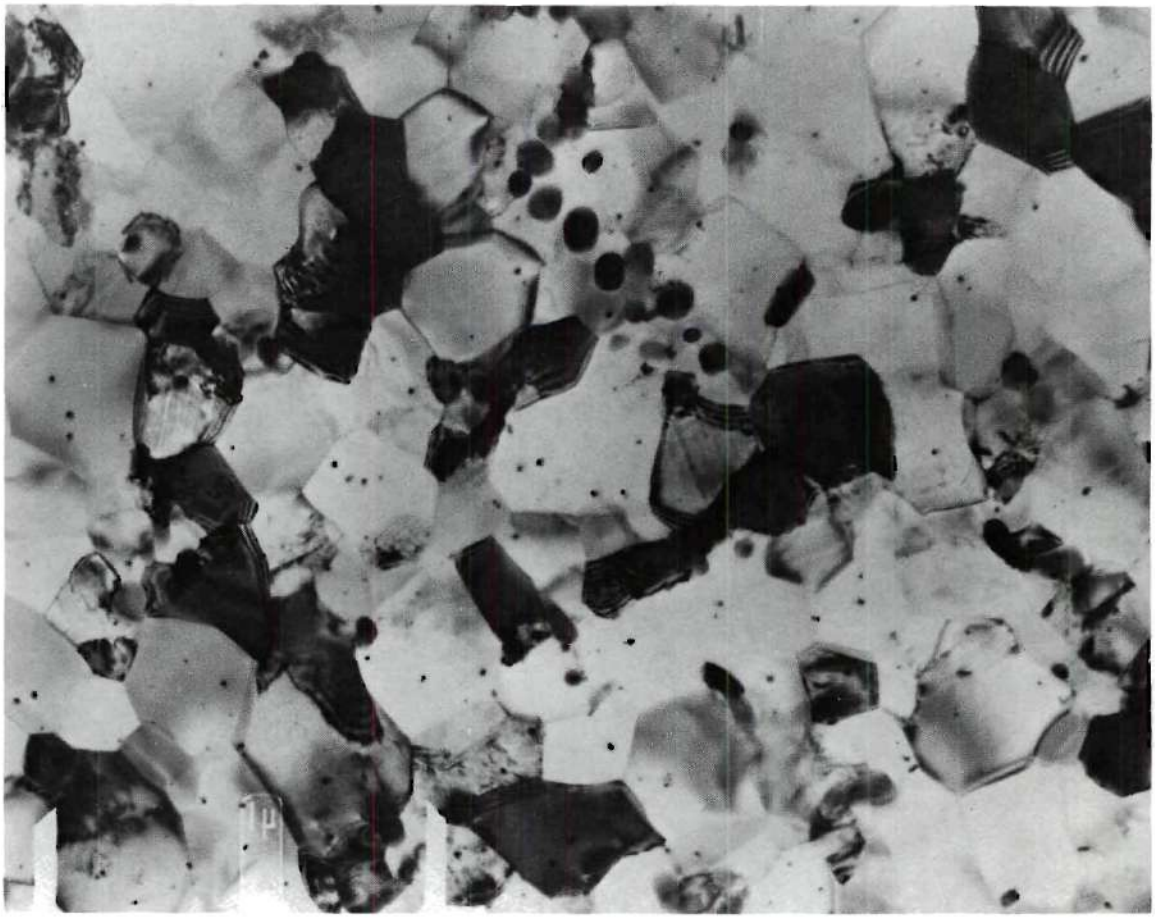

Figure 67. TEM of the Al-Fe-Co Alloy Wire Isochronally Annealed for One Hour at 250°F Showing a Slight Decrease in Dislocation Density.

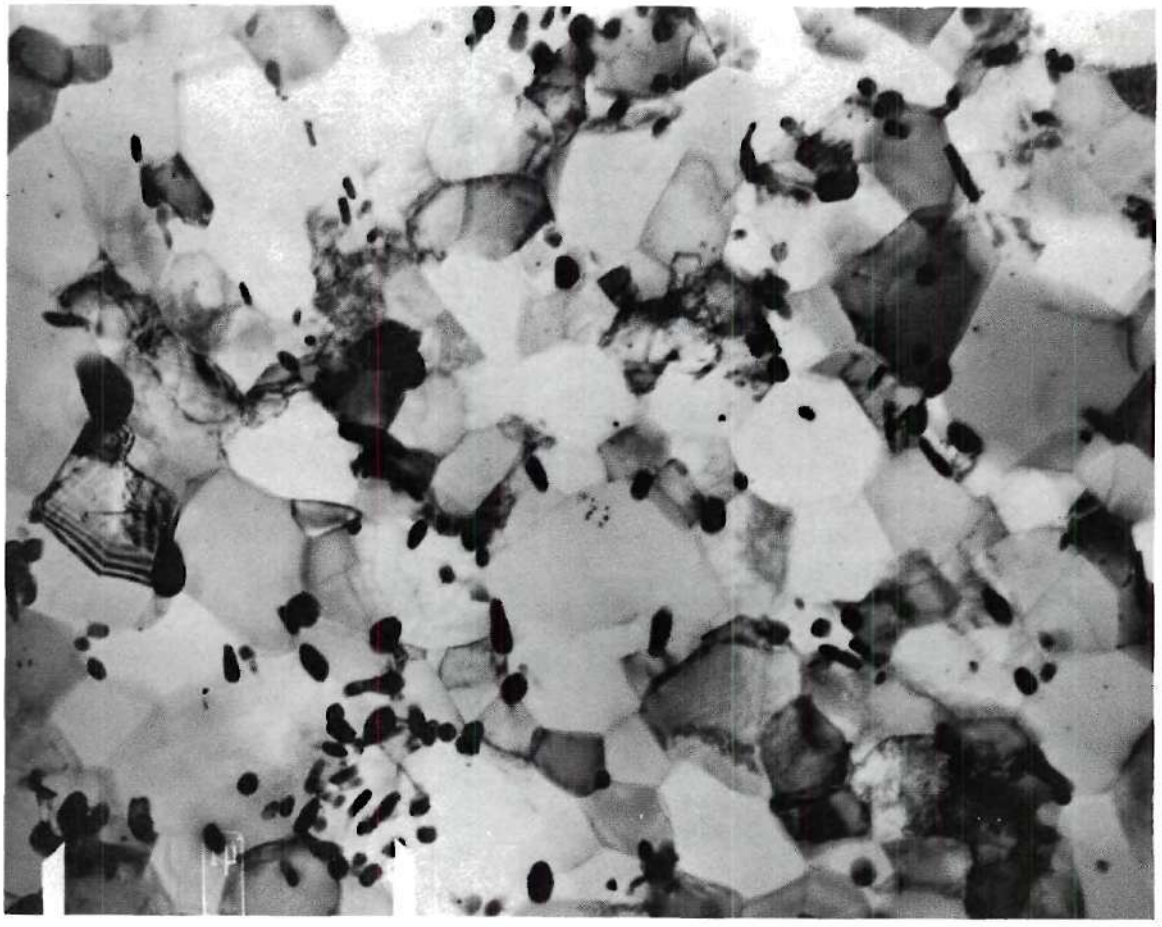

Figure 68. TEM of Al-Fe-Co Alloy Wire Isochronally Annealed for One Hour at 425°F Showing a Significant Decrease in Dislocation Density Due to Static Recovery. Notice the Presence of Small $(Co, Fe)_2Al_9$ Precipitates Still Present in the Structure and the Subgrain Coalescence Which Begins to Take Place.

tion during the early stage of recovery, so that a net increase in ultimate tensile strength and yield strength and a decrease in elongation was produced. The subgrain structure during recovery can grow larger due to a lack of sufficient precipitate particles to act as pinning points during subgrain coalescence. A similar effect for EC aluminum is shown in Figure 69A and B. Roth[104] reported that in hard drawn aluminum wires containing small amounts of iron and traces of silicon, the iron precipitates from solid solution during annealing. This produced a marked increase in tensile strength at low annealing temperatures which denoted the beginning of precipitation.

The strength of the EC aluminum wire, on the other hand, did not increase when annealed at 200°F, 250°F or 300°F, as shown in Figure 70. Thus, no age-hardening took place in this material. Apparently, there was insufficient iron in solid solution at this stage to cause any significant precipitation. The elongation and electrical conductivity, plotted in Figures 71 and 72, showed typical behavior.

Examinations with the transmission electron microscope showed that there were some isolated recrystallization nuclei in the Al-Fe-Co alloy wire isochronally annealed at 475°F for one hour. Such an isolated nucleus is shown in Figure 73. Figure 59 shows that there was a sharp drop in strength of the Al-Fe-Co alloy wire above 400°F and then a marked change in the rate of softening at about 480°F, as shown by a change in the slopes of the tensile and yield strength. The elongation started a sharp climb at 450°F. Furthermore, the temperature at which the subgrain size range became largest due to the onset of recrystallization was at about 475°F. According to Weissman[111] the most active

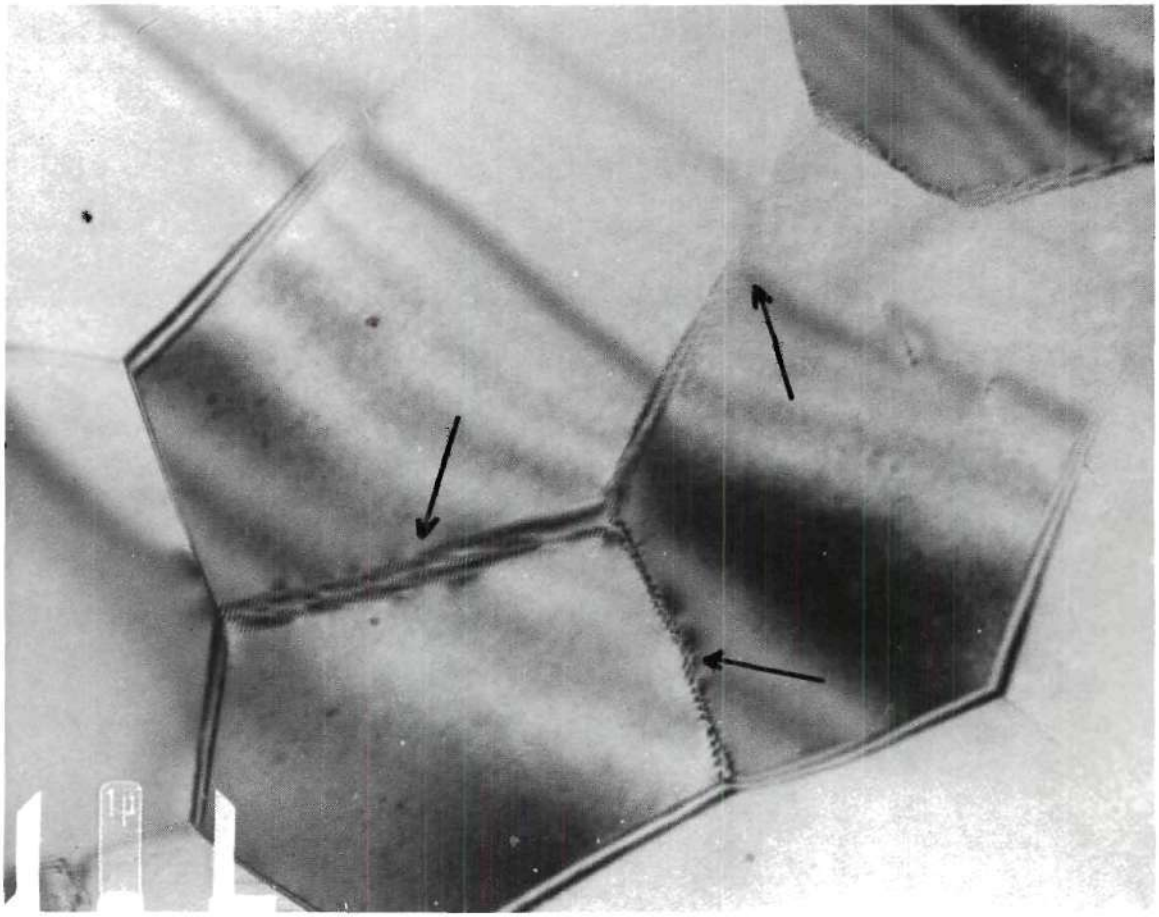

Figure 69A. EC Aluminum Wire Annealed at 500°F For One Hour After Cold Drawing Showing Subgrain Boundaries Disappearing During Subgrain Coalescence. (Shown by the Arrows).

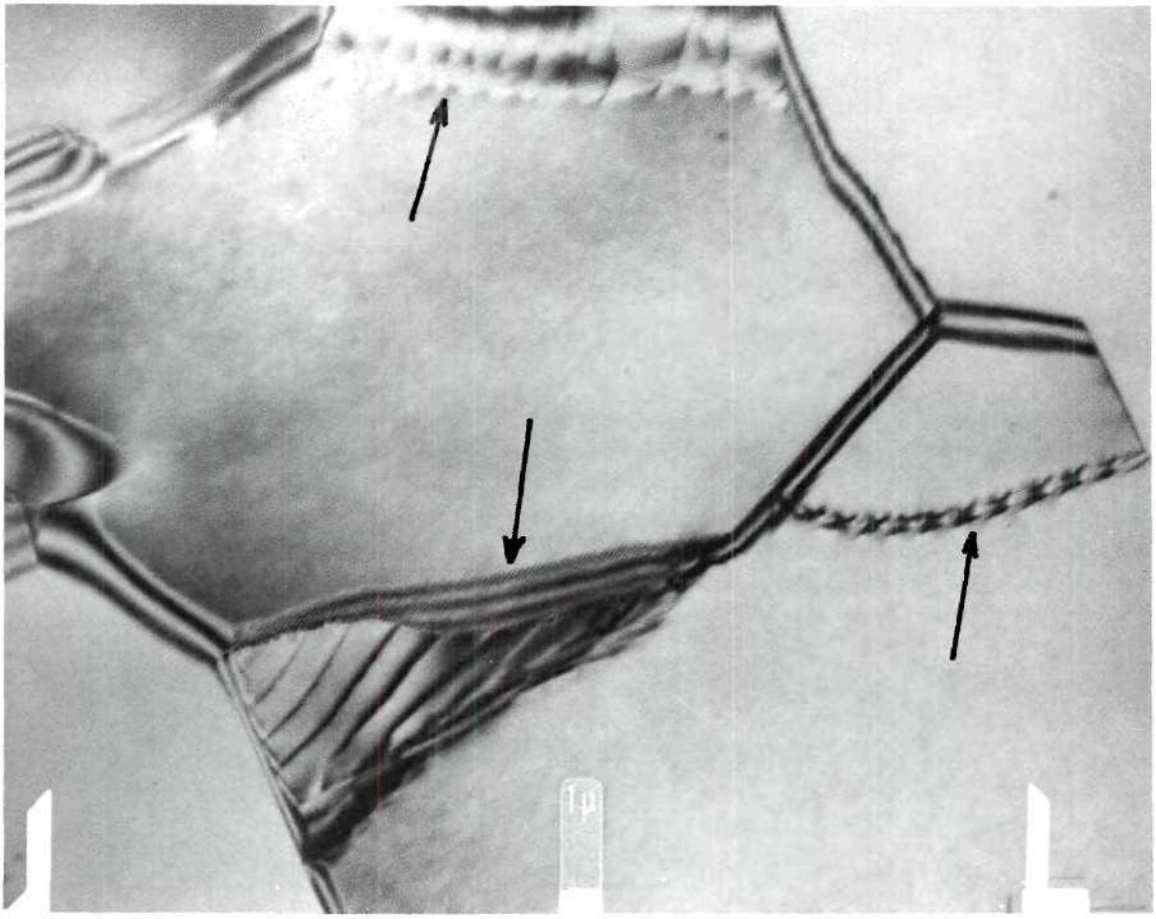

Figure 69B. EC Aluminum Wire Annealed at 500°F for One Hour After Cold Drawing Showing Subgrain Coalescence During Recovery. (Shown by the Arrows)

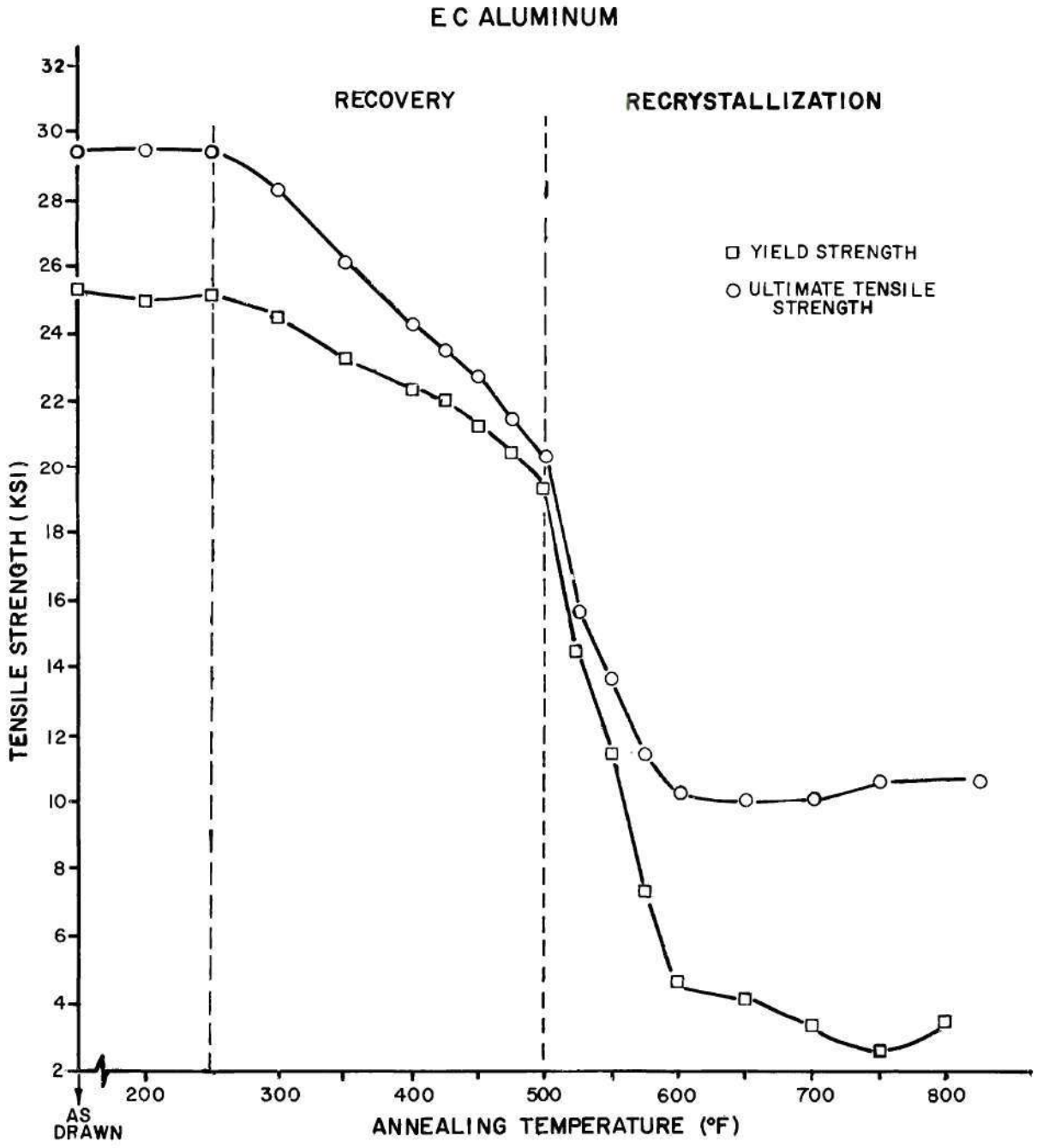

Figure 70. Effect of Isochronal One-Hour Annealing on Ultimate Tensile Strength of 0.105 Inch Diameter EC Aluminum Wire.

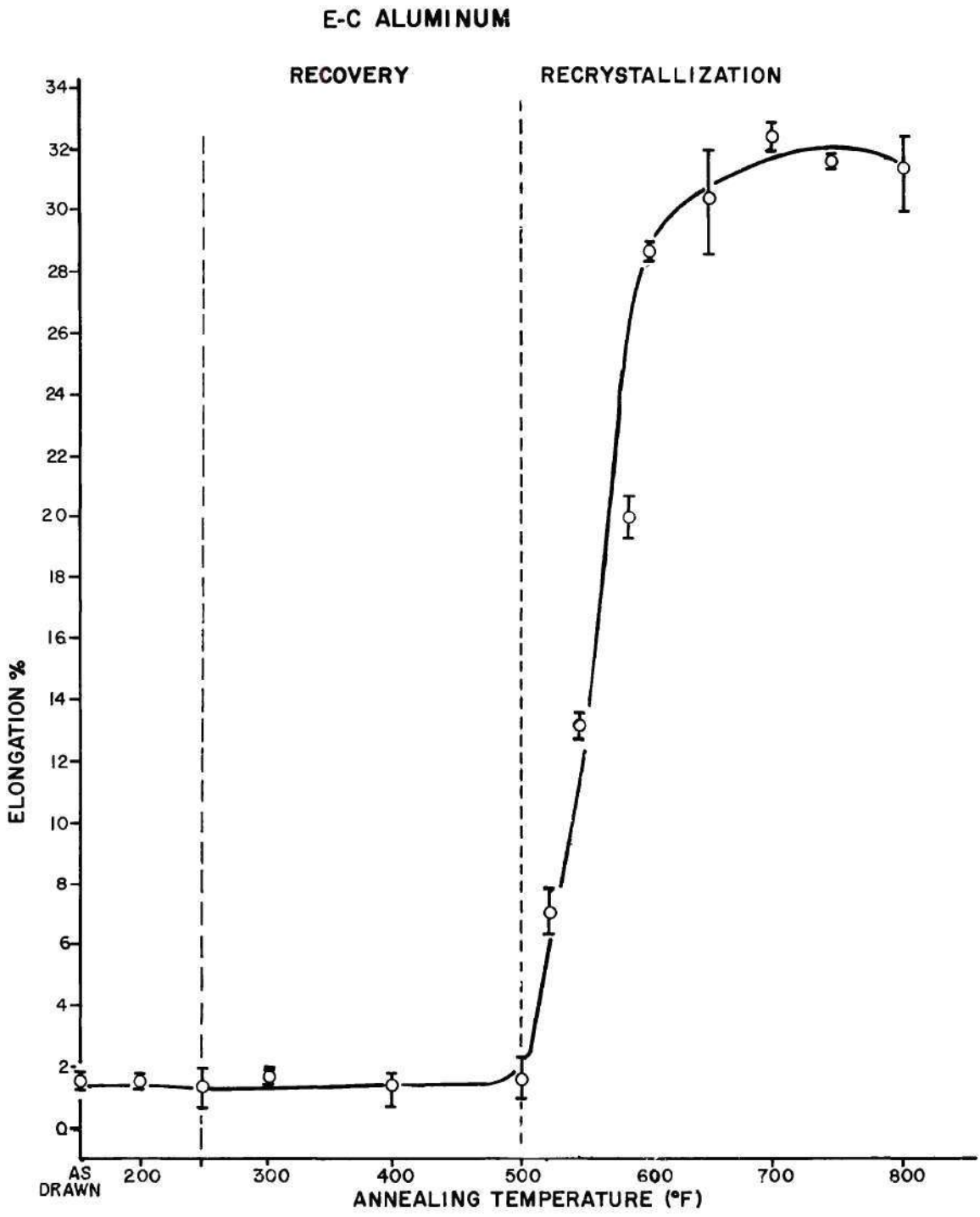

Figure 71. Effect of Isochronal One-Hour Annealing on Percent Elongation of 0.105 Inch Diameter EC Aluminum Wire.

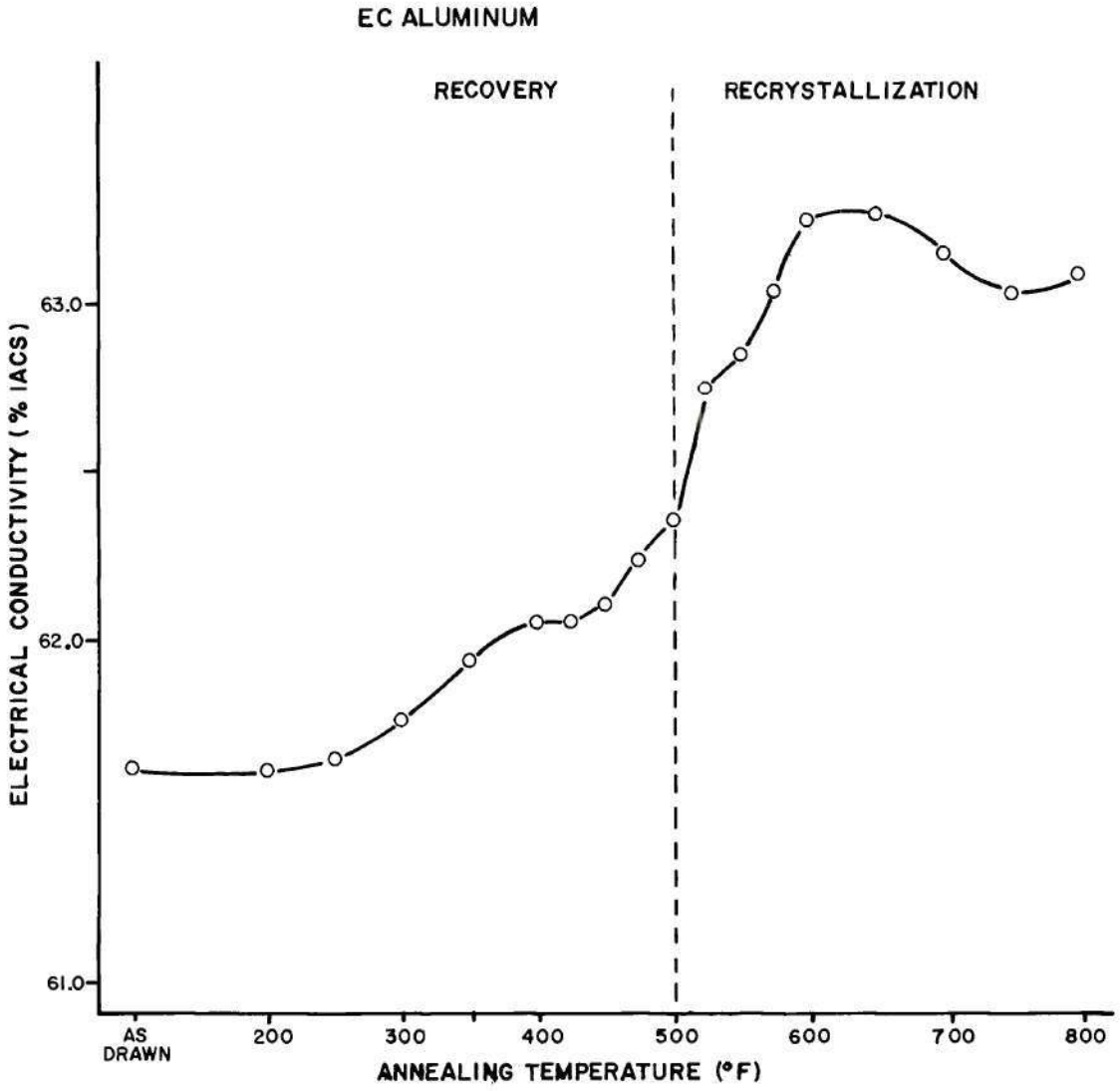

Figure 72. Effect of Isochronal One-Hour Annealing on Electrical Conductivity of 0.105 Inch Diameter EC Aluminum Wire.

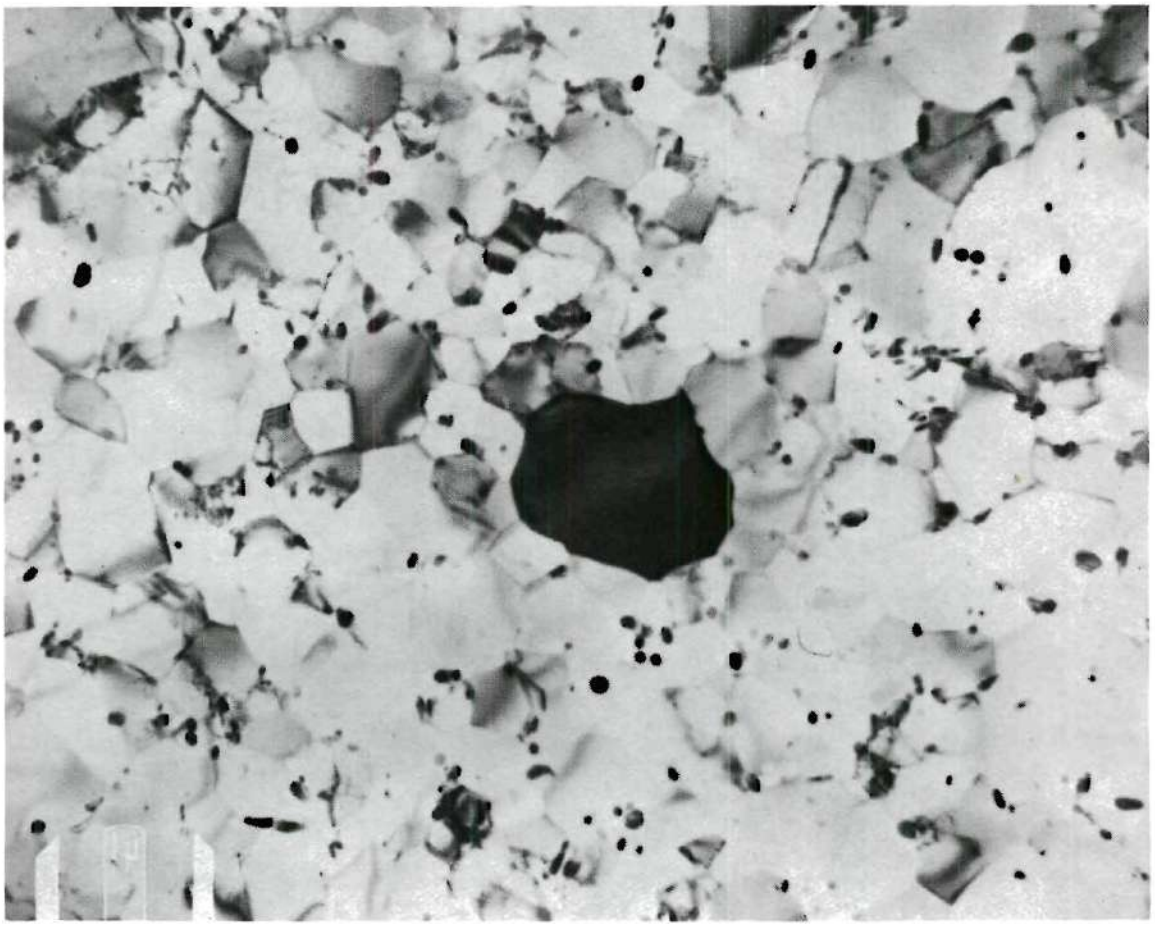

Figure 73. TEM of Al-Fe-Co Alloy Wire Annealed at 475°F for One Hour Showing a Growing Recrystallization Nucleus. The High Degree of Misorientation Between the Nucleus and the Adjacent Subgrains can be Judged by the Relative Difference in Darkness.

recrystallization nuclei are the subgrains which show high angles of misorientation with respect to their neighbors. He also stated that these subgrains attain the highest growth rate during recrystallization. Weissman[112] et al. postulated that high angle boundaries become highly mobile if they have a high degree of misorientation with respect to their surroundings.

The rate of change in yield strength with temperature was measured and plotted as a function of annealing temperature for the Al-Fe-Co alloy in Figure 74 and for the EC aluminum in Figure 75 Mould and Coterill[105] found that the maximum of this curve coincided with the temperature corresponding to 50 percent recrystallization. However, the maximum of the $\frac{\Delta\sigma}{\Delta T}$ curve in this investigation coincided with the onset of recrystallization (475°F) and not with the 50 percent recrystallization. Figure 64 shows that the grain size increased sharply at 475°F and progressively increased until approximately 530°F. Above the latter temperature, the subgrain size remained constant until secondary recrystallization took place. This temperature of 530°F, above which the subgrain size did not continue to increase, also corresponded to the minimum of the $\frac{\Delta\sigma}{\Delta T}$ versus annealing temperature plot in Figure 74. It is at this temperature that the grain size approached the interparticle spacing, as shown in Figures 76 and 77. Several grains were found to have overcome the pinning of the boundaries by the particles in the specimen annealed at 675°F for one hour. Figure 78 shows the grains growing into other grains in this specimen.

During the primary recrystallization stage, the decreases in ultimate tensile strength and yield strength were significantly less than

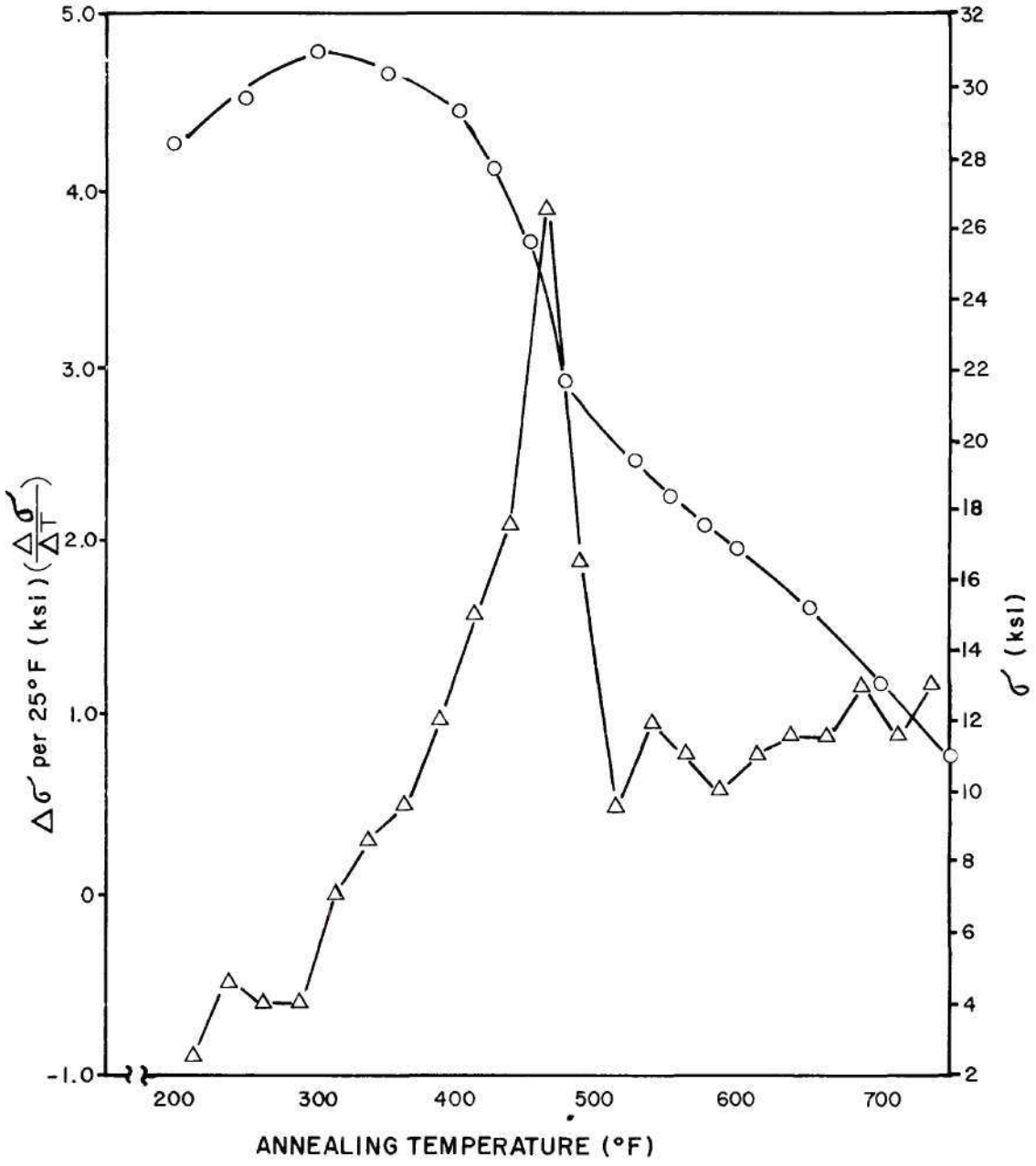

Figure 74. Rate of Change in Yield Strength as a Function of the Annealing Temperature for Al-Fe-Co Alloy.

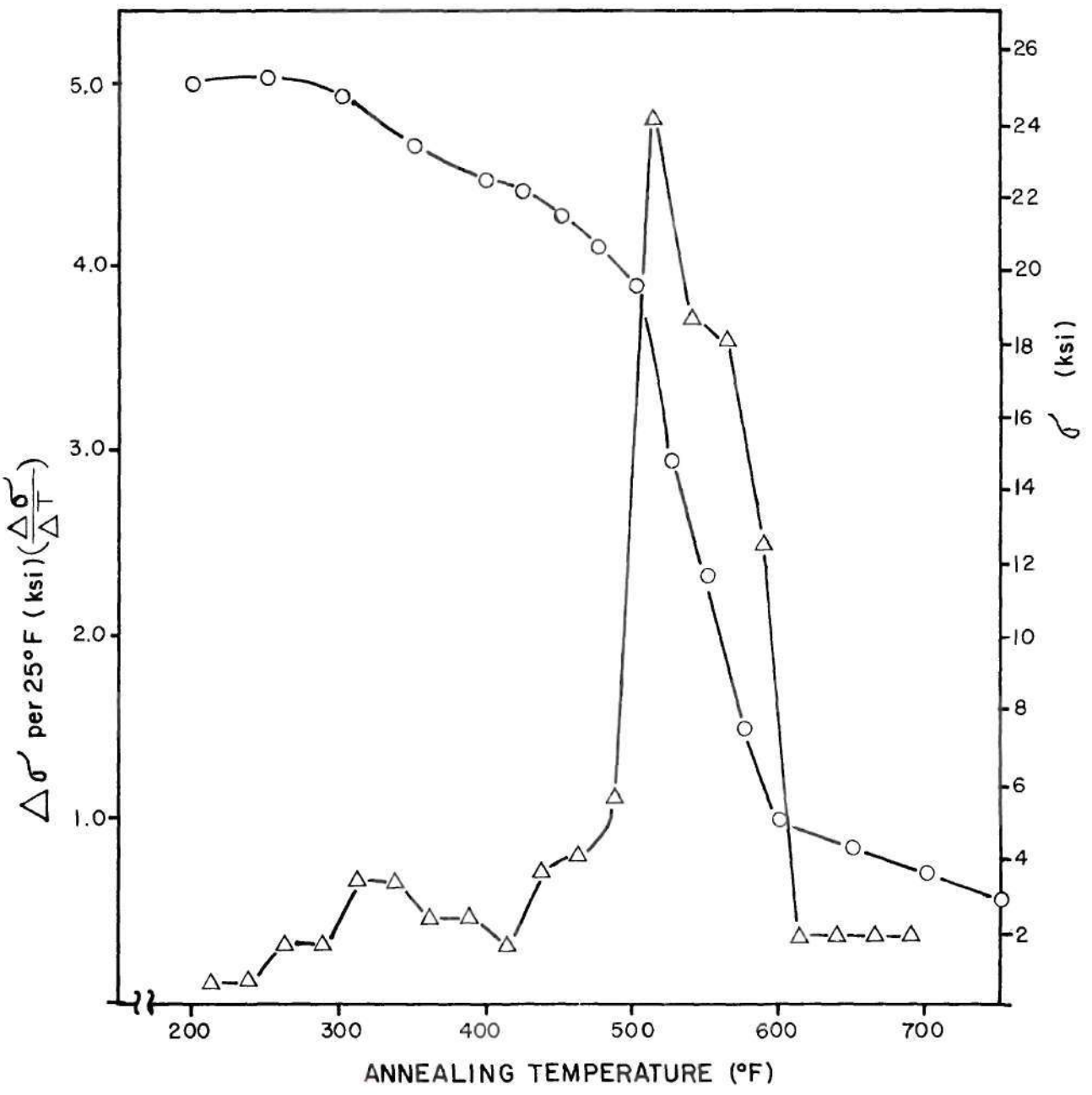

Figure 75. Rate of Change in Yield Strength as a Function of the Annealing Temperature for EC Aluminum.

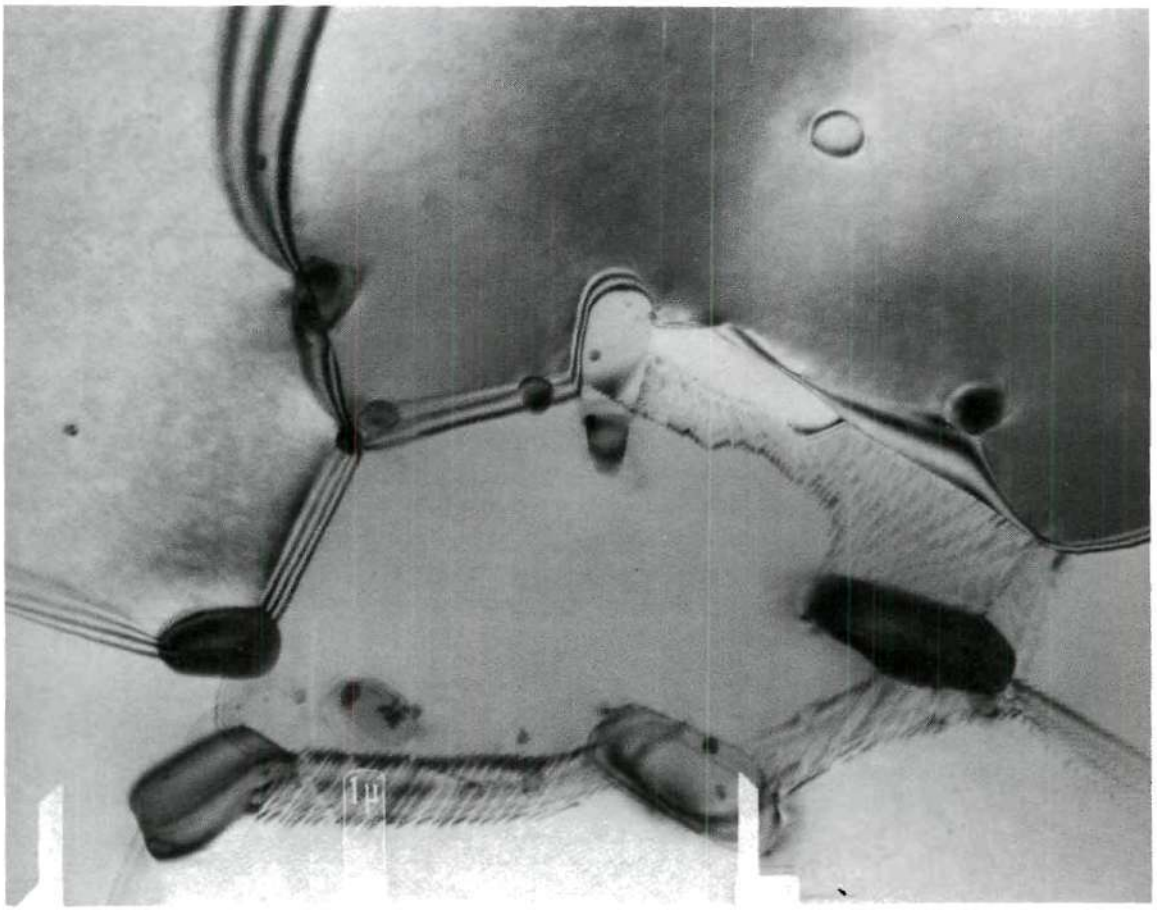

Figure 76. TEM of Al-Fe-Co Alloy Wire Isochronally Annealed at 500°F for 1 hour showing that the Interparticle Spacing has Become of the Same Magnitude as the Subgrain Size. This is Due to the Obstruction of Subgrain Coalescence by the Pinning Effect of the Particles.

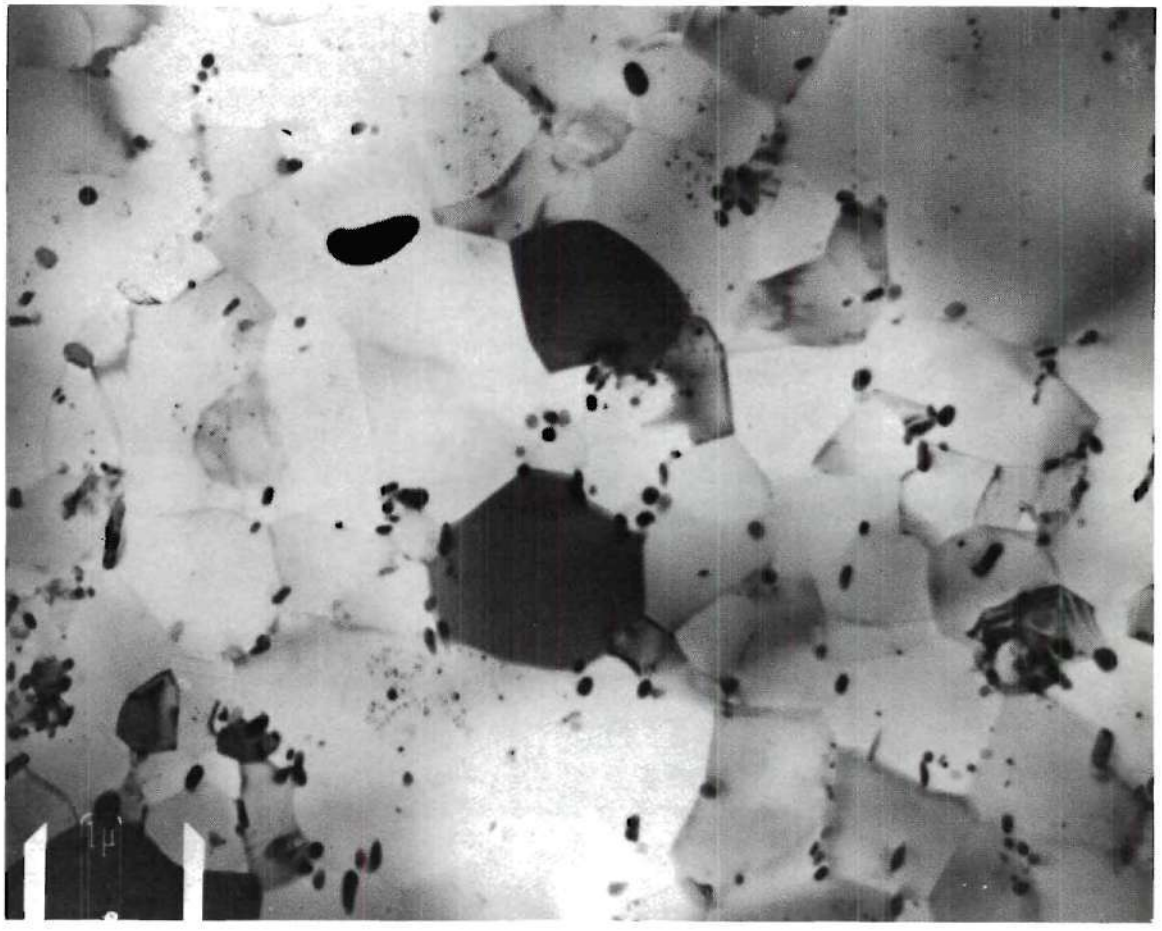

Figure 77. TEM of Al-Fe-Co Alloy Wire Isochronally Annealed at 550°F for One Hour Showing Completely Polygonized Subgrains Which have Recrystallized but have their Boundaries Pinned by Particles and Other Boundaries.

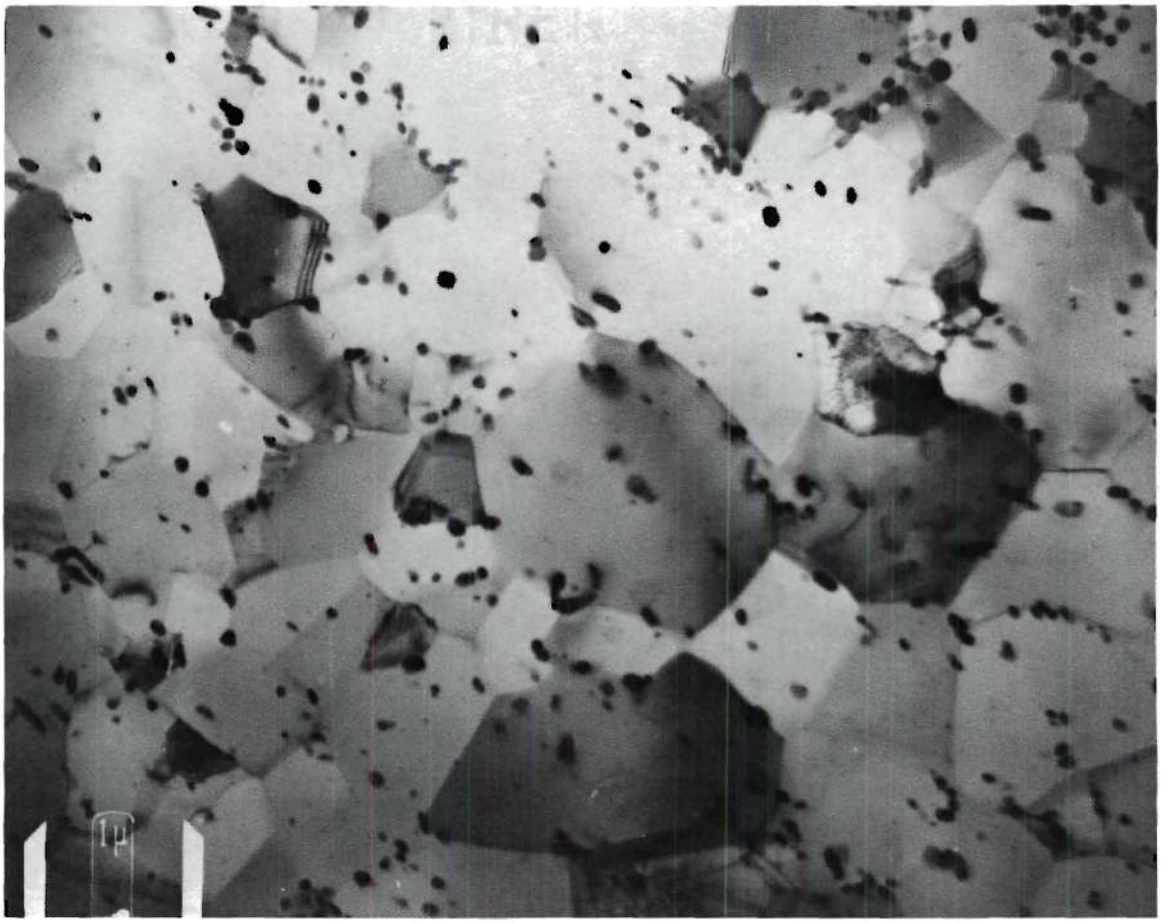

Figure 78. TEM of Al-Fe-Co Alloy Wire Annealed at 675°F for One Hour Showing Subgrains Which Have Overcome the Pinning by the Particles and are Growing into Other Subgrains.

the decreases during the latter phase of recovery. Recrystallization had a greater effect on ductility than did recovery. The elongation decreased from 3% to ½% during recovery, whereas the elongation increased to 17% and 21% during annealing at 525°F and 675°F, respectively. It is significant to point out that the largest increase in the electrical conductivity was obtained during the recovery stage. The electrical conductivity increased from 59.5 percent IACS (International Annealed Copper Standard) to 61.0 percent IACS. During recrystallization the grains became more delineated with thinner walls producing a polygonized structure, as shown in Figure 80. However, the recrystallization stage did not produce a uniform increase in the grain size in the majority of the areas studied. Larger grain size ranges were measured in areas where the precipitate distribution was not uniform, and the absence of precipitates at certain locations allowed the subgrains to coalesce. However, grains such as that shown in Figure 79 were found in several areas. In this case, the subgrain had grown beyond existing precipitate particles producing an anomalously large subgrain. This produced an increase in the size range measured as shown in Figure 64.

Secondary recrystallization was clearly observed in the specimen annealed at 700°F for one hour, as shown in Figure 81. However, large areas of the structure contained grains as those observed in Figure 82 which did not show signs of secondary recrystallization. This was also confirmed by optical microscopy, as shown in Figure 115B. The structure contained several areas of small grains with a size of the same magnitude as the interparticle spacings. Adjacent to these areas there were areas of large grains (as large as 500 microns) which contains in their interior

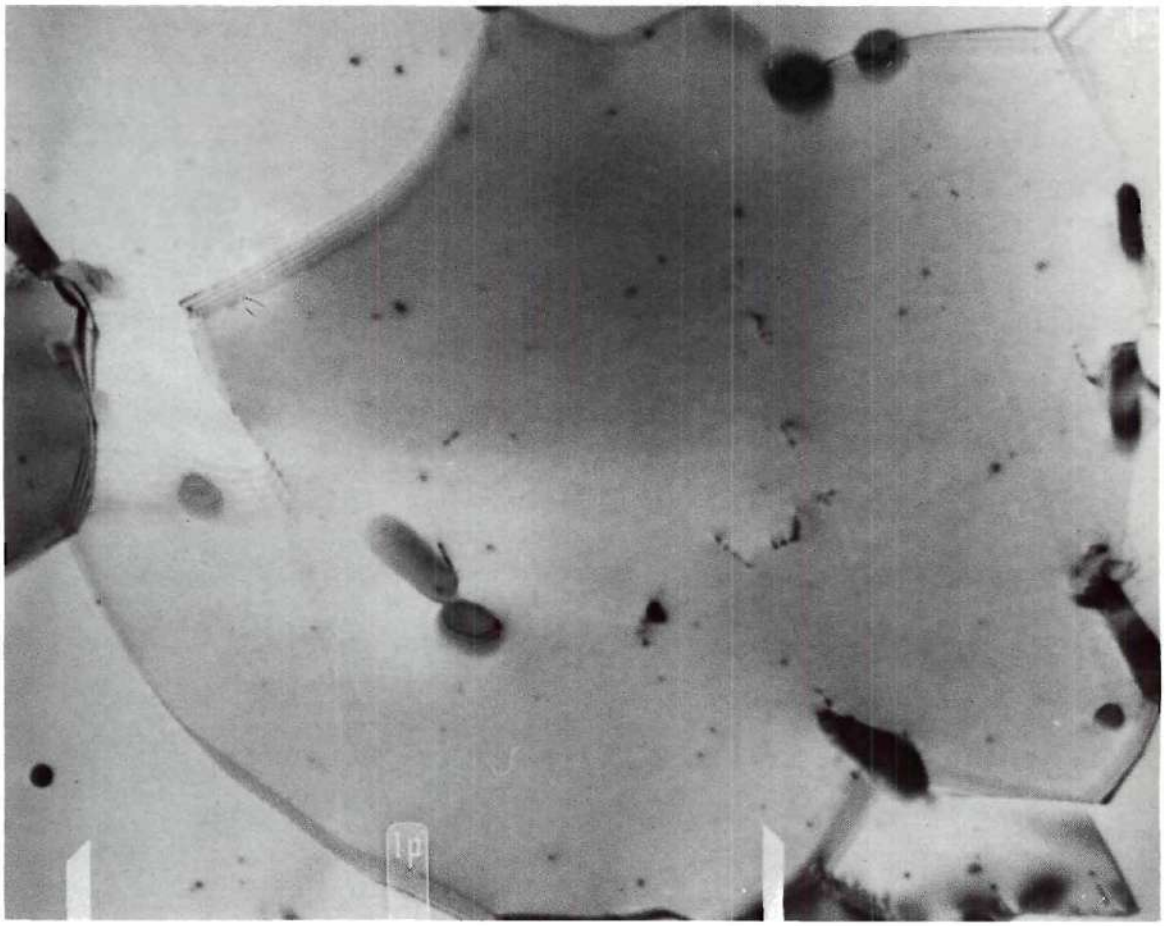

Figure 79. TEM of Al-Fe-Co Alloy Wire Annealed at 500°F for One Hour Showing Excessive Subgrain Coalescence. Note Slip Traces Present Indicating the Migration of Dislocations During Subgrain Coalescence.

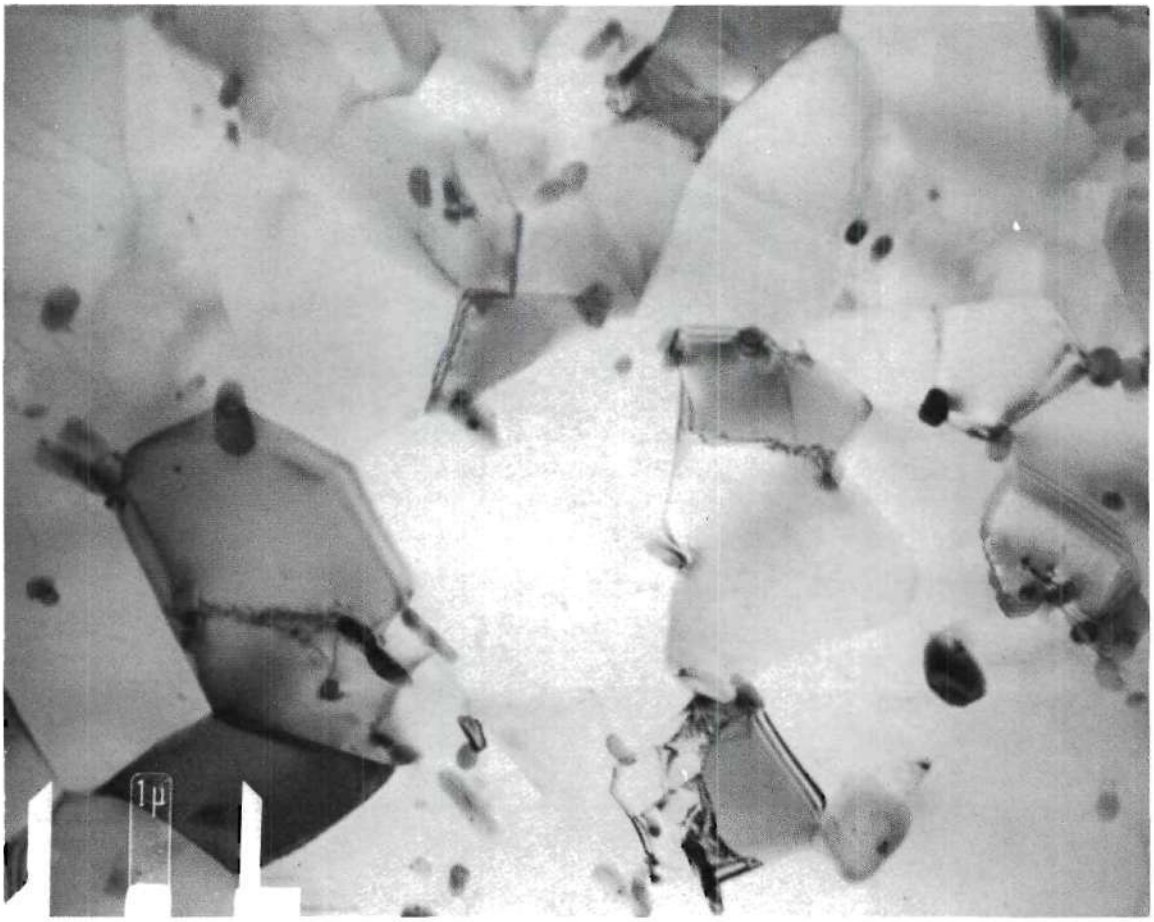

Figure 80. TEM of the Al-Fe-Co Alloy Wire Annealed at 600^{o}F for One Hour Showing Polygonized Subgrains and $(Co,Fe)_2Al_9$ Precipitates.

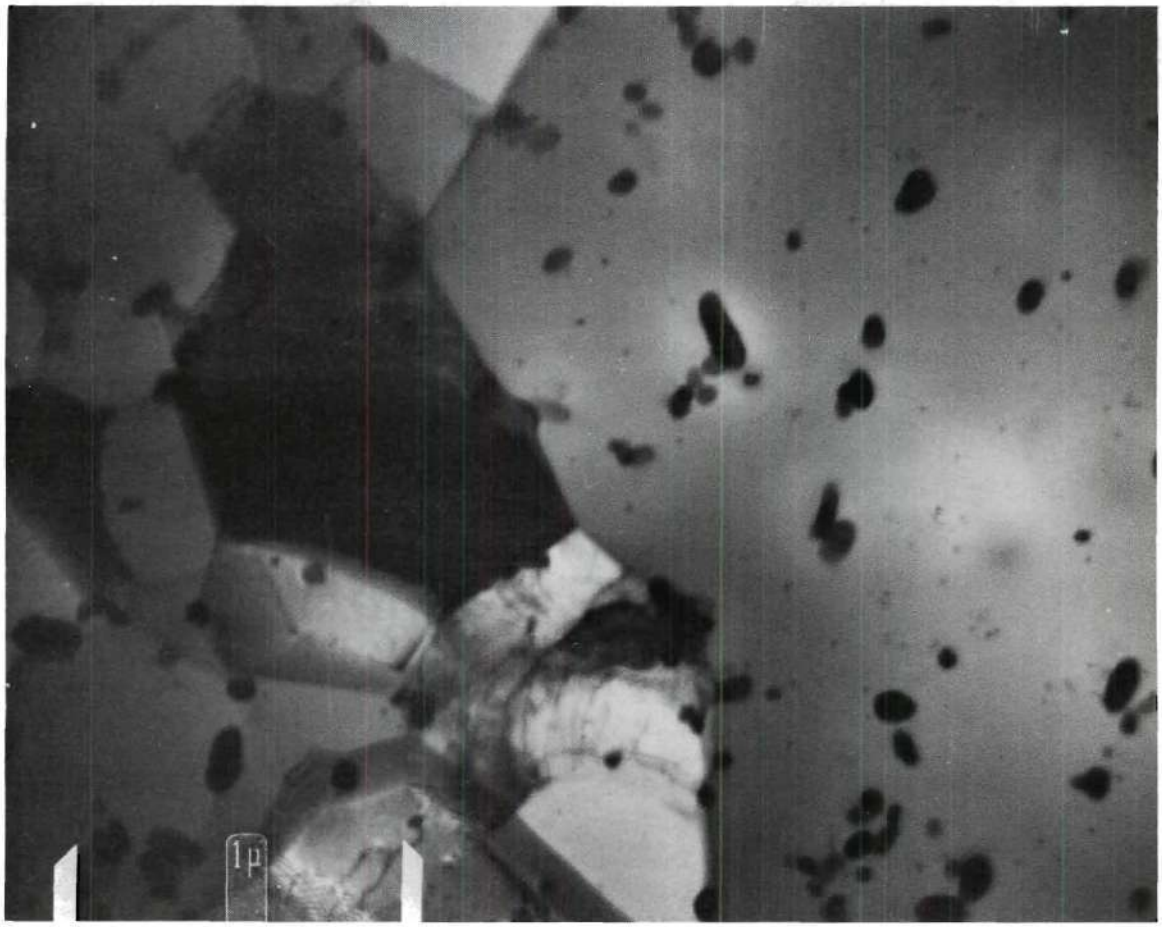

Figure 81. TEM of the Al-Fe-Co Alloy Wire Annealed at 700°F for One Hour Showing a Large Subgrain Which has Formed at the Onset of Secondary Recrystallization.

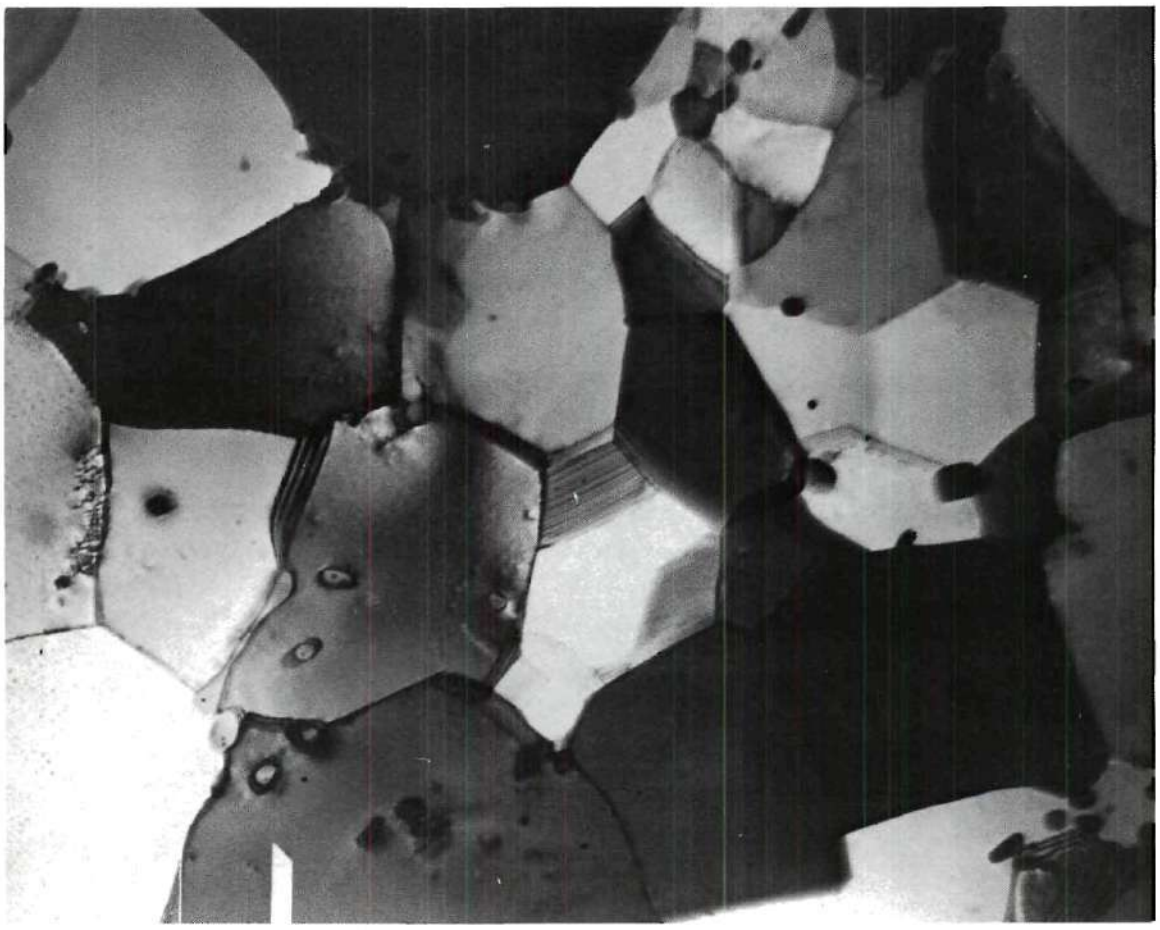

Figure 82. TEM of the Al-Fe-Co Alloy Wire Annealed at 700^{O}F for One Hour Showing Polygonized Subgrains.

a number of precipitate particles. During electron microscopy observations, the specimens were tilted continuously to insure that the large grains were not composed of any subgrains with slight differences in orientations. Above 700°F, the grain size continued to increase as shown in Figure 64 and in Figure 83, which is a TEM of a specimen annealed at 800°F for one hour. This increase in grain size was due to the fact that the supplied energy makes climbing easier and had exceeded the activation energy for boundary migration.[106] This process is quite complex and has been discussed in detail elsewhere.[107,108,109,110]

In comparing recrystallization temperatures, one must be aware of the amount of stored energy retained in a material after a particular reduction in area. An alloy such as the Al-Fe-Co alloy stores a higher amount of energy in the form of dislocations and other defects than does the relatively pure EC aluminum. The large volume fraction of precipitates present in the Al-Fe-Co alloy enhances dislocation multiplication and hinders dynamic recovery resulting in a small subgrain size. Therefore, this alloy has a higher dislocation density than EC aluminum after an equivalent amount of deformation. A large amount of stored energy serves to lower the amount of externally applied energy (kT) needed to initiate recrystallization as indicated by the appearance of a lower effective recrystallization temperature of the Al-Fe-Co alloy as compared to EC (475°F versus 500°F for the onset of recrystallization). However, the precipitates hinder the growth of recrystallization nuclei and the process is more sluggish in the Al-Fe-Co than in EC. This was evident by comparing the slopes of the yield strength versus annealing-temperature curves and the optical microstructures of the two materials. The higher

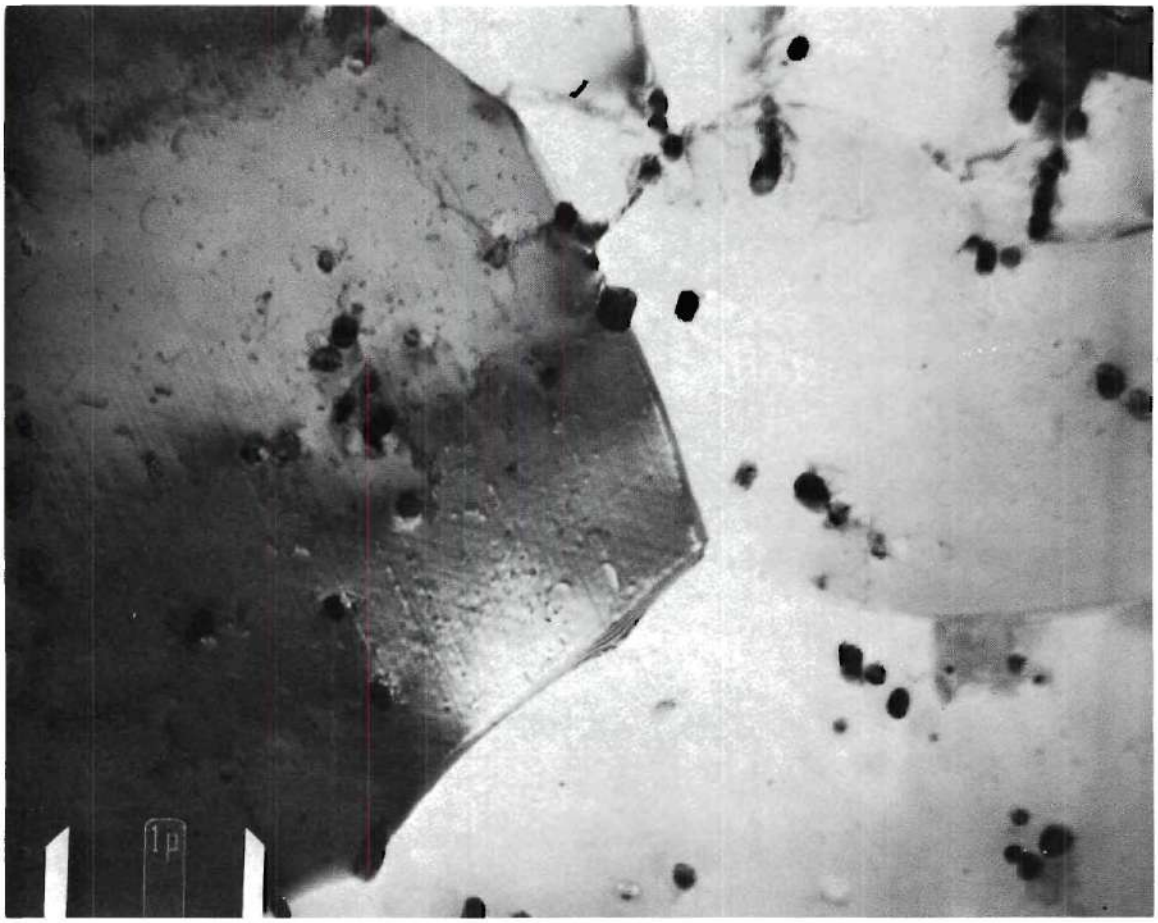

Figure 83. TEM of the Al-Fe-Co Alloy Wire Isochronally Annealed at 800°F for One Hour Showing Large Subgrains with $(Co,Fe)_2Al_9$ Particles Inside.

degree of internal energy present in the Al-Fe-Co alloy was manifested by the greater amount of dislocations in the cell interior, as may be seen by comparing Figures 84 with Figure 85.

The structural changes which took place in 0.105 inch diameter cold drawn EC aluminum during annealing were also studied with the electron microscope. In addition, the subgrain size of each wire, after annealing, was measured and plotted in Figure 86.

Recovery in the EC aluminum took place from about 250°F to about 500°F as shown by the gradual decrease in ultimate tensile strength and yield strength (Figure 70) and by subgrain coalescence. However, subgrain coalescence was not very pronounced and it took place in a small temperature range. Figure 87 is a transmission electron micrograph of EC aluminum wire annealed one hour at 400°F. Salient features in the structure were the clearing of dislocations from the interior of the subgrains together with some polygonization.

Primary recrystallization occurred in EC aluminum above 500°F. The ultimate tensile strength and yield strength started a sharp decrease which corresponded to a dramatic increase in grain size from 0.6 microns at 500°F to 1.4 microns at 525°F. Structures after annealing at 525°F are shown in Figures 88A. and 88B. Certain portions of the material were completely polygonized showing large grains with thin, delineated walls as those shown in Figure 88A. Figure 89 shows the structure of the partially recrystallized specimen annealed at 550°F for one hour. Significant growth of subgrains from recrystallization nuclei occurred. After a one hour anneal at 600°F, the EC aluminum exhibited a completely recrystallized grain structure, as shown in Figure 90.

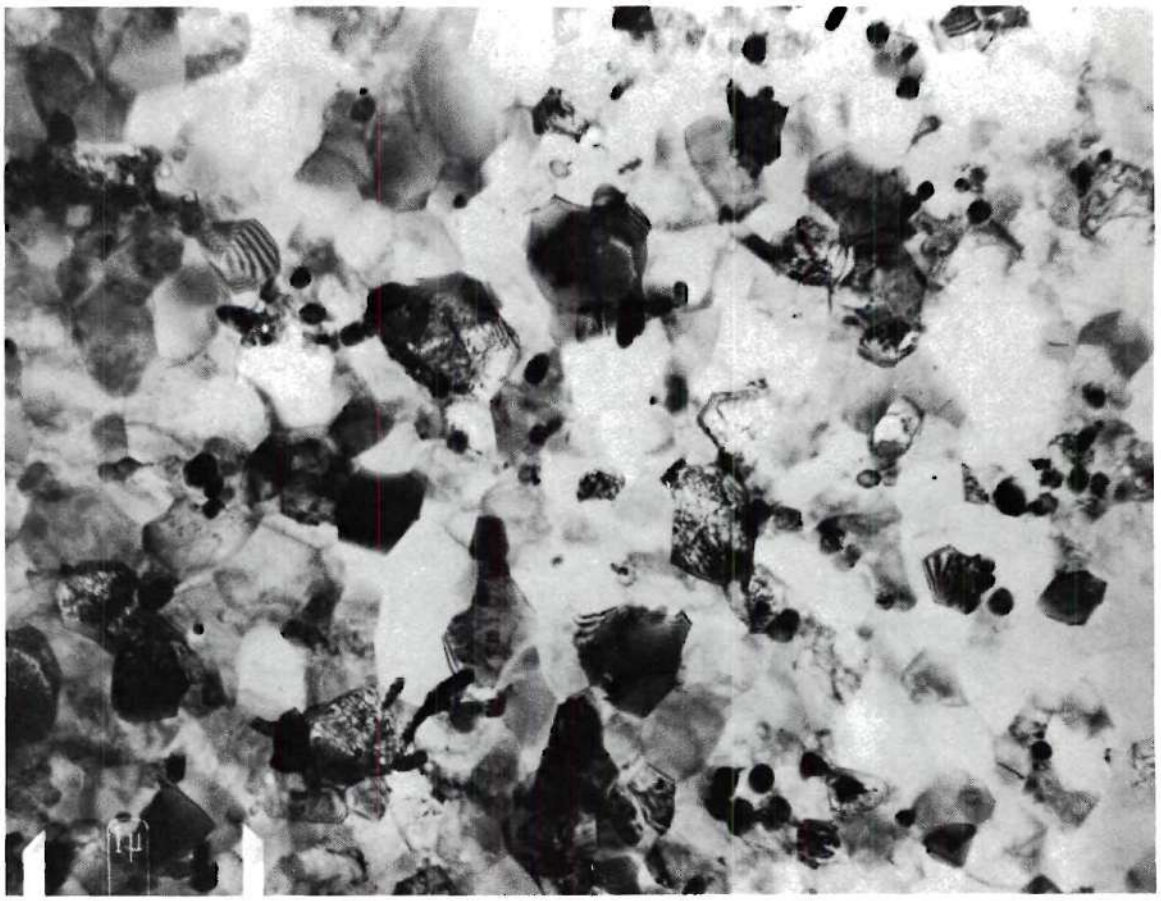

Figure 84. TEM of Al-Fe-Co Alloy Wire in the As-Drawn Condition Showing Heavy Dislocation Tangles and Heavy Cell Walls.

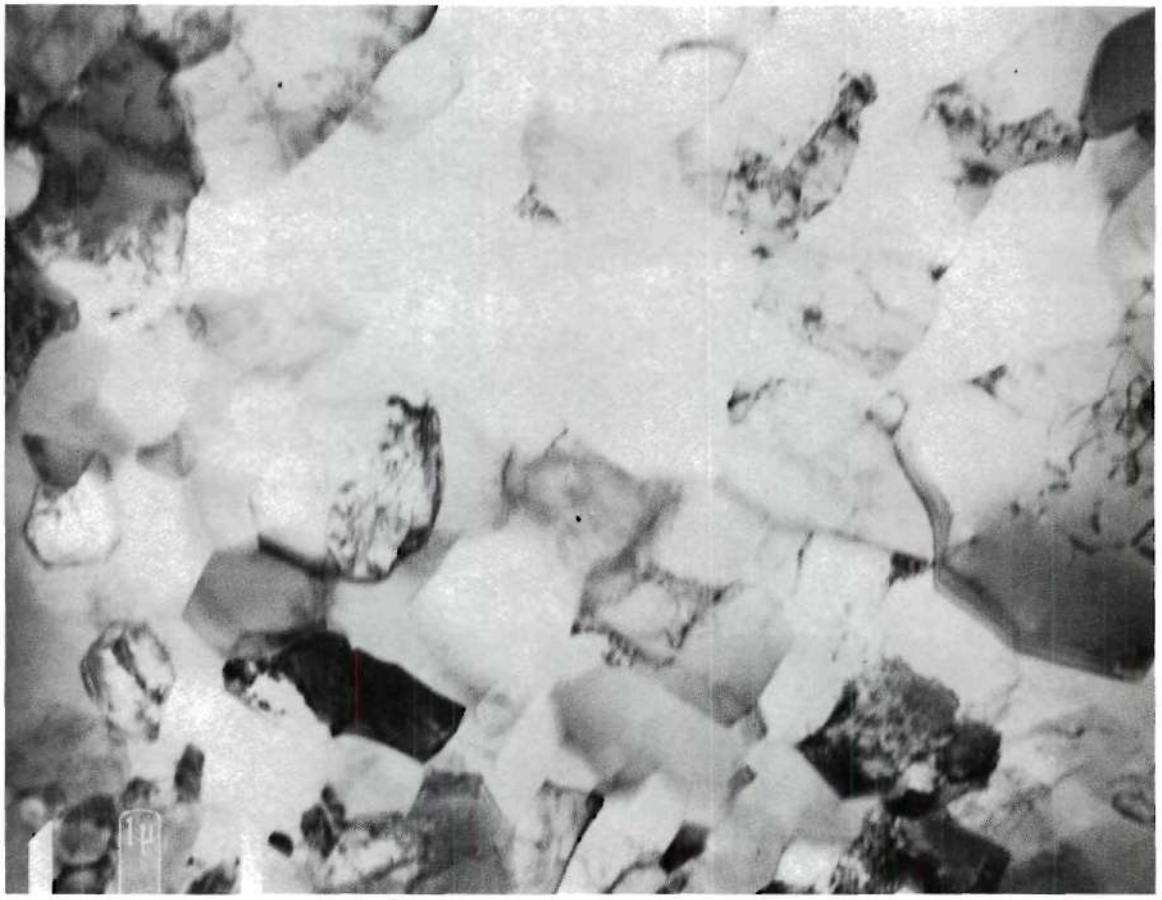

Figure 85. TEM of EC Aluminum Wire in the As-Drawn Condition Showing Cell Structure.

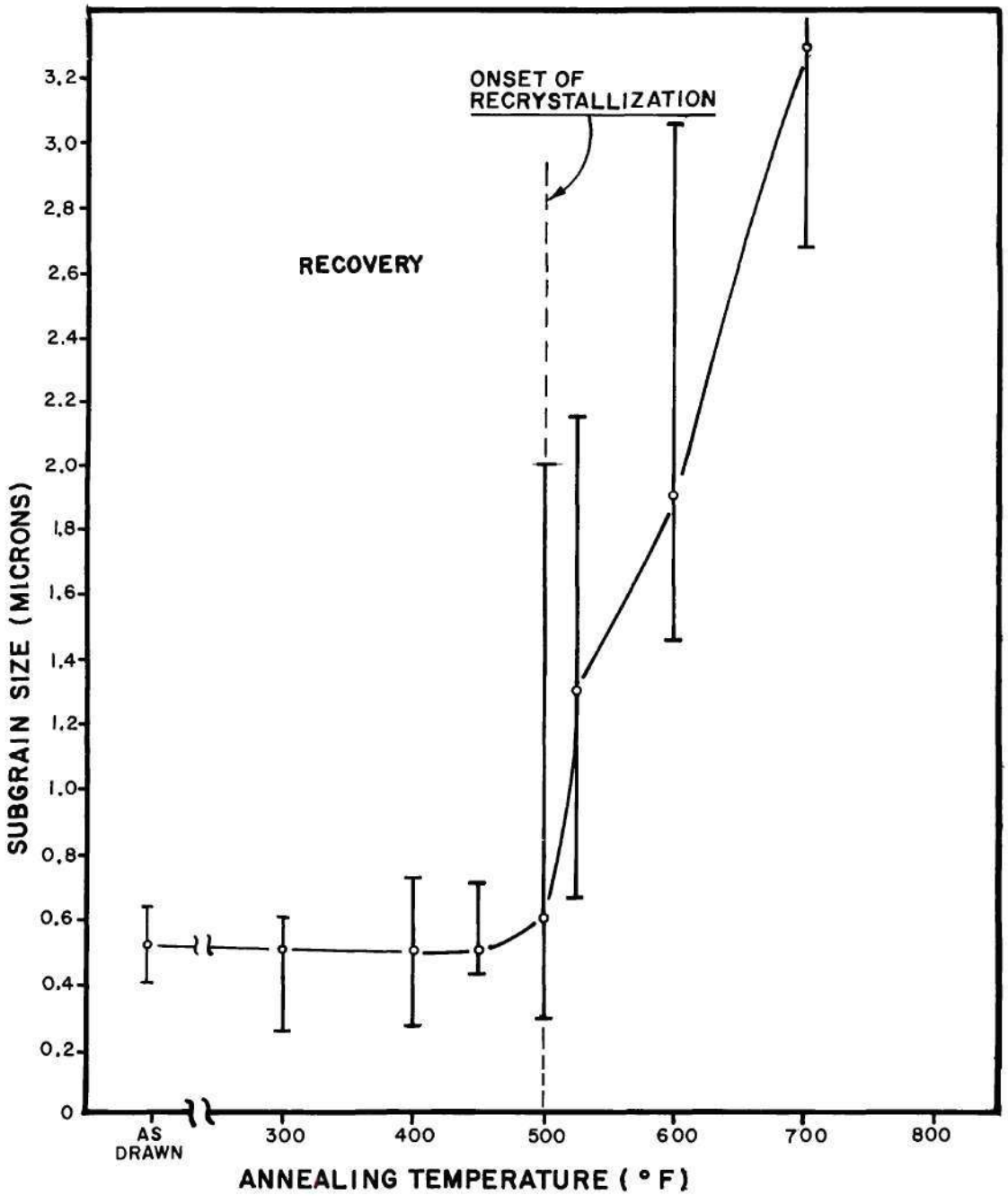

Figure 86. Effect of One Hour Isochronal Annealing on the Subgrain Size of EC Aluminum Wire.

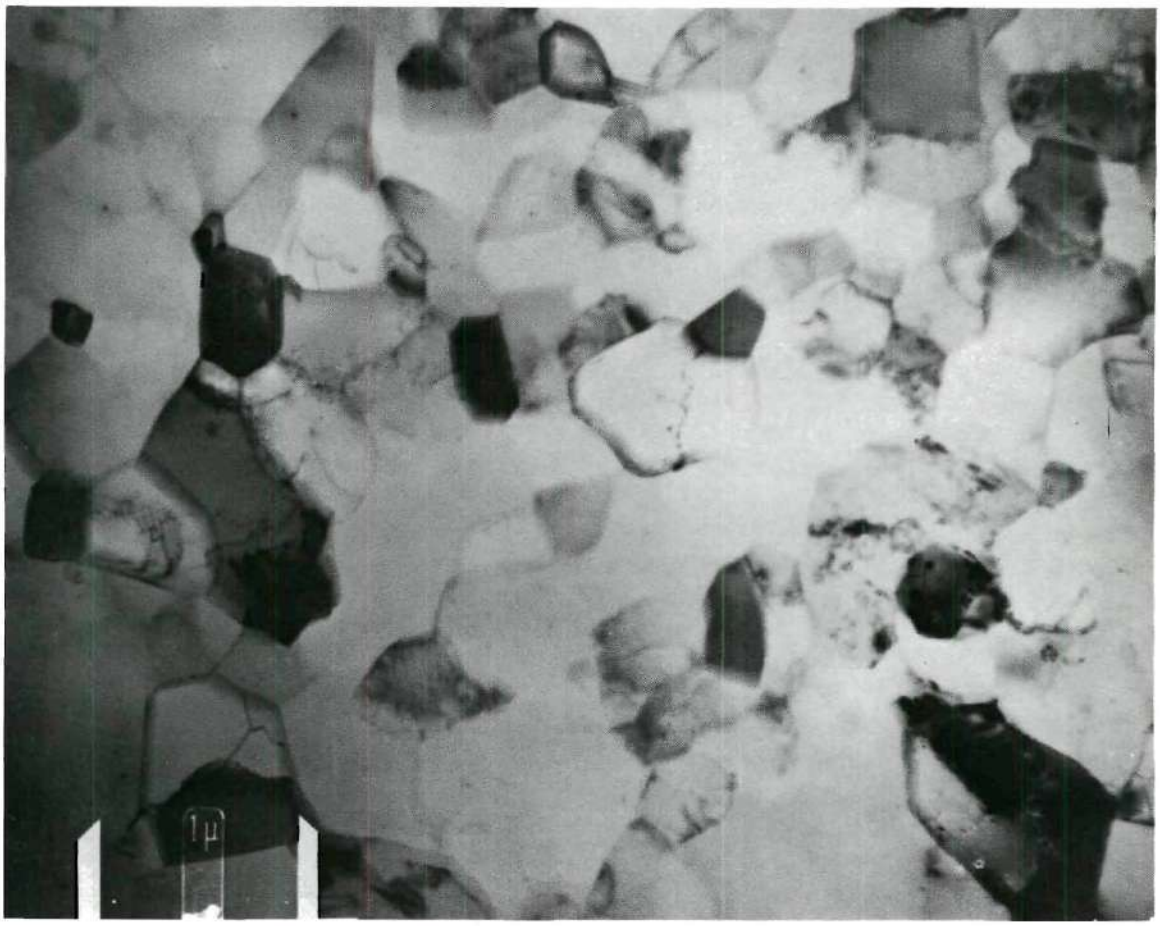

Figure 87. TEM of EC Wire 0.105 Inch Diameter Annealed for One Hour at 400°F Showing Dislocation Clearing from the Cell Interiors. A certain Amount of Polygonization is Observable.

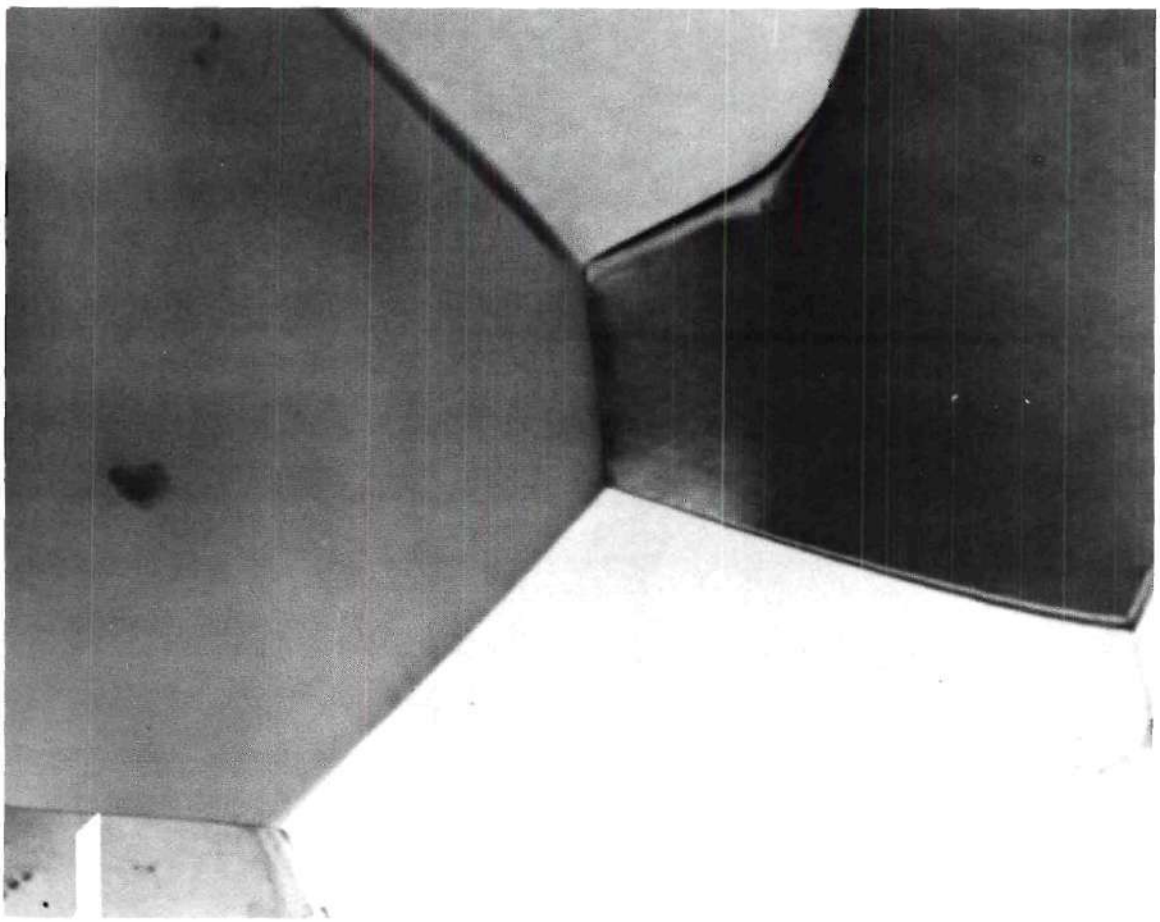

Figure 88A. TEM of EC Wire Annealed for One Hour at 525°F Showing Completely Polygonized Subgrains Corresponding to the Recrystallized Regions.

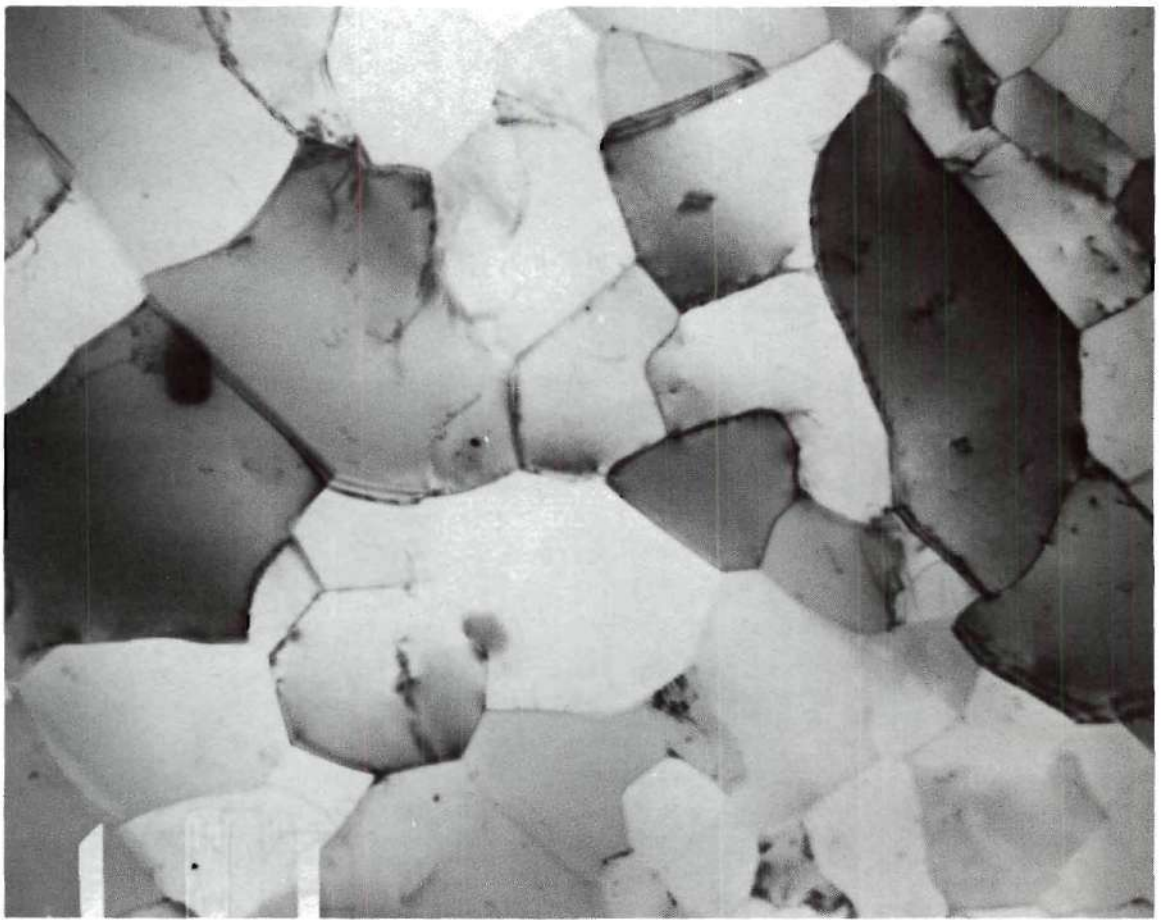

Figure 88B. TEM of EC Wire Annealed for One Hour at 525°F Showing Areas Which Have not Recrystallized.

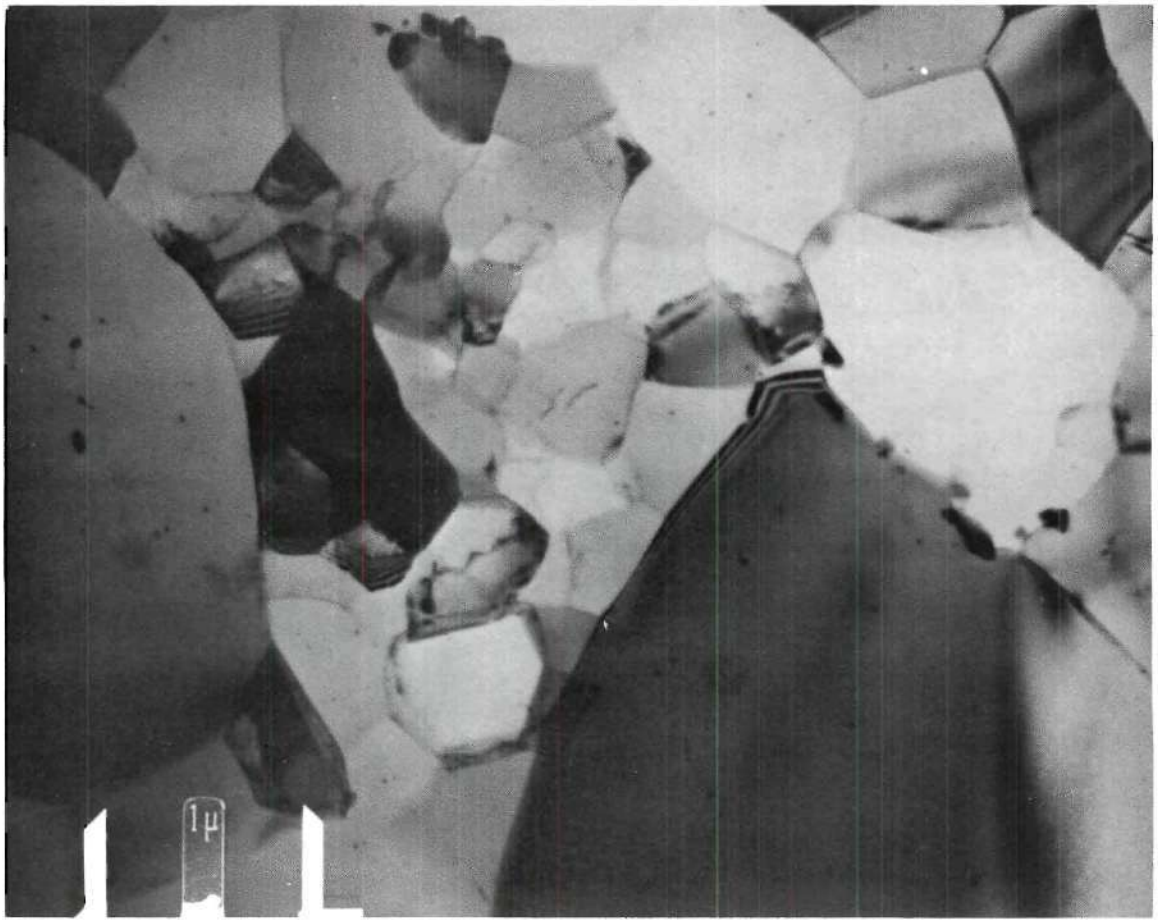

Figure 89. TEM of EC Wire Annealed at 550°F for One Hour Showing a Non-Uniform Subgrain Structure.

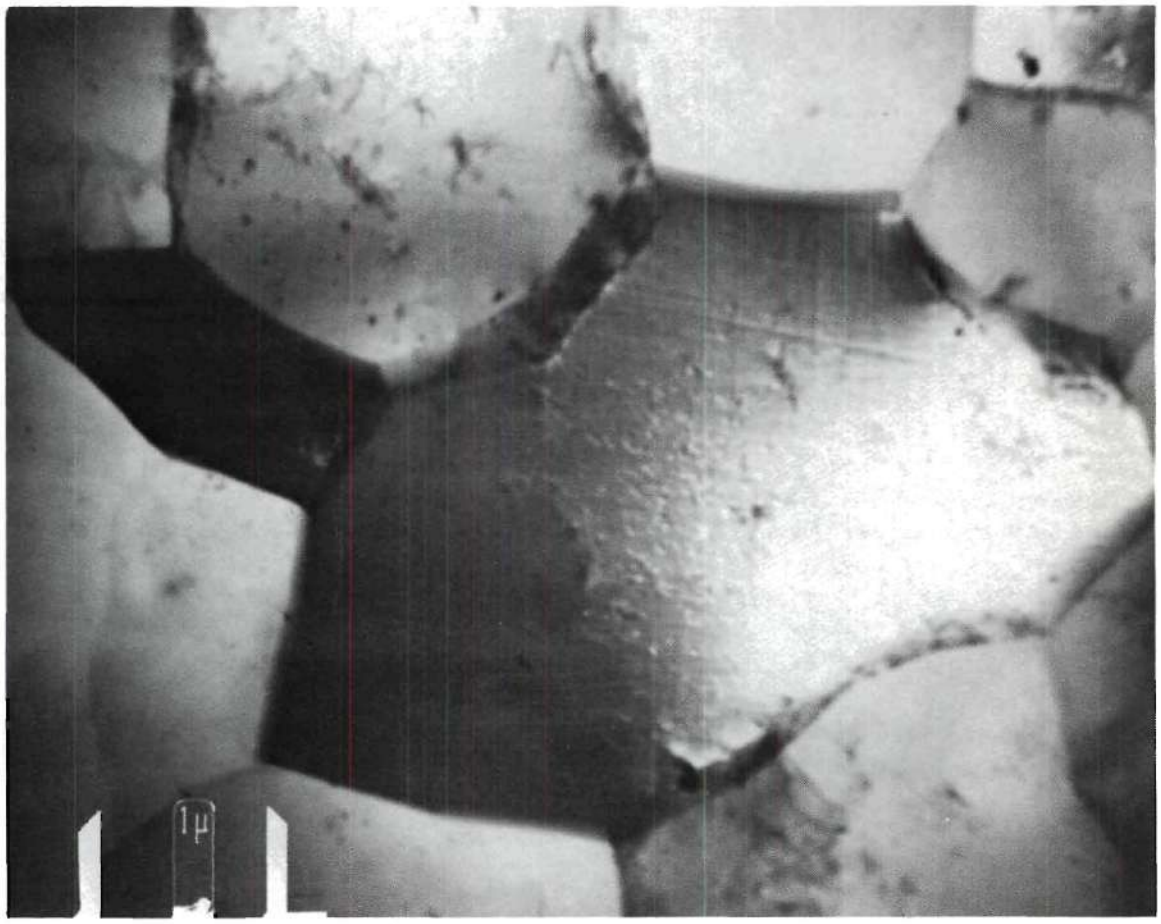

Figure 90. TEM of EC Wire Annealed at 600°F for One Hour Showing Large, Recrystallized Subgrains.

Optical Microstructures

In order to observe the effect of isochronal annealing on the microstructure of Al-Fe-Co alloy and EC aluminum, optical micrographs were taken from as-drawn to annealed at 800°F for one hour at 50°F intervals.

In the Al-Fe-Co alloy, the recrystallized grains are not clearly resolvable at 100X (Figure 91). However, selected area diffraction determinations and high magnification observation of these microstructures in the electron microscope showed the presence of recrystallization nuclei in the specimen annealed at 475°F for one hour as shown in Figure 73. The progress of recrystallization can be observed optically in Appendix II. The recrystallized grains are not resolvable at 100X magnification due to the pinning effect exerted by the precipitates in the matrix. Consequently, a recrystallized fraction count would not be accurate. This also implies that the end of recrystallization cannot be definitely ascertained.

The onset of secondary recrystallization can be observed in the specimen annealed one hour at 700°F. (Figure 92A) The amount of secondary recrystallized grains increases with increasing annealing temperatures, however, the specimen annealed at 850°F for one hour does not present a completely secondary recrystallized structure. (Figure 92B)

A side-by-side comparison of Al-Fe-Co and EC specimens isochronally annealed is shown in Appendix I. It can be observed that the EC specimens show the onset of recrystallization optically when annealed between 525°F and 550°F. Complete recrystallization was observed in the specimen annealed one hour at 600°F.

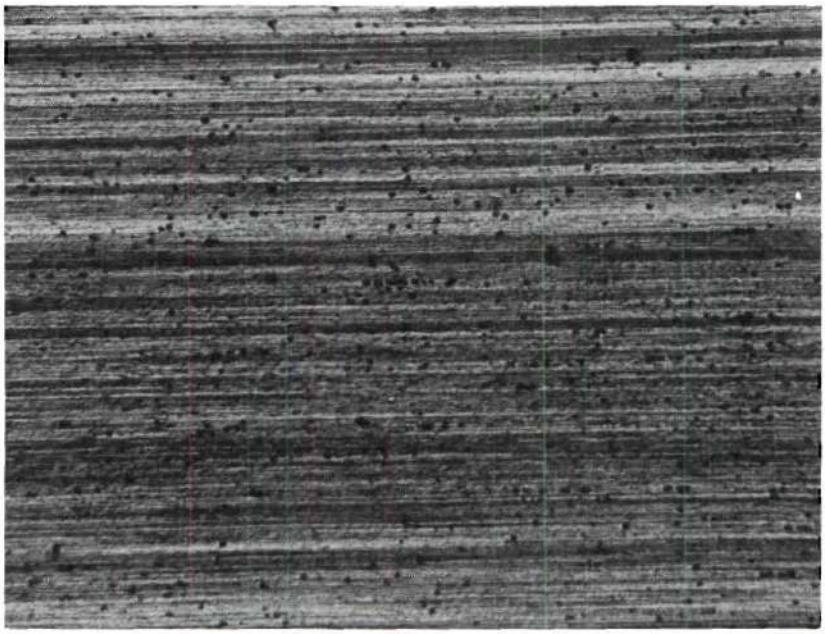

Figure 91A. Al-Fe-Co Alloy Wire in the Cold Drawn Condition. Polarized Light 100X

Figure 91B. Al-Fe-Co Alloy Wire Annealed One Hour at 625°F Showing Even, Small Recrystallized Grains. Note the Lack of Resolution of Individual Grains Due to the Small Size of the Subgrains. The Pinning of the Boundaries by the Precipitates Prevents them from Coalescing.

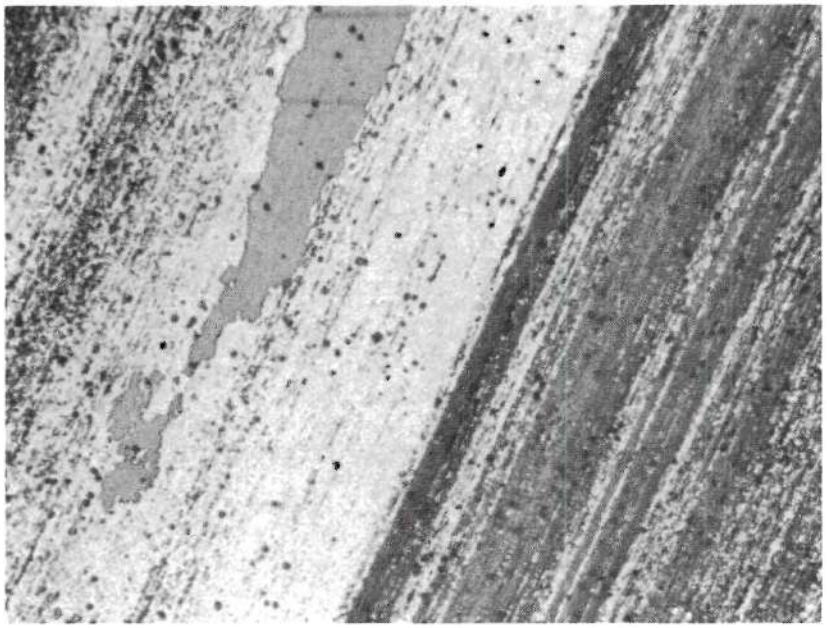

Figure 92A. Al-Fe-Co Alloy Wire Annealed One Hour at 700°F Showing the Onset of Secondary Recrystallization.

Polarized Light 100X

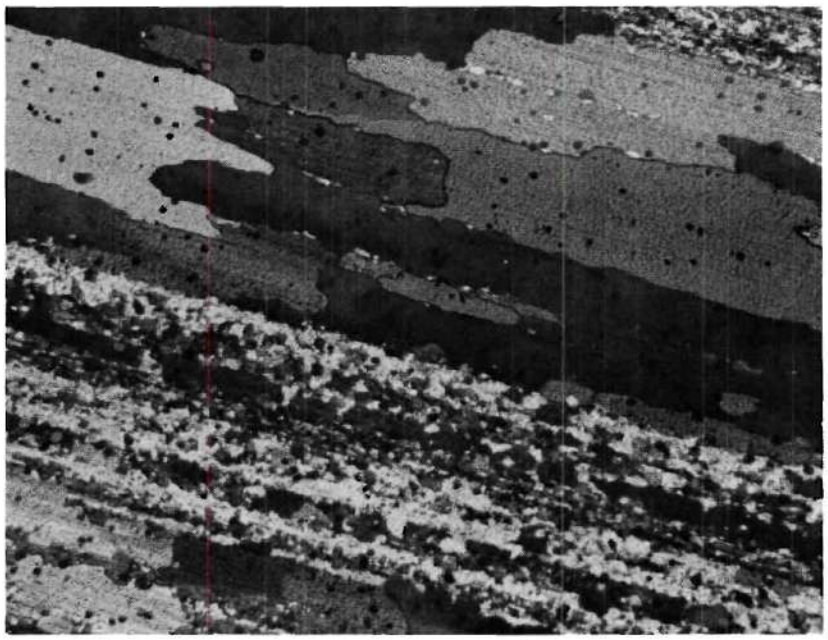

Figure 92B. Al-Fe-Co Alloy Wire Annealed One Hour at 850°F Showing Large Areas of Grains Which have Secondarily Recrystallized.

Polarized Light 100X

Continuous grain growth is visible from 600°F to 800°F with an absence of secondary recrystallization. Appendix II contains the optical microstructural sequence of the isochronally annealed Al-Fe-Co alloy.

In summary, the present research has shown that in order to produce a final wire product with small, uniformly distributed precipitate particles, rapid solidification producing a small interdendritic spacing is necessary.

During hot-rolling, once the critical amount of strain has been achieved, deformation of the alloy proceeds uniformly. Optimum rolling conditions consist of a high strain rate with the maximum cooling attainable during deformation to produce a good dispersion of particles and a small cell structure.

Annealing the hot rolled rod before cold drawing was proven to have a detrimental effect on the mechanical properties of the finished wire. This is due to the excessive growth of the subgrains before cold work and to the precipitation of the compounds before final annealing. It was also found that the obtained dispersion of particles in the cold drawn wire acts as pinning points to the movement of the subgrain boundaries during annealing. It was found that the high degree of thermal stability achieved in the aluminum, 0.5 percent iron, 0.5 percent cobalt alloy was due to the pinning effect produced by the precipitate particles on the growing subgrain boundaries after primary recrystallization. This effect is responsible for producing a finish-wire product which possesses a stable subgrain structure and consequently, excellent mechanical and electrical properties.

CHAPTER V

CONCLUSIONS

1. The rapidly solidified Al-Fe-Co aluminum alloy exhibits a fine network of $(Co,Fe)_2Al_9$ and $FeAl_3$ eutectic compounds in the as-cast structure, which results in a fine distribution of precipitates in the final wire product and excellent mechanical and electrical properties.

2. The slowly solidified Al-Fe-Co alloy cast bar exhibited a non-uniform structure characterized by the presence of patches or colonies of eutectic compound between large aluminum crystals. This structure produced a non-uniform distribution of precipitates large cells and poor mechanical properties in the hot-rolled rod and finished wire product. This results from the slow solidification which allows all of the cobalt and iron to precipitate as large particles in non-uniformly distributed eutectic colonies. The large areas devoid of precipitates cannot resist the movement of the grain boundaries and therefore subgrain coalescence takes place.

3. During hot rolling, the ultimate tensile strength of the Al-Fe-Co alloy sharply increases above 90 percent reduction. The elongation of the Al-Fe-Co sharply decreases with reductions above 90 percent. This is due to the high degree of work hardening and the negligible amount of dynamic recovery taking place after this reduction which are produced by the high rolling speeds and low rolling temperatures.

4. Subgrains are formed after 37 percent reduction in area during hot rolling. The subgrains form initially between rows of precipitates which act as dislocation sources during deformation. The subgrain size decreases progressively until 95 percent reduction. Further reductions do not significantly reduce the cell size; however, the dislocation density in the cells increases significantly.

5. Annealing the hot-rolled Al-Fe-Co rod 650^{o}F for three hours before cold drawing produces a finish wire with larger subgrains and poorer mechanical properties than the wire produced from non-annealed rod.

6. Static recovery of 0.5 percent Cobalt 0.5 percent iron aluminum alloy starts to take place at approximately 300^{o}F for one hour. Precipitation, which begins to take place at 200^{o}F, for one hour appears to be responsible for the increase in mechanical properties after annealing at 200^{o}F, 250^{o}F and 300^{o}F. The EC aluminum wire shows a steady increase in subgrain size during static recovery which continues during static recrystallization.

7. Primary recrystallization starts at about 475^{o}F in the cold-rolled Al-0.5% Fe-0.5% Co alloy wire produced from the rapidly solidified ingot. The onset of recrystallization is marked by the coalescence of certain subgrains to form the recrystallization nucleus. The nucleus grows to form a high-angle boundary grain structure with thin, delineated grain walls. During recrystallization subgrain growth is inhibited by the presence of precipitate particles, which act as pinning points to the movement of the subgrain boundaries. Thus, the resulting average size of the recrystallized subgrains in the annealed wire is of the same magnitude as the average interparticle spacing.

8. Secondary recrystallization takes place at 700°F for one hour in the Al-Fe-Co alloy when the pinning effect of the precipitates is overcome by the introduced energy.

9. The Al-Fe-Co alloy strengthening obeys the Orowan mechanism. In a matrix containing subgrains, the strength is determined by a combination of precipitate and subgrains effect. The combination of this duplex strengthening mechanism probably prevents any direct correlation with either Hall-Petch or Langford-Cohen equations.

APPENDIX I

MISORIENTATION ANGLES

In order to determine the misorientation angle between adjacent subgrains in a specimen annealed one hour at 750°F, selected area diffraction (SAD) patterns were taken of each subgrain in the areas shown in Figure 93. The obtained angles between subgrains and their respective orientation are shown in Figure 94. As can be observed the smallest measured angle was 11.5° between (112) and (334) and the highest angle was 46.5° between (334) and (001). Table 10.

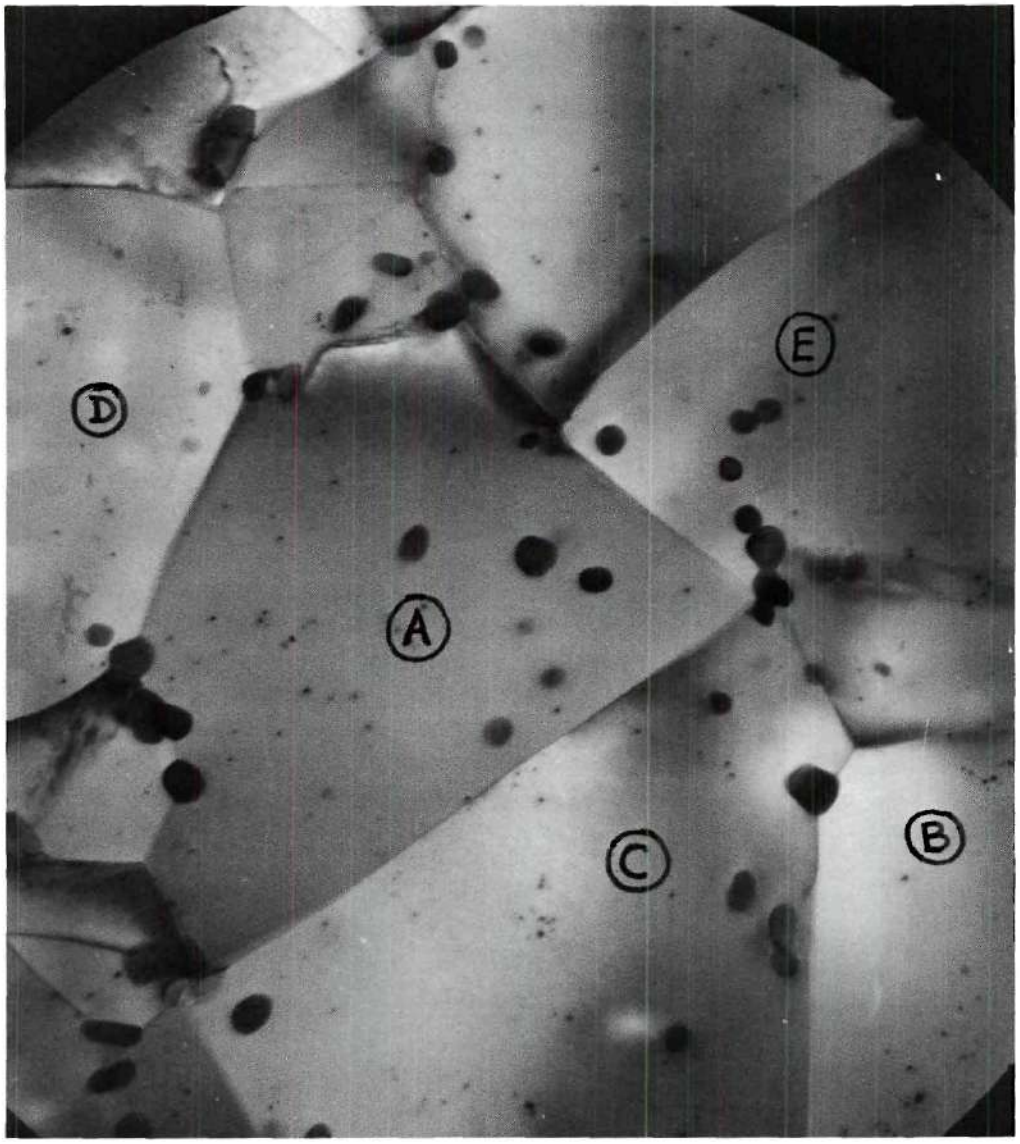

Figure 93. TEM of the Location of the Selected Area Diffraction Determination.

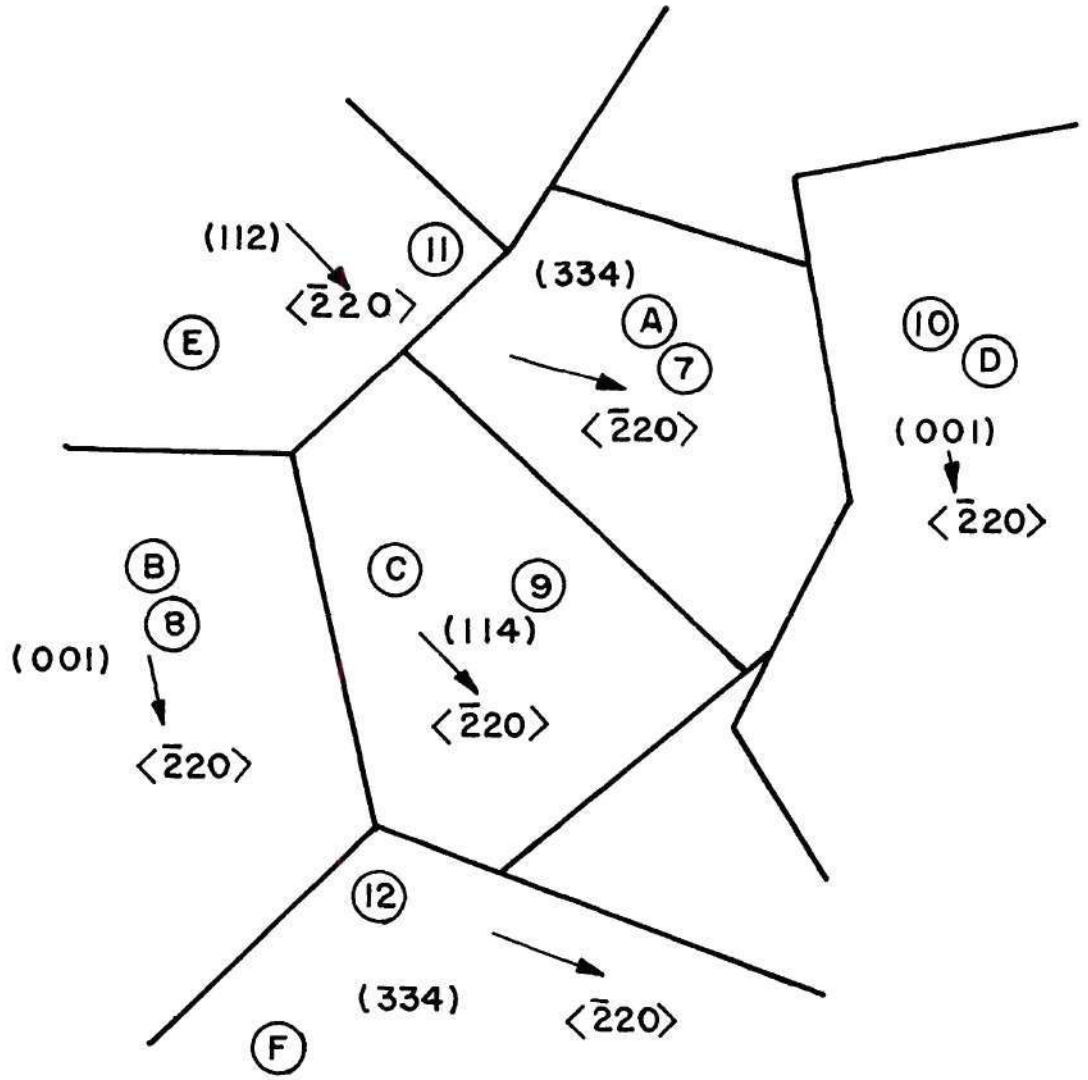

Figure 94. Sketch of the SAD Location Showing Subgrains' Orientations.

Table 10. Angles of Misorientation Between Subgrains

SUBGRAIN	PLANE	ANGLE
A	(334)	46.5°
D	(001)	
A	(334)	27°
C	(114)	
B	(001)	19.5°
C	(114)	
E	(112)	35°
B	(001)	
E	(112)	11.5°
A	(334)	
E	(112)	16°
C	(114)	

APPENDIX II

ISOCHRONAL ANNEALING

Optical micrographs at 50X magnification of the aluminum 0.5 percent iron 0.5 percent cobalt alloy and EC alloy wires are included in Figures 95 to 105. The specimens were cold drawn to 0.105 inch and isochronally annealed for one hour at various temperatures. The photomicrographs were taken using polarized light in the direction parallel to the drawing axis.

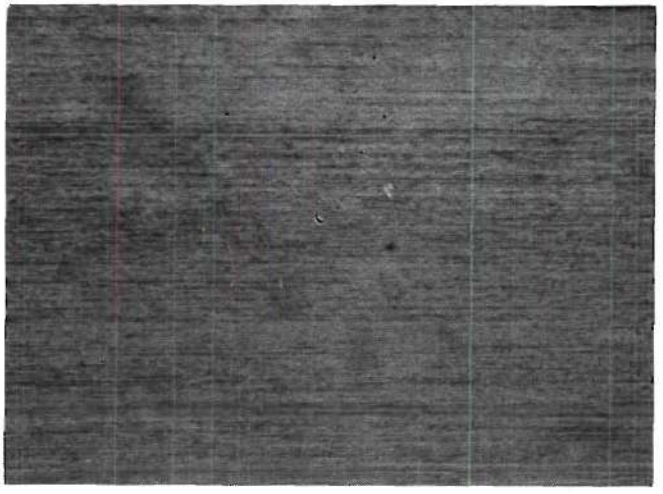

Figure 95A. Al-Fe-Co Alloy Hard Drawn Wire 50X

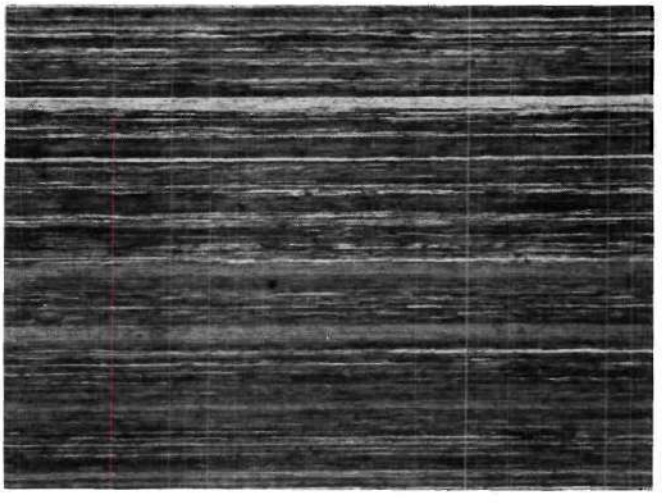

Figure 95B. EC Hard Drawn Wire 50X

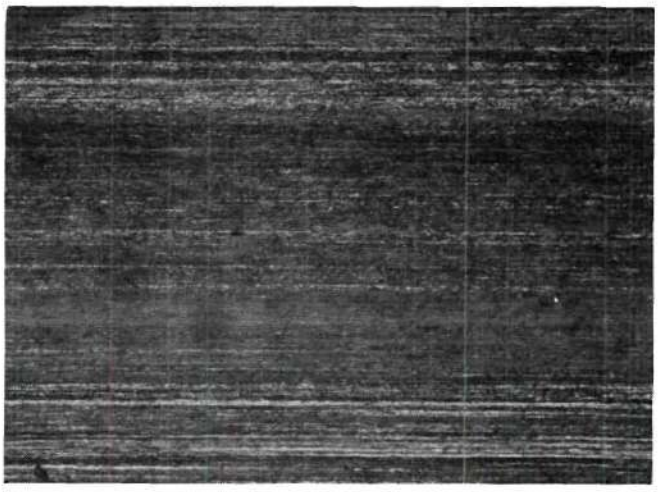

Figure 96A. Al-Fe-Co Alloy Annealed at 475°F for One Hour 50X.

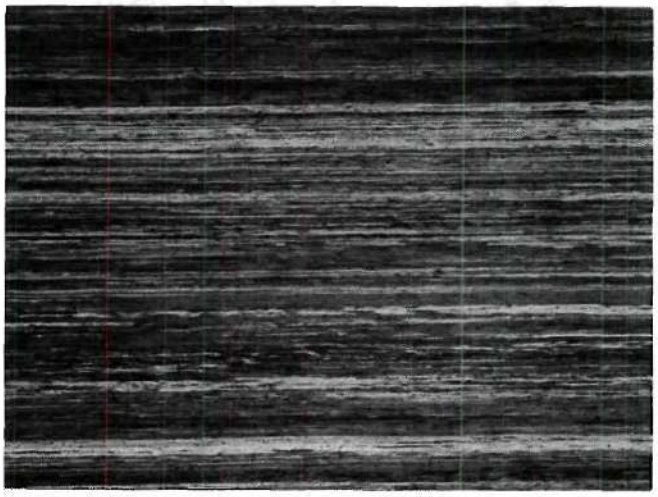

Figure 96B. EC Alloy Wire Annealed at 475°F for One Hour. 50X

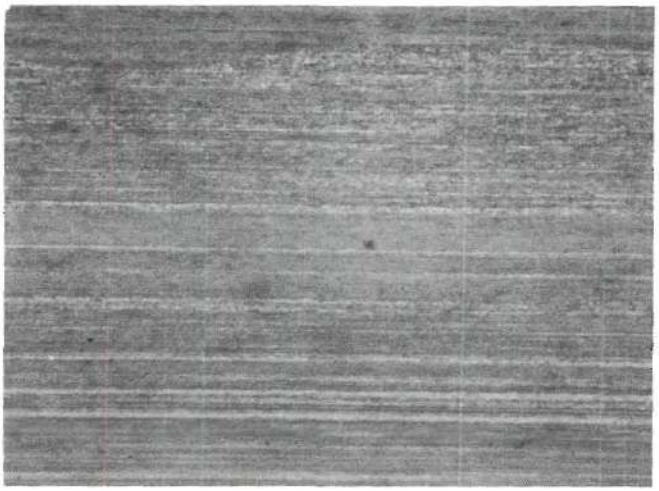

Figure 97A. Al-Fe-Co Alloy Wire Annealed at 500°F for One Hour. 50X

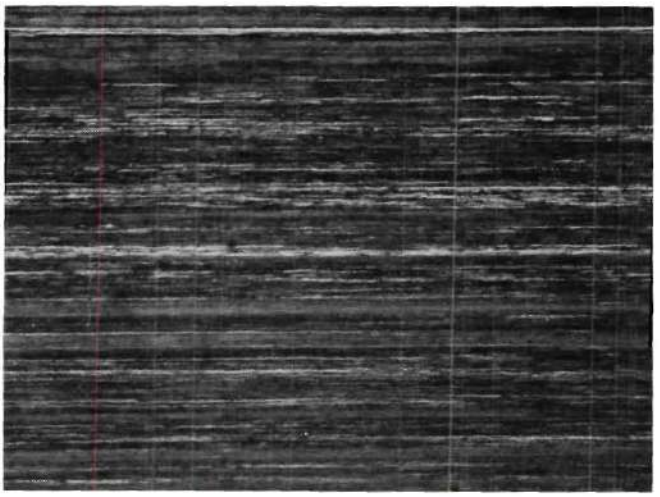

Figure 97B. EC Alloy Wire Annealed at 500°F for One Hour. 50X

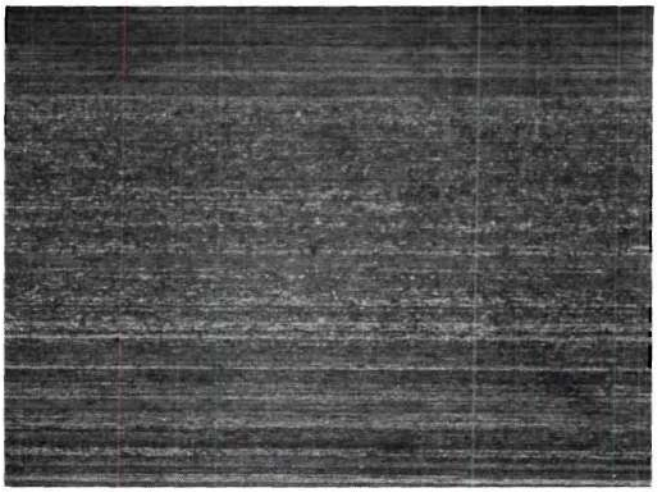

Figure 98A. Al-Fe-Co Alloy Wire Annealed at 525°F for One Hour. 50X

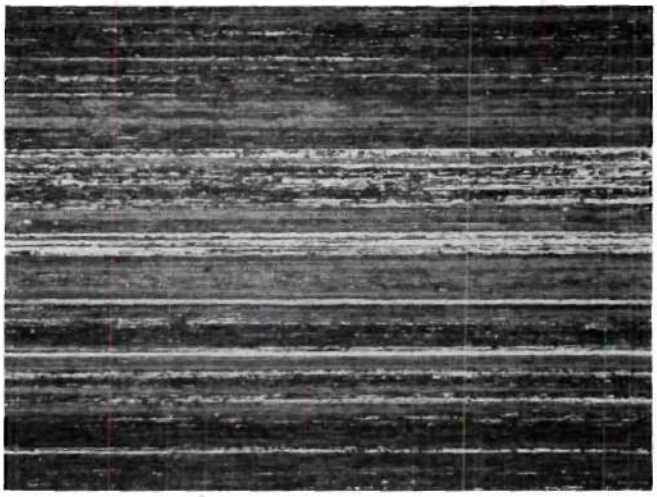

Figure 98B. EC Alloy Wire Annealed at 525°F for One Hour. 50X

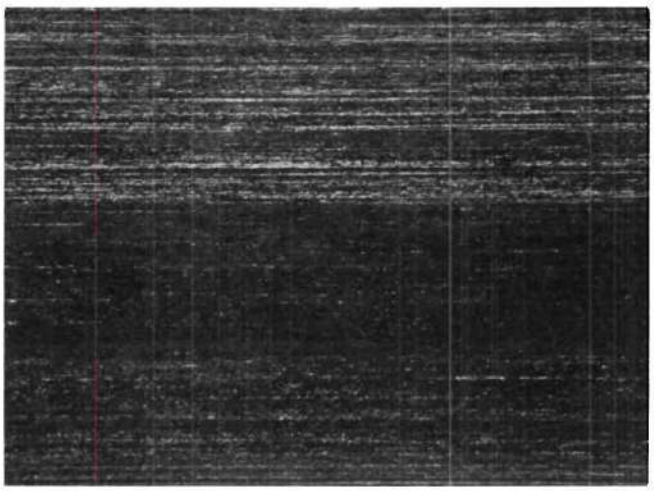

Figure 99A. Al-Fe-Co Alloy Annealed at 550°F for One Hour. 50X

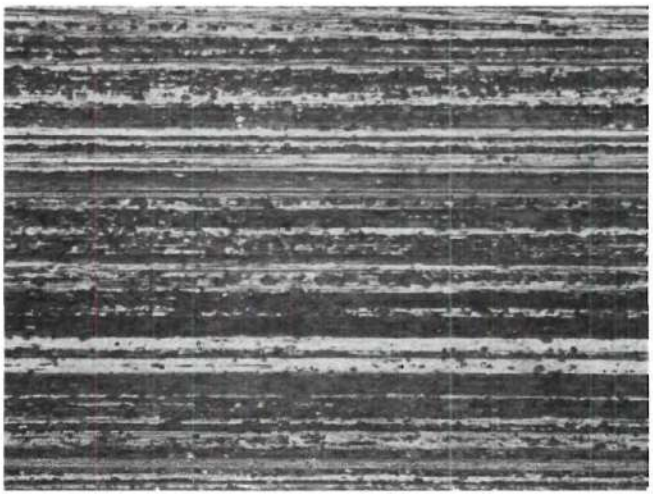

Figure 99B. EC Alloy Wire Annealed at 550°F for One Hour. 50X

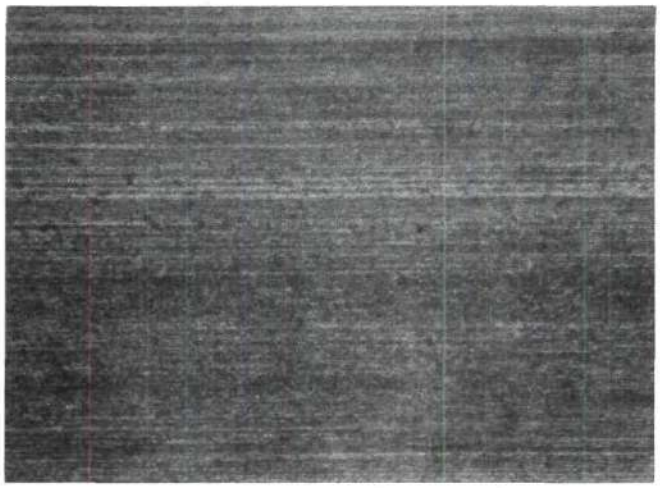

Figure 100A. Al-Fe-Co Alloy Wire Annealed at 575°F for One Hour. 50X

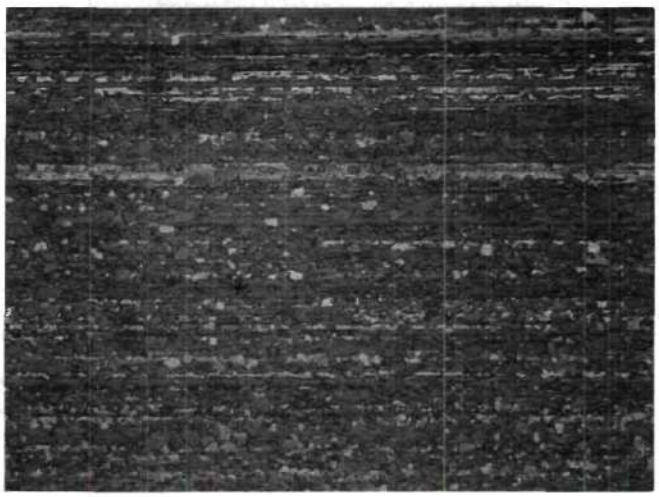

Figure 100B. EC Alloy Wire Annealed at 575°F for One Hour 50X

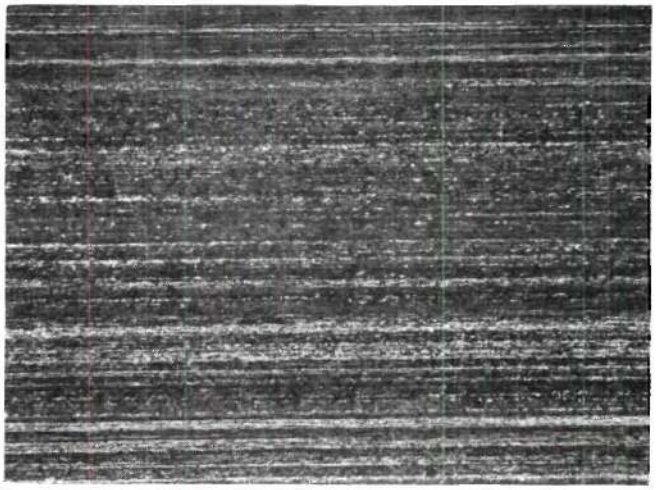

Figure 101A. Al-Fe-Co Alloy Annealed at 600°F for One Hour. 50X

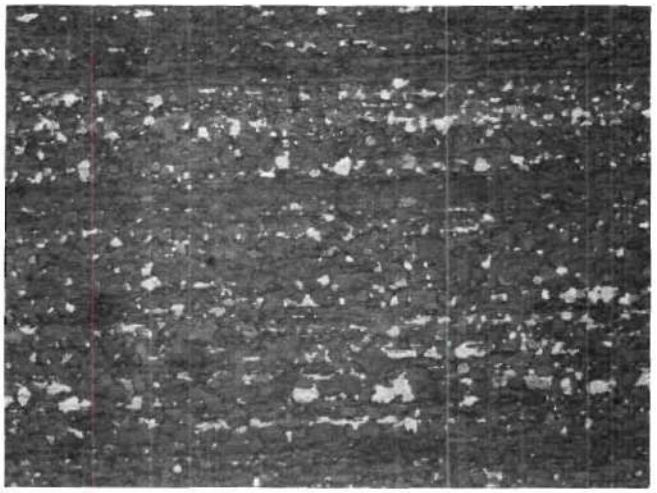

Figure 101B. EC Alloy Wire Annealed at 600°F for One Hour. 50X

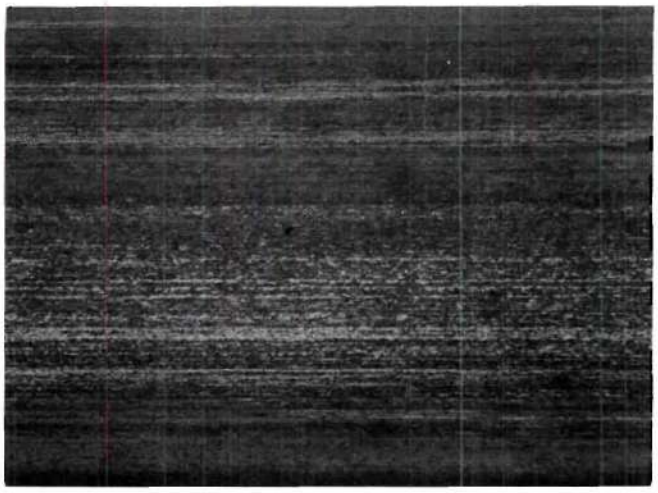

Figure 102A. Al-Fe-Co Alloy Annealed at 650°F for One Hour. 50X

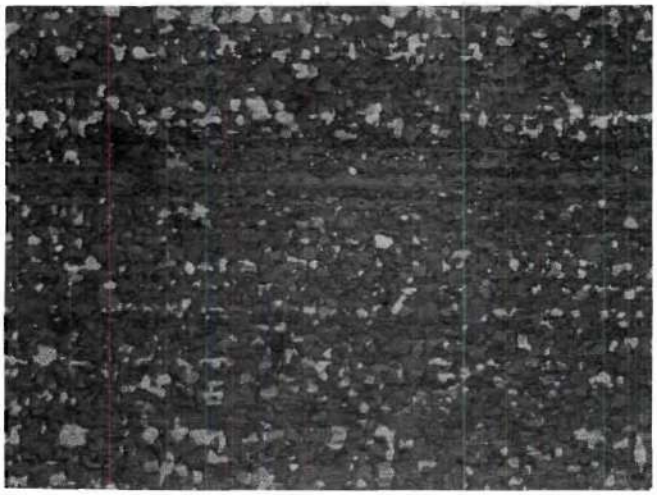

Figure 102B. EC Alloy Wire Annealed at 650°F for One Hour. 50X

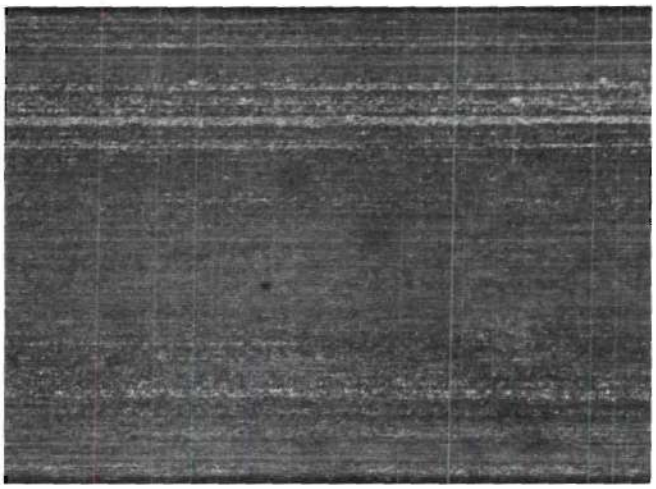

Figure 103A. Al-Fe-Co Alloy Annealed at 675°F for One Hour. 50X

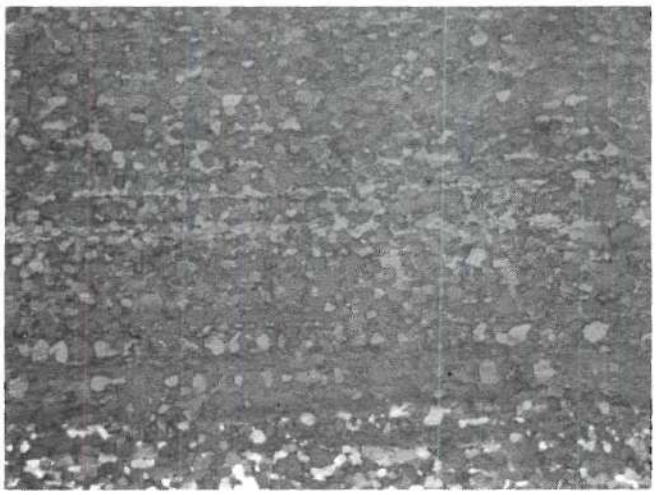

Figure 103B. EC Alloy Wire Annealed at 675°F for One Hour. 50X

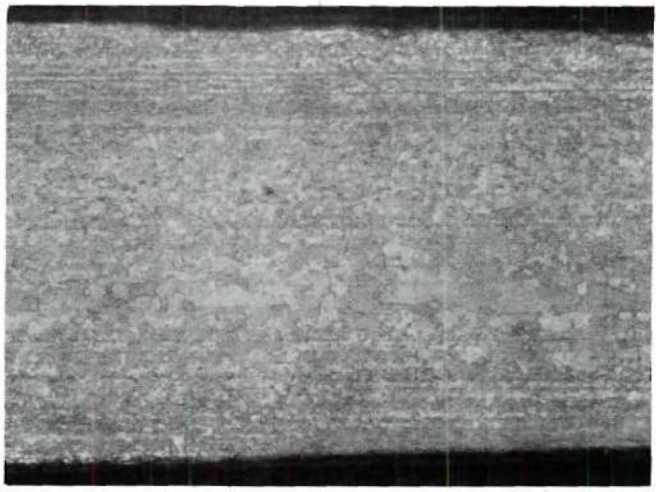

Figure 104A. Al-Fe-Co Alloy Annealed at 700°F for One Hour. 50X

Figure 104B. EC Alloy Wire Annealed at 700°F for One Hour. 50X

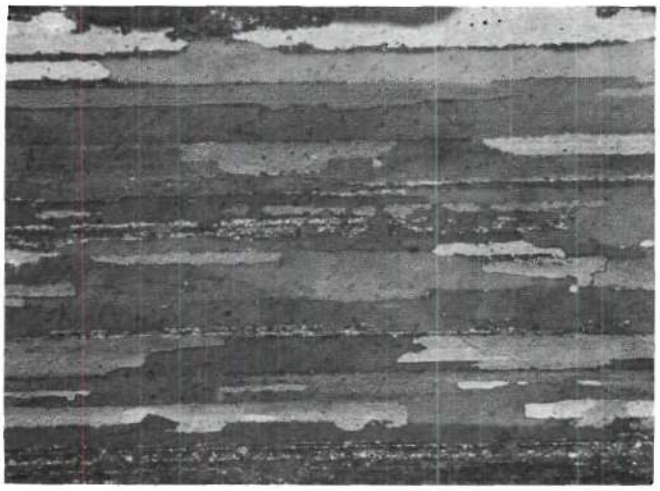

Figure 105A. Al-Fe-Co Alloy Annealed at 800°F for One Hour. 50X

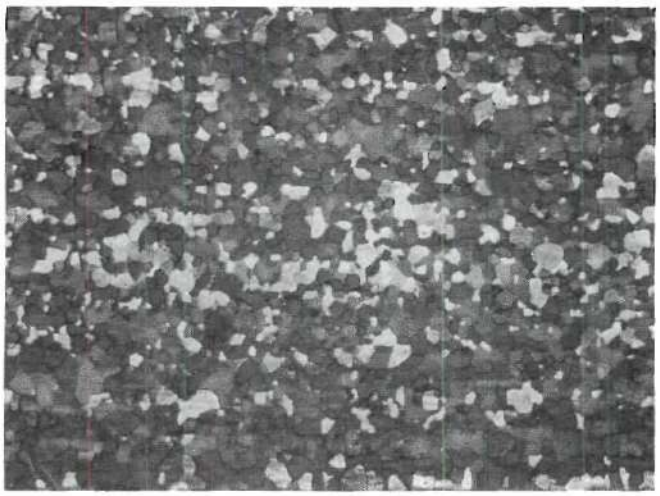

Figure 105B. EC Alloy Wire Annealed at 800°F for One Hour. 50X

APPENDIX III

ISOTHERMAL ANNEALING

The change of mechanical properties during isothermal annealing of the Al-Fe-Co and EC alloy wires are included in Figures 106 to 111. The material was cold drawn to 1.105 inch diameter and isothermally annealed at 500,550,600 and 650 degrees Fahrenheit. During the first hour of annealing, specimens were tested every 10 minutes in order to study the softening characteristics. Isothermal annealing was carried on the specimens to 420 minutes.

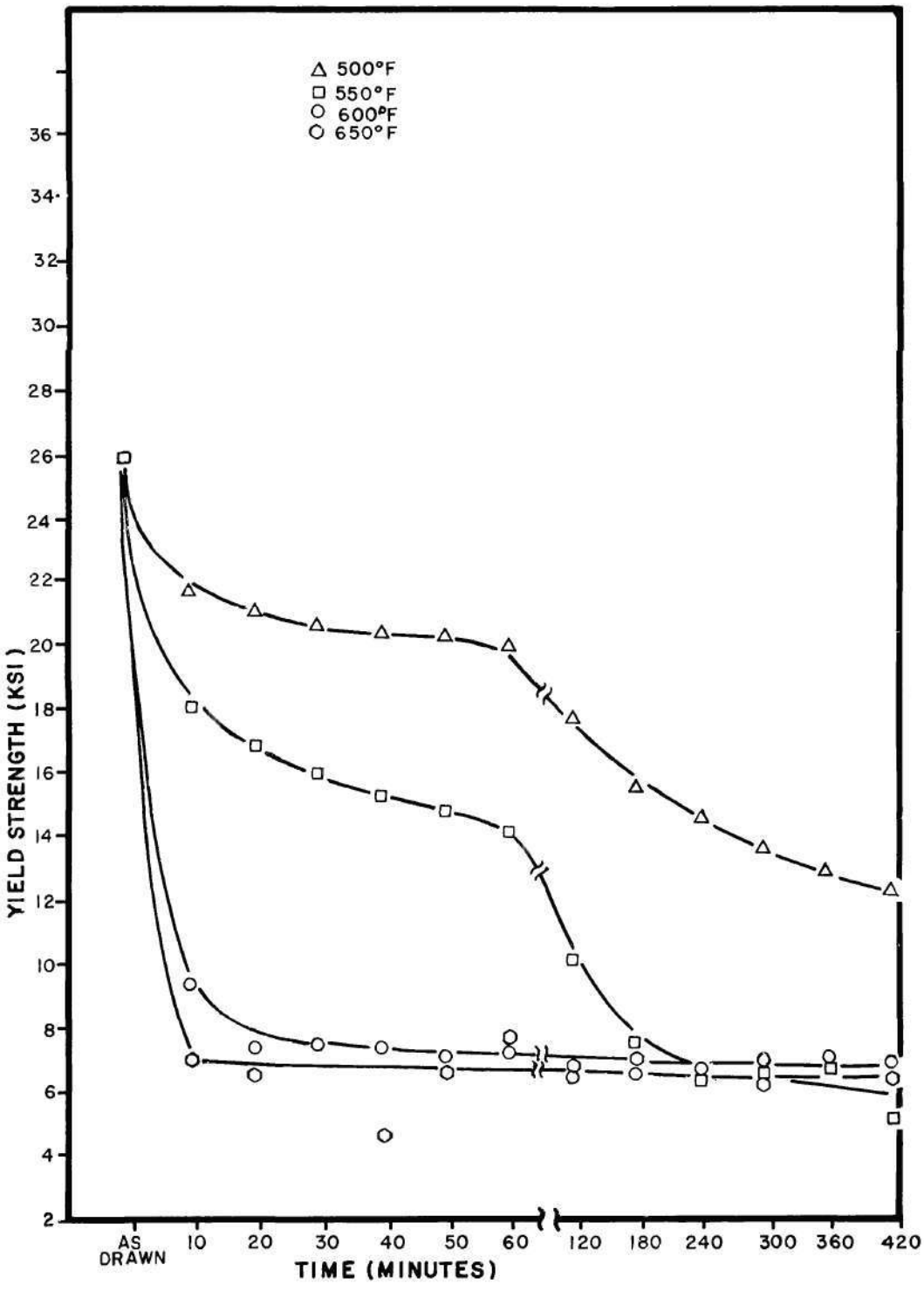

Figure 106. Variation of the Yield Strength During Isothermal Annealing of EC Cold Drawn Wire (0.105 Inch Diameter).

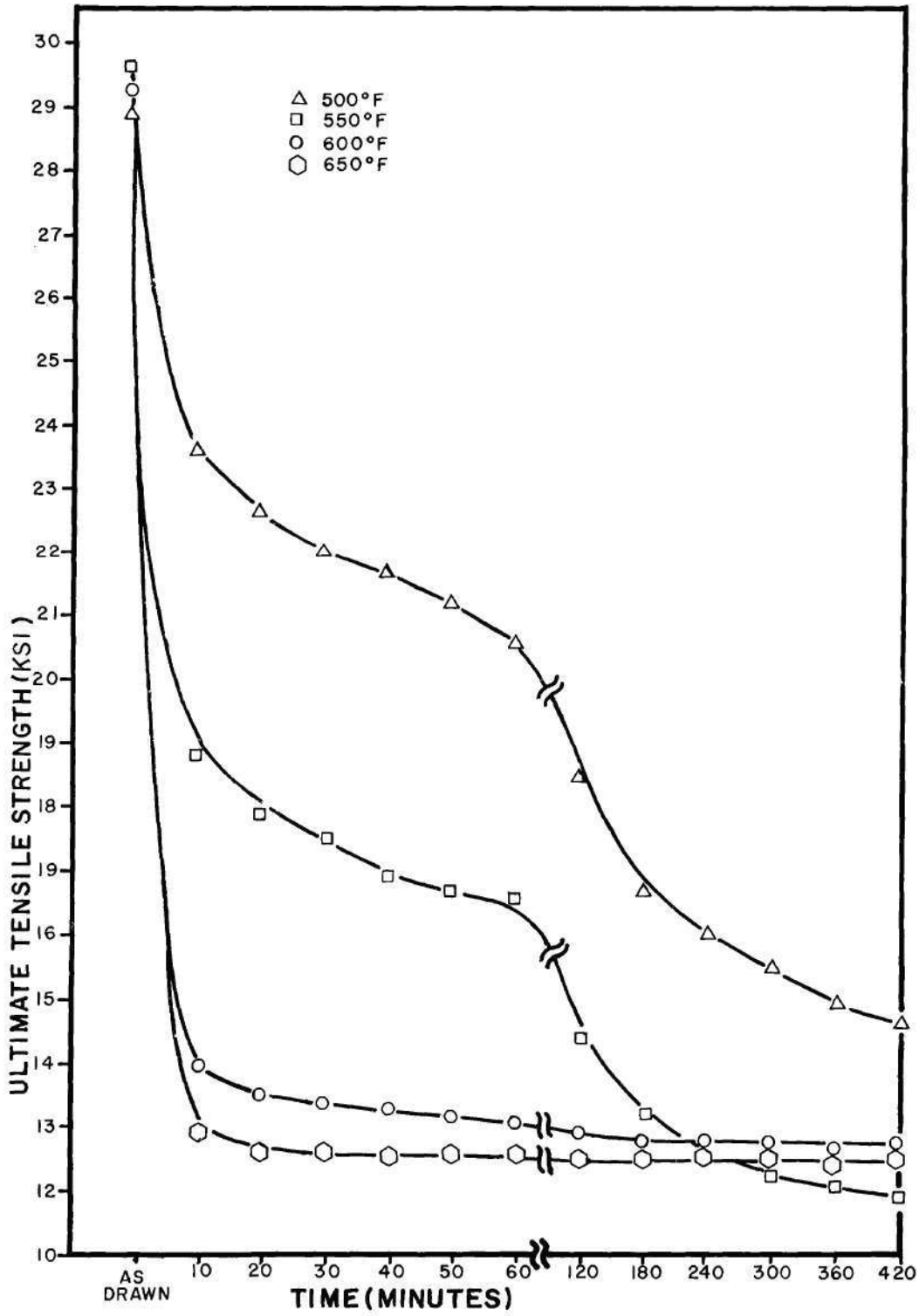

Figure 107. Variation of the Ultimate Tensile Strength During Isothermal Annealing of EC Cold Drawn Wire. (0.105 Inch Diameter).

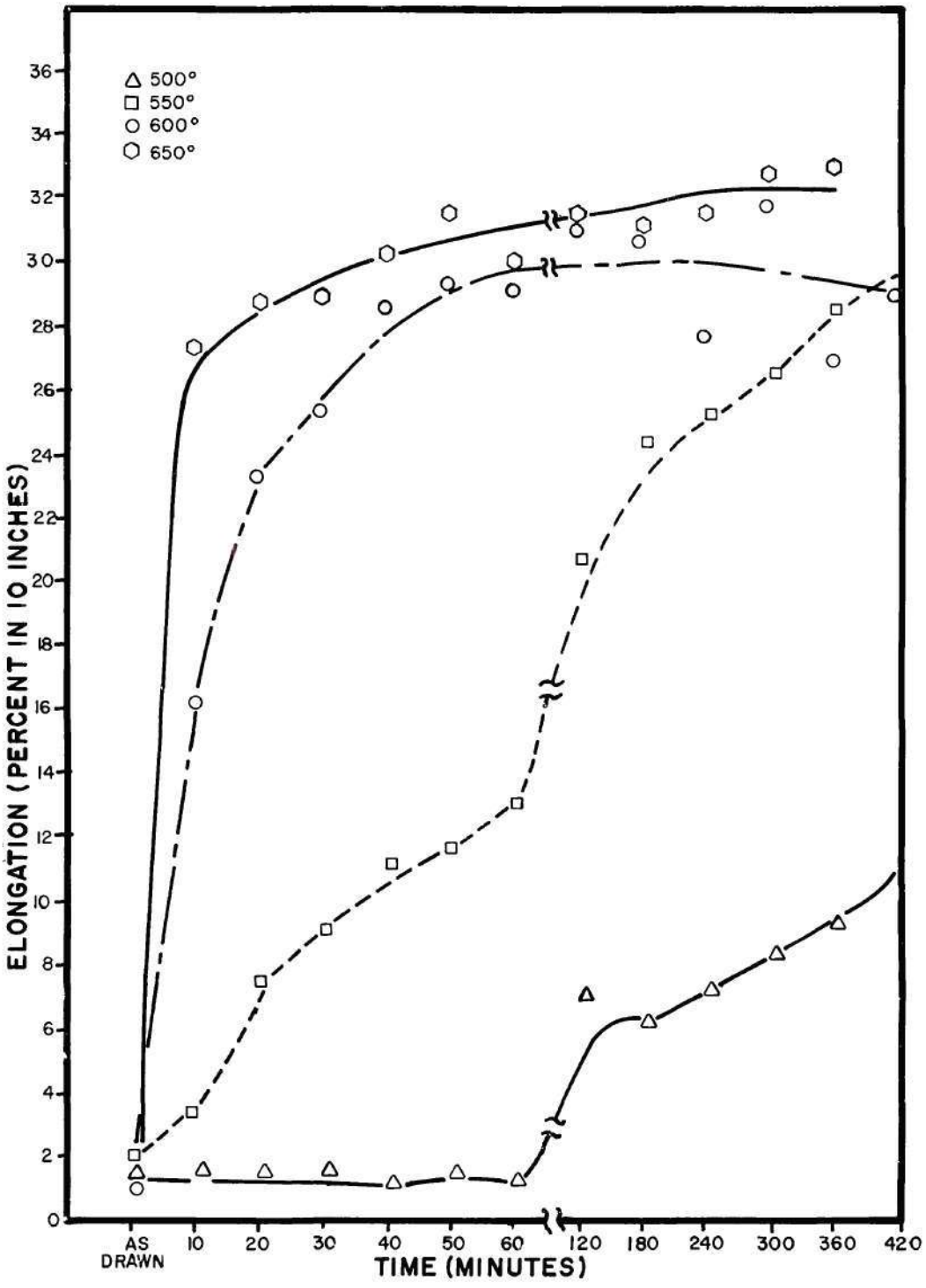

Figure 108. Variation in the Percent Elongation During Isothermal Annealing of EC Cold Drawn Wire (0.105 Inch Diameter).

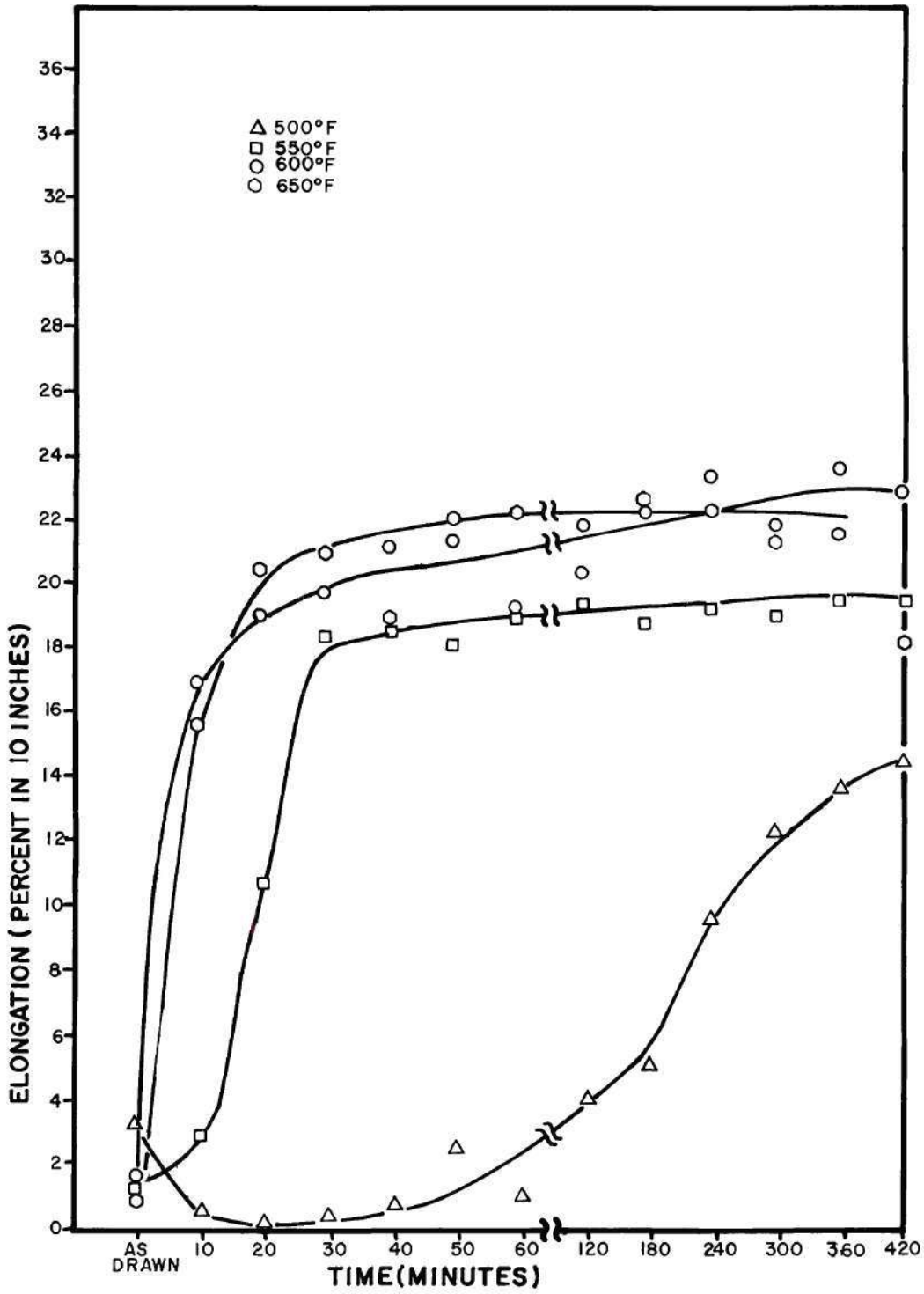

Figure 109. Variation in the Yield Strength During Isothermal Annealing of Al-Fe-Co Cold Drawn Wire. (0.105 Inch Diameter)

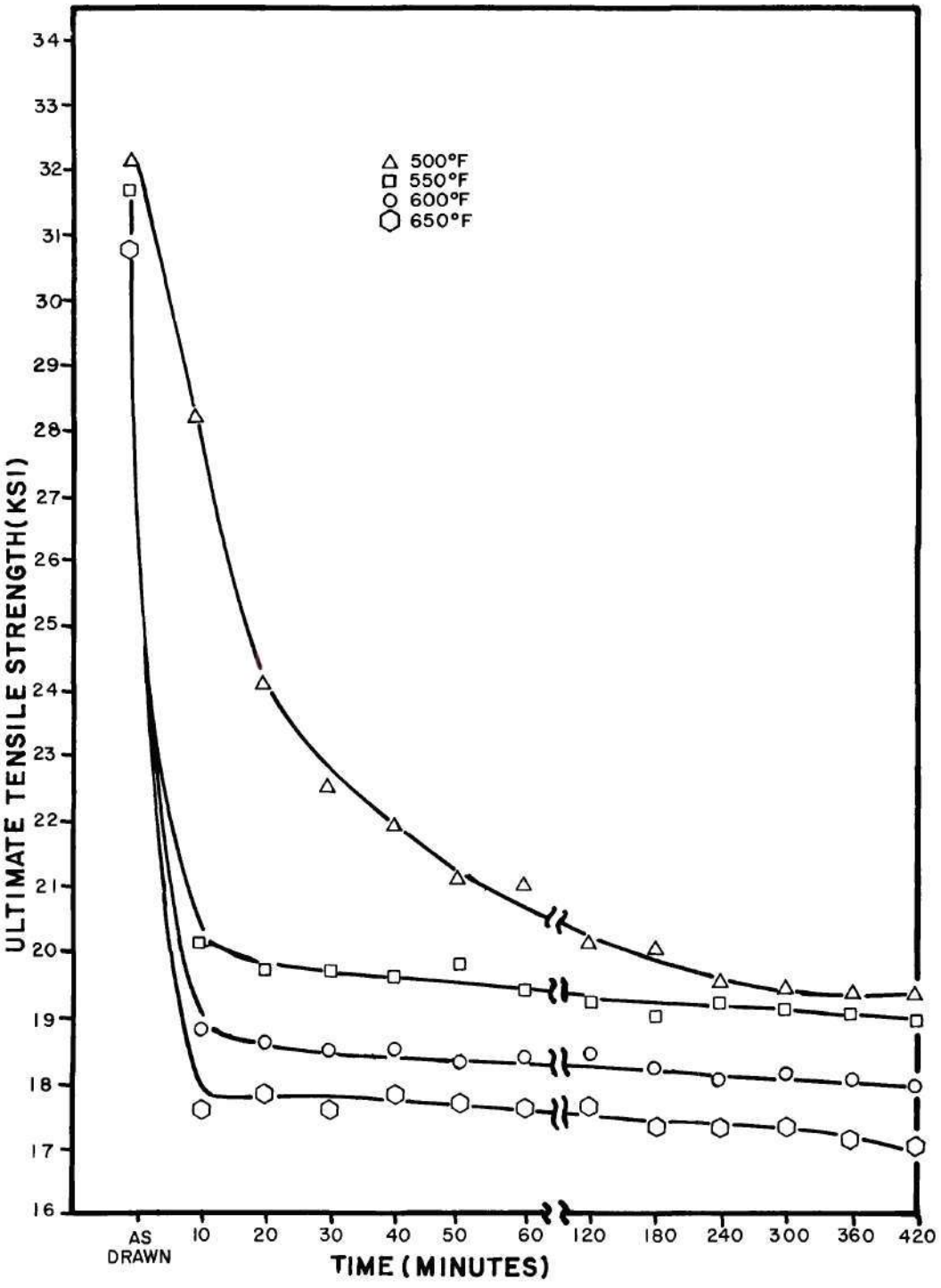

Figure 110. Variation of the Ultimate Tensile Strength During Isothermal Annealing of Al-Fe-Co Cold Drawn Wire. (0.105 Inch Diameter)

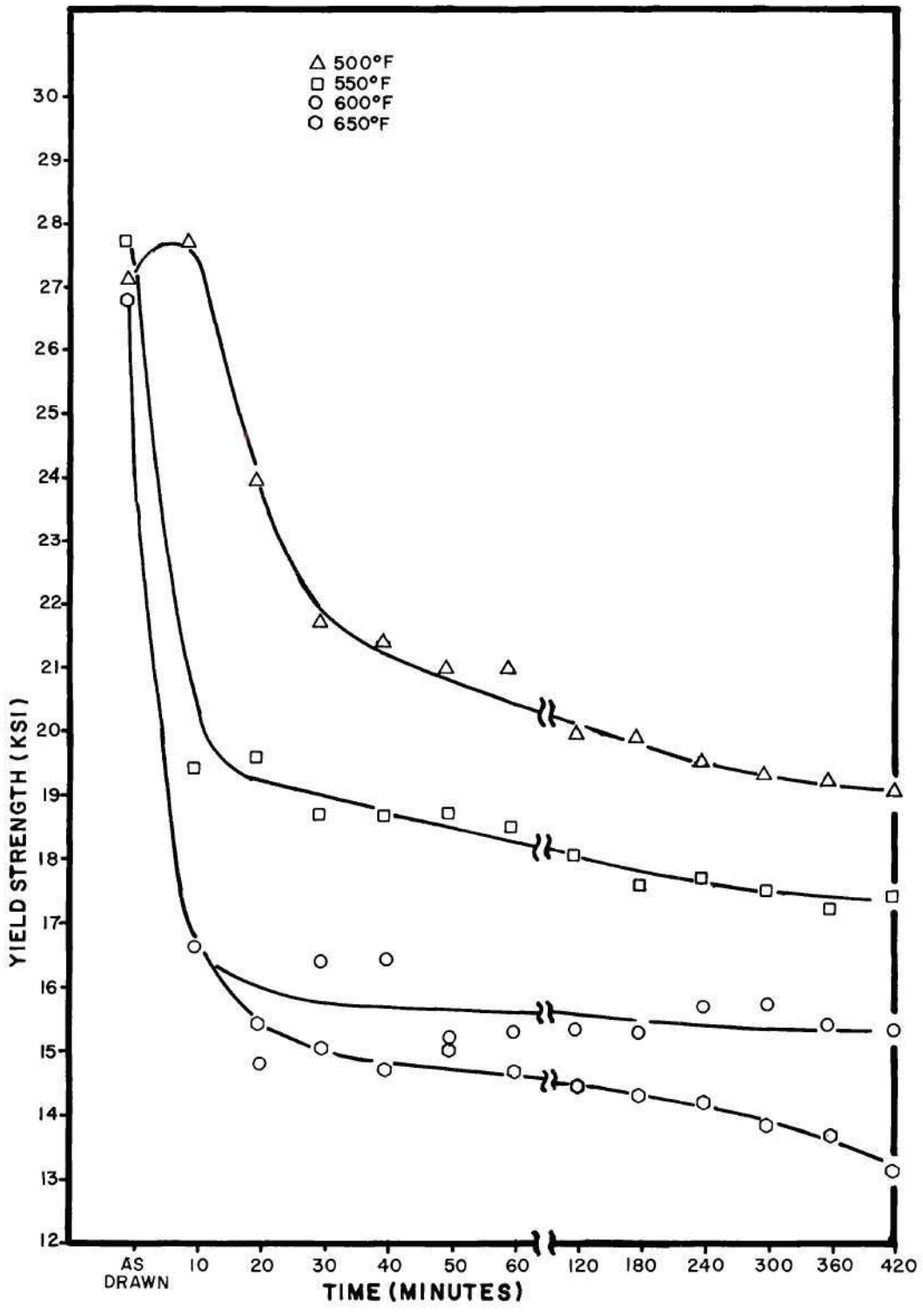

Figure 111. Variation of the Percent Elongation During Isothermal Annealing of Al-Fe-Co Cold Drawn Wire. (0.105 Inch Diameter)

APPENDIX IV

ISOCHRONAL HIGH TEMPERATURE ANNEALING

The change in mechanical properties after one hour isochronal annealing for Al-Fe-Co and E alloy is shown in Figures 112 and 113. The specimens were annealed for one hour after cold drawing to 0.105 inch diameter (92.2 percent total reduction in area) at 25 degrees intervals from 600 to 850 degrees Fahrenheit.

The corresponding optical micrographs are included in Figures 114 to 118. The photomicrographs were taken in the longitudinal direction at 100X magnification using polarized light.

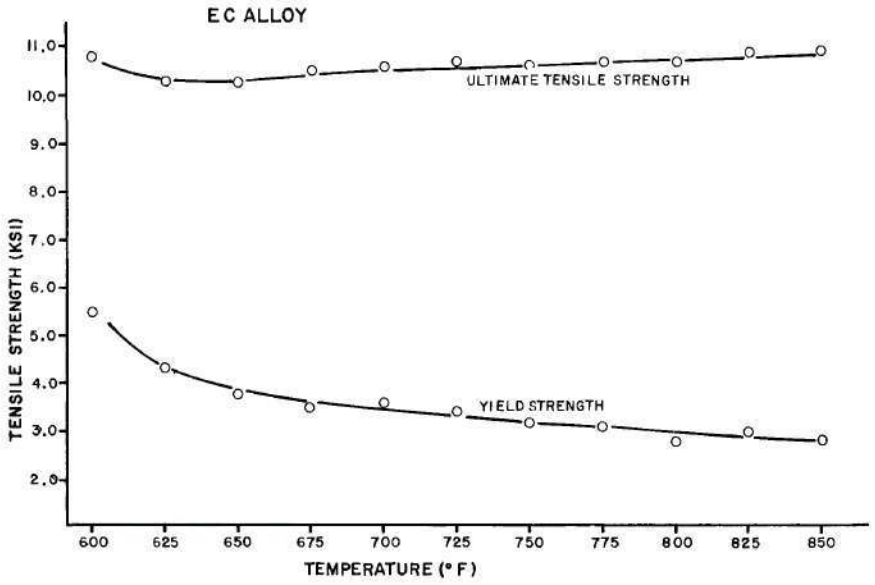

Figure 112A. Isochronal Annealing of 0.105 Inch Diameter EC Aluminum Wire After Cold Drawing - Ultimate and Yield Strength.

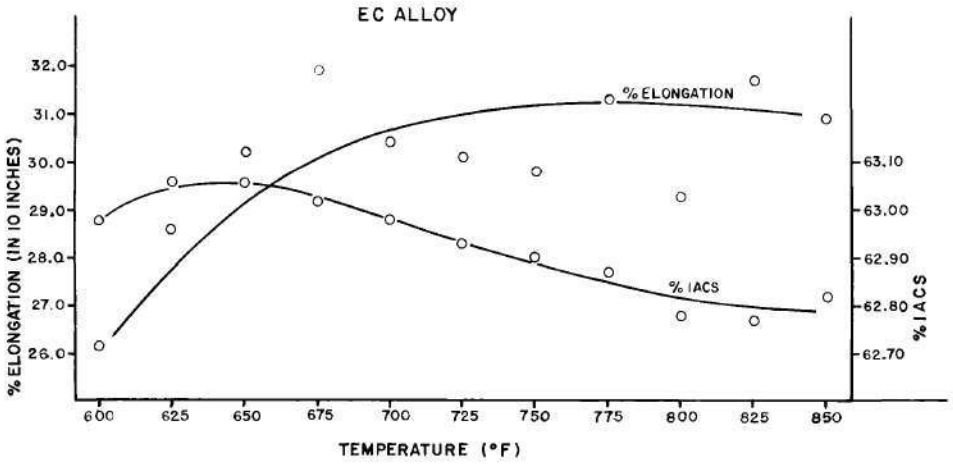

Figure 112B. Isochronal Annealing of 0.105 Inch Diameter EC Aluminum Wire After Cold Drawing - Percent Elongation and Electrical Conductivity.

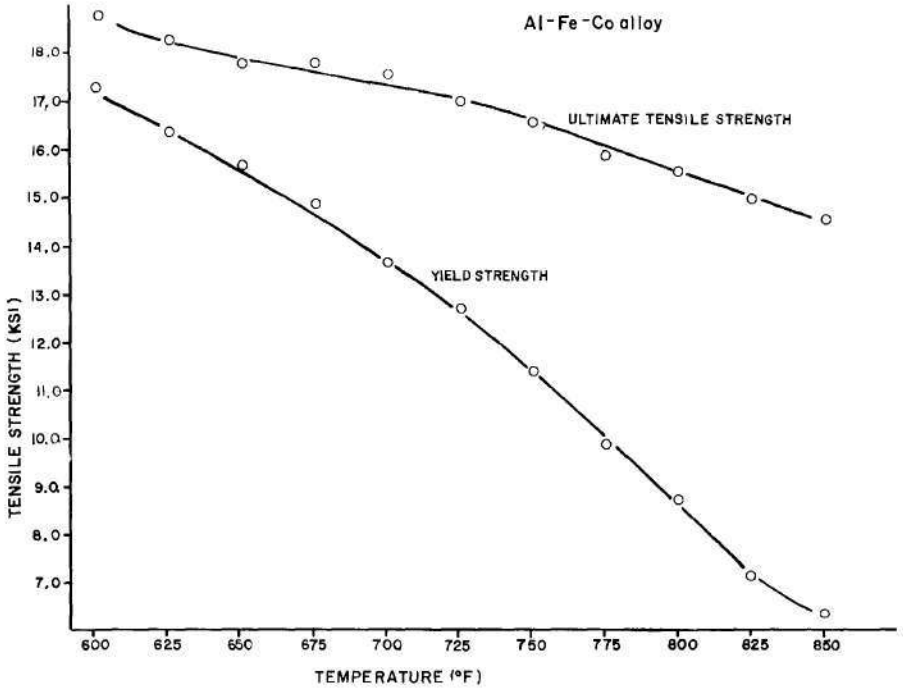

Figure 113A. Isochronal Annealing of 0.105 Inch Diameter Al-Fe-Co Alloy Wire After Cold Drawing - Ultimate and Yield Strength.

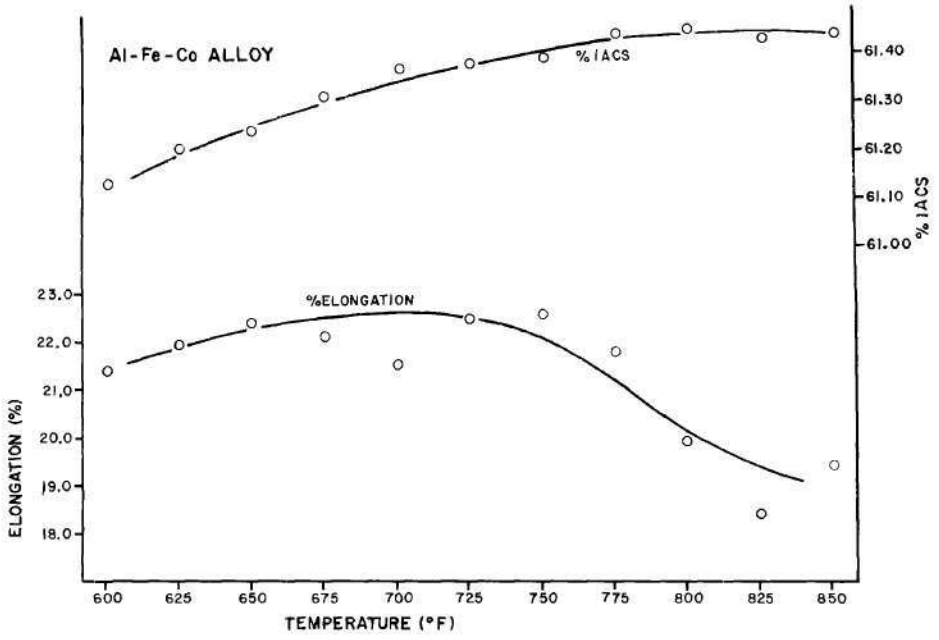

Figure 113B. Isochronal Annealing of 0.105 Inch Diameter Al-Fe-Co Alloy Wire After Cold Drawing - Percent Elongation and Electrical Conductivity.

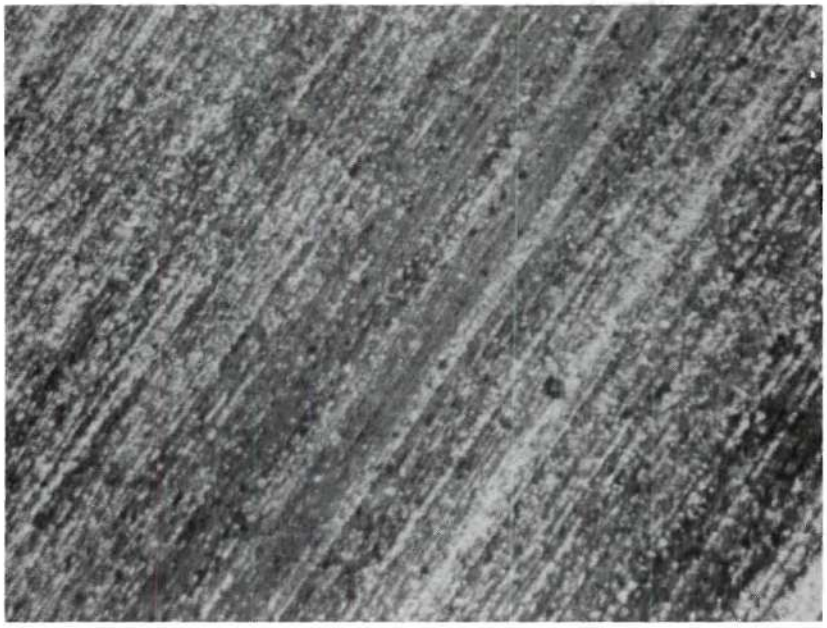

Figure 114A. Al-Fe-Co Alloy Wire Annealed at 625°F for One Hour. 100X

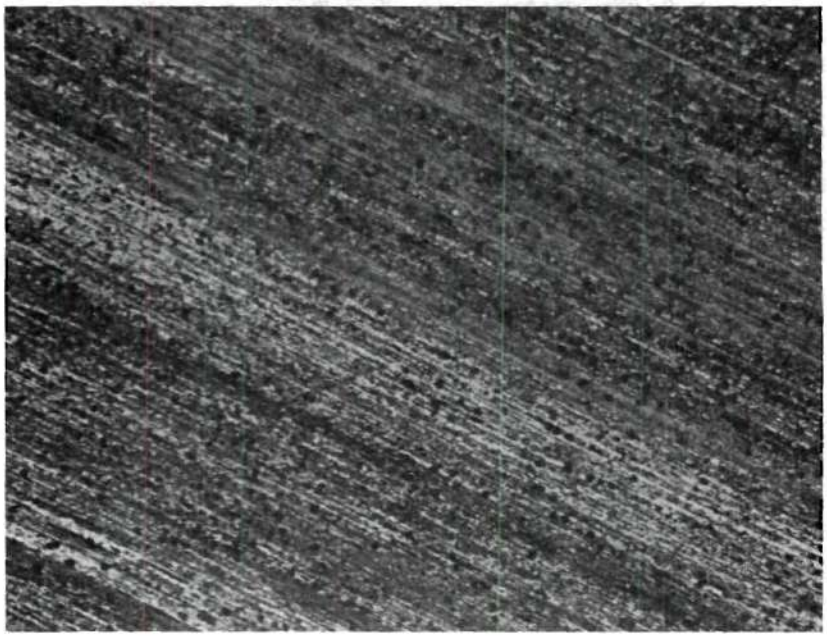

Figure 114B. Al-Fe-Co Alloy Wire Annealed at 650°F for One Hour. 100X

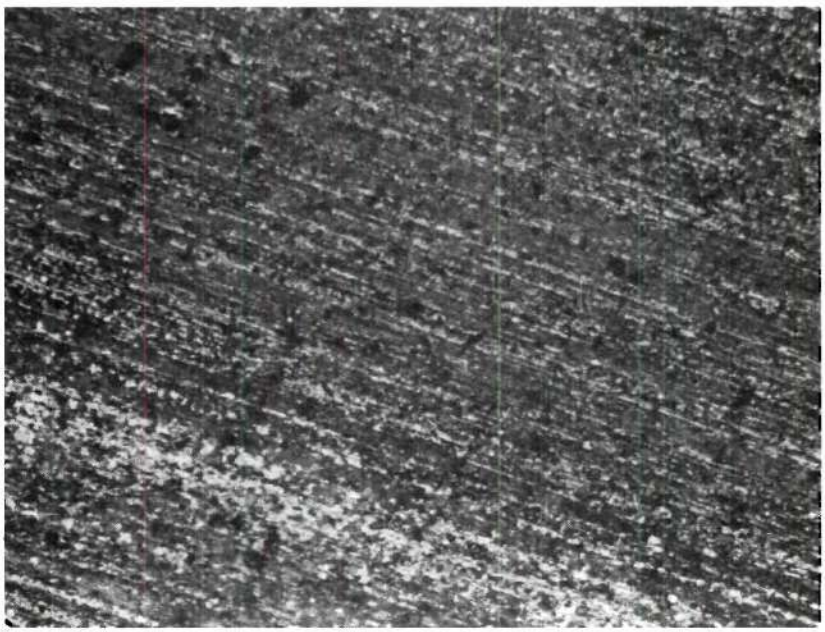

Figure 115A. Al-Fe-Co Alloy Wire Annealed at 675°F for One Hour. 100X

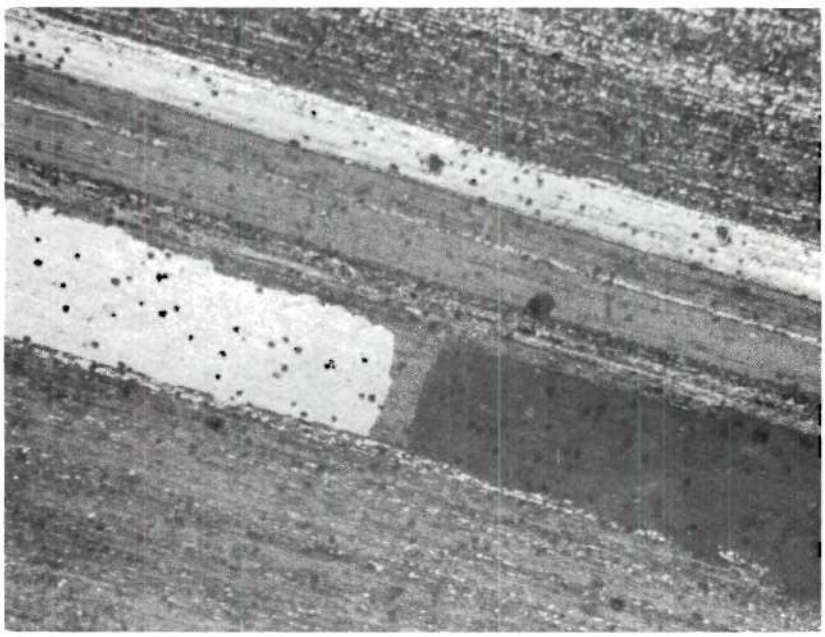

Figure 115B. Al-Fe-Co Alloy Wire Annealed at 700°F for One Hour. 100X

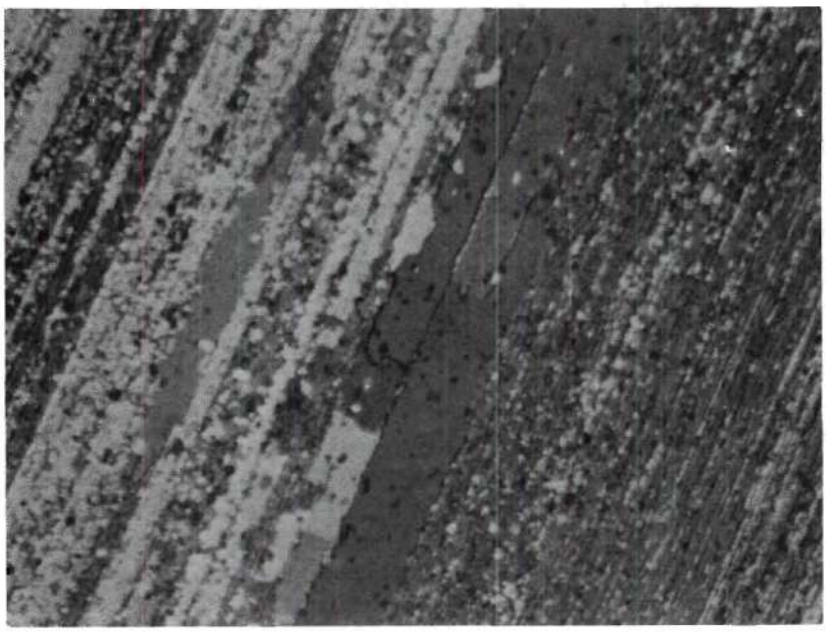

Figure 116A. Al-Fe-Co Alloy Wire Annealed at 725°F for One Hour. 100X

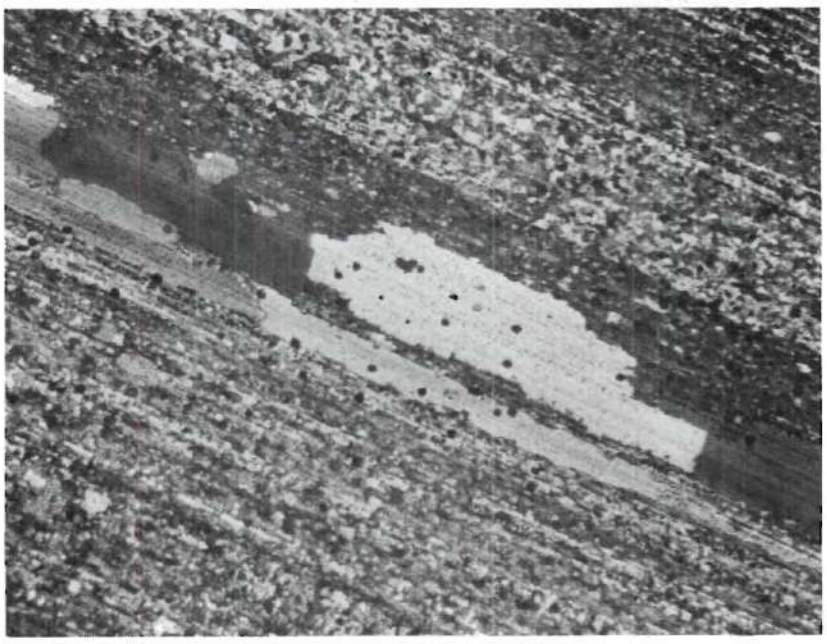

Figure 116B. Al-Fe-Co Alloy Wire Annealed at 750°F for One Hour. 100X

Figure 117A. Al-Fe-Co Alloy Annealed at 775°F for One Hour. 100X

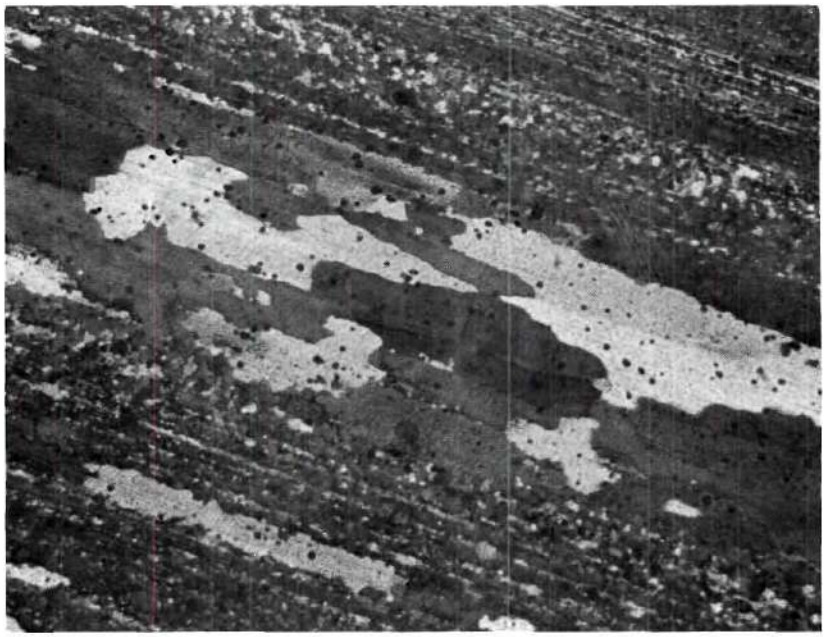

Figure 117B. Al-Fe-Co Alloy Wire Annealed at 800°F for One Hour. 100X

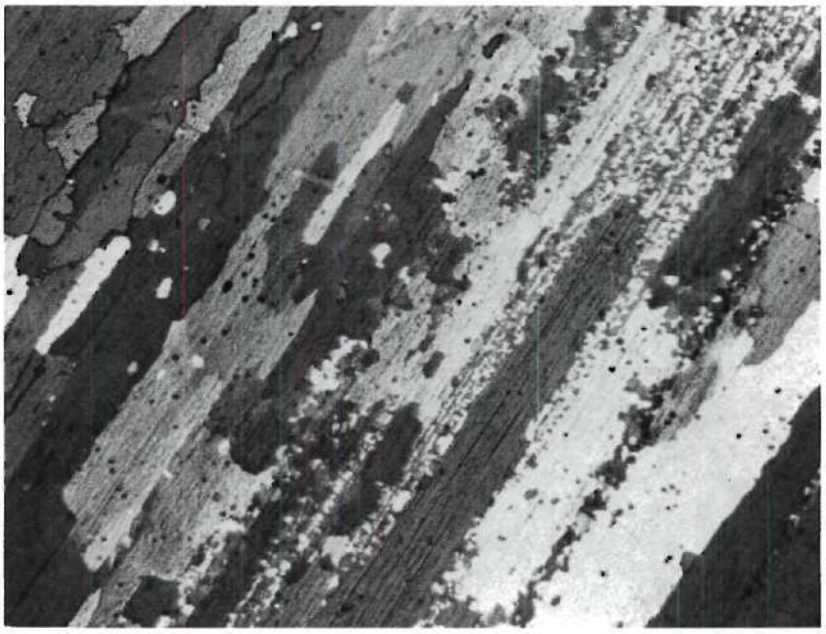

Figure 118A. Al-Fe-Co Alloy Wire Annealed at 825°F for One Hour. 100X

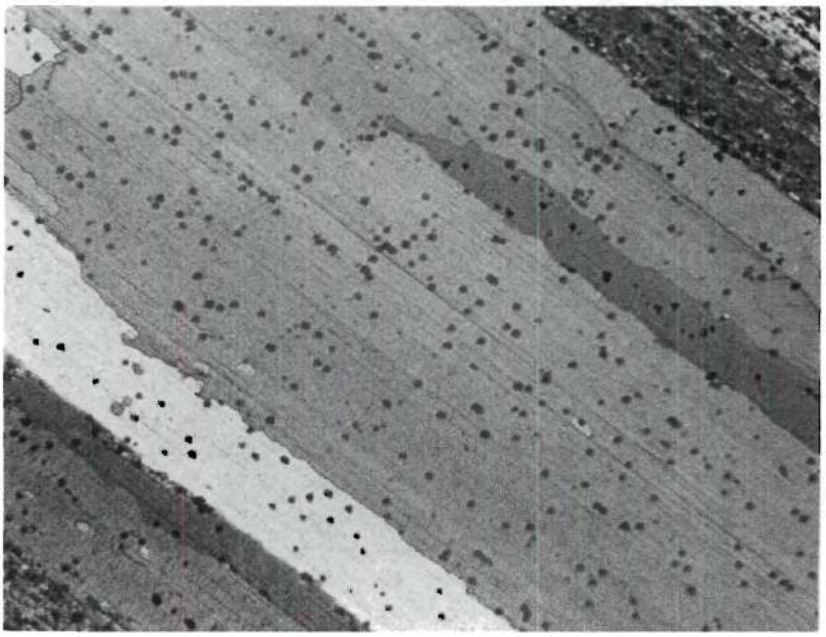

Figure 118B. Al-Fe-Co Alloy Wire Annealed at 850°F for One Hour. 100X

BIBLIOGRAPHY

1. Chia, H. C., Wire & Wire Products, October, 1971.

2. Kelly, A., and Nicholson, R. B., "Precipitation Hardening," Progress in Material Science, Bruce Chalmers ed. Vol. 10, Pergamon Press, New York, 1963.

3. Starke Jr., E. A., Journal of Metals 22 (1970) 54.

4. Brook, G. B., Precipitation in Metals, Special Report No. 3, Fulmer Research Institute, 1964.

5. Polmear, K. J., J. Australian Institute of Metallurgy, 11, (1966) 246.

6. Mould, P. R. and Cotterill, P., "The Effect of Particle Content on the Recrystallization of Two-Phase Aluminum-Iron Alloys," J. Met. Sci., Vol. 2, 1967, p. 241.

7. Leslie, W. C., Michalak, J. T. and Auld, F. W., "Iron and Its Dilute Solid Solutions," Interscience, N.Y., pp. 119-216

8. Chia, H. C. and Starke, Jr., E. A., Wire Journal, September 1971.

9. Ling, Fu-Wen and Starke, Jr., E. A., J. Appl. Cryst. 3 (1970) p. 407.

10. Sellars, C. M. and McG Tegart, W. J., Mim. Sci. Rev. Met. 63 (1966), p. 731.

11. Hirsch, P. B., Internal Stresses and Fatigue in Metals, Elsevier, New York 1958.

12. Amelinckx, S., "The Direct Observation of Dislocations" Solid State Physics 6, Academic Press, New York, 1964.

13. Jonas, J. J., Sellars, C. M., and McG. Tegart, W. J., Met Rev. 14, No. 130 (1969).

14. McQueen, H. J., Journal of Metals, April, 1968.

15. Thornton, P. H., and Cagn, R. W., J. Inst. Met., 1960-61, Vol. 89, p. 455.

16. Chia, H. C. and Starke, Jr., E. A., Aluminum, Vol.47 (1971) pp. 429-431.

17. Gay, P. Hirsch, P. B., and Kelly, A., Acta Cryst., Vol. 7, p. 42 (1954).

18. Perryman, E. C. W., Acta Met., Vol. 2, p. 26 (1954).

19. Vandermeer, R. A.and Gordon, P., "The Influence of Recovery on Recrystallization in Aluminum" in "Recovery and Recrystallization of Metals," Gordon and Breach, N. Y., 1962, p. 211-239.

20. Cahn, R. W., J. Inst. Met., Vol. 76, 1949, p. 121.

21. Leighly, H. P., Perkins, F. C. and McCune, R. A., J. Inst. Met. Vol. 92, 1964, p. 364.

22. Li, J. C. M., J. Appl. Phys., Vol. 33, 1962, p. 2958.

23. Bailey, J. E., and Hirsch, P. B., Proc. Roy Soc., London, Vol. A-267, 1962, p. 11.

24. Beck, P. A. and Sperry, P. R., J. Appl. Phys., Vol. 21, (1950), p. 150.

25. Cottrell, A. H., "Theory of Dislocations", Progress in Metal Physics, Interscience, N. Y., 1953, Vol. 4, p. 206.

26. Hu, H., "Annealing of Silicon-Iron Single Crystals," Recovery and Recrystallization of Metals, Interscience, N. Y., 1963, p. 270.

27. Dunn, C. G. and Koh, P. K., "Simple Orientation Relationships for Secondary Recrystallization in Silicon-Iron," J. of Met., Vol. 9, 1957, p. 82.

28. Doherty, R. D., "The Deformated State and Nucleation of Recrystallization," Metal Science, Volume 8, pp. 132-142.

29. Fujita, Hiroshi, "Direct Observations of Subgrain Growth of Cold Worked Aluminum by Means of Electron Microscope," Journal of the Physical Society of Japan, Vol. 16, No. 3, 1961.

30. Schweizer, M., and Form, W., "New Concepts of the Recrystallization Phenomenon," Journal of the Inst. of Metals, Vol. 101, January, 1973.

31. Hall, E. O., Proc. Phys. Soc., Vol. 64, 1951, p. 747.

32. Petch, N. J., J. Iron Steel Inst., Vol. 174, 1953, p. 25.

33. Rezek, J. and Graig, G. B., Trans. Met. Soc. AIME, Vol. 221, p. 715, 1961.

34. Ball, C. J., J. Iron Steel Inst., Vol. 191, p. 232, 1959.

35. Warrington, D. H., J. Iron Steel Inst., Vol. 201, p. 610, 1963.

36. Abson, D. J. and Jonas, J. J., Met. Sci. J., 1970, 4.

37. Embury, J. D., Keh, A. S. and Fisher, R. M., "Substructural Strengthening in Materials Subject to Large Plastic Strains," Trans. AIME, Vol. 236, (1966), p. 1252.

38. Korbel, A., and Swiatkowski, K., "The Role of Strain Rate in the Formation of Dislocation Structure and its Influence on the Mechanical Properties of Aluminum" Metal Sci. Journal, Vol. 6, 1972, p. 60.

39. Abson, D. J. and Jonas, J. J., Metal Sci. J., Vol. 4, 1970, p. 24.

40. Ball, J. C., "The Flow Stress of Polycrystalline Aluminum"

41. Kelly, A., Acta Cryst. 1954, Vol. 7.

42. Swann, P. R., Electron Microscopy and Strength of Crystals, Interscience, New York, 1963.

43. Gay, P., Hirsch, P. B., and Kelly, A., Acta Cryst., 1954, Vol. 7.

44. Jonas, J. J. and McQueen, H., "Recovery and Recrystallization," To be Published.

45. Langford, G. and Cohen, M., "Strain Hardening of Iron by Severe Plastic Deformation," Trans. ASM, Vol. 62, 1969, pp. 623-638.

46. Thompson, A. W. and Baskes, M. I., "The Influence of Grain Size on the Work Hardening of Face Centered Cubic Poly-Crystals," Phil. Mag., Vol. 29, No. 2, 1973, p. 301.

47. Li, J. C. M., Trans. Met. Soc. AIME, Vol. 227, 1963, p. 239.

48. Kocks, U. F., Met. Trans. Vol. 1, 1970, p. 1121.

49. Hirth, J. P., Met. Trans. Vol. 3, 1972, p. 3047.

50. Kosik, O., Abson, D. J. and Jonas, J. J., Journal of the Iron and Steel Institute, August, 1971.

51. Lequet, R., Whitwham, D., and Herenguel, J. Me'm. Sciet. Revue Me'tell., 1962, Vol. 59.

52. Auld, J. H., Garrod, R. I. and Thomson, T. R., Acta Met., 1957, Vol. 5, p. 741.

53. Friedel, "Dislocations," Pergamon Press, 1964, p. 351.

54. Preston, O. and Evant, N. J., "Dispersion Strengthening of Copper by Internal Oxidation," Trans. AIME, Vol. 221, 1961, p. 164.

55. Doherty, R. D. and Martin, J. W., "Recrystallization in Two-Phase Aluminum-Copper Alloys," Trans. ASM, Vol. 57, 1964, pp. 628-629.

56. Humphreys, F. J. and Martin, J. W., "The Effect of Dispersed Silica Particles on the Recovery and Recrystallization of Deformed Copper Crystals," Acta Met., Vol. 14, 1966, p. 775.

57. Hornbogen, E., "Electron Microscopical Investigation of the Recrystallization of Alloysin Which Precipitation Can Occur," Prak, Metall., Vol. 9, 1970, pp. 349-360.

58. Embury, J. D., "Strengthening Methods in Crystals," John Wiley & Sons, p. 356, 1971.

59. Cahn, J. W., "The Kinetics of Grain Boundary Nucleated Reactions," Acta Met., Vol. 4, 1956, p. 449.

60. Preston, O. and Grant, N. J., "Dispersion Strengthening of Copper by Internal Oxidation," Trans. AIME, Vol. 221, 1961, p. 164.

61. Martin, J. W., "Some Observations on the Effect of a Dispersed Phase on the Recrystallization of Copper," Metallurgia, 1957, p. 162.

62. Humphreys, F. J. and Martin, J. W., "Recrystallization in Copper-Silica Crystals," Acta.Met., Vol. 14, 1966, p. 793.

63. Gatti, A. and Fullman, R. L., "A Study of the Recrystallization Kinetics and Tensile Properties of an Internally Oxidized Solid-Solution Aluminum-Silver Alloy," Trans. AIME, Vol. 215, 1959, p. 763.

64. Lucke, K., and Detert, K., "A Quantitative Theory of Grain Boundary Motion and Recrystallization in Metals in the Presence of Impurities," Acta Met., Vol. 5, 1957, p. 628.

65. Raynor, G. V. and Waldron, M. B., Proc. Roy. Soc., Volume 194, 1948.

66. Waldron, M. B., Met. Abstracts, Vol. 16, p. 266.

67. Dr. L. R. Mondolfo, by Private Communication.

68. Buckerud, L., Jernkont. Ann. 152 (1968).

69. Hollingsworth, E. H., Frank, G. R. and Willet, R. E., Trans. IAME, Vol. 224, Feb. 1962.

70. U. S. Patent No. 3,592,637, issued to Union Carbide.

71. Dubose, E. K. H. and Jones, C., "The Preparation of Transmission Electron Microscopy Specimens from Tubing," Metallography, 2, No. 1, 1969.

72. Underwood, E. E., by Private Communication.

73. "Tension Testing of Metallic Materials," American Society for Testing and Materials, Specification E-8, 1969, pp. 430-435.

74. Chia, E. H.,"Optimization of the Yield Strength Determination in Aluminum Wires," Wire Journal, 1973.

75. "Aluminum Wire EC-H16 or -H26 for Electrical Purposes," American Society for Testing and Materials, Specification B-262-69.

76. "Resistivity of Electrical Conductor Materials," American Society for Testing and Materials, Specification B-193-65.

77. Orowan, E., "Symposium on Internal Stresses in Metals and Alloys," Inst. Metals, 1948, p. 451.

78. Foreman, A. J. E., and Makin, M. J., Canad. J. Physics. Vol. 45, 1967, p. 511.

79. Ashby, M. F., "Strengthening Mechanisms in Crystals," Elsevier, 1971, p. 137.

80. Koster, U., "Recrystallization Involving a Second Phase," Metal Science, Vol. 8, pp. 151-159.

81. Higgins, G. T., "Grain-Boundary Migration and Grain Growth," Metal Science, Vol. 8, pp. 143-149.

82. McElroy, R. J. and Szkopiak, E. C., "Dislocation-Substructure - Strengthening and Mechanical-Thermal Treatment of Metals," Int. Met. Revs., Vol. 17, 1972.

83. Kelley, P. M., International Met. Reviews, Vol. 18, 1973.

84. Ashby, M. F., Phil. Mag., Vol. 21, 1970, p. 399.

85. Hansen, N. and Lilholt, H., "Modern Developments in Powder Metallurgy," Vol. 5, 1971, p. 339.

86. "Mechanical Behavior of Materials," by McClintock and Argon, Addison-Wesley, 1966.

87. Trans. AIME 245, B83 (1969).

88. Starke, Jr., E. A., Kralik, G. and Gerold, V., "Plasticity of Al-Ge Single Crystals Containing Small Fractions of Precipitates," Mat. Sci. and Eng., 11 (1973) 319-323.

89. Ashby, M. F., Ansell, G. S., Cooper, T. O., Lenel, F. V., "Oxide Dispersion Strengthening," Proc. Second Bolton Landing Conf., Gordon and Breach, 1968.

90. Thomas, G., "Transmission Electron Microscopy of Metals," John Wiley & Sons, N.Y., 1966, p. 75.

91. Beck, P. A., Holzworth, M. L. and Sperry, P. R., "Effect of a Dispersed Phase on Grain Growth in Al-Mn Alloys," Trans. AIME, Vol. 180, 1949, p. 163.

92. Marchant, G., "The Influence of Manganese in Solid Solution on the Recrystallization Temperature and Grain Size of Pure Aluminum Sheet," Can. J. Tech., Vol. 31, 1952, p. 16.

93. Day, M. K. B., "Relation entre les Conditions de Fabrication, la Structure et le properties des alliages d'aluminum a 1.25% de Manganese," Revne de Met., Vol. 56, 1956, p. 202.

94. Decroix, J. H., Nevev, R. J., Castro, "Deformation Under Hot Working Conditions," Pub. 108, Iron and Steel Inst., London, 1969.

95. Sellars, C. M. and McG Tegart, W. J., "Hot Workability," Inst. Met. Rev., no. 158, Vol. 17, 1972, p. 19.

96. Leech, E. A., Gregory, P. and Eborall, R., Inst. Met., 1954, Vol. 83, p. 343.

97. Starke, Jr., E. A., Spooner, S., "The Influence of Processing on the Structure and Properties of Aluminum Rod and Wire," Southwire Co Internal Report, January 1974.

98. Lee, E. V., Kranzlein, H. H., and Underwood, E. E., "Dynamic Recovery in Aluminum," Met. Sci. Eng. 7, (1971) 348-356.

99. Bailey, J. A. and Singer, A. R., J. Inst. Metals, Vol. 92, 1963, p. 404.

100. Ommerod, H. and McG. Tegart, W. J., J. Inst. Metals, Vol. 89, 1960, p. 94.

101. Jonas, J. J., McQueen, H. J. and Wong, W. A., "Dynamic Recovery During the Extrusion of Aluminum," Iron Steel Inst., London, Spec. Rept. 180, 1968, pp. 49-59.

102. Jonas, J. J. McGill University, Montreal, Canada, by Private Communication.

103. Vandermeer, R. A., Gordon, P., "the Influence of Recovery on Recrystallization in Aluminum," AIME Symposium, New York, 1962.

104. Roth, A., "On the Solubility of Iron in Aluminum," Z. Metallkunde, Vol. 31, 1939, pp. 299-301.

105. Mould, P. R. and Coterill, P., "The Effect of Particle Content and Matrix Grain Size on the Recrystallization of Two-Phase Aluminum-Iron Alloys," J. Met. Sci. 2 (1967), p. 241-255.

106. Gordon, P. and Vandermeer, R. A., Trans. Met. Soc. AIME, Vol. 224, (1962).

107. Lucke, K. and Stuwe, H. P., "Recovery and Recrystallization of Metals," Interscience, New York, 1963, p. 171.

108. Gordon, P. and Vandermeer, R. A., "Recrystallization, Grain Growth and Textures," ASM, Metals Park, 1966, p. 205.

109. Turnbull, D., Trans. AIME, Vol. 191 (1951) p. 661.

110. Beck, P., Sperry, P. and Hu, H., J. Appl. Phys., Vol. 21 (1950) p. 420.

111. Weissman, S. Trans. ASM, Vol. 53 (1961) p. 265.

112. Weissman, S., Imura, T., Hosokawa, N., "Recovery and Recrystallization of Metals," Interscience, New York (1963) p. 241.

113. Aust, K. T. and Rutter, J. W., "Grain Boundary Migration" in "Recovery and Recrystallization of Metals," Interscience, New York (1963) p. 134.

114. Brimhall, J. L., Klein, M. J. and Huggins, R. A., "Influence of a Finely Dispersed Second Phase on Recrystallization," Acta Met., Vol. 14, 1966, p. 459.

VITA

E. Henry Chia was born in Cienfuegos, Cuba on October 14, 1940. He attended Marist Schools and graduated from Institute de Cienfuegos in 1958. He attended the School of Chemical Engineering at the University of Santa Clara, Cuba from 1959 to 1961. He entered West Georgia College in Carrollton, Georgia in January 1962 while employed at Southwire Company as a laboratory technician. In 1964, he graduated from West Georgia College with a Bachelors Degree in Chemistry.

In September, 1964 he enrolled in the Graduate Division of the Georgia Institute of Technology and received the degree Master of Science in Metallurgy in June 1967. During this year he was employed by Southwire Company as a Metallurgist.

In September 1970 he enrolled again in the Graduate Division of the Georgia Institute of Technology to pursue the degree of Doctor of Philosophy in the School of Chemical Engineering (Metallurgy). During this time he was Manager of the Metallurgy Laboratory, Research and Development, of Southwire Company. He was awarded the "Best Paper of the Year" Award by the Wire A sociation in 1971 for the paper "The Metallurgy of Triple E: A New Alloy Concept" co-authored by Dr. E. A. Starke, Jr.

He is a member of the Institution of Metallurgists, the Wire Association, the American Institute of Mining and Metallurgical Engineers, the American Society for Testing and Materials, the International Metallographic Society, the Honorary Society of

Sigma Xi and the American Society for Metals.

He is married to the former Diana Beguiristain and has two daughters Laura Maria and Lisa Maria.